DEVELOPMENT OF SUSTAINABLE MASONRY BRICK

Tintu Kizhakkethundathil Tomy

A Thesis Submitted to the Faculty of Graduate Studies

in Partial Fulfillment of the Requirements

for the Degree of Master of Applied Science

Graduate Program in Civil Engineering

York University

Toronto, Ontario

December 2019

Abstract

Implementation of environmentally-friendly and cost-effective building designs has been a persistent challenge to the civil engineering community. The current study aims to develop innovative masonry bricks which could open up the prospects in the future for inexpensive construction. It is also envisioned that if adopted, the proposed process of the brick fabrication could benefit the brick manufacturing industry by curtailing the carbon dioxide foot-print and firing energy levels without compromising the prescribed mechanical and physical properties of the resulting product. The research explores the potential of incorporating HBS-polymer which is a biologically-inert product produced after various treatment processes in the Environmental Laboratory of Lassonde, and Incinerated Sewage Sludge Ash (ISSA) obtained from biological treatment facilities as alternative raw materials in manufacturing low cost and environmentally-friendly masonry bricks. The development of geopolymer masonry bricks, that ensures minimum of 40% reuse of waste glass by weight per brick is an another actively pursued area of the current research. The geo-polymerization process was done using quarried shale, Recycled Crushed Glass (RCG) and sodium silicate. In contrast to the conventional masonry bricks fired exclusively over 1000 degree Celsius for no less than 24 hours, the geopolymer bricks were made at a firing temperature of 400 degree Celsius for four hours. In both cases the materials considered are used in partial replacement of shale, which in turn makes the geopolymer bricks and the Incinerated Sewage Sludge Ash bricks a potentially sustainable construction material in the sense that it uses wastes to replace the use of irreplaceable natural resources. The resulting hybrid bricks will be tested for the effect in compressive strength, flexural strength, split tensile strength, ultrasonic pulse velocity, cold as well as hot water absorption, saturation coefficient, efflorescence, freeze thaw damage, and resonant frequency, all being part of the established quality control procedures in this industry. For the HBS-polymer bricks, the findings indicate that, while the compressive strength, hot as well as cold water absorption and resistance to freeze-thaw damage of hybrid bricks was on par with the control brick without any shale replacement, HBS polymer bricks were much lighter (apparently owing to a better distribution of fine pores and without a commensurate increase in water absorption capacity). The results from the study of the Geo-polymer bricks, Bio-polymer bricks and SSA bricks suggest that they can be a promising solution for the long debated economical building construction with a reduced carbon footprint and firing energy while offering an alternative to landfill disposal of waste.

Acknowledgements

I would like to extend my sincere and wholehearted appreciation to my dear supervisor Dr. Pantazopoulou from the Department of Civil Engineering at the York University, for her acceptance, guidance, advice and encouragement throughout the most challenging two years of my master's degree. I would never have been able to finish my degree and dissertation without her valuable guidance and support. It has been an honor and a privilege to work with her during these two years.

Also, I would like to deeply thank Dr. Ahmed Eldyasti, for his generosity and kindness in helping me with the aspects of Environmental Engineering and his interest in my research and the valuable feedback.

To extend, I would like to thank Civil Engineering Department lab technicians Kunjan Rupakheti, Riad Rajab, Melessa Salem for their high spirit and continuous support. Appreciation also goes to Brampton Bricks, The Ashbridges Bay Wastewater Treatment Plant, Toronto for providing me the research materials.

Special love and gratitude goes to my parents, sister , brother and my husband, Nobish Varghese for being a constant source of motivation and supporting me through good and bad times. I cannot leave out my little girl, Iza Maria who missed out many fun moments with me in the course of this endeavour. Further, I can not thank enough all my friends and colleagues including Michael, Kitty, Rita, Nicolas, Zoi, Kostas, Adrien, Sebnem, Satbir, Ismail and Fergala. Furthermore, I would like to thank Ahmed Elzoghby for his wonderful support during the initial stages of my research.

Last but not least, I thank Almighty for giving me the strength for accomplishing the desired goal.

Table of Contents

[x]

List of Tables

Chapter 2

Chapter 3

Chapter 5

Chapter 6

Chapter 7

Appendix

List of Figures

Chapter 4

Chapter 5

Chapter 6

Appendices

List of Acronyms

US DoE   United States Department of Energy

HBS   High Bio-polymer Sludge

ISSA   Incinerated Sewage Sludge Ash

CB   Control Bricks

GB   Geo-polymer bricks

BP   Bio-polymer bricks

ISSAB   Incinerated Sewage Sludge Ash Bricks

RCG   Recycled Crushed Glass

GBFS   Granulated blast furnace slag

FA   Fly-Ash

RFT   Resonant Frequency Test

UPV   Ultrasonic Pulse Velocity Test

FEM   Finite Element Model

EPA   The United States Environmental Protection Agency

SMM   Sustainable Materials Management

CRT   Cathode Ray Tubes

KTS   Kaolin Tailing Sand

CFBA	Circulating Fluidized -Bed Adsorber
NIST	National Institute for Standards and Technology's
BEES	Building for Environmental and Economic Sustainability
BKBA	Brick Kiln Bottom Ash
PMS	Paper Mill Sludge
WMP	Waste Marble Powder
WGS	Waste Glass Sludge
SCBA	Sugar Cane Bagasse Ash
SF	Silica Fumes
GRPd	Glass Reinforced Plastic Dust
NaOH	Sodium Hydroxide
Na_2SiO_3	Sodium Silicate
ASTM	American Society for Testing and Materials
LL	Liquid Limit
PL	Plastic Limit
PI	Plasticity Index
LHBS	Liquid High-Biopolymer Sludge
PHA	Poly Hydroxy Alkanoate

LHBS-1   Liquid High-Biopolymer Sludge Type 1

LHBS-2   Liquid High-Biopolymer Sludge Type 2

DHBS-3   Dried High-Biopolymer Sludge Type 3

SAP   Super Absorbent Polymer

SPB   Shale-Poraver®- Bricks

SPSB   Shale-Poraver®-Slag Bricks

SPSSB   Shale-Poraver®- Na_2SiO_3 Bricks

GB-20   Geo-polymer-20 Bricks

GB-30   Geo-polymer-30 Bricks

GB-40   Geo-polymer-40 Bricks

SSSB   Shale-Slag-Na_2SiO_3 Bricks

SFSSB   Shale-Flyash-Na_2SiO_3 Bricks

SAB   Sludge Ash Bricks

SSAB-15   Sewage Sludge Ash Bricks -15

SSAB-30   Sewage Sludge Ash Bricks -30

CWA   Cold Water Absorption

HWA   Hot Water Absorption

SC   Saturation Coefficient

CAN/ CSA A82   Material standards for Fired masonry brick made from clay or shale

FEA   Finite Element Analysis

GUI   Graphical User Interface Method

List of Symbols

Hc   Composite Correction

ρ_{dry} Optimum Dry Density

Wd   Dry weight of the half brick in grams**,**

W_s^2 Saturated weight of the half brick after 24 hours submersion in cold water

W_b^5 Saturated weight of the half brick after an hour submersion in boiling water

[k]   Element stiffness matrices

[K]   Global stiffness matrix

$\{U\}$ Nodal displacements

F   Externally applied loads

f'_c Compressive strength

Ec, E   Modulus of elasticity

ρ Density

μ Poisson's ratio

f_t Tensile Strength

$f_{c\ trans}$ Compressive Strength in transverse direction

$f_{c\ long}$ Compressive Strength in longitudinal direction

$f_{t\ flex}$ Flexural Strength

$f_{t\ split}$ Split Tensile Strength test

T   Values of correction factor

Chapter1. Introduction

1.1 Background

Implementation of sustainable, environmentally-friendly and cost-effective building design and construction has been a persistent challenge to the civil engineering community. Construction materials cost a major share of the total cost of the building and the production of these materials involve several steps including procurement and processing of raw materials, manufacture, transport as well as assembly. These steps are extremely energy intensive and leave a considerable level of carbon footprint during the process. As per the United States Department of Energy (US DoE), production of construction materials constitutes around 13% of the energy requirement of the country and is one of the major sources of greenhouse emissions. Similarly, the Indian construction industry accounts for nearly 22% of the total greenhouse emissions [EIA., 2019]. With the exception of renewable energy production mechanisms, most traditional forms of energy production requires material consumption and therefore carbonization of the environment; material production, in turn, requires energy. This vicious cycle of energy demand for material production so as to produce more energy but also to produce new materials for construction so as to meet the needs for development is known as the energy-material nexus: apart from the emission of CO_2 in the environment, an equally serious implication of the continued quarrying of raw materials is depletion of natural resources. One example is the shale used by the masonry industry, limestone used by the cement industry, bauxite used by the aluminum industry, coal used for electricity and so on.

The Paris agreement sets a goal for de-carbonization of energy production by 2030, a target that is hard to meet by developed and developing countries together, whereas several of the polluting industries are in denial regarding the effects of pollution on climate [Gibson et.al., 2019]. However, even if the energy part of the nexus is addressed, depletion of natural resources for the need of construction are not yet part of the ongoing discourse. Sustainable development and stability of society, along with the increasing standards of living throughout the globe place the need for continued production of construction materials at the core of stable growth.

At the same time, the annual volume of global waste generation has exceeded 2.01 billion tons and is expected to increase considerably by 2050 to 3.40 billion tons [Kaza et.al., 2018]. Most recent research in sustainable construction materials has included waste generation and disposal

in its ongoing agenda. Reuse rather than disposal, but without compromise in quality and safety has become an urgent priority. For example research is ongoing, with remarkable success, in the introduction of recycled aggregate resulting from demolition of older structures in new concrete; industrial by-products such as ashes and slags are used as cement replacement showing exceptionally favorable performance to physical or chemical attack; ground recycled glass has been shown to possess hydraulic behavior (i.e. reacting with water to produce solids) and is being introduced in the cement industry.

Much less risky exploration regarding implementation of unconventional materials as replacement of raw materials are considered by the brick manufacturing industries. Manufacturing processes are set and centered around the quarry and use of shale in lieu of pure clay as the main ingredient for the red-brick masonry production. Although the cement-industry is considered a main culprit for CO_2 emissions, the masonry industry has been partly spared the controversy. However, the fact remains that clay resources are depleting, and that brick firing to over 1200ºC for several hours is an energy intensive process. Therefore, developing a rational alternative that would reduce the raw material exploitation in red-brick manufacturing is an important challenge. In this regard, past work that has been done by a few researchers [Tay, 1987] around the globe has been focused in the potential use of treated sludge, a by-product of solid waste treatment plants which is currently deposited in landfills.

For example, in Canada, the rate of municipal solid waste generation crossed 34 million tons in 2016 and 73% of these wastes is sent to landfills [Statistics Canada 2016]. Further, the building industry contributes towards 40% of energy usage and 30% of greenhouse emissions in the world [Lemmet, 2009]. Based on a study from the U.S Environmental Protection Agency (EPA), around 160 million tons of waste is generated annually from construction and demolition activities. As the current technology of recycling is not quite adapted in construction industry on account of lack of established codes and standards regarding structural performance, demolished construction materials are often landfilled at the end of their useful lives. Being one of the most extensively used and highly sought-after building material, it is important that the case is no different for masonry bricks. A tremendous amount of energy which is about 2.800 MJ/kg is required for producing bricks and 150 kJ/kg of it is spent in firing kilns [Moedinger, 2003]. Additionally, the process also releases an array of harmful air pollutants including carbon as well

[2]

as Sulphur oxides and particulate matter such as black carbon which in turn can cause a remarkable influence on human health and climate change.

1.1.1 Resource Depletion

Resource depletion is a serious roadblock for the growth of the construction sector. The construction industry is one of the greatest consumers of natural resources worldwide. Unfortunately, it relies heavily on non-renewable raw materials owing to the technological barriers in producing sustainable construction materials and the relative ease in using the available supply of resources [Schilling & Chiang, 2009]. As of now, most of the widely used construction materials or composites including concrete, metals and asphalt are associated with conventional natural reserves in one or other way. While several petroleum products are indispensable and directly used in construction, production of other materials such as cement and metallic structures use them as the source of energy. In the same way, most of masonry bricks produced in the world use coal or natural gas as the source of energy. Additionally, clay used as the major raw material in brick manufacture is procured from top soil and cause depletion in the availability of farmable land. An alternative to clay known as shale is a non-replaceable natural resource. Based on current trends, this level of consumption will continue to increase due to the rapid development and technological progress. Consequently, the natural stock of resources is at the brink of disappearance. Furthermore, with the increase in population, processing and disposal of municipal waste has been a serious issue across the globe. The need for proper disposal of sludge waste from biological treatment facilities has created heavy financial and technological burdens [Abdel-Shafy & Mansour, 2018]. The sludge generated in a treatment facility need to be removed periodically and disposed of in sanitary landfills or by incineration. Incineration is a process of high energy demand and emits greenhouse gases. On the other hand, disposal in sanitary landfills requires transportation to secluded landfill sites which in turn utilize non-renewable fuel reserves and cause air pollution. Additionally, there is concern regarding the re-entrance of heavy metals and other pollutants through the water cycle (e.g. high amounts of endocrine-stimulating or immune-suppressing complexes) in the solid waste that are potentially dangerous to long term health of both plant and animal life [Smith, 2008].

1.2 Use of Sustainable Construction Materials

A feasible solution to the environmental issues caused by the construction industry is the use of sustainable construction materials that are abundantly available and easy to procure without damaging the environment [Kadir et al., 2011]. Avoiding use of non-replaceable natural reserves and the use of renewable materials that generate less waste are paramount in preserving the existing natural resources [Owusu & Asumadu-Sarkodi, 2016]. Likewise, usage of source materials with lower embodied energy and prevention of waste going to landfill is important in reducing the negative impact on the environment. The recent trend in this direction points towards the renewable bio-based composites with diminished environmental footprint from cradle to grave of the material. Moreover, these materials offer further benefits such as the reduction in total embodied energy of constructed structures, curtailing volatile organic compound off-gassing and improvement in mechanical and chemical properties such as density, elasticity, absorption as well as resistance to salt and freeze-thaw damage.

1.3 Thesis Objectives

This study aims to address some of the environmental challenges of the masonry construction industry as well as municipal waste disposal by using waste as a source material to produce masonry bricks. In this endeavor, the feasibility of incorporating a variety of waste materials into the proposed hybrid masonry bricks are investigated. The study includes a detailed experimental component, where the proposed partial replacement of shale is carried out through all the steps of the manufacturing process as well as in terms of evaluation of mechanical and physical performance of the developed product in order to assess the feasibility of each waste type considered as source material.

Polyhydroxyalkanoates are biogenic polyesters with similar properties with those of synthetic plastics such as polypropylene and they improve several characteristics of bricks such as strength, density and absorption when used as partial clay replacement in the form HBS-polymer. While this offers a viable solution for the envisioned attainment of 'low-cost, low-emissions' buildings in the construction sector, the concept is also to create a new application for HBS-polymers that are currently produced from environmental treatment processes in the Environmental Engineering Facilities of Lassonde, thereby reducing the landfills and rendering the biological treatment facility as a productive and futuristic industry.

[4]

Along those lines, Incinerated Sewage Sludge Ash (ISSAB) – a brick source material obtained by incinerated treated waste generated in municipal sewage treatment facilities, is also considered as a promising solution for low cost environmentally friendly construction. With the inherent simplicity in the technique and time-tested durability of structures, masonry bricks remain as one of the preferred choices in construction industry although the process of bricks' fabrication evolved continuously over thousands of years [Fernandes, Lourenço & Castro, 2010; Campbell & Pryce, 2003]. Several research studies that investigated the feasibility of brick manufacture from sewage [Okuno and Takahashi, 1997; Wiebusch and Seyfried, 1997; Samadikun et al, 2018] have suggested that sewage sludge is a prospective brick source material. A few other studies [Lin Deng-Fong & Weng Chih-Huang, 2001] have explored the feasibility of utilizing incinerated sewage sludge as an admixture in brick manufacturing. The results from their tests conducted on the fabricated bricks indicated that up to 40% of ash incorporation yielded compressive strengths comparable to those of control bricks although 10% was found to be the optimal ratio of incorporation. Further, addition of incinerated ash decreased the firing shrinkage and weight loss.

Glass, being an indispensable commodity used by the modern society for an assortment of purposes, also generates vast amounts of waste. Although a limited fraction of the waste glass is recycled directly, the remaining portion, dumped as waste material, is a cheap and readily accessible source material for brick manufacture. Finely pulverized glass has been shown to have pozzolanic activity by virtue of its amorphous state and presence of silicon and calcium in sizeable quantities [Dyer and Dhir, 2001]. These beneficial characteristics of recycled waste glass make it an optimum choice as additive in the brick manufacturing process. Previous studies have investigated the usefulness of various forms of waste glass including recycled glass [Chidiac and Federico, 2007; Demir, 2009; Smith, 2014], personal computer panels [Dondi et al., 2009], cathode ray tube glass [Lee et al., 2016] and solar panel glass waste [Lin et al., 2012] in brick manufacture.

Municipal sewage waste and waste glass are the some of the categories of waste that are available easily and abundantly. Their availability and the emerging awareness to seek engineering solutions that would reduce the cost of construction, the carbon dioxide foot-print and firing energy levels that plague the masonry fabricating industry, as well as the urgency to put a check on 'the extent' of natural resources being dug out of the ground every day for brick manufacture were

motivating concepts for the present research. This was also paired with the innovative idea of using the masonry bricks as a host of various wastes- a solution to reducing wastes containing undesirable compounds in landfills.

As a result, the following objectives pursued in the current research thesis:

1. To develop hybrid masonry bricks from waste materials especially with municipal sewage sludge and waste glass without compromising the prescribed mechanical and physical properties.

2. To explore futuristic (hybrid) brick designs as alternative construction products that enable the effective use of other types of industrial wastes:

   i.   Bricks containing Geo-polymer technologies (GB)

   ii.   Bio-polymer bricks containing Bio-materials (BP)

   iii. Bricks that contain incinerated sewage sludge ash (ISSA) in partial replacement of raw shale

1.4 Thesis Outline

The aforementioned objectives have been accomplished by the following steps. All these steps are described in several chapters.

1.4.1 Chapter 2- Review of Literature

A literature review has been conducted to develop a better understanding of the previously conducted research studies on the utilization of waste materials for production of added-value construction materials. The contents of this chapter are divided into two sections – discussing the quest for sustainable and inexpensive construction and the utilization of waste materials for brick manufacture.

1.4.2 Chapter 3- Preliminary Phase of the Research

The preliminary phase of the Research focusses on investigating the level of improvement that is effected in structural and mechanical properties of bricks after partial replacement of principal source material, quarried shale, with waste products. As a first step toward the research, the shale sample was subjected to exhaustive geotechnical analyses prior to the commencement of brick

production to characterize the constituent components and to investigate the ambient casting mix conditions such as the allowed level of moisture content.

In this regard, Control Bricks (CB) were made without any replacement of shale, and hybrid bricks with varying shale replacement rates were fabricated using several waste materials including HBS-polymers, Incinerated sludge ash (ISSA) provided by the Municipal wastewater treatment facilities, Poraver® expanded glass powder, Recycled Crushed Glass (RCG), Granulated blast furnace slag (GBFS), fly-ash (FA) etc. Additionally, reference brick specimens were produced without any shale replacement. All experimental units including the reference bricks were produced in few trial specimens for each material combination. Then the preliminary analysis was done considering a range of standardized tests proofing the mechanical and physical performance of the trial mixes.

1.4.3 Chapter 4- Main Phase of the Experimental Research

The results of the trial investigations were used to guide the formulation of the main phase of the research. At this stage Control bricks, Geo-polymer bricks, Dried High Bio-polymer bricks and Sewage Sludge Ash bricks were made in sizable numbers on account of their sustainability and better performance during the trials. Among them, Geopolymer bricks and sludge ash bricks were made in several percentage replacement of shale with recycled glass powder and sewage sludge ash respectively.

1.4.4 Chapter 5- Experimental Results

Several experiments including physical and mechanical tests have been conducted on all the bricks made during the final phase of the research, replicating the quality control procedures prescribed by the Masonry Design Code for the characterization of a masonry product in the market. Tests conducted may be classified into non-destructive and destructive tests. The non-destructive mechanical tests conducted were, the Resonant Frequency Test (RFT) and Ultrasonic Pulse Velocity Test (UPV). The destructive mechanical tests conducted were indirect tensile strength tests such as flexural strength and splitting tensile strength test and compression tests in longitudinal and transverse directions. Other durability tests performed include resistance to freeze-thaw damage, efflorescence and water absorption.

1.4.5 Chapter 6- Numerical Simulation for Inverse Analysis

Finite Element Modelling (FEM) of the mechanical tests conducted during the experimental phases on control as well as hybrid bricks was conducted to relate the mechanical behavior with the essential material mechanical properties. The tests included flexural strength, splitting tensile strength and compression tests in longitudinal as well as transverse directions. Input material properties used in the FEM models were obtained after iteration to match the load displacement response of the specimens with the analytical estimation in a consistent manner. This computer-assisted inverse extraction of the actual characteristic material properties was necessary because tensile strength and strain capacity are both material properties that cannot be measured directly but are routinely obtained through inverse analysis of indirect tests (e.g. flexure, splitting) for all brittle and semi-brittle materials. In this regard, the advanced nonlinear finite element platform, VecTor2, developed at the University of Toronto was used in the simulation studies.

1.4.6 Chapter 7- Correlation Analysis

In this chapter, correlation between the various mechanical and durability test parameters extracted from the experiments was sought, aiming to obtain simple predictors of properties that are difficult to measure or are fraught with uncertainty, from the values obtained either in standard (e.g. compression) or otherwise, non-destructive tests.

1.4.7 Chapter 8- Summary and Conclusions

This chapter summarizes the findings of the research. It also provides recommendations that could be adopted in future projects for continuation of the exploration for alternatives to shale in brick manufacturing.

Chapter 2. Review of Literature

2.1 Overview

The volume of municipal solid waste generation is increasing drastically with the rise in population and rate of urbanization across the globe. The annual volume of global waste generation has exceeded 2.01 billion tonnes and is expected to increase considerably by 2050 to 3.40 billion tonnes [Kaza *et al*., 2018]. In Canada, the rate of municipal solid waste generation crossed 33 million tonnes and over 74% of these wastes is sent to landfills [Statistics Canada, 2016b, Statistics Canada, 2016a]. Furthermore, the building industry is responsible for 40% of the energy usage and contributes towards 30% of greenhouse emissions in the world [Lemmet, 2009]. Meanwhile, the growing cost of construction materials makes affordable housing a distant dream for large groups of the earths' population [World Economic Forum, 2019]. In light of this state of affairs regarding the energy-materials nexus, utilization of waste materials in the manufacture of construction materials is an obvious solution, which can also be sustainable provided the necessary technologies are developed. The United States Environmental protection Agency (EPA) has been working effectively on the waste management in the past 30-35 years; now thinking beyond waste, they have transitioned from focusing on waste management to focusing on Sustainable Materials Management (SMM), which refers to the use and reuse of materials across their entire life cycle. SMM conserves resources, reduces waste and minimizes the environmental impacts of materials we use (EPA, 2018). It is very important to conserve and recycle the resources in all possible sectors like the construction industry for the overall development of the world economy and to contribute towards a sustainable environment. Figure 2-1 shows the current national waste management of the United States.
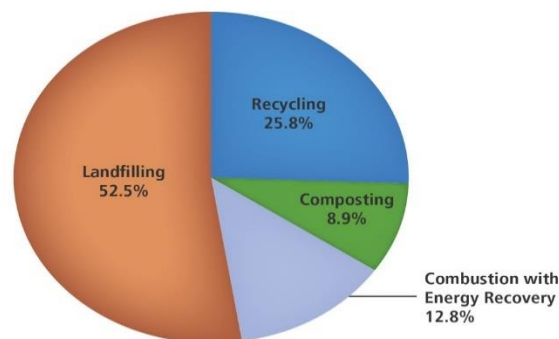
Figure 2-1: The current national waste management of the United States (EPA,2018)

[9]

Following up on this consideration, the present chapter summarizes the previously conducted research studies on the utilization of waste materials for construction materials. The contents of the chapter are divided into two sections – the first referring to the quest for sustainable and inexpensive construction and the second to the utilization of waste materials for brick manufacture.

2.2 The Quest for Sustainable and Inexpensive Construction

Before the massive displacement of the masonry by the reinforced concrete, up to the early 20th century, masonry was the preferred choice in building construction. However, masonry is still used for the construction in many parts of the world, mainly because of its ecological and economical advantages, as well as for aesthetic reasons [Pardalopoulos, Karantoni, Pantazopoulou, 2019]. While sustainable development is one of the difficult tasks of the last two centuries [e.g. Sachs & Warner, 1995], the same holds true for the masonry industry as well. With the extent of pollution, waste generation and resource depletion caused by the construction industry [Dixon, 2010], the significance of measures to ensure sustainability is paramount. Further, the complexity and financial burden of waste disposal makes it a strenuous process. Incorporation of waste in construction materials offers a promising solution to curtail these issues simultaneously.
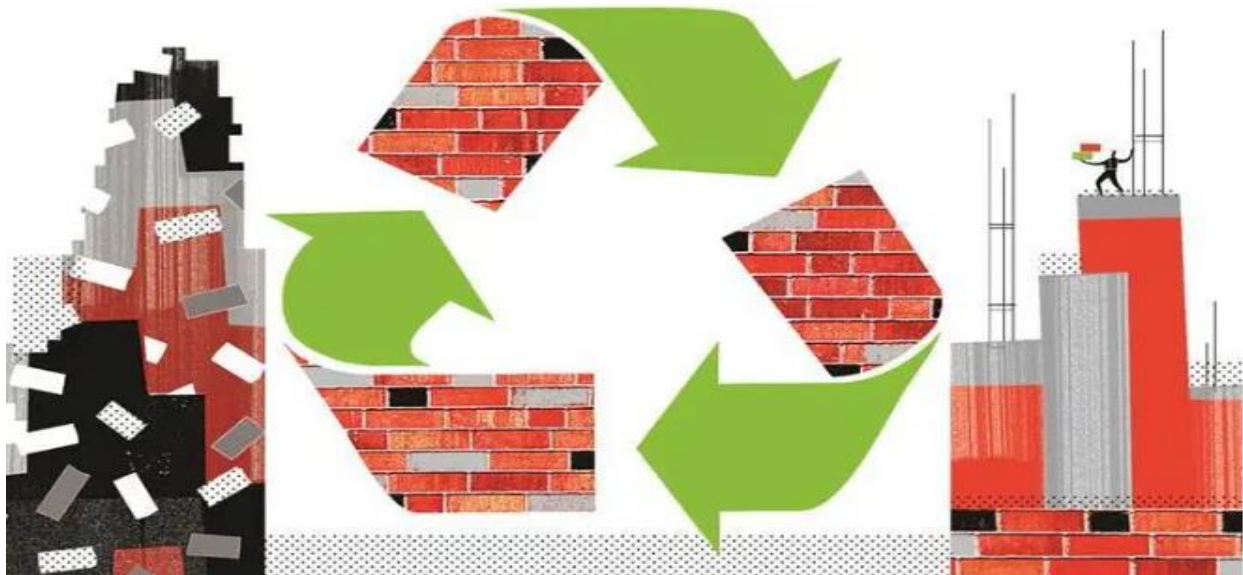
Figure 2-2: Depicts reuse and recycling by the incorporation of waste in construction materials (Sasikumar ,2010)

The drive for sustainable construction has paved the way for characterization of numerous waste products as valuable source materials. Finely pulverized glass is theoretically pozzolanic by virtue of its amorphous state and presence of silicon and calcium in sizeable quantities [Dyer and Dhir, 2001]. Moreover, its cementitious properties have been illustrated before [Archibald *et al*., 1995]. These beneficial characteristics motivated the scientific community to explore the feasibility of recycled glass as sand replacement in construction. The utility of recycled glass as an admixture for partial sand replacement has been explored in various parts of the world [Bashar & Ghassan, 2009; Kim, Choi, & Yang, 2018; Cabrera-Covarrubias, Gomez-Soberon, Almaral-Sanchez, Arredondo-Rea, & Mendivil-Escalante, 2018; Chandra Paul, Šavija, & Babafemi, 2018]. Correspondingly, Cathode ray tubes (CRT), dumped as waste products by the advent of the new generation widescreen televisions are recycled by utilizing them in the production of high-strength mortars. Waste cathode ray tubes are ground, sieved and used as aggregate component in the mortar.

Investigation of mechanical properties of the resulting cementitious compounds have revealed increased compressive strength upon the incorporation of waste CRT glass [Maschio, Tonello, & Furlani, 2013]. Utilization of sea shells in cement products is an eco-smart concept enabling the replacement of fine and coarse aggregates with natural substances. Crushed and sieved mussel shells [Martínez-García, González-Fonteboa, Martínez-Abella, & Carro- López, 2017] as well as waste oyster shells [Eo & Yi, 2015] have been tested for their utility as partial aggregate replacement in concrete structures. When sea shells are used as cheap natural nanoplatelets, they enhance the pore structure and improve the durability of cement-based products. During such a process, sea shells are rinsed, dried, crushed and subjected to alkali treatment before they are used as nanoplatelets. Research studies demonstrate significant increase in compressive strength and drop in chloride penetration of cement paste and mortar after these nature friendly nanoplatelets are incorporated in the minute scale [Huang, Lv, Liao, Lu, & Xu, 2018]. Feasibility studies investigating the usefulness of excavation soil as an alternative source material for sand replacement have yielded positive results although the soil had to be stabilized beforehand [Priyadharshini , Ramamurthy, & Robinson, 2018]. Mining and metallurgical industry is one of the sources for waste or by-products that could be used as construction grade raw materials. Kaolin Tailing Sand (KTS), a by-product from kaolin mining industry has been used to replace fine aggregates in concrete structures and resulted in the improvement of the compressive

as well as splitting strengths [Xu *et al*., 2018]. Likewise, blast furnace slag, a non-metallic by-product of iron ore purification process is a potential Portland cement replacement in the manufacture of ecofriendly concrete [Mehta & Siddique, 2018].

Agro-waste, generated during agricultural activities is also considered a promising source material for construction. For instance, the use of composite materials consisting of pea nut shells and plaster improves the thermal properties of buildings. In other words, the composite material exhibits significantly reduced thermal conductivity and diffusivity in comparison with a simple plaster material [Lamrani *et al*., 2017]. Agricultural waste products such as coconut fibre, rice husk and oil palm empty fruit bunch have been tested for their effectiveness as filler materials in the manufacture of concrete paving blocks [Lutfi, Yamin, Rahman, & Ginsel Popang, 2018]. Similarly, light weight concrete structures are produced using coconut fibres. On top of the significant weight reduction achieved, coconut fibre reinforcement improved the toughness of the concrete structure while maintaining comparable physical and mechanical properties at low proportion of fibre incorporation [Hasan, Sobuz, Sayed & Islam, 2012]. Coarse and fine aggregates such as crushed stone are indispensable constituents of concrete mix design. The relative scarcity and steep increase in the cost of these materials over the years led to the investigation for alternatives. Interestingly, agricultural waste products have been proved to be a valuable resource in this endeavor. Various agricultural waste products such as oil palm shells [Alengaram *et al*., 2013; Khankhaje, Salim, Mirza, Hussin & Rafieizonooz, 2016], coconut shells [Kumutha, Vijai, & Vijayragavan, 2018] , groundnut shells [Sada, Amartey,& Bako, 2013], saw dust [Kumar, Singh, Kumar& Gupta,2014] and walnut shells [Kamal *et al*., 2017 ; Mirza, Anwar, Samarul & Mohd, 2017] have been identified to be promising options and enabled significant proportion of aggregate replacement without considerable drop in physical and mechanical properties of concrete structures.

Incinerated residues of several agro-waste products possess pozzolanic activity and this characteristic qualify them as supplementary cementitious materials [ASTM C125-16]. Scientific exploration in this direction investigated the efficacy of an array of agro-waste ash including wheat straw ash [Qudoos, Kim, Atta-ur-Rehman, & Ryou, 2018], rice husk ash [Chindaprasirt, Rukzon, 2015], sugar cane bagasse ash [Akkarapongtrakul, Julphunthong, Thanongsak, 2017], palm kernel nut waste ash [Joshua *et al*., 2017] and corn stalk ash [Raheem, Adedokun, Adeyinka, & Adewole, 2017], cork waste ash [Ramos , Matos & Sousa–Coutinho, 2014], groundnut shell ash [Arshad ,

Kumar, 2017; Olutoge, Buari & Adeleke,2013] and saw dust ash [Auta *et al.*,2016] as raw materials for cement replacement. Evidently, such studies established the prospects of agricultural waste products as prospective components for partial cement replacement. The construction and demolition sector constitute a considerably large proportion of waste generated globally and surpassed 3 million tonnes per year across 40 countries by 2012 [Akhtar & Sarmah, 2018]. Recycled concrete waste that can be segregated from demolition waste can be used as coarse aggregates in green concrete mixtures to achieve sustainable development without impacting the massive landfills. Nevertheless, a thorough segregation, cleaning as well as grinding is mandatory before recycled concrete can be used as a well graded aggregate admixture [Jain, Garg, & Minocha, 2015; Wentao & Jason, 2010].
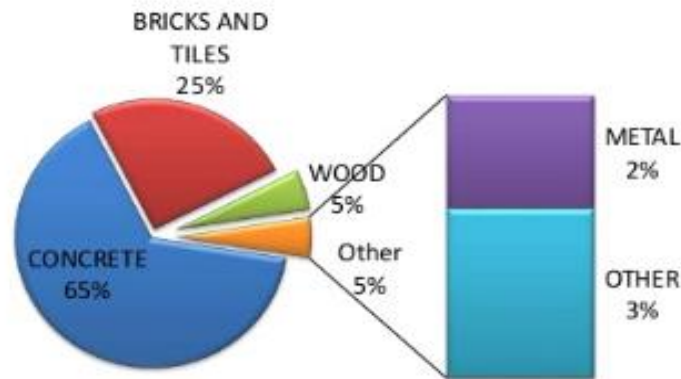
Figure 2-3: Typical percentage of demolition waste of a developing nation (Thakkar, 2017)

Incorporating industrial waste materials among construction materials have the double advantage of cost reduction and as a means of waste disposal. A multitude of waste products including porcelain polishing waste [Matos, Prudêncio, Oliveira, Pelisser, & Gleize, 2018], brine sludge [Garg & Pundir, 2014], fly ash [Naganathan, 2015], co-fired blended ash [Ram & Ralegaonkar, 2018] have been used as concrete admixtures. Concrete bricks made with Circulating Fluidized-Bed Adsorber (CFBA), which is a by product from the power plant industry, demonstrated 61% reduction in thermal conductivity. This by-product exhibits physical and chemical properties similar to portland cement. In the same way, sintered sludge material obtained from copper slag recycling facilities have proved to be an effective aggregate replacement [Tay Joo-Hwa, Hong Sze-Yunn, & Show Kuan-Yeow, 2000].

Sewage sludge incorporated soil was used in pavement sub layers and the mechanical properties of soil samples with varying sludge proportions indicated that the stabilized soil sludge mixtures have significant prospects in pavement construction [de Figueirêdo Lopes Lucena, Thomé Juca, Soares, & Portela, 2014]. Further, ground sludge ash has been used as cement replacement in mortar blocks [Pinarli & Kaymal, 1994].

A number of other waste products have been recognized as viable choices for incorporating into construction materials. While waste packaging tape [Hu *et al*., 2018] and engine oil [Liu, Peng, Wu, & Zhou, 2018] improved the rheological properties of bitumen, waste engine oil inclusion resulted in a drop of viscosity which is helpful in reducing the construction temperature and energy consumed. Introduction of waste metal in asphalt enabled enhanced resistance to skid and scraping without considerable changes in mechanical properties of bitumen [Ajam, Gómez-Meijide, Artamendi, & Garcia, 2018]. Considerable scale of plastic waste incorporation as aggregate replacement in non-structural concrete offers additional benefit of reduced thermal conductivity up to seven times compared to conventional concrete [Záleská *et al*., 2018].

2.3 Utilization of Waste Materials in Brick Manufacture

Masonry bricks represent one of the ancient and widely used construction methods across the globe that gained widespread popularity during the Mesopotamian, Egyptian and Roman era. With the inherent simplicity in the technique and time-tested durability of structures, they remain as one of the preferred choices in construction industry although the process of brick fabrication evolved continuously over thousands of years [Fernandes, Lourenço & Castro, 2010; Campbell & Pryce, 2003]. Traditional masonry bricks exhibit modest level of specific strength, fire resistance, chemical as well as corrosion resistance and durability. However, despite these appealing factors, their dependence on natural resources and energy intensive manufacturing processes undermines the vision of sustainable construction.

2.3.1 Limitations of Conventional Masonry Bricks

2.3.1.1 Resource depletion

Brick industry is heavily dependent on vast amounts of natural resources such as clay and shale. Evidently, a growing demand for bricks is taking a toll on the availability of these natural reserves in various parts of the world. In the same way, construction industry has a major role in the

depletion of world's fossil fuel reserves. Unchecked clay usage for brick manufacture has reduced the area of arable land and is threatening the future of agriculture in China and India [Bhushan, Basu, Yadav & Kumar, 2016], [Reddy, 2004], [Zhang, 2013]. In China, over a billion square meters of clay resources is used annually for brick manufacture which in turn is equivalent to the destruction of 500 thousand acres of farmable land [Xu, 2010]. In addition, roughly 7 thousand tons of coal is used every year in the country, resulting in the release of approximately 18 thousand tons of carbon dioxide emissions [China Coal Information Institute, 2015]. As per a survey by World Energy Council, the global energy demand may increase by over 50% by 2050 and the global fossil fuel reserves are therefore in great peril if their consumption continues at this alarming rate.

2.3.1.2 Significant level of embodied energy

The term 'embodied energy' refers to the total energy used for the manufacture of construction materials. It is described as the energy spent in the extraction of raw materials, manufacture and transport of materials from the plant to the construction site [Fay *et al*., 2000]. As per Thormark [Thormark, 2002], the embodied energy can contribute towards nearly 45% of a building's total energy needs in a life span of 50 years. Construction materials like fired masonry clay bricks are manufactured through energy intensive processes and have relatively high embodied energy. Based on the data from National Institute for Standards and Technology's (NIST) Building for Environmental and Economic Sustainability (BEES) Database 4.0, the annual embodied energy of clay bricks manufacture in United States is 86000000 Million British Thermal Units (BTU). The same resource estimates that roughly 6000 BTUs of fossil fuels are spent in average in making a fired clay brick [NIST , BEES 4.0].

2.3.1.3 Environmental pollution

Coal based brick factories generate significant level of brick kiln bottom ash (BKBA) that contaminate soil and water environments of nearby areas through leaching of toxic metals [Mondal *et al*., 2017]. Firing of conventional bricks in kilns involves very high temperature around 1400 degree Celsius and consumes large quantities of fuel resulting in the release of polluting gases such as carbon monoxide, carbon dioxide and ammonia [Heindl & Pendergast,1929].

2.3.2 Incorporation of Waste Materials for Manufacture of Sustainable Hybrid Bricks

In light of the fact that conventional bricks do not adhere to the principles of sustainable construction, there is an urgent need for innovative solutions that can develop sustainable and less expensive alternatives with comparable mechanical, physical as well as thermal performance. Utilization of waste materials in brick manufacture is a multi-pronged approach that enables green construction and waste recycling simultaneously.

During the last few decades, research has been done to incorporate various type of waste materials into the production of bricks including sludge [Lutfi, Yamin, Rahman, & Ginsel Popang, 2018], [Lamrani, Laaroussi, Khabbazi, Khalfaoui, Garoum, & Feiz, 2017], [Taha & Nounu , 2009], [Zhang & Ingham, 2010], pulp and paper mill residue [Goel & Kalamdhad 2017], olive industry waste, biomass ash [Iwuagwu & Ugwuanyi 2014], boron waste, spent coffee grounds, and cigarette butts. Researchers have tried to also use waste materials such as blast furnace slag, iron tailings, and sludge waste.

The feasibility of utilizing incinerated sewage sludge as an admixture in brick manufacturing [Lin Deng-Fong & Weng Chih-Huang, 2001]. The results from the tests conducted on the fabricated bricks indicated that up to 40% of sludge ash incorporation yielded compressive strengths comparable to that of control bricks. However, 10% was found to be the optimal ratio of incorporation with a compressive strength of 150kg/cm^2. Further, addition of sludge ash decreased the firing shrinkage by 8% and weight loss by 15%.

The prospects of using paper mill sludge (PMS) was also explored in lightweight brick manufacture. Drained PMS and soil samples were dried and milled before they were incorporated in the brick mixture [Goel & Kalamdhad, 2017]. The fabricated bricks were tested for their mechanical properties and results showed considerable reduction in weight by 24% compared to conventional bricks. It was noticed that bricks made with PMS incorporation up to 10% by weight conformed to the required specifications.

Another investigation looked into the viability of using waste marble powder (WMP) in making bricks [Munir, Abbas, Nehdi, Kazmi, & Khitab, 2018]. Bricks fabricated with WMP content ranging from 0 to 25% was tested for mechanical and durability characteristics. The results from the tests specified that the bricks containing up to 10% of WMP satisfied the minimum compressive strength and flexural strength with only 8% and 3.3% reduction respectively from the

control specimens with regards to these properties.Besides, usage of up to 5% of WMP resulted in bricks with no efflorescence and sulphate attack compared to the control bricks.

The feasibility of using sludge from sand beneficiation treatment plant in brick manufacture was explored by [G. Reddy and Babu, 2013]. Results of experiments on the fabricated bricks showed that up to 40% sludge by weight of clay could be used to make bricks without loss in strength whereas other brick characteristics were considered satisfactory for conventional purposes.

Boro-gypsum generated by the boric acid production industry for making bricks and improving their properties was analysed. In the case of bricks fabricated with 0-15% of boro-gypsum were subjected to physical and mechanical tests including compressive strength, water absorption and resistance to freeze thaw damage [Emrullahoglu, 2014]. The results indicated that the bricks made with up to 10% of boro-gypsum incorporation had a compressive strength of 40 MPa and water absorption of 8%. Besides, addition of boro-gypsum reduced the brick density and increased freeze/thaw resistance.

The utilization of waste glass sludge (WGS) in the fabrication of burnt clay bricks. Up to 25% by clay weight of WGS procured from industrial scale glass polishing and cutting facilities was added as partial clay replacement [Kazmi *et al*, 2017]. It was observed that the compressive strength of the bricks was increased 37% by the additions of WGS. Further, WGS incorporated bricks were lighter in weight and showed reduced water absorption. Furthermore, there are no signs of efflorescence, sulphate attack and freeze-thaw damage was better after WGS was included as a raw material.

Using sugar cane bagasse ash (SCBA) and silica fume (SF) wastes as a raw material in making bricks were also studied [Jiménez-Quero *et al*, 2017]. Bricks incorporated with SCBA and SF were tested for physical and mechanical characteristics and the results showed that bricks made with incorporation of up to 40% by clay weight of SF had no change in physical and mechanical properties with those of control bricks without clay replacement while the addition of SCBA significantly reduced the physical and mechanical characteristics of the fabricated bricks especially with a reduction in compressive strength by 100kg/cm^2.

The viability of incorporating several waste materials including demolished bricks, fly ash and rice husk ash into environmentally-friendly and cheaper fired clay bricks is motivating the

present research [Hossain *et al*., 2018]. The study also analyzed the effect of glass cullet addition in the characteristics of the resultant bricks. The results from mechanical, physical and thermal tests on the manufactured bricks indicated that that those with up to 80% of waste incorporation still complied with the technical specifications for masonry units. Note that the disposal of tons and tons of glass in the form of glass containers in the landfills leads to the emission of green house gases [Vossberg, 2014], whereas recycling of these waste materials instead of disposing them in the landfills would help to save 27% of the energy and would achieve a 37% reduction in greenhouse gas emissions per year.

The applicability of a sea weed based biopolymer known as alginate as a constituent in unfired clay blocks was explored [Dove et al., (2016]. A number of alginate and soil samples were tested, and physical and mechanical tests were performed on the fabricated bricks [Hossain *et al*., 2018]. Also, these bricks are compared with control bricks in relation to flexural and compressive strength, microstructure, abrasive strength and hygroscopic behaviour. The results showed that the mechanical properties on the blocks was dependent on the choice of alginate source and constituents of the soil used. The bricks crafted with the alginate form *Laminaria Hyperboria* showed 52% increase in compressive strength compared to that of the control blocks.

A research study on the viability of using glass reinforced plastic dust (GRPd) waste in making bricks was also conducted recently [Mobili *et al*., 2018]. The clay was partially substituted by a maximum of 10% of GRPd and the fabricated bricks were tested for changes in compressive and flexural strengths, porosity, density and water absorption. The results revealed that GRPd incorporation reduced the compressive strength by 46% though there was an increase in total (connected) porosity and water absorption of 29%. An older laboratory and pilot plant study [Giugliano *et al*., 1985] had shown that tannery sludges could also be used in brick manufacture for up to 10% of the dry weight of bricks. They were made at a firing temperature of 950 °C; masonry units made with the incorporation of tannery sludge had higher porosity, and similar flexural strength and frost resistance to that of control brick. Another work was fabricating brick fabrication by mixing the raw materials, tannery sludge and clay together in different proportions illustrated that the mechanical and physical properties like water absorption, porosity, linear shrinkage, leaching and transverse rupture strength of the brick samples made with up to 30% replacement of clay with tannery sludge were similar to those characteristics specified for control bricks [Basegio *et al*., 2002]. The physical and mechanical properties conducted on the prepared

brick specimens indicated that bricks prepared with 40% and 50% of dried sludge and sludge ash respectively resulted in good workability and energy saving of 15–47% for 10-40% replacement of clay with sludge.

Dried sludge and sludge ash from the waste water treatment plant is a promising source material for the manufacture of masonry bricks. In a pioneering research study, [Tay, 1987] explored the feasibility of using waste water sludge in making eco-friendly bricks. While dewatered sludge from wastewater treatment plants creates problems of disposal, incineration might be an alternative solution for urban areas due to the limited land space for the landfill. Dried and oven fired sludge samples were ground and bricks samples were prepared with varying proportions of sludge and sludge ash. The results of the bricks made by the utilization of dried sludge and sludge ash showed that the maximum replacement ratios of dried sludge and sludge ash that could be mixed with clay for brick making are 40% and 50% respectively. The compressive strength of the bricks found to be 87.2 MPa for 0% sludge, decreasing to 37.9MPa for 40% clay replacement with dried sludge, and 69.4MPa for 50% replacement with sludge ash.

Another study envisioned to craft sustainable bricks from sewage sludge ash [Okuno,1997] made use of the fact that there are eight full scale sewage sludge incineration plants in Japan. The researchers fabricated masonry bricks from 100% sewage sludge ash by firing them at about 1000°C. The bricks made with 100% replacement of clay with sewage sludge ash are now widely accepted for public works such as flooring of plazas or pedestrian walk ways. The overall quality of the sewage sludge ash brick was not competitive enough initially because of the moss growth on the exposed surface of the brick owing to its high moisture content and efflorescence by Calcium Carbonate leaching. These problems were solved by increasing the firing temperature and application of chemical coating. Masonry brick properties like shrinkage, water absorption, compressive strength, flexure strength, leaching behaviour and energy consumption were tested and found similar to control bricks.

In Germany, several aspects of using ashes from sewage sludge incineration in the brick and tile industry have been examined [Wiebusch *et al*., 1997]. It was found that the use of precipitation agents containing heavy metals like iron during the event of dewatering of sludge, influence the quality of sludge ash as the effects of ash on the brick properties may vary based on the chemical composition of the sludge. This particular research replaced up to 40% of clay with sewage sludge ash and found that the water absorption, density and compressive strength similar

[19]

to the control bricks. However, greater than 40% replacement reduced the compressive strength by 30%.

In one of the studies that aimed on manufacture of geopolymer based bricks from abundantly available waste materials [Ferone *et al*., 2015] clay sediments from the water reservoir in Italy was used along with ground granulated blast furnace slag (GBFS), Sodium hydroxide (NaOH) and Sodium silicate (Na_2SiO_3). While up to 30% GBFS the researchers used a maximum percentage of NaOH in the order of 10%. The crafted hybrid bricks were studied by X-ray diffraction, differential thermogravimetry, Fourier transformed infrared (FTIR) spectroscopy and 27Al and 29Si Magic Angle Spinning Nuclear Magnetic Resonance (MAS-NMR) spectroscopy for characterization. The researchers found the characteristics of the hybrid bricks as ideal when clay sediments were heated at 750°C. Also, a good compressive strength with a range between 28 MPa to 38.1 MPa were obtained for bricks made with heat treated clay sediments.

A slightly different approach was taken towards the geopolymer bricks' manufacture [Arulrajah *et al*.,2016]. The objective of this research was to evaluate the strength development in bricks made by the industrial by-products, including Recycled Glass (RG) and Fly Ash (FA). This geopolymer bricks were made with fly ash (30%), Glass waste (<4.75 mm/70%) and a mixture of Na2SiO3 and NaOH at 90/10, 70/ 30 as well as 50/50 combinations. The resultant bricks made were cured for 7 days at 50 °C in order to achieve maximum strength development. The authors discovered that 30% content of FA was sufficient for geo-polymerization to occur and the resulting bricks had good compressive strength. Moreover, all the source materials used were industrial by-products, which in turn enabled efficient waste management, through the production of these hybrid masonry units.

Use of Biosolids in the manufacturing of bricks was another milestone in the history of masonry industry. Biosolids are the by-product from the wastewater treatment process or the less watery component derived from wastewater sludge. The use of biosolids in fired-clay bricks was also studied [Ukwatta, 2015]. For this purpose, biosolids had been collected from the Eastern Treatment Plant (ETP) in Melbourne, Australia for manufacturing masonry units. The suitability of biosolids as a partial replacement material for the clay in fired-clay bricks was assessed during the research and bricks were made with up to 25% clay replacement by biosolids. The resulting bricks were tested for the mechanical properties including the compressive strength and shrinkage

as well as density, Initial Rate of Absorption (IRA), thermal conductivity and water absorption. Furthermore, scanning electron microscopy (SEM) was performed to elucidate the microstructure of the fired-clay bricks. The results showed that the compressive strength of clay–biosolids bricks were 25.9MPa for the bricks with the 25% biosolids which is greater than the standard compressive strength for first class bricks. The biosolid fired-bricks also had higher apparent porosity and thus lower density. However, the compressive strength of the control fired-clay bricks was 36.1 MPa, thus a 30% reduction of strength was effected by the use of the biosolids. To better understand the role of the minerals and particle sizes on the performance of the biosolid bricks, the chemical composition of the clay and biosolids were compared in Table 1a and 1b below. Note the substantive difference in the Aluminum Hydroxide Silicate content which is an effective binder at the firing temperatures of the brick, in favor of the lower strength content of Calcium; also note is the high content of Carbon in the organic biosolid material, which during firing will cause increased porosity in the resulting product and therefore some degree of strength reduction, approximately 1.4% (strength in semi-brittle materials such as concrete and masonry is inversely related to porosity).

The chemical and mineral composition of clay and biosolids and the particle size analysis was done for the brick manufacturing [Moreno et al., 2016].The results from the analysis is given in Table 2-1. Table 2-1 (a) shows the chemical composition of clay and biosolids, Table 2-1 (b) shows the mineral composition of clay and biosolids and Table 2-1 (c) shows the finer particle content in clay and Biosolids.

Table 2-1(a): The chemical composition of clay and biosolids (Moreno et al., 2016)

Sample	Element						
	O	Al	Si	Fe	K	Ca	C
Clay (%)	49.23	8.75	38.72	6.93	-	-	-
Biosolid (%)	31.4	4.35	8.65	6.33	0.92	2.81	46.02

(a)

Table 2-1 (b) The mineral composition of clay and biosolids (Moreno et al., 2016)

Mineral	Clay (%)	Biosolid (%)
Silicon Oxide (Quartz)	74	71.3
Aluminium Hydroxide Silicate (Kaolinite 2)	13	-
Aluminium Silicate Hydroxide (Kaolinite 1)	11	9.9
Iron Oxide Hydroxide (Goethite)	2	-
Calcium Carbonate (Calcite)		6.9
Aluminum Hydroxide (Gibbsite)		11.9

(b)

Table 2-1 (c) The finer particle content in clay and Biosolids (Moreno et al., 2016)

Content of fines in Biosolid			Content of fines in Biosolid		
Clay (%)	Silt (%)	Sand (%)	Clay (%)	Silt (%)	Sand (%)
15.99	18.94	65.06	40	32	28

Chapter 3. Preliminary Phase of the Research

This study investigates the level of improvement that is effected in structural and mechanical properties of bricks after partial replacement of principal source material, quarried shale, with waste products. For the needs of the study, Quarried Shale was procured from 'Brampton Bricks' during the facility tour in May 2018 which in turn was an occasion to learn extensively regarding the industry standards and procedures of manufacturing and testing of masonry bricks. The primary ingredients in the quarried shale are sand, clay and silt which is a combination of calcite and quartz. In this regard, hybrid bricks with varying shale replacement rates are fabricated using several waste materials including HBS-polymers which are non-pathogenic products of novel environmental processes developed in the Environmental Laboratories at Lassonde, Incinerated Sewage Sludge Ash (ISSA) provided by the Municipal wastewater treatment facilities, Poraver® expanded glass powder, Recycled Crushed Glass (RCG), Granulated blast furnace slag (GBFS), fly-ash etc. Additionally, reference brick specimens termed hereon as Control Bricks (CB) are produced without shale replacement as benchmarks of all the other trials. In the initial phase of the experimental work, which is the subject of the present chapter, all experimental units including the reference bricks were produced in few numbers for each material combination. Then the preliminary analysis was done through a cycle of mechanical and physical tests in order to help identify those cases that warranted further exploration in the main phase of the study.

3.1 Methods and Standards of the Experimental Program

3.1.1 Geotechnical Analysis

As first step toward the research, the shale sample was subjected to exhaustive geotechnical analyses prior to the commencement of brick production to characterize the constituent components and to investigate the ambient casting mix conditions such as the allowed level of moisture content required for the fabrication of control brick.

3.1.1.1 Gradation

To determine the particle size distribution of the shale sample, gradation has been done. Since the specimen contains a wide range of particle sizes, gradation has been done using two methods. The particle size distribution of coarser particles with size greater than 75μm was done using ASTM D6913M - 17 Standard test methods for particle-size distribution (gradation) of soils through sieve

analysis. For the finer particles with size lower than 75µm, the ASTM D7928 - 17, Standard test method for particle-size distribution (gradation) of fine-grained soils using the sedimentation (hydrometer) analysis has been used.

3.1.1.1.1 Gradation by sieve analysis

The sieve shaker from Rotary Lab Sifter and the US standard sieve series were used in the sieve analysis, as per ASTM D6913M – 17. The equipment used in this part of the study are depicted in Figures 3-1, to 3-4.

Figure 3- 1 : Sieve shaker from Rotary Lab Sifter

Figure 3-2: The US standard sieve series.
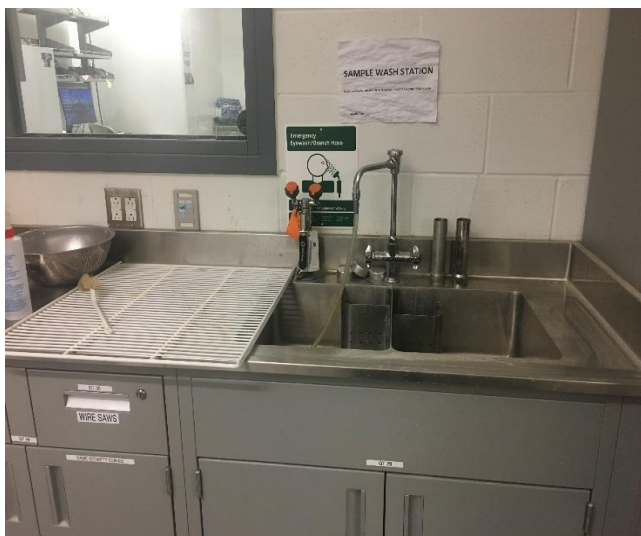
Figure 3-3: Washing Station

Figure 3-4: Wash Sieve

The procedure used was as follows: first, 326gg of shale was taken and prior to sieving, the material was washed with 75μm wash sieve to remove finer particles in the washing sink with a spray nozzle. A washing station with sink having a spray nozzle attached to a flexible line to facilitate the washing and material transferring processes without spillage was used. In addition, the rate of water flow through the spray nozzle was easily controlled. After removing the finer particles, the weight of the sample recorded was 156.1g. Then, the sample was oven dried for 24 hours. The weight of the sample was recorded again after the oven drying process. The dried sample was then put into the top sieve of the pre-arranged set of sieves which was in the order of 4.75 mm, 2.36 mm, 2mm, 1.18mm, 600 μm, 425 μm, 300 μm, 150 μm, 75 μm pan and kept in a mechanical sieve shaker for 10 minutes. Further the mass of particles retained on each sieve was determined. The results were tabulated as the number of sieve sizes versus percent passing. Later, the tabulated results in Table 3-1 were plotted graphically to obtain the gradation curve, which is a plot of the percent passing versus the log of the particle size in mm and is shown in Figure 3-5.

Table-3-1 Gradation by Sieve Analysis

Sieve Size (mm)	Retained Weight (g)	Retained Percentage (%)	Cumulative Weight (%)	Percentage Finer
4.75	0.0	0.0	0.0	100.0
2.36	0.4	0.3	0.3	99.7
2	2.4	1.5	1.8	98.2
1.18	36.2	23.2	25.0	75.0
0.6	52.9	33.9	58.9	41.1
0.424	18.0	11.5	70.4	29.6
0.3	16.5	10.6	81.0	19.0
0.15	19.3	12.4	93.3	6.7
0.075	10.1	6.5	99.8	0.2
0.01	0.2	0.1	99.9	0.1
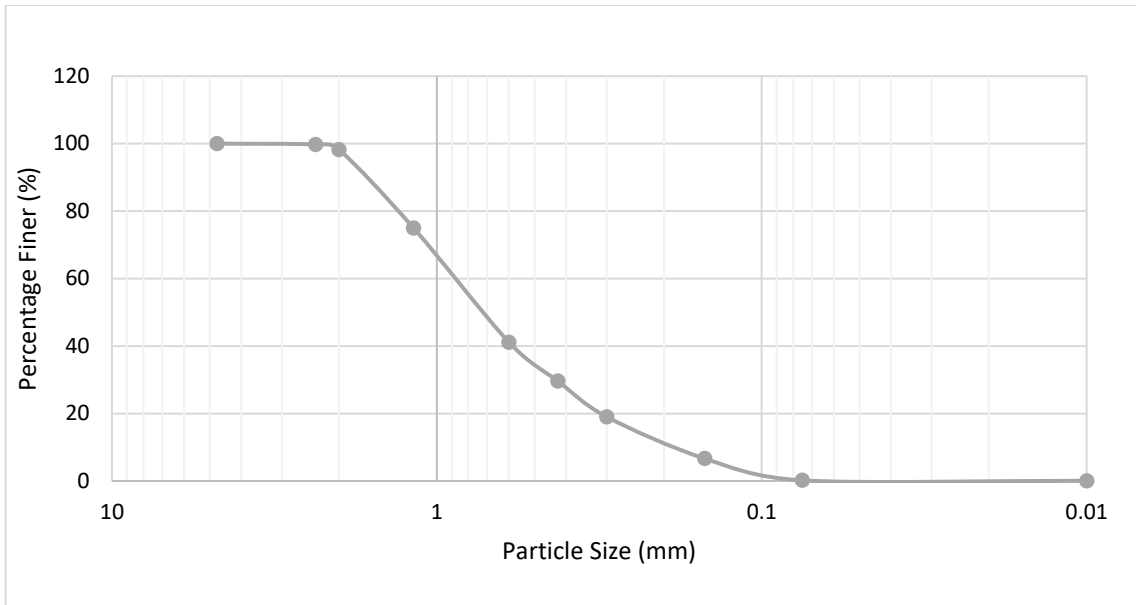
Figure 3-5: Particle Size distribution by sieve analysis

3.1.1.1.2 Gradation by sedimentation (hydrometer) analysis

In order to determine the size of the finer particles in the shale, hydrometric analysis was done as per ASTM D7928 – 17. For this test, Sample 1 has been made by taking 50gms of shale that in turn has been sieved through 2mm sieve in a 250ml beaker and mixed uniformly with 125ml of hydrometric solution which is sodium hexametaphosphate (dispersant). The mixture was covered properly to prevent evaporation and was allowed to stand in room temperature for 24 hours.

Subsequently, Sample 2 was prepared by taking 125 ml of hydrometric liquid in a separate 1000 mL glass cylinder, mixing well with water and filling to the line without soil. After the mixing, a hydrometer was inserted, and the reading was taken. This reading was recorded as the composite correction Hc, which was used to compute the calculations.

After 24 hours, the entire Sample 1 was then poured into the mechanical mixer using the spray bottle to extract the remaining soil particles. Then, water was added to the mixing cup until it was 2/3 full. The sample was mixed for about 2 minutes. The mixed Sample 1 was carefully poured into another 1000 mL glass cylinder and filled with distilled water up to the mark, closed with a stopper and mixed by hand for 1 min by inverting the cylinder about once per second. The cylinder was then placed in a fixed location without any disturbances. The hydrometer was then placed carefully within the cylinder containing Sample 1 and immediately the stop-watch was started. Hydrometer and thermometer readings was taken at 0 s, 30 s, 1 min, 2 min, 5 min, 15 min, 30 min,

[26]

1 hr, 2 hrs 4 hrs and 24 hrs. The correction hydrometer and thermometer readings were 7mm and 24 °C respectively and was constant throughout the process.

After taking the readings, the particle diameter was calculated by multiplying the temperature constant, K with $\sqrt{L/t}$, where, L is the effective depth of the hydrometer and t is the elapsed time in minutes. The 95% of the particles were of size less than 49.7 microns, 85.1% of the particles were of size less than 6.76 microns, 63.1% of the particles were of size less than 1.36 microns.

3.1.1.1.3 Gradation by particle size analyze

Particle size analysis or particle size distribution of the quarried shale, the primary raw material was also performed using a particle size analyser. Three samples were analyzed by this method. A detailed and more accurate particle size distribution was observed through this analysis as shown in Figure 3-6.
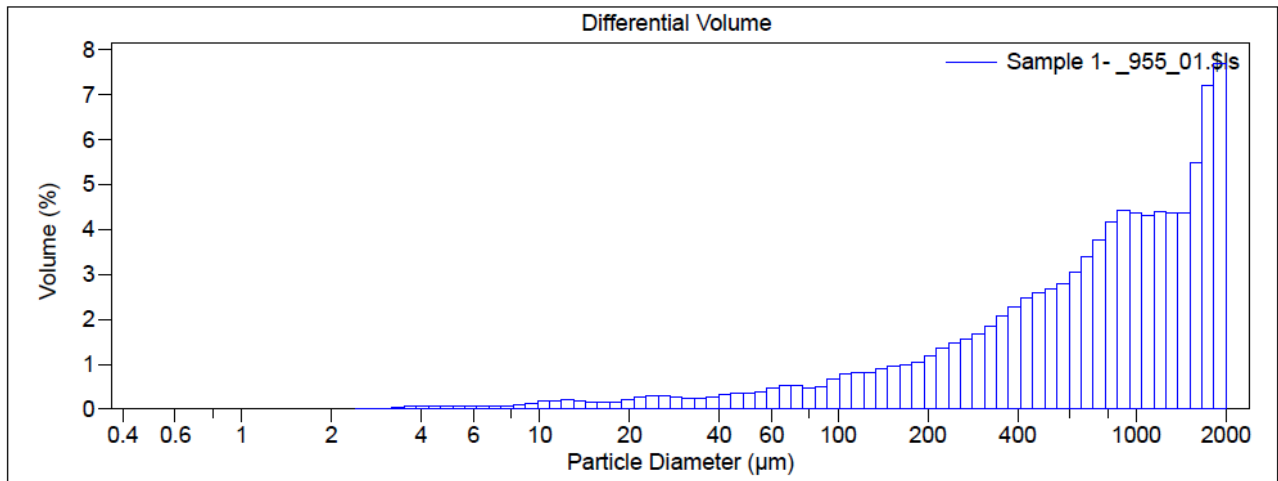
(a)
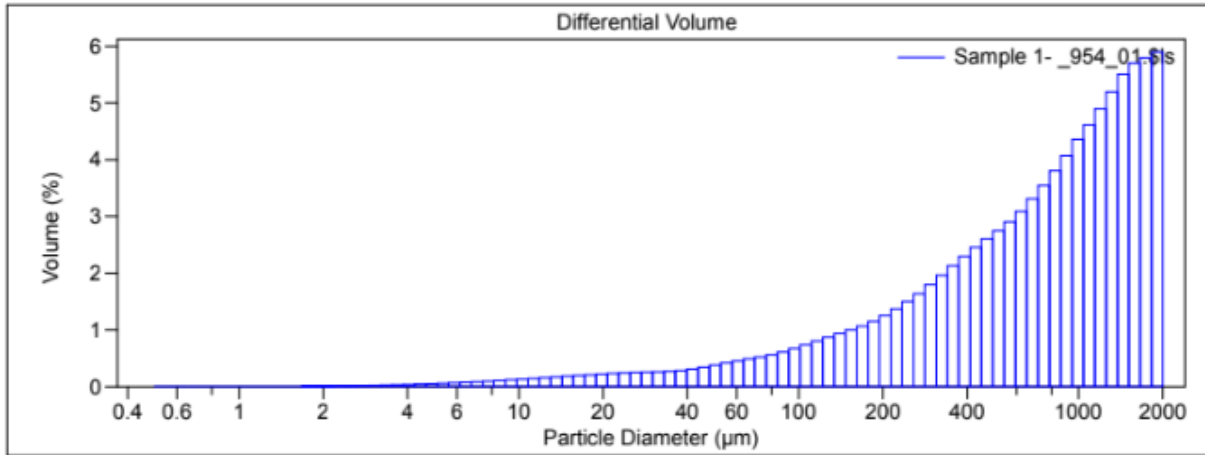
(b)
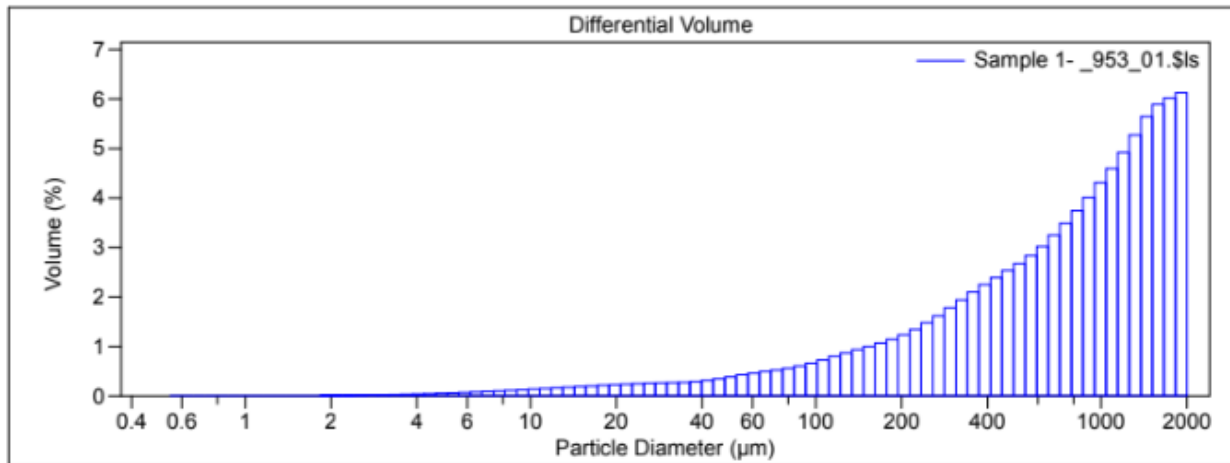
(c)

Figure 3-6: Gradation by Particle Size Analyzer, (a) Sample 1, (b) Sample 2, (c) Sample 3

From the particle size analysis, it was observed that, 10% of the particles were of size less than 118.3 μm, 25% of the particles were of size less than 354.5 μm, 50% of the particles were of size less than 801.9 μm, 75% of the particles were of size less than 1371 μm, 90% of the particles were of size less than 1770 μm and 99.8% of the particles were of size less than 2000μm.

3.1.1.2 Atterberg limits

The 'Atterberg limit' was calculated as per the American Society for Testing and Materials ASTM_D4318 Standard Test Methods for Liquid Limit, Plastic Limit, and Plasticity Index of Soils for determining the compatibility of the shale for brick fabrication. Specifically, the 'Plastic

limit', 'liquid limit' and 'plasticity index' as well as 'in-situ moisture content' of shale were calculated.

3.1.1.2.1 Liquid Limit (LL)

Liquid limit (LL) of shale is the water content at which the shale changes from plastic to the liquid form. At this point, the shale possesses only a very low shear strength. The LL of the shale was analyzed by the Fall cone penetrometer method. In this method, the shale sample was placed in a 55 mm diameter and 40 mm deep brass container. A stainless-steel cone with shaft weighing 80 g having a 30° angle is positioned, so that its tip just touches the sample in the container. The cone was then released for 5 seconds so that it gets to penetrate the shale sample. The liquid limit is defined as the water content of the soil which allows the cone to penetrate exactly 20 mm during that period of time. Since it is difficult to obtain a test with exactly 20 mm penetration, the procedure was performed five times for a range of water content and the penetration depth corresponding to each moisture content was noted from the digital display in the apparatus. The relationship between the depth of cone penetration and moisture content was plotted in semi-log paper.
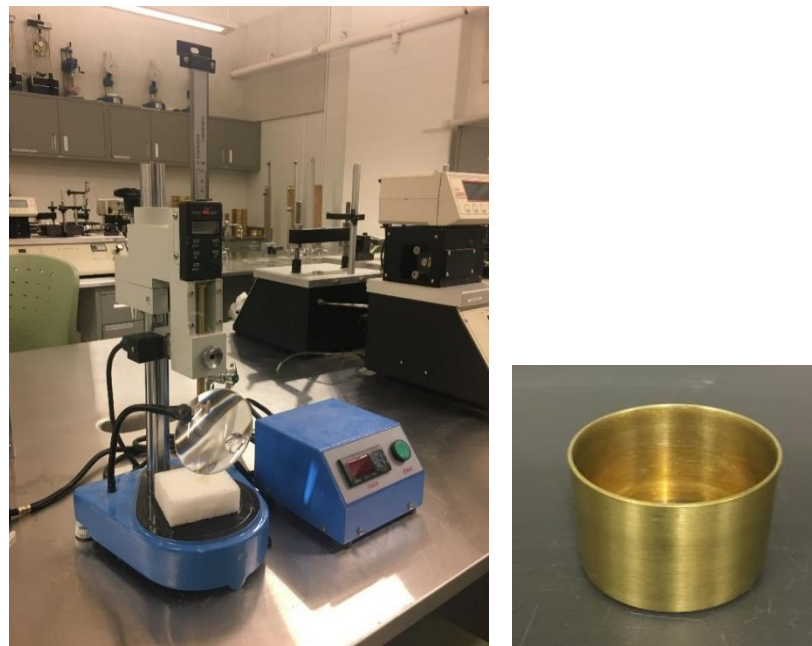
(a)

Figure 3-7(a) :Fall cone penetrometer and container

Moisture content corresponding to a cone penetration of 20 mm was taken as the liquid limit of the sample. The fall cone penetrometer used is shown in Figure 3-7a. The Liquid limit of the shale sample from six trials was obtained as 27.50.

3.1.1.2.2 Plastic Limit (PL)

Plastic limit (PL) is the water content in shale, at which it no longer behaves like a plastic material. The PL of the shale was examined by the Rolling Thread Method wherein PL is the water content at which the shale starts to crumble when rolled in threads of 3 mm diameter. At this water content, the soil losses its plasticity. Figure 3-8 shows the plate used for plastic limit test.
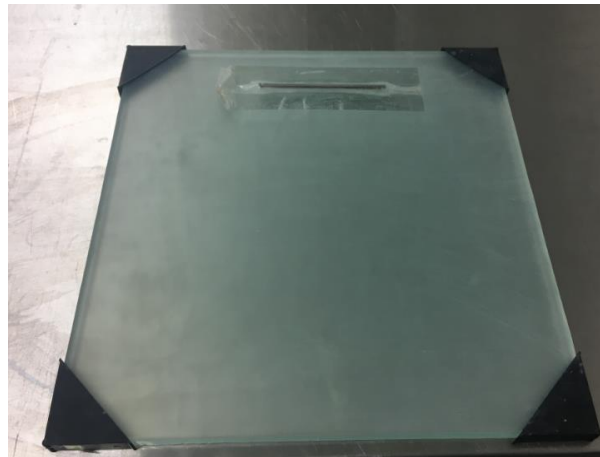
Figure 3-8: Plastic Limit test Apparatus

The Plastic Limit was calculated as,

$$P.L = \frac{M2 - M3}{M3 - M1} \tag{3.1}$$

Where, M1 = Mass of the container (g),

M2 = Mass of the threaded sample and container (g),

M3 = Mass of the oven dried threaded sample (M2) and container (g)

The Plastic limit for the shale from six trials was found to be 15.64 which shows that the shale has more clayey particles.

[30]

3.1.1.2.3 Plasticity Index (PI)

The Plasticity Index, PI of the soil/shale is the difference between the liquid limit and plastic limit. For the shale sample it was computed as 11.86.

A higher value of plasticity index, exceeding 17, shows the presence of clay content in the sample. The PI value between 7 and 17 highlights medium plasticity and has comparatively lesser clay content. On the other hand, PI value less than 7 corresponds to slightly plastic sample with significantly less clayey content and if the PI value is equal to zero, which means the liquid limit is less than or equal to the plastic limit, then, there wouldn't be any clay content in the sample. In other words, the sample will be non-plastic [Sowers, 1979].

The shale sample tested for the current study was medium plastic and suitable for brick fabrication. The results from this analysis are included in Figure 3-9(b). By oven drying method the in-situ moisture content of the shale sample was found to be between 6 and 7%/wt.

(a)   *(b)*
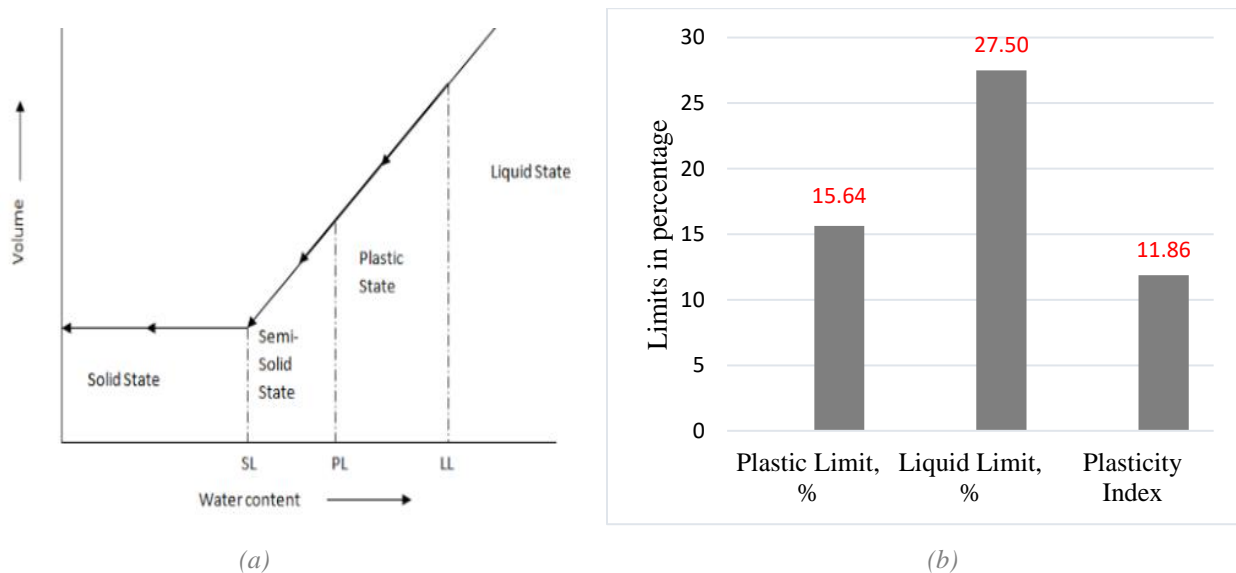
Figure 3-9(a) :Atterberg Limits Graph (civilseek.com); (b): Atterberg Limits for the shale sample

3.1.1.3 Proctor compaction test

The 'proctor compaction test' was performed as per ASTM D698 - 12e2, 'Standard Test Methods for Laboratory Compaction Characteristics of Soil Using Standard Effort' to compute the

'optimum dry density' of shale in order to figure out the required quantity of casting mix for the specific mold in use and for estimating the allowed moisture content for making high quality bricks. The standard proctor compaction apparatus is shown in Figure 3-10.

Figure 3-10 :Standard proctor compaction test apparatus

The test determined the optimum dry density as 1.97g/cm^3 and the optimum moisture content as 14%. In order to calculate the mass of the material to be used the mold intended for the fabrication of bricks was considered;

The optimum dry density, $\boldsymbol{\rho}_{dry}$ = mass/ volume ;   (3.2)

Therefore,

Mass=volume x optimum dry density

$$= 14.0*5.8*2.6*1.97$$

$$=416 \text{ g of the mixture per mold.}$$

Since the shale has an in-situ moisture content of 6 - 7%, the amount of water that was necessary to be added was 8%.

3.1.2 Fabrication of Bricks

As the lab settings are completely different compared to those of the commercial brick manufacturing facilities like 'Brampton Bricks', a custom protocol for making bricks was

developed by improving the same sequentially during the trial runs, often making innovative adaptations. In such a way a general procedure was obtained. It involves the design and fabrication of acrylic molds, weighing and addition of solids as well as liquid constituents of the casting mix in multiple sessions followed by thorough compaction and homogenization. The bricks within the molds could dry in air as well as in the oven before they would be fired with gradual increase in the temperature. After the bricks were removed from the kiln, they were examined for cracks and subjected to physical and mechanical tests including compressive strength, flexural strength, splitting tensile strength, water absorption tests, efflorescence test, Freeze-thaw resistance, ultrasonic pulse velocity and resonance frequency according to prevalent standards. The development of cracks which had been a persistent issue was resolved by increasing the drying as well as firing temperature gradually and allowing additional drying within the mold at room temperature.

The hybrid bricks are compared to control bricks made without any shale replacement in terms of compressive strength, flexure strength, split tensile strength, ultrasonic pulse velocity, cold as well as hot water absorption, saturation coefficient, efflorescence, dimensional change, freeze thaw damage and resonant transverse frequency. Even though the fabrication procedure is similar in general for all the varieties of the bricks, each type of bricks required minor modifications in the casting procedure owing to the consistency of the raw material.

3.1.2.1 Design of the mold

The mold for brick fabrication was custom designed and made by laser cutting at The Sand Box Prototyping Lab at York University that has a laser cutting facility. The drawings pertaining to the custom design are given in Appendix A. As a trial, a single mold and a plunger was made initially. The material used for making the mold was Acrylic plastic. In order to perform uniform compaction of the casting mixture, a plunger was also made as shown in Figure 3-11(a) and 3-11(b).
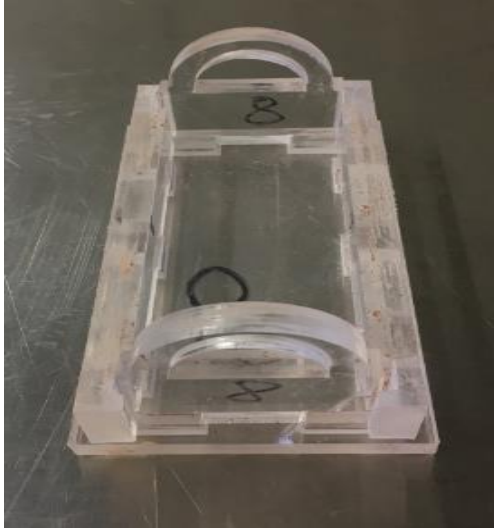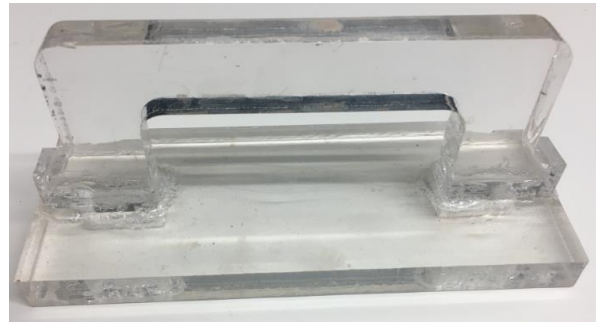
Figure 3-11(a) :Acrylic Brick Mold (b):Acrylic Plunger

3.1.2.2 Control Bricks (CB)

For the fabrication of the control bricks (CB), the shale was mixed for 2 minutes in a mixer to eliminate any clusters. Subsequently, the water was added gradually in aliquots of one quarter of total amount and mixing was continued for 3 minutes. Later on, the bricks were molded and kept at room temperature for 2 hours. The bricks were then demolded and placed in the oven for drying with a gradual increase in temperature from 30°C to 110°C for 24 hours. The temperature increment was 20°C/hour. Afterwards, the bricks were kept in the furnace for firing with a gradual increase in temperature from 110°C to 1100°C for 24 hours with a temperature increment of 200°C per hour.

Figure 3-12:Quarried Shale

Figure 3-13:Water

Figure 3-14 :Mixing

Figure 3-15:Molding
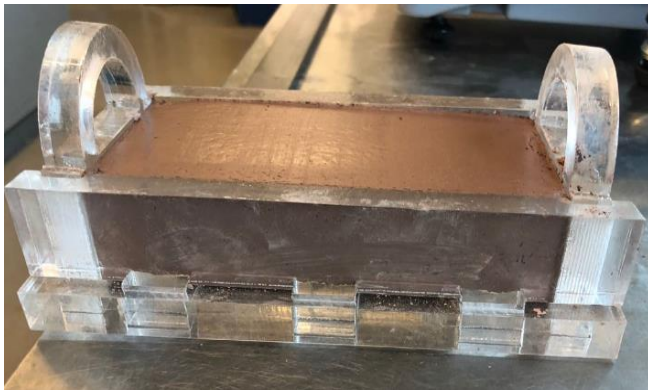
Figure 3-16: Air Drying

Figure 3-17: Firing in the Furnace

Figure 3-18:Control Brick

3.1.2.2.1 Chemistry and thermodynamics of control brick firing

From the mineral analysis, the main mineral constituents of shale (Appendix II) are mainly siliceous and micaceous matters like $Al_2 O_3 .2SiO_2 .2H_2O$, $K_2O. Al_2O_3 .6SiO_2$, Fe_2O_3, CaO, MgO, Na_2O and K_2O. During the firing process, at a temperature ranging from 450-650°C, the combined

matters will be decomposed into its constituent minerals like SiO_2, Al_2O_3 etc. The firing of brick comprises three main stages: The burning out of carbonaceous matter and combustible sulfur present in the shale, the breakdown of carbonates present in the clay to give off carbon dioxide during $400\text{-}900\,^{o}C$, and finally the release of insitu and the added water during the mixing process from the brick until $1100\,^{o}C$ [Akinshipe & Kornelius 2017].

3.1.2.3 High Bio-Polymer Sludge Bricks

As a part of the development of sustainable masonry bricks, a solution to the environmental challenge is explored by the use of processed Liquid High-Biopolymer Sludge (LHBS) as a source material in brick manufacturing.

The main goal was to develop innovative technologies and methods for incorporating Poly Hydroxy Alkanoate (PHA) polymer that is generated as a waste from the modern biological wastewater treatment facilities in the form of high biopolymer sludge (HBS), in the production of building products with the required strength, stability, and physical properties. It is envisioned that this hybrid construction material will enable low cost housing and general-purpose construction, while moderating the amounts of firing energy and CO_2 emissions.

The LHBS offers partial replacement for the shale content and was expected to improve the final properties of the brick as well. The concept presents a great opportunity for the masonry industry in reducing impact to the environment resulting from clay-quarries while having a societal impact as it facilitates an opportunity for disposal of the massive waste product in an industry that may support low cost environmentally friendly housing (brick masonry) for the exploding population needs. Additionally, this offers a new application for the LHBS and creates a high gain opportunity for the wastewater industry. The important steps required in the process of implementation of the concept, through preconditioning, mixing, and enhancing the shale-sludge mix so as to obtain desirable strength and physical properties and in eliminating the organic content was also developed during the preliminary phase of the research.

3.1.2.4 High Bio-Polymer Sludge Bricks Type 1 (LHBS-1)

The first trial of hybrid bricks development was performed with the partial replacement of shale with liquid high biopolymer sludge bricks type 1 (LHBS-1). The type identifiers as used here are meant to distinguish the percentage of solid Biopolymer content in the LHBS used. These hybrid

bricks were made exactly like the control bricks with the exception that the original constituents of the casting mix were partially replaced with the liquid high biopolymer sludge type 1 (LHBS-1). Partial substitution with biopolymer sludge involved the computation of the liquid volume equivalent to the chosen percentage of biopolymer dry weight as well as making the required modifications in the volume of water to be added by taking account of the liquid content of biopolymer sludge before the constituents are added to the mix. In this regard, the LHBS type 1 has 36g of solid biopolymer content per litre of LHBS.

3.1.2.4.1 LHBS-1-0.24

Liquid High Biopolymer sludge type 1 (LHBS-1-0.24) refers to the hybrid brick category made with partial replacement of shale with 0.24% by weight. The lower percentage of the shale replacement was considered on account of s the fact the LHBS was 'waterier' and had only a very little percent-36g of solid biopolymer/L of LHBS-1.
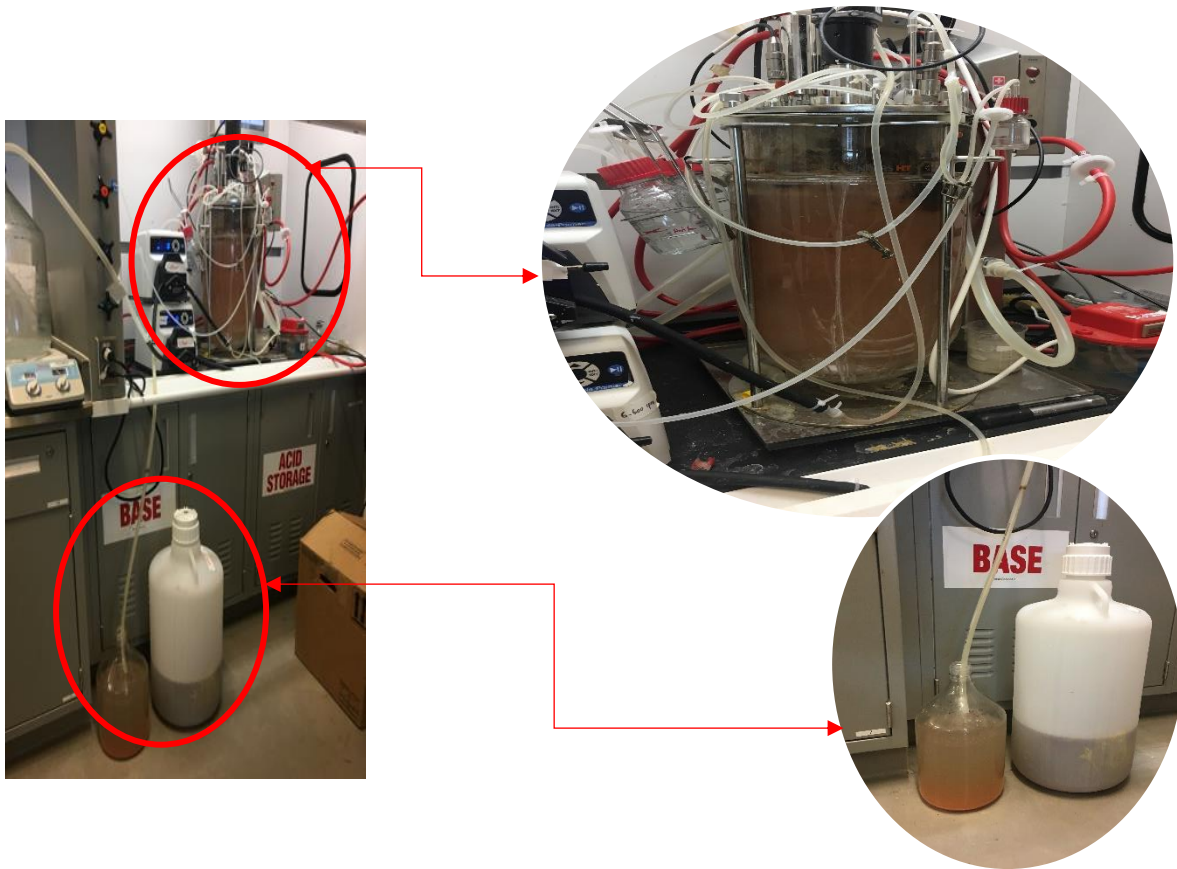
Figure 3-19(a) :High Bio-polymer Sludge extraction process from sewage waste water sludge at the Enviromental Engieering Lab, York University

Figure 3-19 (b): Liquid High Biopolymer Sludge Type 1.   Figure 3-20 :LHBS-1-0.24 Bricks

3.1.2.4.2 LHBS-1-0.40

Liquid High Biopolymer sludge type 1 (LHBS-1-0.40) was used for hybrid bricks having partial replacement of shale with 0.4% by weight. Here as well, the lower percentage of the shale replacement is due to the 'waterier' LHBS-1.

Figure 3-21 :Liquid High Biopolymer Sludge Type 1-0.4 Brick(LHBS-1-0.4)

3.1.2.4.3 Mix composition for Liquid High Biopolymer Sludge Type 1 Bricks

The amount of materials used for the fabrication of two Liquid High Biopolymer Sludge Type-1 Brick and the percentage of shale replaced by weight are given in Table 3-2.

[38]

Table 3-2 Mix composition for Liquid High Biopolymer Sludge Type-1 Brick

LHBS-1 Type	Shale(g)	LHBS-1(ml)	Water(ml)	Percentage replacement of shale by weight (%)
LHBS-1-0.24	894.8	60	14.16	0.24
LHBS-1-0.4	896.4	-24.4	100	0.40

3.1.2.5 High Bio-Polymer Sludge Bricks Type 2 (LHBS-2)

The second trial of hybrid bricks development was with the partial replacement of shale with liquid high biopolymer sludge bricks type 2 (LHBS-2). These hybrid bricks were made exactly like the LHBS-1 with the exception that the percentage of solid Biopolymer present in the LHBS-2 was 64 g/L. While type I was made with 0.24% and 0.4% substitutions using the 36g/L HBS sample, 0.25%, 0.4%, 0.5% as well as 1% substitutions were attempted with the 64g/L HBS sample.
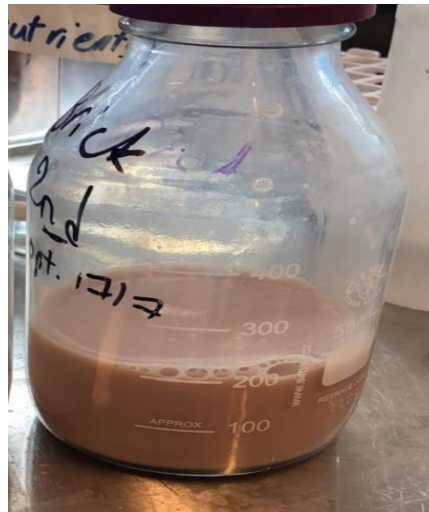
Figure 3-22 :Liquid High Biopolymer Sludge Type 2 (LHBS-2)

3.1.2.5.1 LHBS-2-0.25

Liquid High Biopolymer sludge type 2 (LHBS-2-0.25) is the hybrid brick made with partial replacement of shale with 0.25% by weight. Although the percentage of solid biopolymer in the LHBP-Type 2 is higher than that of LHBP-type 1, the percentage of the shale replacement is still lower due to the 'watery' nature of LHBS-2 as shown in Figure 3-22. Trial LHBS-2-0.25 bricks are shown in Figure 3-23.

Figure 3-23 :Liquid High Biopolymer Sludge Type 2-0.25 Brick (LHBS-2-0.25)

3.1.2.5.2 LHBS-2-0.40
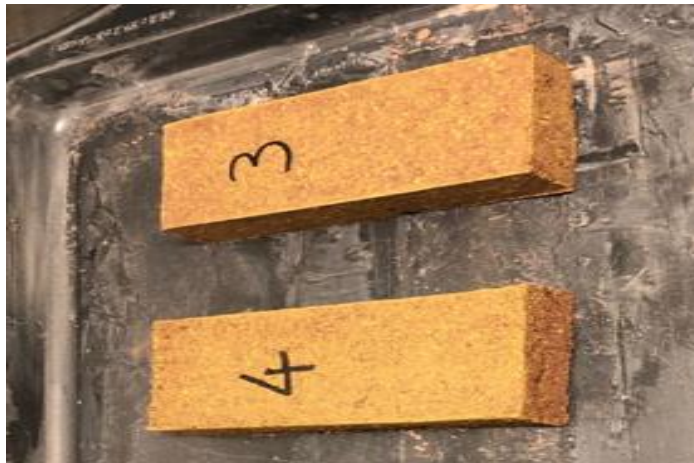
Figure 3-24 :Liquid High Biopolymer Sludge Type 2-0.40 Brick (LHBS-2-0.40)

Liquid High Biopolymer sludge type 2 (LHBS-2-0.40) refers to the hybrid brick made with partial replacement of shale with 0.25% by weight. Trial LHBS-2-0.4 bricks are shown in Figure 3-24.

3.1.2.5.3 LHBS-2-0.50

Similarly, to the preceding the Liquid High Biopolymer sludge type 2 (LHBS-2-0.50) refers to hybrid bricks made with partial replacement of shale with 0.50% by weight. Trial LHBS-2-0.5 bricks are shown in Figure 3-25.

Figure 3-25 :Liquid High Biop.loymer Sludge Type 2-0.50 Brick (LHBS-2-0.50)

3.1.2.5.4 LHBS-2-1

Figure 3-26: Liquid High Biopolymer Sludge Type 2-0.40 Brick (LHBS-2-1)

Liquid High Biopolymer sludge type 2 (LHBS-2-1) refers to hybrid bricks made with partial replacement of shale with 1.00% by weight. Trial LHBS-2-1 bricks are shown in Figure 3-26.

3.1.2.5.5 Mix composition for Liquid High Biopolymer Sludge Type 2 Bricks

The amount of materials used for the fabrication of two Liquid High Biopolymer Sludge Type-2 Brick and the percentage of shale replaced by weight are given in the Table 3-3.

Table 3-3 Mix composition for Liquid High Biopolymer Sludge Type-2 Brick

LHBS-1 Type	Shale(g)	LHBS-1(ml)	Water(ml)	Percentage replacement of shale by weight (%)
LHBS-2-0.25	897.8	34.38	39.83	0.25
LHBS-2-0.40	896.4	56.25	19.35	0.40
LHBS-2-0.50	895.5	70.31	6.19	0.50
LHBS-2-1.00	891.0	140.625	-59.00	1.00

3.1.2.6 Dried High Biopolymer Sludge Brick Type 3 (DHBS-3)

As an advanced version of Liquid High Biopolymer Sludge Type 1 and 2, High Bio-Polymer Sludge Brick Type 3 (DHBS-3) was developed with an intention of achieving a higher replacement of shale. The High Bio-Polymer Sludge Brick Type 3 (DHBS-3) used more concentrated LHBS generated using several dewatering techniques to remove the excess moisture in LHBS.

3.1.2.6.1 Dewatering techniques to remove the excess moisture.

During the initial stages of the research, the bricks made with the addition of LHBS were light-weight, yet strong even with a small percentage of LHBS. However, both the LHBS types were in a very dilute form and for this reason, various methods have been investigated to reduce the excess water content in the LHBS so as to incorporate higher concentrations of LHBS-polymer in the bricks.

3.1.2.6.1.1 Centrifugation

Centrifugation is a sedimentation technique used for the separation of solid particles from a solution depending on the various parameters including the size, shape, density, viscosity of the solution and the speed of the rotor in the equipment. The Liquid High Biopolymer Sludge with higher percentage of water and lower percentage of solid biopolymer is poured in the centrifugation bottles and these bottles were placed in the rotor inside the centrifugation equipment. The equipment was spun at a specific speed for less than 30 minutes. However, no

remarkable reduction in the percentage of moisture content was observed even after the centrifugation. The centrifuge and the centrifugation bottle used are shown in Figure 3-27 and 3-28 respectively.

Figure 3-27: Centrifugation Equipment from Beckman Coulter

Figure 3-28: Centrifugation Bottle

3.1.2.6.1.2 Use of Super Absorbent Polymer (SAP)

One of the several alternative methods considered for dewatering the LHBS was the use of Super Absorbent Polymer (SAP) as shown in the Figure 3-29. Superabsorbent polymers (SAP) are materials that have the ability to absorb and retain large volumes of water and aqueous solutions. This makes them ideal for use in water absorbing applications such as baby diapers. In this process, SAP was tied in a damp cloth and immersed in a container with LHBS. However, this approach was not successful as a reverse process was observed.

Figure 3-29: Super Absorbent Polymer

Hydrogen bonds are formed by the electrostatic interactions between molecules, i.e., when the molecule with hydrogen atom combines with electronegative atoms like O, N and F as shown

in Figure 3-30. The positive hydrogen atom in the SAP gets attracted by the oxygen in the water molecules leading to hydration. However, the electropositive and electronegative reaction isn't occurring, and SAP could not absorb water from the 'watery' High Bio-Polymer Sludge.
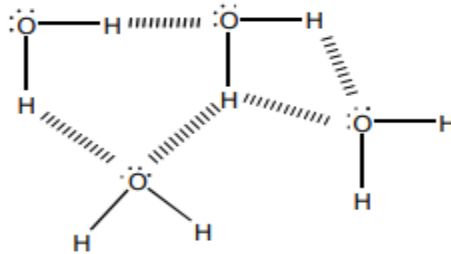
Figure 3-30: Electrostatic interactions between H and O molecules (Elliott, BASF)

3.1.2.6.1.3 Drying in heat control room

Another method used for the removal of the excess water in the LHBS was evaporation. This was achieved by drying of the LHBS polymer in a heat control room at 28°C, in the Environmental Engineering Laboratory, York University. By this method, the amount of dried solid biopolymer retrieved was 35-40 g from 25Lof LHBS. The LHBS used for the drying in the heat control room had less than 5g of solid biopolymer content in it. Among the various options used for dewatering the Liquid High Biopolymer Sludge, the drying of LHBS in a heat control room was the most successful method.

For the fabrication of the new and advanced hybrid brick - the Dried High Bio-Polymer Sludge Brick Type 3 (DHBS-3), the shale was partially replaced with the Dried High Bio-Polymer Sludge obtained from the drying method. The trial run of the process involved five percent by weight of shale replacement. The Dried High Bio-Polymer Sludge shown in Figure 3-31 was powdered using a mortar and pestle (Figure 3-32) and the size of the powdered DHBS-3 was less than 2mm.

Figure 3- 31: DHBS before grinding into powder　　　　*Figure 3-32: Mortar and Pestle used for powdering DHBS*

The shale was mixed for two minutes in a mixer to eliminate any clusters and then the powdered Bio-Polymer was added gradually. After three minutes of mixing, water was added gradually in aliquots and mixing was continued for three more minutes. Thereafter the bricks were molded and kept at room temperature for three hours. The bricks were demolded and placed in the oven for drying with a gradual increase in temperature from 30°C to 110°C for 24 hours (the temperature increment was 20°C/hour). Subsequently, the bricks were kept in the furnace for firing with a gradual increase in temperature from 110°C to 1100°C for 24 hours. The DHBS brick made is shown in Figure 3-33.

Figure 3-33:Dried HBS brick

3.1.2.7 Shale-Poraver®- Bricks (SPB)

The next attempt towards the development of sustainable hybrid bricks was done with the incorporation of Poraver® (Figure 3- 34)- expanded glass powder, which is a versatile lightweight aggregate having size that ranges from 0.1 to 0.3mm, made from post-consumer recycled glass.

0.1 – 0.3 mm

Figure 3-34 :Poraver®

The shale was mixed for two minutes in a mixer to eliminate any clusters and then the Poraver® was added gradually. After three minutes of mixing, water was added gradually in aliquots and mixing was continued for three more minutes. Thereafter, the bricks were molded and kept at room temperature for three hours. The bricks were demolded subsequently and placed in the oven for drying with a gradual increase in temperature from 30°C to 110°C for 24 hours (the temperature increment was 20°C/hour). Then the bricks were kept in the furnace for firing with a gradual increase in temperature from 110°C to 1100°C for 24 hours. The initial trial of waste incorporation was performed with 30% replacement of shale with Poraver®. However, when the Poraver® reacted with shale under high temperature, during high temperature firing at 1100 °C, the resulting hybrid bricks formed cracks (Figure 3-35). The replacement percentage of shale with Poraver® was 30 % by weight. The composition of the brick casting mix included 46% of shale by weight, 30% of Poraver® by weight and 24 % of water by weight.

Figure 3-35 :Poraver® Bricks with shale replacement of 30% by weight

3.1.2.8 Shale-Poraver®-Slag Bricks (SPSB)

Figure 3-36 :Granulated Blast Furnace Slag (GBFS)   *Figure 3-37 :Shale-Poraver®-Slag Bricks (SPSB)*

As a follow up to the Shale-Poraver Bricks (SPB), a binder in the form of Granulated Blast Furnace Slag (GBFS) was added to control the crack formation. With this, the next trial involved the fabrication of bricks with shale as the primary ingredient, along with Granulated Blast Furnace Slag (Figure 3-36) and Poraver® as incorporated waste materials.

The granulated blast furnace slag (GBFS) is obtained during the extraction process of any metal from its raw ore. After the desired quantity of metal has been separated, the by-product obtained is known as molten slag. This molten slag is rapidly chilled with water and finely powdered to obtain the granulated blast furnace slag (GBFS). This material is known for its highly reactive behavior and hydration properties when exposed to water.

[47]

For the fabrication of Shale-Poraver®-Slag Bricks (SPSB), the Poraver® was mixed with granulated blast furnace slag (GBFS) for 2 minutes. Thereafter, the shale was added gradually and mixed for two more minutes. Then, water was added gradually, and mixing was continued for three more minutes. Then the bricks were molded and kept at room temperature for three hours. Thereafter, the bricks were demolded and placed in the oven for drying with a gradual increase in temperature from 30°C to 110°C for 24 hours (the temperature increment was 20°C/hour). The bricks were kept in the furnace for firing with a gradual increase in temperature from 110°C to 800°C for 24 hours. Shale-Poraver®-Slag Bricks (SPSB) were made with mix composition of 52% shale by weight, 15% Poraver by weight, 15% slag by weight and 18% water by weight.

The Shale-Poraver®-Slag Bricks (SPSB) maintained their shape like SPB bricks as shown in Figure 3-37. Although the bricks were dried and fired gradually at a seemingly lower temperature of 800 °C, they still developed cracks because of the inadequate workability of GBFS with the Poraver.

3.1.2.9 Shale-Poraver®- Na_2SiO_3 Bricks (SPSSB)

Since crack development was a primary issue in the brick design with mineral waste incorporation, the subsequent trials used sodium silicate also known as water glass in order to encourage geo-polymerization of the alkaline materials [Nour et al., 2018]. As a solution for the cracks formed in the Shale-Poraver®- Bricks (SPB), Sodium silicate- Na_2SiO_3 (Figure 3-38) was added to the mix in order to control the cracks. Previous researchers have shown that sodium silicate has a crack sealant/healing property in concrete [Prabakar, et al, 2017]. The sodium silicate added was sodium meta silicate 38%, that contained 9% of sodium oxide and 29% silicon dioxide.

Figure 3-38: Sodium Silicate 38% (pottery supply house)

For the fabrication of Shale-Poraver®- Na_2SiO_3 Bricks (SPSSB), Poraver® was mixed in a planetary mixer and the sodium silicate was added gradually and mixed for two minutes. Afterwards, shale was added gradually and mixed for three minutes. Later on, water was added gradually, and mixing was continued for an additional three minutes. Subsequently, the bricks were molded and kept at room temperature for three hours. Then the bricks were demolded and placed in the oven for drying with a gradual increase in temperature from 30°C to 110°C for 24 hours (the temperature increment was 20°C/hour). Then the bricks were kept in the furnace for firing with a gradual increase in temperature from 110°C to 1100°C for 24 hours. Several Shale-Poraver®- Na2SiO3 Bricks (SPSSB) were made with different percentage replacement of shale with Poraver®. The table below shows the mix composition of different Shale-Poraver®- Na_2SiO_3 Bricks (SPSSB).

3.1.2.9.1 Mix composition (by weight) percent for Shale-Poraver®- Na_2SiO_3 Bricks (SPSSB)

Table 3-4 Mix composition of Shale-Poraver®- Na_2SiO_3 Bricks (SPSSB)

Shale	Poraver	Sodium Silicate	Water
77.6	10	10	2.4
64.5	20	10	5.5
52	30	10	8.0
39.4	40	10	10.6
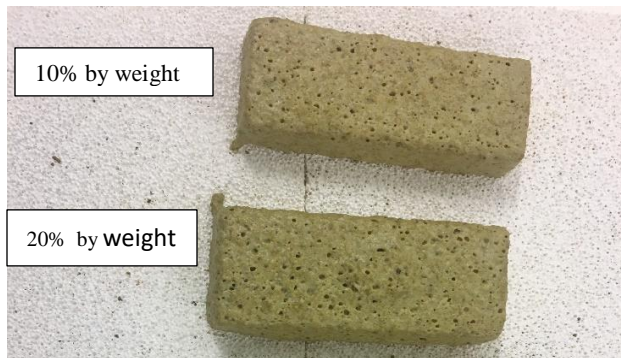
Figure 3- 39: SPSS-10 , SPSS-20 Bricks
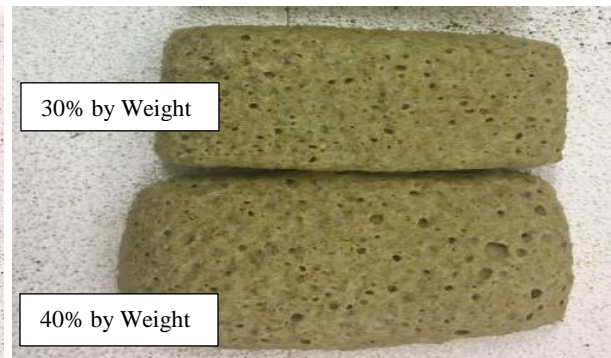
Figure 3-40: SPSS -30, SPSS-40 Bricks

Even though the resulting bricks were not cracked, they were spread out of shape and highly porous. The reason for this phenomenon is the effect of Sodium Silicate during the firing process. The addition of Sodium Silicate controlled the cracks by acting as a binder and sealant, however, the property of Sodium Silicate was incompatible for the fabrication of highly fired masonry bricks as, it hardens at a temperature of 100-110°C and melts again when heated at a temperature that exceeds 550-600°C. With this, all of the Shale-Poraver®- Na_2SiO_3 Bricks (SPSSB) were not completely successful. However, the brick appeared strong and had a 'Stoney' nature.

3.1.2.10 Geo-polymer Bricks (GB)

The addition of Poraver® was found to be incompatible for the fabrication of high-quality sustainable brick. So, the Poraver® was replaced by the Recycled Crushed Glass (RCG), whose surface had been roughened and therefore was more reactive. The next set of experiments that were conducted were focussed on making geo-polymer bricks (GB). Geo-polymer bricks are made by the geo-polymerization technology wherein the geopolymer chemistry is governed by covalent bonding mechanism of the repeating units of silico-aluminate (-Si-O-Al-O-). Fabrication of Geopolymer Bricks involved the partial replacement of shale with Recycled Crushed Glass (RCG) and Na_2SiO_3.

The Geopolymerization process was performed using quarried shale, Recycled Crushed Glass (RCG - Figure 3-41) from 'Opta Minerals' of size from 0.1mm-0.5mm and sodium silicate (Na_2SiO_3). Quarried Shale and Recycled Crushed Glass are used as binder materials while the alkaline solution of Sodium Silicate was used as an alkali-activator in the geo-polymerization process. The chemical reaction of the solid aluminosilicate with sodium silicate, makes the brick a hardened and strong construction material.

Figure 3-41: Recycled Crushed Glass (RCG)

3.1.2.10.1 Geo-polymer Bricks (GB-20)

Geo-polymer Brick samples (GB-20) were fabricated by mixing the Sodium silicate gradually to the recycled crushed glass in a mixer. Thereafter the shale was added gradually and mixed for three minutes to get rid of any clusters. Later on, the bricks were molded and kept at room temperature for 48 hours and were then demolded and put in the oven for firing with a gradual increase in temperature from 100°C to 400 °C for four hours. The temperature increment was 100°C/hour.

As a pilot experiment, GB-20 was made as a cube in a silicon mold with 20 % replacement of shale by weight with Recycled Crushed Glass as shown in Figure 3-42. For the mix, sodium silicate was added as 13% of the weight of the RCG plus Shale; no water was added.

Figure 3-42: Geopolymer Bricks (GB-20)

3.1.2.10.2 Geo-polymer Bricks (GB-30)

Geo-polymer Bricks (GB-30) was made exactly like Geo-polymer Bricks (GB-20). However, an important difference is in the percentage of recycled crushed glass added. As a trial experiment, GB-30 was also made as a cube in a silicon mold as shown in Figure 3-43. For the Geo-Polymer Bricks (GB-30), the mix composition was 30% replacement of shale with recycled crushed glass. Sodium silicate was added as 13% of the weight of the RCG plus Shale, with no water.

Figure 3-43: Geopolymer Bricks (GB-30)

3.1.2.10.3 Geo-polymer Bricks (GB-40)

Geo-polymer Bricks (GB-40) were also fabricated in the same manner as Geo-polymer Bricks (GB-20). In fact, the only difference was in the percentage of recycled crushed glass added. As a trial experiment, GB-40 was also made as a cube in a silicon mold as shown in Figure 3-44. For the Geo-polymer Bricks (GB-40), the mix composition was 40% replacement of shale with recycled crushed glass. Sodium silicate was added as 13% of the weight of the RCG plus Shale. No water was added.

Figure 3-44: Geopolymer Bricks (GB-40)

All of the geopolymer cubes were strong, and no imperfections were found. Addition of RCG not only reduced the shale consumption in the process, but also made the geopolymer bricks an inexpensive construction material and a useful host of waste glass. In addition, while the

conventional masonry bricks are fired exclusively over 1100 °C for no less than 24 hours, the geopolymer bricks were made with three times less firing energy utilization.

3.1.2.10.4 Mix composition (by weight) percent for the Geopolymer Bricks

Table-3-5 Mix composition for the Geopolymer Brick

Brick Type	Shale	RCG	Sodium Silicate (% of solids)
GB-20	80	20	13
GB-30	70	30	13
GB-40	60	40	13

3.1.2.11 Chemistry of Geopolymer brick

From the mineral analysis, the primary constituents in RCG and shale are SiO_2, Al_2O_3, Fe_2O_3 and CaO (Appendix II). The chemical reaction between these minerals with the Na_2SiO_3 makes the brick a hardened construction material.

3.1.2.12 Shale-Slag-Na$_2$SiO$_3$ Bricks (SSSSB)

The next trial performed involved the combination of Granulated Blast Furnace Slag, Na_2SiO_3 and shale. The experiment was repeated using various percentages of slag. The first casting mixture for this trial was prepared with 75% of shale by weight, 25% of slag by weight and 10% of sodium silicate by weight of the solid components. Shale-Slag-Na_2SiO_3 Bricks (SSSSB) was fabricated by mixing the shale and slag for two minutes in a mixer. Later on, the sodium silicate was added gradually and mixed for three minutes.

The second type of mixture for SSSS bricks was prepared with 50% of shale by weight, 50 % of slag by weight and 10% of sodium silicate by weight of the solid components. Subsequently, the bricks were molded and kept at room temperature for 24 hours. Then the bricks were demolded and placed in the furnace for firing with a gradual increase in temperature from 100°C to 600 °C for 24 hours. The temperature increment was 100°C/hour.

Since addition of sodium silicate enabled low temperature firing, bricks were fired at 600 °C. Upon visual testing, it was observed that both categories of the resulting bricks were not strong

enough and they accumulated a white powdery substance on the brick faces as shown in Figure 3-45a, Figure 3-45b.

(a)   *(b)*

Figure 3-45(a): SSSS-25 brick (b):SSSS-50 brick

3.1.2.13 Shale-Fly Ash-Na$_2$SiO$_3$ Bricks (SFSSB)

With the possibility that the blast furnace slag is the reason for the white deposit on the brick faces, slag was replaced by fly-ash *(*Figure 3-46a*)*, in the subsequent trial. So, bricks were made by Partial replacement of shale with fly-ash and Na$_2$SiO$_3$. The first trial used 75% of shale by weight, 25 % of fly-ash by weight and 10% of sodium silicate by the weight of solids. Shale-Fly Ash-Na$_2$SiO$_3$ Bricks (SFSSB) were fabricated by mixing the shale and fly-ash for two minutes in a mixer. Then the sodium silicate was added gradually and mixed for three minutes.

The second type of mixture for SFSS bricks was prepared with 50% of shale by weight, 50 % of fly-ash by weight and 10% of sodium silicate by weight of the solid components. Thereafter, the bricks were molded and kept at room temperature for 24 hours. Later on, the bricks were demolded and placed in the furnace for firing with a gradual increase in temperature from 100°C to 600 °C for 24 hours. The temperature increment was 100°C/hour.

As the addition of sodium silicate enabled low temperature firing, these bricks were also fired at 600 °C. Inspection of the resultant bricks showed signs of cracks and lack of strength as shown in Figure 3-47 and Figure 3-48. The cracks were even more prominent for SFSS-50.

Figure 3-46 fly-ash

Figure 3-47 SFSS-25 brick

Figure 3-48 SFSS-50 brick

3.1.2.14 Sludge Ash Bricks (SAB)

The next series of experiments involved the utilization of SSA as a partial replacement of shale. For that, I have contacted one of the Municipal wastewater treatment facilities Ashbridges Bay waste-water treatment plant in downtown Toronto for the sludge ash. The process of firing of sludge cake also known as dewatered sludge to produce sludge ash was as follows: The dewatered sludge (Figure 3-50(a)) was kept in the oven in ceramic crucibles for firing. The firing temperature of the oven was gradually increased from 20°C to 900°C.The temperature increase from 20°C to 300°C was faster when compared to the temperature increment from 300°C to 900°C in order to evaporate the humidity of the dewatered sludge. The ramping of temperature for the incineration process is shown in Figure 3- 49. 100 g of dewatered sludge yielded approximately 14 %-15% of sludge ash. The color transformation of sludge ash from black (Figure 3-50(b)) to red (Figure 3-50(c)) takes place between 550°C and 650 °C. The addition of iron during the dewatering technique of the sewage sludge, causes the red color of the sludge ash upon burning. The sludge ash was very similar to the quarried shale and was very light in weight. The sludge ash was ground

again, and the size of the ground sludge ash was less than 2mm. The experiment was performed with two fractions of sludge ash as the partial replacement of shale.

Incineration Process of Dewatered Sludge

Data points: 0, 30; 15, 90; 30, 150; 45, 210; 60, 300; 120, 400; 180, 500; 240, 600; 300, 700; 360, 800; 420, 900

X-axis: Time (minutes)
Y-axis: Temperature (°C)
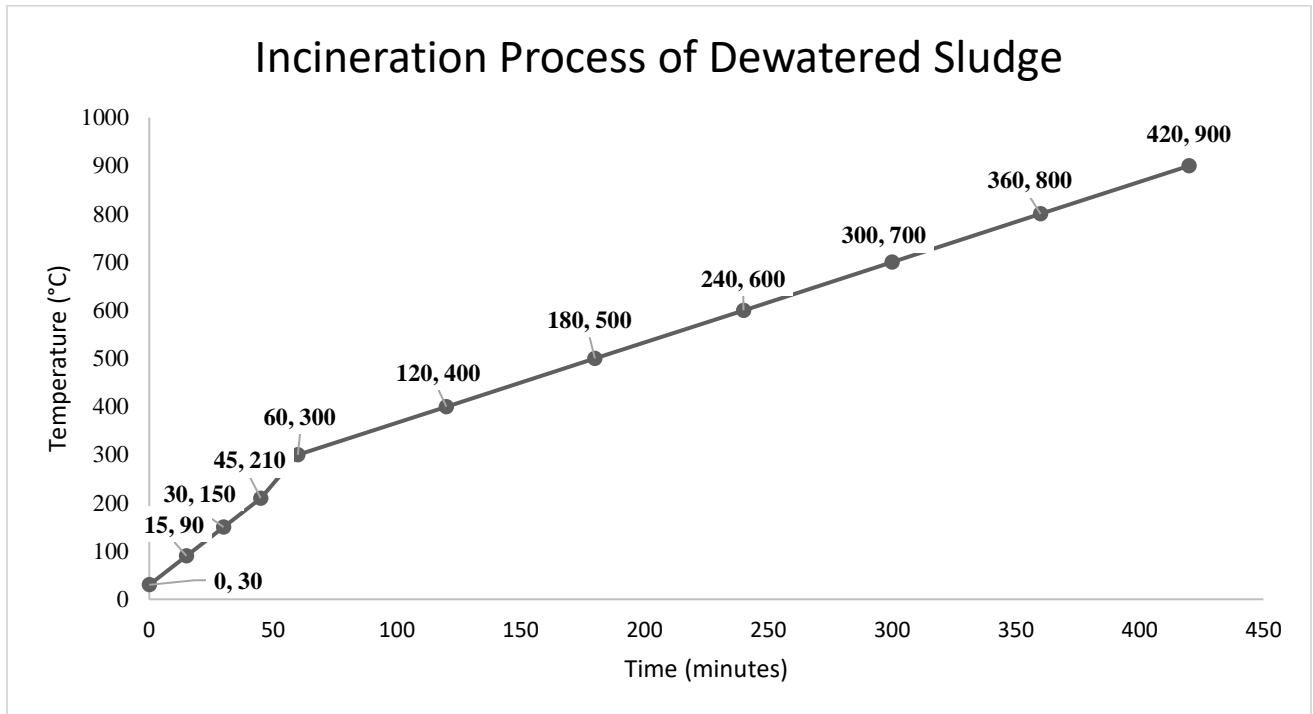
Figure 3-49:Incineration process of dewatered sludge

(a)

Figure 3-50 (a): Dewatered Sludge; (b): Incinerated Sludge Ash burned at 550°C (c): Incinerated Sludge Ash burned at 900°C

3.1.2.14.1 Sewage Sludge Ash Bricks (SSAB-15)

As the first trial, 15% replacement of shale with sludge ash was considered. For the fabrication of Sewage Sludge Ash Bricks SSAB-15, Shale was mixed for 2 minutes in a mixer to eliminate any clusters and then the sludge ash was added gradually. After 3 minutes of mixing, water was added gradually in quarter amount and mixing was continued for 3 minutes. Then, the bricks were molded and kept at room temperature for 3 hours. Later on, the bricks were demolded and placed in the oven for drying with a gradual increase in temperature from 30°C to 110°C. The temperature increment was 20°C/hour. Thereafter, the bricks were kept in the furnace for firing with a gradual increase in temperature from 110°C to 1100°C for 20 hours.

The mix composition for Sewage Sludge Ash Bricks (SSAB-15) was 85% of quarried shale, 15% of sludge ash and 13% of water by the weight of the solids. The bricks obtained from this trial mix were lighter and strong from the initial visual inspection.

3.1.2.14.2 Sewage Sludge Ash Bricks (SSAB-30)

The next trial involved partial replacement of shale with an increased percentage of Sewage Sludge Ash. For that, the mix composition was 70% of quarried shale, 30% of sludge ash and 13% of water by the weight of the solids. The fabrication procedure for Sewage Sludge Ash Bricks (SSAB-30) was the same as Sewage Sludge Ash Bricks (SSAB-15).

[57]

3.1.2.15 Chemistry of sewage sludge ash bricks

Raw sewage sludge contains SiO_2, $CaSO_4$, $CaSO_4.2H_2O$, and $NaCaSi_4Al_4O_8$ minerals [Tantawy et al., 2012]. $CaCO_3$ appears after incineration of sewage sludge at 500°C. This may be due to carbonation of some calcium compounds by CO_2 produced from combustion of organic matter. After incineration of sewage sludge at 800 and 950°C, these minerals constituents present in the sewage sludge ash decomposes into SiO_2, Al_2O_3, Fe_2O_3, CaO, MgO and P_2O_5 which are the same constituents present in shale with an exception of phosphorous pentoxide. The mineral composition of SSA used in the present study is given in Appendix II.

3.1.2.16 Crushed Bricks as a replacement for shale

Figure 3-51: Crushed Bricks

Crushed waste bricks is yet another source material that was considered as a shale replacement in making hybrid bricks. Unfortunately, no supplier or source for crushed bricks was found and in the absence of waste crushed bricks, tested control bricks were crushed in this endeavor (Figure: 3-51). However, as the control bricks were strong, that option was rather difficult to implement.

3.1.3 Preliminary Test Results

During the preliminary phase of the research, a multitude of hybrid bricks were made and the basic properties of the masonry units such as compressive strength and water absorption were analysed. Among the several categories of the bricks made, only few of them were identified as sustainable, economical and most promising brick types. These are, the Geo-polymer bricks, Liquid Bio-polymer bricks, Dried Biopolymer Bricks and Sewage Sludge Ash bricks. All these categories of bricks were gone through the preliminary analysis.

The Compressive strength tests on bricks are carried out to determine the load carrying capacity of brick under compressive load and it represents the most rudimentary material characterization test for all brittle and semi-brittle materials. The test was carried out in a control pilot compression testing machine. The compressive strength values and the standard deviation are given in Figure 3-52. The strength values for all bricks except for GB-20, GB-30, GB-40, SSAB-15, SSAB-30 are twice higher when compared with the other bricks because of the friction created between the brick surface and the loading plate, However, to get the actual compressive strength, in the remainder of the test program, all other bricks were tested using teflon plate of thickness 6mm on the top and bottom of the brick to avoid the frictional effect.

The water absorption of brick indicates the porosity of the brick – this is a most basic quality control test. The cold-water absorption refers to the larger pores that can hold water and hot-water absorption refers to the finer set of connected pores that can only store water in the form of steam. Asper the CAN/ CSA A82– Material standards for Fired masonry brick made from clay or shale, the percentage of cold-water absorption should be less than 15% of the total weight of the brick for the first-class bricks and the percentage of hot water absorption should be less than 17% of the total weight of the brick. For all the bricks tested for water absorption the observed percentage was less than the allowed value

3.1.3.1 Compressive Strength Test
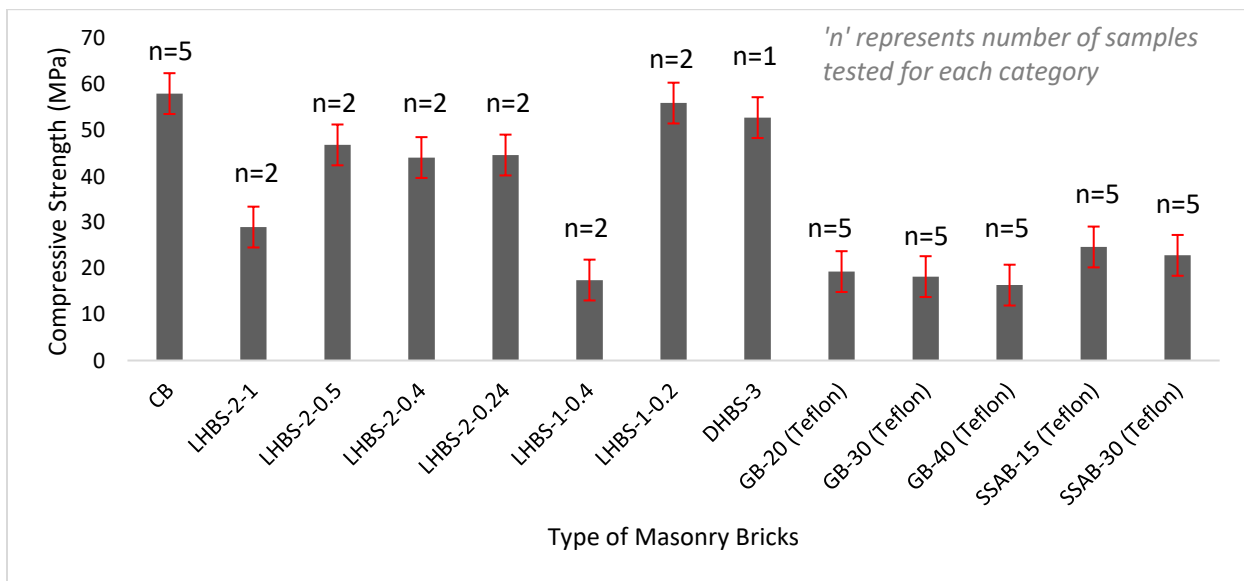
Figure 3-52: Preliminary Compressive Strength results of hybrid bricks

3.1.3.2 Water Absorption Tests
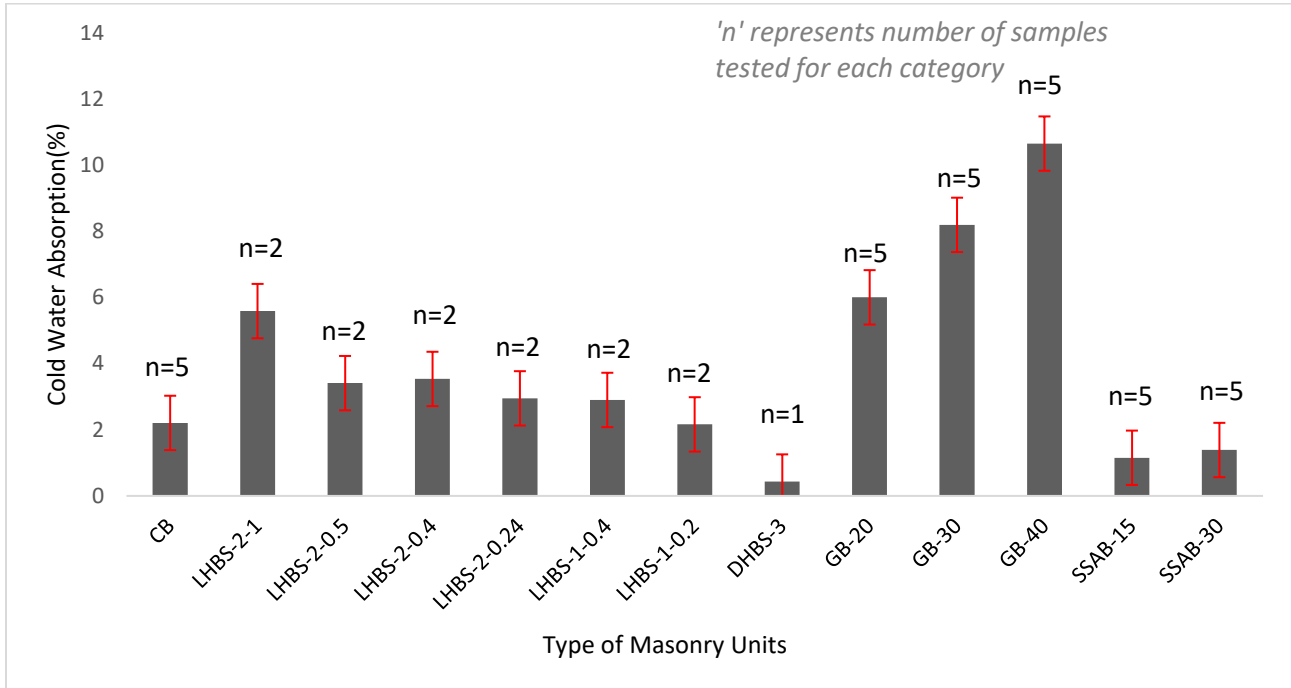
Figure 3-53: Preliminary cold -water absorption results of hybrid bricks
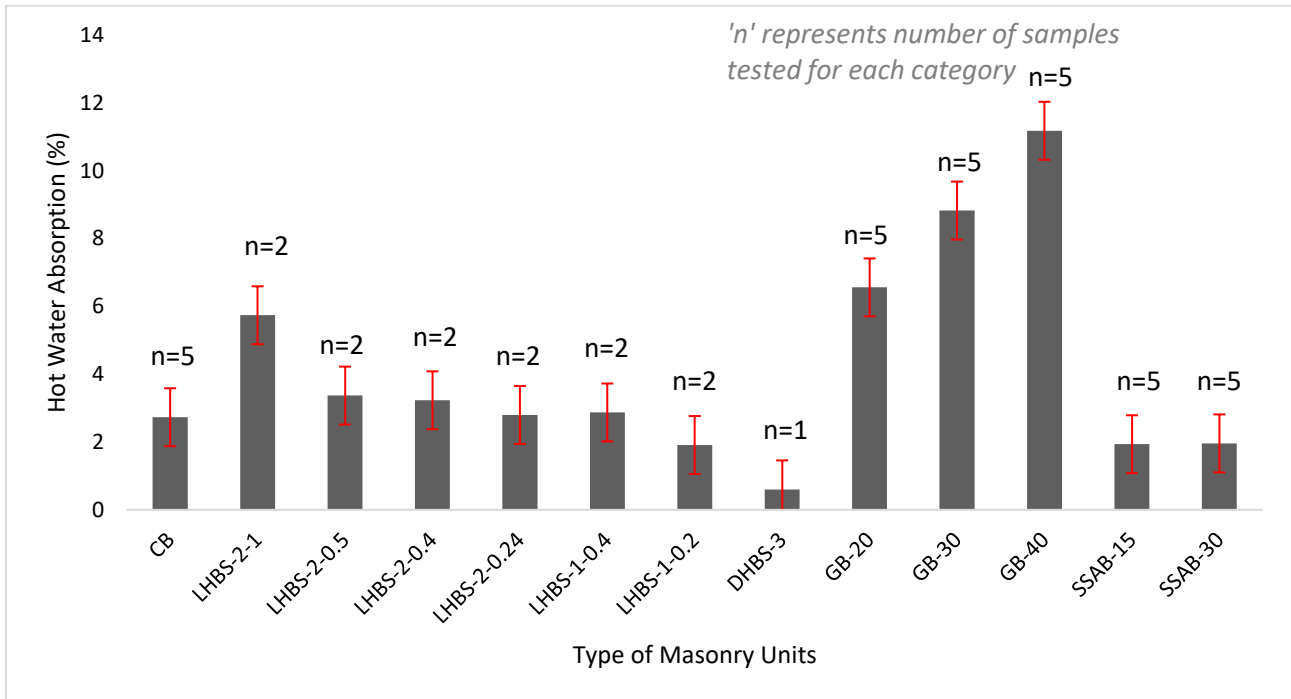
Figure 3-54: Preliminary hot- water absorption results of hybrid bricks

3.1.3.3 Weight of the Bricks
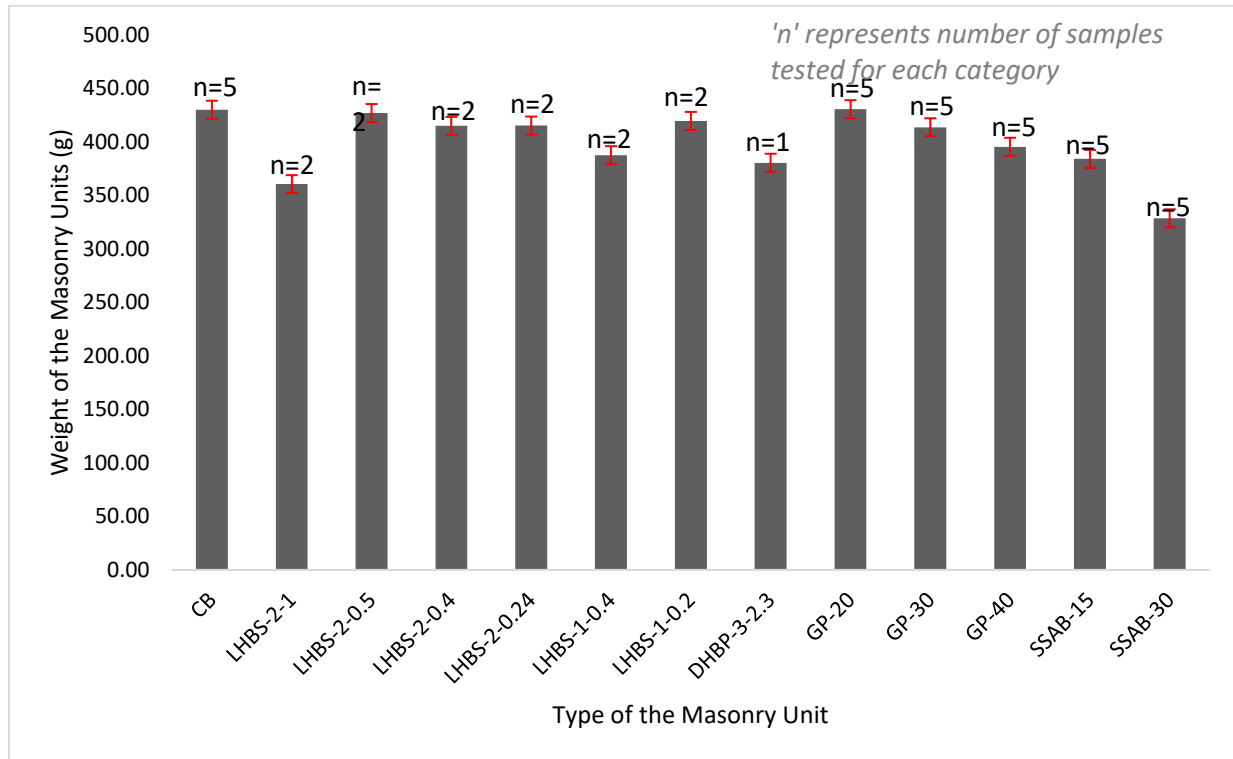
Figure 3-55 :Preliminary weight results of hybrid bricks

Chapter 4. Main Phase of the Experimental Study

The preliminary phase of the experimental work gathered helpful information on several promising source material combinations for the manufacture of hybrid bricks. Primary and crucial property tests like hot and cold-water absorption and compressive strength were performed for Geo-polymer bricks, Liquid High Biopolymer Sludge bricks, Dried High Bio-polymer bricks and Sewage Sludge ash bricks. Further, the weight of the hybrid bricks was compared with that of control bricks. From the preliminary experimental results as described in Chapter 3, three categories of hybrid bricks – Geo-polymer bricks, Dried High Bio-polymer bricks and Sewage Sludge ash bricks were identified as the most promising types of bricks and proceeded for the main phase of the research study.

4.1 Fabrication of Bricks

During the final phase of the research, control bricks, Geo-polymer bricks, Dried High Bio-polymer bricks and Sewage Sludge ash bricks were made. Among them, Geopolymer bricks and sludge ash bricks were made in several combinations of shale replacement with recycled glass powder and sewage sludge ash respectively. As a first step, a total of fourteen acrylic molds for the fabrication and two plungers for the compaction during the fabrication of the final bricks as shown in the Figure 4-1. Fourteen molds are made to fabricate fourteen brick for all categories which are necessary for the testing which are described in the Chapter 5.

Figure 4-1:Fourteen Acrylic brick molds made for the main phase of the experimental research

4.1.1 Control Bricks (CB)

The first category of brick made was the Control Bricks (CB) with no shale replacement. The materials used comprised 92% of shale and 8% of water. The method of fabrication was exactly the same as in the preliminary phase of the research. In total, fourteen control bricks of size 140mm x 58mm x 26mm and three cubes of size 50mm were made for the final tests and analysis.

4.1.2 Geo-polymer Bricks (GB)

The second category of bricks made was a type of hybrid bricks called Geopolymer Bricks (GB). The Geopolymer Bricks were made with varying percentages of shale replacement with Recycled Crushed Glass (RCG) and sodium silicate (Na_2SiO_3). All the Geopolymer Bricks were made in exactly the same way as in the preliminary phase of the research.

The types of the Geopolymer bricks were, Geo-polymer Bricks (GB-20) where, the shale is replaced by 20% of the recycled crushed glass and 13% of Sodium Silicate; Geo-polymer Bricks (GB-30) where, the shale is replaced by 30% of the recycled crushed glass and 13% of Sodium Silicate; Geo-polymer Bricks (GB-40) where, the shale is replaced by 40% of the recycled crushed glass and 13% of Sodium Silicate. The manufactured Geopolymer bricks are shown in Figure 4-2, 4-3 and 4-4. Fourteen specimens of each types of Geopolymer bricks, of size 140mm x 58mm x 26mm and three cubes of size 50mm were made for the final tests and analysis.

Figure 4-2: Geo-polymer Bricks (GB-20)   *Figure 4-3: Geo-polymer Bricks (GB-30)*

Figure 4-4: Geo-polymer Bricks (GB-40)

4.1.3 Dried High Bio-Polymer Bricks (DHBS)

The next category of hybrid bricks made was the Dried High Bio-Polymer Sludge Bricks (DHBS), with the partial replacement of shale with the Dried High Bio-Polymer Sludge obtained from the drying method as outlined in section 3.1.2.6.1.3 .The percentage of shale replaced was 2.3% by weight. The DHBS is shown in Figure 4-3. Fourteen number of DHBS bricks of size 140 mm x 58 mm x 26 mm and three cubes of size 50 mm were made for the final tests and analysis.

Figure 4-5: Dried High Bio-Polymer Sludge Bricks (DHBS)

4.1.4 Sewage Sludge Ash Bricks (SSAB)

The last category of hybrid bricks was made with the Sewage Sludge Ash (SSA) as a partial replacement for shale. Two fractions of sludge ash were used as the partial replacement of shale

during this process. The resultant hybrid bricks are Sewage Sludge Ash Bricks (SSAB-15) where, 85% of quarried shale, 15% of sludge ash by weight of solids, and 13% of water by the weight of the solids was used and Sewage Sludge Ash Bricks (SSAB-30) where, 70% of quarried shale, 30% of sludge ash by weight and 13% of water by the weight of the solids was used in the process. The two types of Sewage Sludge Ash Bricks (SSAB) made are shown in Figure 4-4a and 4-4b. Fourteen specimens of each type of SSAB of size 140mm x 58mm x 26mm and three cubes of size 50mm were made for the final tests and analysis.

Figure 4-6 Sewage Sludge Ash Bricks (SSAB-15)   *Figure 4-7 Sewage Sludge Ash Bricks (SSAB-30)*

Chapter 5. Experimental Results

Several experiments including physical and mechanical tests have been conducted on all the bricks made during the final phase of the research. Objective was to characterize their mechanical properties according with the established standards, to verify that they pass the quality control tests and to seek relationships between the many indices of mechanistic and physical behavior.

The tests conducted are classified in two groups: (a) Non destructive tests to assess durability and quality of the units; (b) Destructive, to assess the mechanical strength of the masonry units. The two groups are listed below. A standard number of five identical specimens was tested in each type of test.

Non-Destructive and Durability Tests: Cold Water Absorption; Hot Water Absorption; Ultrasonic Pulse Velocity Test; Efflorescence; Freeze thaw tests followed by transverse frequency measurements.

Destructive Tests: Compressive Strength in Transverse and Longitudinal direction, Splitting Tensile Strength Test and Flexural Strength Test.

5.1 Destructive Mechanical Tests

The destructive mechanical tests were done as per ASTM C67 / C67M Standard Test Methods for Sampling and Testing Brick and Structural Clay Tile. The destructive tests performed are the flexural or three-point bending test, split tensile strength test and the compressive strength test. Among these tests, the flexural bending test and split tensile strength tests are indirect methods for measuring the tensile strength of the material. This is done following the same procedure as in all semi-brittle materials (e.g. concrete), since it is difficult to conduct direct tension experiments not only for lack of an acceptable test specimen form, but also because the test hardware used to grip the specimens in the direct tension experiment may generate additional stress often leading to premature failures and yielding inaccurate results. In the current study, the direct tensile strength was determined using iterative numerical simulation through an advanced finite element platform, VecTor 2 described in Chapter 6. Compressive strength was also tested for the brick units. This destructive mechanical test - is a benchmark for all properties of semi-brittle materials and structural elements such as concrete, masonry blocks and wallettes. However, in testing brick compressive strength, a primary concern is the direction of compression with respect to the

longitudinal brick axis. Many of the reported test values are obtained from tests where compressive pressure is applied over the largest prism side (wherein the longitudinal axis of the brick is placed in the horizontal orientation, referred to in the remainder as "horizontal" for brevity). However, concerns may arise from the triaxial state of stress generated in that condition owing to the stocky aspect ratio of the specimen. To evaluate this effect compression tests were also done on bricks placed so that the longitudinal axis is oriented vertically, parallel to the direction of the compression load. In the remainder of this chapter this type of test will be referred to as 'vertical'.

5.1.1 Flexural Strength Test

The flexural or the bending strength of a masonry wall is an important mechanical property as it attempts to quantify the structural strength to tensile loads. Such examples include shear, bending and service life deflections. When scaling up from the masonry unit to the wall, occasionally, the mechanical response in tension is controlled by the mortar used for pointing which is the weakest material. However, measuring directly the tensile strength of the masonry units is not possible on account of the brittleness of the material. To address this problem several researchers as well as code standards prescribe the execution of a flexural test – one where the masonry unit is loaded as a beam with simple supports and a point load in the middle, to generate tension and therefore cracking failure in the midspan. This type of test is conducted in the present research to extract the tensile strength of the masonry unit indirectly, either from the stress formulae at the end of the ascending branch of the load-displacement curve, or through iteration by matching of the experimental responses with similar responses obtained after finite element simulations. Five masonry bricks from each category were tested in three-point bending to assess the flexural strength. The test unit was placed flatwise on two rollers having diameter of 25 mm, as bottom supports. The top and bottom surfaces of the bricks were plastered using a high strength (1-hour compressive strength of 27.6MPa) plaster hydro-stone gypsum cement from USG Industrial & Specialty Solutions (Figure 5-2(a)) to make the surfaces of the brick levelled and smooth so as to avoid any possible errors during the testing. For 200 grams of hydro-stone plaster, 55 grams of water was used for the right consistency as shown in Figure 5-2(b).

Loading was applied by the roller to the brick through the steel bearing plate (Figure 5-1) placed on the top at the centre of the brick. The load was applied in the direction of the depth of

the specimen's section. The size of the steel bearing plate was 6 mm in thickness, 30 mm in width and the length was 58 mm which is equal to the width of the specimen. This particular dimension for the plate has been chosen based on the aspect ratio of the masonry brick. The test set up for the flexural strength test is shown in Figure 5-1 and 5-3.

To capture the images of the testing to see the failure pattern, Canon DSLR camera and appropriate lighting system was used as shown in Figure 5-3(a).

(a)

(b)
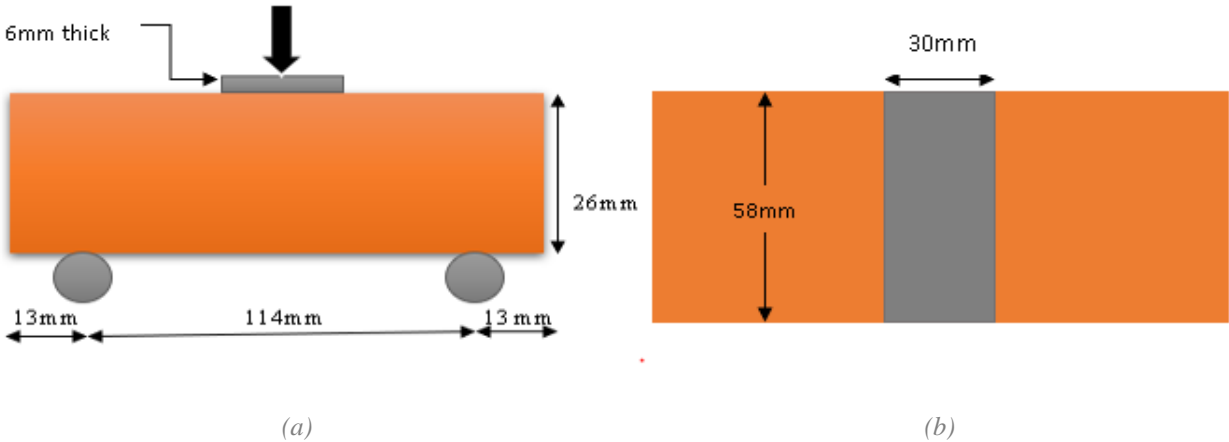
(c)

Figure 5-1 :Dimensions for three-point loading test (a) front view   (b) plan (c) The steel bearing plate of size 30x55x6 mm

<table>
<tr><td>(a)</td><td>(b)</td></tr>
</table>

5.2 (a): Gypsum cement used for plastering (b): After mixing with water

(a)
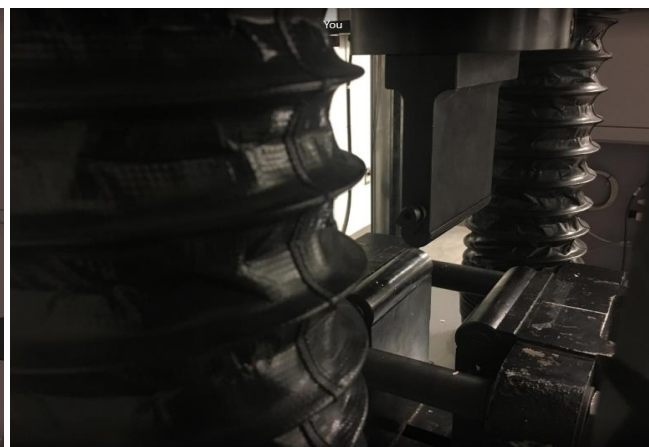
<table>
<tr><td>(b)</td><td>(c</td></tr>
</table>

(d)   (e)

Figure 5-3 (a) : Camera and lighting (b) Typical flexural strength test set up on MTS (c) Bottom and top rollers(d)
Loading on brick (e) Typical Flexural strength test set up

5.1.1.1 Peak load and Flexural Strength calculation

The Peak load and the flexural strength were calculated as per the ASTM C67 / C67M Standard
Test Methods for Sampling and Testing Brick and Structural Clay Tile. The flexural strength is
calculated by Equation (5.1):

$$f_{t\ flex} = \frac{3W(L/2 - x)}{bd^2}$$
(5.1)

$f_{t\ flex}$ = Flexural strength of the specimen at the plane of failure in Pa,

W = Maximum load indicated by the testing machine in N,

L = Distance between the supports in mm,

b = Net width of the specimen at the plane of failure in mm,

d = Depth from bed surface to bed surface, of the specimen at the plane of failure in mm, and

x = average distance from the midspan of the specimen to the plane of failure measured in the
direction of the span along the centerline of the bed surface subjected to tension in mm.

[70]

Table 5-1 Flexural Strength of the Control Bricks (CB)

W (kN)	L (mm)	b (mm)	d (mm)	$f_{t\,flex}$, Flexural Strength (MPa)
3.18	133.00	56.37	25.16	14.14
3.30	136.87	56.80	25.82	16.19
3.05	136.52	55.80	25.30	15.44
3.12	138.30	56.21	25.84	14.25
3.25	136.58	54.98	25.80	16.66
				15.34

Table 5-2 Flexural strength of the Dried High Biopolymer Bricks (DHBS)

W (kN)	L (mm)	b (mm)	d (mm)	$f_{t\,flex}$, Flexural Strength (MPa)
2.90	136.80	55.08	25.18	14.58
2.91	134.78	57.35	25.39	15.92
2.99	138.15	56.52	25.29	14.38
2.89	137.07	57.38	25.16	15.12
2.79	137.09	55.41	25.98	14.43
				14.88

Table 5-3 Flexural strength of the Geopolymer Bricks (GB-20)

W (kN)	L (mm)	b (mm)	d (mm)	$f_{t\,flex}$, Flexural Strength (MPa)
1.92	138.80	55.68	25.25	9.05
2.50	138.12	55.44	25.48	12.20
1.96	139.57	55.36	25.19	10.50
2.02	138.09	55.87	25.98	10.40
1.85	139.95	56.91	25.93	9.75
				10.42

Table 5-4 Flexural strength of the Geopolymer Bricks (GB-30)

W (kN)	L (mm)	b (mm)	d (mm)	$f_{t\,flex}$, Flexural Strength (MPa)
1.72	138.00	55.01	25.01	8.22
1.79	139.12	56.42	26.00	7.06
1.74	138.92	56.37	25.83	7.65
1.76	139.58	56.53	25.00	8.63
1.80	138.86	56.34	25.70	9.24
				8.16

Table 5-5 Flexural strength of the Geopolymer Bricks (GB-40)

W (kN)	L (mm)	b (mm)	d (mm)	$f_{t\,flex}$, Flexural Strength (MPa)
1.25	139.71	56.92	26.00	6.27
1.35	139.59	56.03	25.85	6.57
1.12	139.01	57.11	25.92	6.06
1.22	138.08	57.08	25.40	6.30
1.43	139.98	56.13	25.27	7.05
				6.45

Table 5-6 Flexural strength of the Sewage Sludge Ash Bricks (SSAB-15)

W (kN)	L (mm)	b (mm)	d (mm)	$f_{t\,flex}$, Flexural Strength (MPa)
2.81	136.28	56.08	25.15	14.36
2.76	136.19	56.85	25.85	13.36
2.87	135.36	56.25	25.98	13.85
2.96	137.07	56.53	25.41	15.30
2.63	137.51	58.00	25.37	14.03
				14.18

Table 5-7 Flexural strength of the Sewage Sludge Ash Bricks (SSAB-30)

W (kN)	L (mm)	b (mm)	d (mm)	$f_{t\ flex}$, Flexural Strength (MPa)
2.51	136.81	56.13	25.17	12.42
2.86	136.92	56.35	25.13	14.12
2.60	136.19	57.09	25.80	11.62
2.49	136.29	56.87	25.27	12.92
2.77	135.85	55.38	25.09	13.12
				12.84
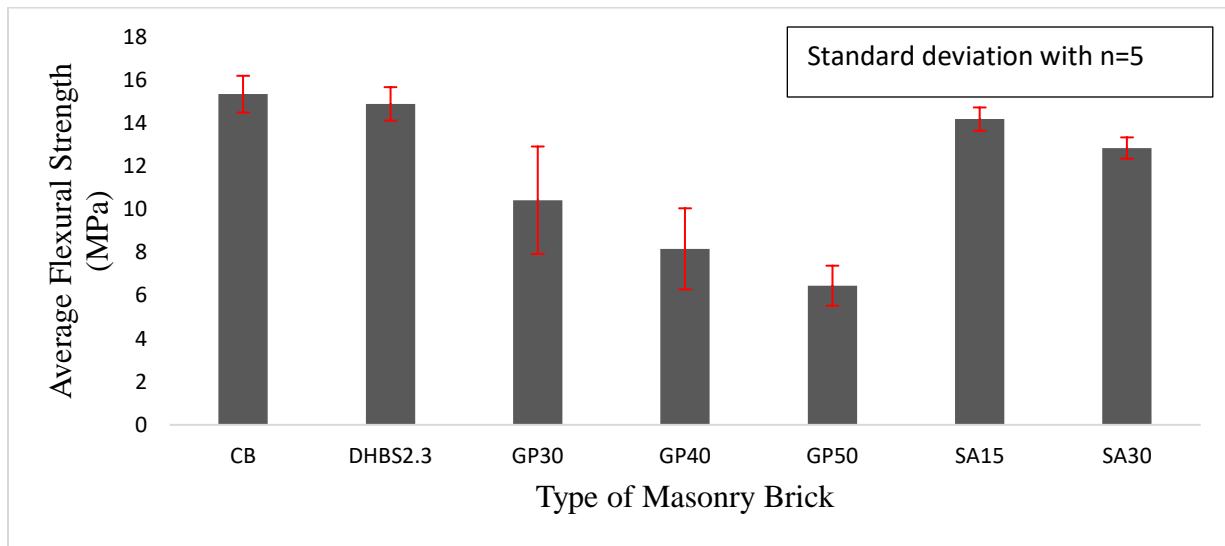
(a)
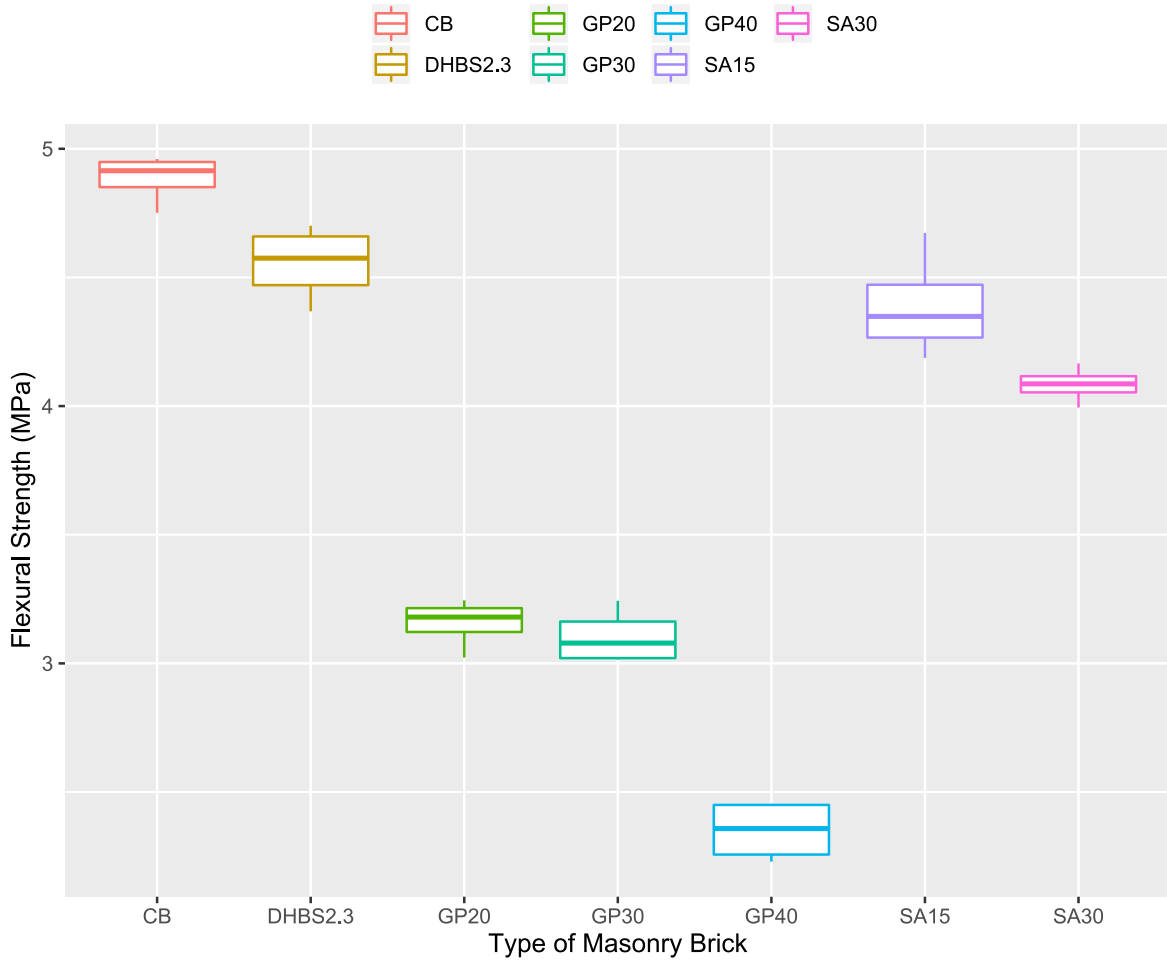
(b)

Figure 5-4 (a): Average Flexural strength of brick (b): Box plot for flexural strength of all brick

5.1.1.2 Failure pattern

The Failure patterns observed for the control bricks as well as the hybrid bricks are shown in the figures below. The failure crack occurred near the mid point, where the top loading roller was placed for all the categories of the bricks. Furthermore, all the failure modes were brittle.

(a)   (b)

Figure-5-5(a) Test Set up (b) : Failure Pattern of Control Brick (CB)

(a)   (b)

Figure-5-6(a) Test Set up (b): Failure Pattern of Dried High biopolymer Brick (DHBS)

(a)   (b)

Figure-5-7(a) Test Set up (b): Failure Pattern of Geopolymer Brick (GB-20)

(a)	*(b)*

Figure-5-8(a) Test Set up (b): Failure Pattern of Geopolymer Brick (GB-30)

(a)	*(b)*

Figure-5-9 (a) Test Set up (b): Failure Pattern of Geopolymer Brick (GB-40)

(a)	*(b)*

Figure-5-10 (a) Test Set up (b) :Failure Pattern of Sewage sludge ash Brick (SSAB-15)

(a)   *(b)*

Figure-5-11 (a) Test Set up (b) :Failure Pattern of sewage sludge ash Brick (SSAB-30)

5.1.1.3 Load-deformation response from the Flexural Strength test

The average load-deformation response of all the categories of brick from the flexural strength test is shown in Figure 5-12. The peak load and the mid displacement was calculated. For the five-control brick tested, the displacement corresponding to the peak load of 3.18 kN, 3.25 kN, 3.30 kN was 0.028 mm, and for the peak load of 3.05 kN and 3.18 kN, the displacement was 0.029 mm.

Similarly, for the DHBS brick, the displacement for the peak load was much higher when compared to the control bricks. The peak load values of the DHBS bricks were 2.90 kN, 2.91 kN, 2.99 kN, 2.89 kN and 2.79 kN and the displacement for them were 0.036 mm for all bricks except for the brick with a peak load of 2.79 kN. The displacement for that brick was 0.035 mm.

Comparably, the SSAB bricks has also showed a close load-deformation response. For SSAB-15 the peak load values were in the range of 2.62 kN and 2.95 kN. The displacement for the peak load of 2.62 kN was found to be 0.0.034 mm and for 2.95 kN, the displacement was 0.037 mm. Closely, for the SSAB-30 bricks as well, the peak load values were between 2.49 kN and 2.86 kN and the displacement ranged between 0.030m and 0.032 mm. Interestingly enough, the displacement for SSAB-30 was lower than SSAB-20 bricks.

For the GB-20 bricks, the peak load was lower than the control bricks and ranged between 1.84 kN and 2.5 kN. The displacement was found between 0.021 mm and 0.022 for all the GB-20 bricks. Likewise, for GB-30 and GB-40 bricks, the peak load values were in between 1.72 kN to

[77]

1.80 kN and 1.12 kN to 1.43 kN respectively. The peak load and the displacement for all the GB-30 and GB-40 bricks were lower than GB 20 bricks. From the analysis, it is clear that GB has much lower load carrying capacity when compared to the other categories of bricks.
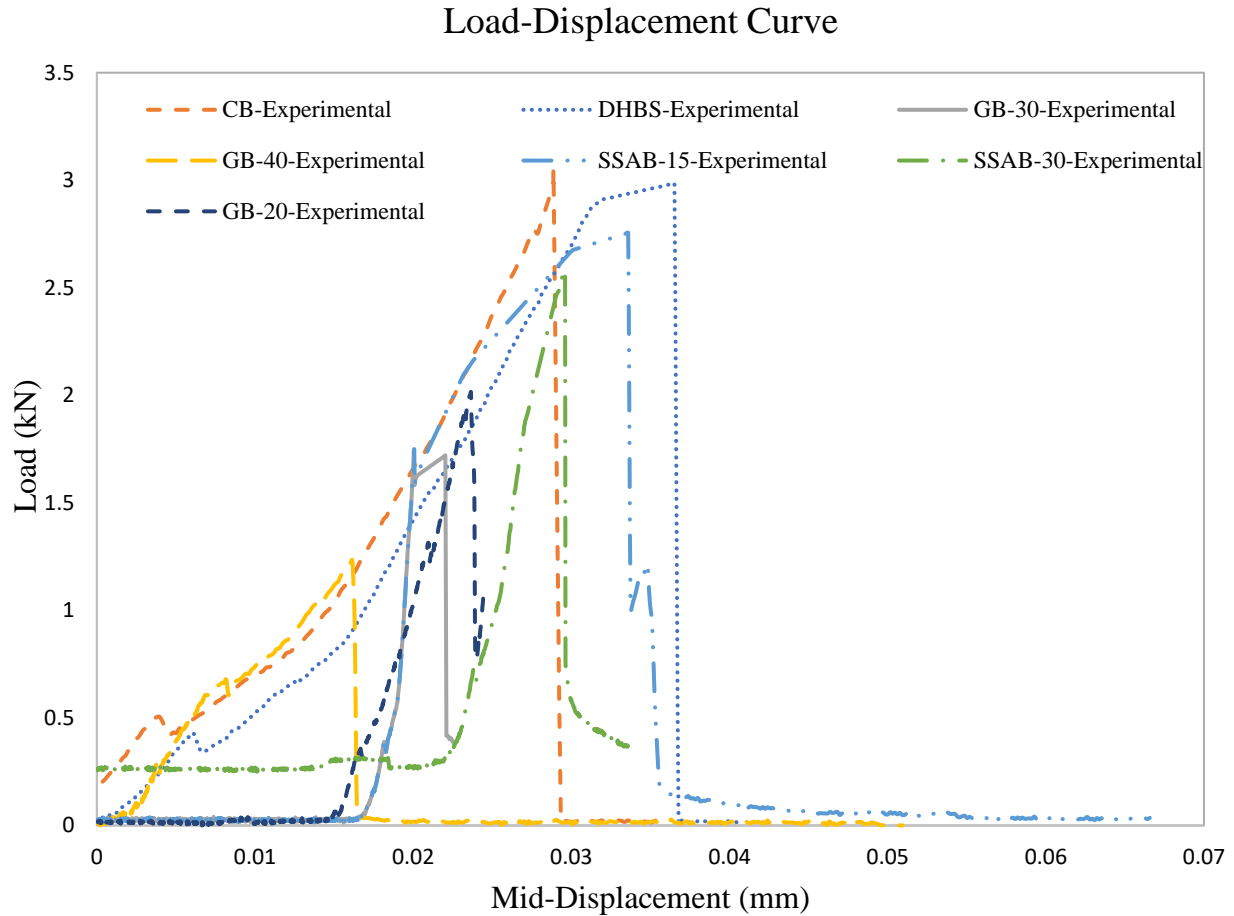
Figure 5-12: Load-deformation response curve from the flexural strength test

5.1.2 Splitting Tensile Strength Test

The second type of destructive mechanical test conducted was the indirect tensile strength tests known as splitting tensile strength test. Tensile strength of masonry is a fundamental material characteristic used to predict crack formation under both compressive loading (cracks oriented parallel to compression) or under diagonal tension (e.g. due to shear, where cracks may run perpendicular of even inclined to the brick axis at testing). The splitting tests were done according with ASTM C1006 / C1006M -Standard Test Method for Splitting Tensile Strength of Masonry Units.

Four masonry bricks were tested for the transverse splitting tensile strength test. The test was done in the Controls Pilot testing machine for the compression test. The compressive load is applied through a steel bearing rod of diameter 3 mm at the top and bottom bed surfaces. Fresh hydrostone-gypsum capping compound was used to keep the bearing rods along the bed surface on the each of the centrelines at the top and bottom of the bricks. For that, one of the bearing rods was placed into the capping compound and pressed until contact has been made with the brick. After the capping compound had set, the second bearing rod was placed parallel to the first on the opposite bed surface using a rafter square. A typical set up for the split tensile strength test is shown in Figure 5-13 (a) to (e).

(a)

(b)

(c)

(d)

(e)
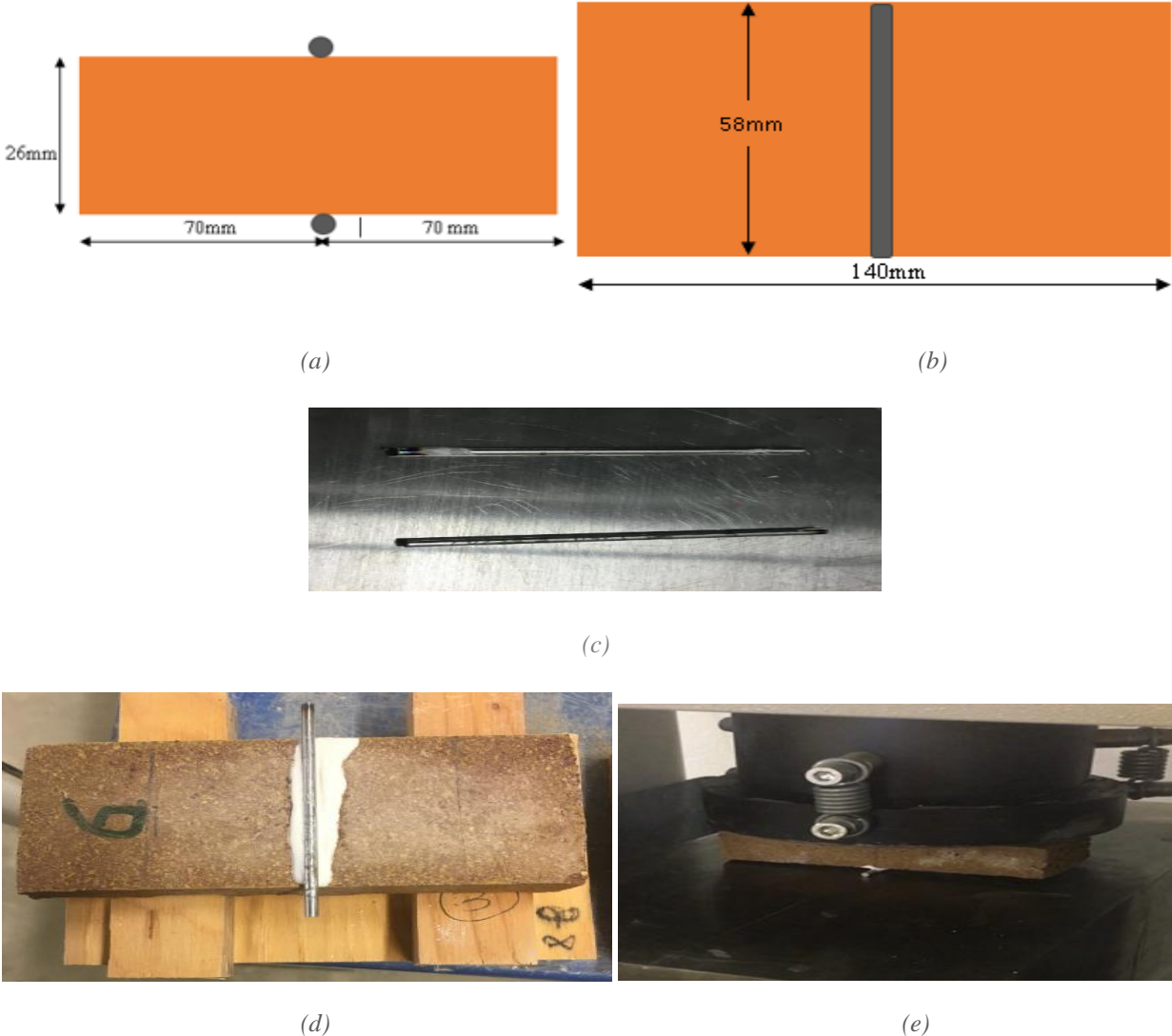
Figure-5-13: Dimensions for splitting tensile strength test (a) : front view (b) plan (c): steel bearing rods

5.1.2.1 Splitting Tensile strength Calculation

The maximum splitting tensile strength in the center of the masonry brick is calculated from the following Equation (5.2)

$$f_{t\ split} = \frac{2P}{\pi LH} \tag{5.2}$$

Where:

$f_{t\ split}$ = the splitting tensile strength of the masonry brick in kPa,

P = the maximum applied load indicated by the testing machine in kN,

L= the gross split length of the masonry brick in m (measured in the width), and

H = is the height of the masonry brick in m

Table 5-8 Split Tensile strength of the Control Bricks (CB)

P (kN)	Width of the specimen, L (mm)	Height of the specimen, H (mm)	Split tensile Strength (Mpa)
11.50	56.23	26.67	4.88
11.03	55.80	26.50	4.75
11.20	57.53	25.00	4.96
11.40	55.60	26.41	4.94
			4.89

Table 5-9 Split Tensile strength of the Dried High Biopolymer Bricks (DHBS)

P(kN)	Width of the specimen, L (mm)	Height of the specimen, H (mm)	Split tensile Strength (Mpa)
10.60	55.62	26.13	4.65
10.40	55.00	26.74	4.50
10.09	57.18	25.73	4.37
10.80	58.00	25.23	4.70
			4.55

Table 5-10 Split Tensile strength of the Geopolymer Bricks (GB-20)

P(kN)	Width of the specimen, L (mm)	Height of the specimen, H (mm)	Split tensile Strength (Mpa)
7.60	56.28	26.84	3.20
7.30	57.52	25.62	3.16
7.64	56.53	26.53	3.24
7.20	57.17	26.54	3.02
			3.16

Table 5-11 Split Tensile strength of the Geopolymer Bricks (GB-30)

P(kN)	Width of the specimen, L (mm)	Height of the specimen, H (mm)	Split tensile Strength (Mpa)
7.10	55.60	25.94	3.14
7.00	55.63	26.52	3.02
6.80	55.63	25.82	3.02
7.40	56.50	25.72	3.24
			3.10

Table 5-12 Split Tensile strength of the Geopolymer Bricks (GB-40)

P(kN)	Width of the specimen, L (mm)	Height of the specimen, H (mm)	Split tensile Strength (Mpa)
5.70	56.35	26.30	2.45
5.80	57.25	26.34	2.45
5.40	57.04	26.61	2.27
5.30	56.08	27.00	2.23
			2.35

Table 5-13 Split Tensile strength of the Sewage Sludge Ash Bricks (SSAB-15)

P(kN)	Width of the specimen, L (mm)	Height of the specimen, H (mm)	Split tensile Strength (Mpa)
9.90	56.50	26.00	4.29
10.40	57.23	26.28	4.40
9.80	56.94	26.18	4.19
10.80	57.50	25.60	4.67
			4.39

Table 5-14 Split Tensile strength of the Sewage Sludge Ash Bricks (SSAB-30)

P(kN)	Width of the specimen, L (mm)	Height of the specimen, H (mm)	Split tensile Strength (Mpa)
9.60	56.18	26.55	4.10
9.80	56.50	26.52	4.17
9.50	56.00	26.53	4.07
9.30	55.73	26.61	3.99
			4.08
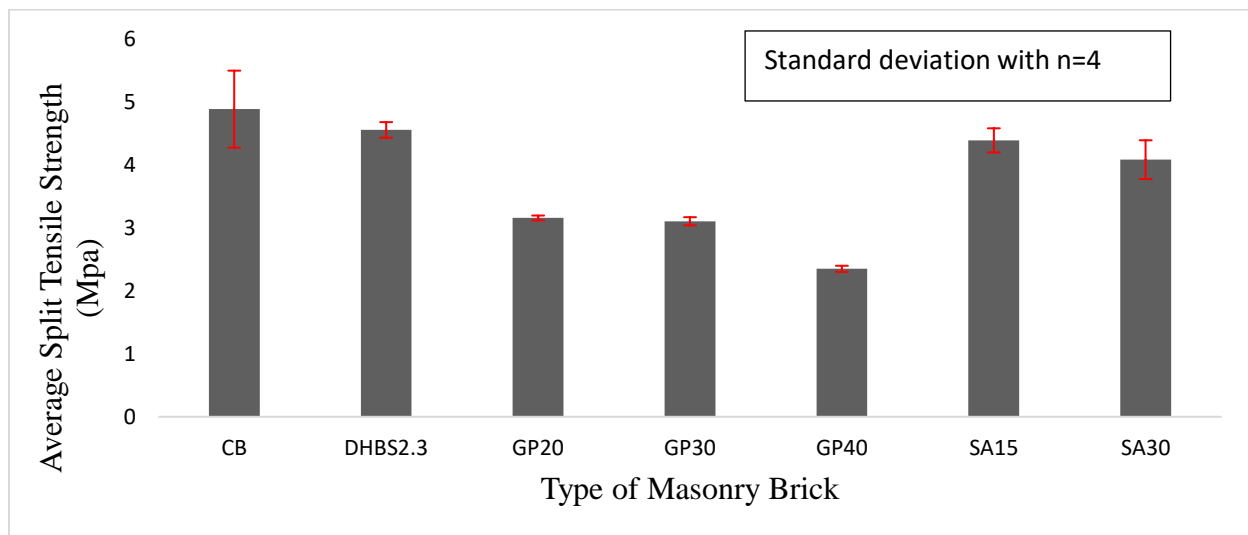
(a)
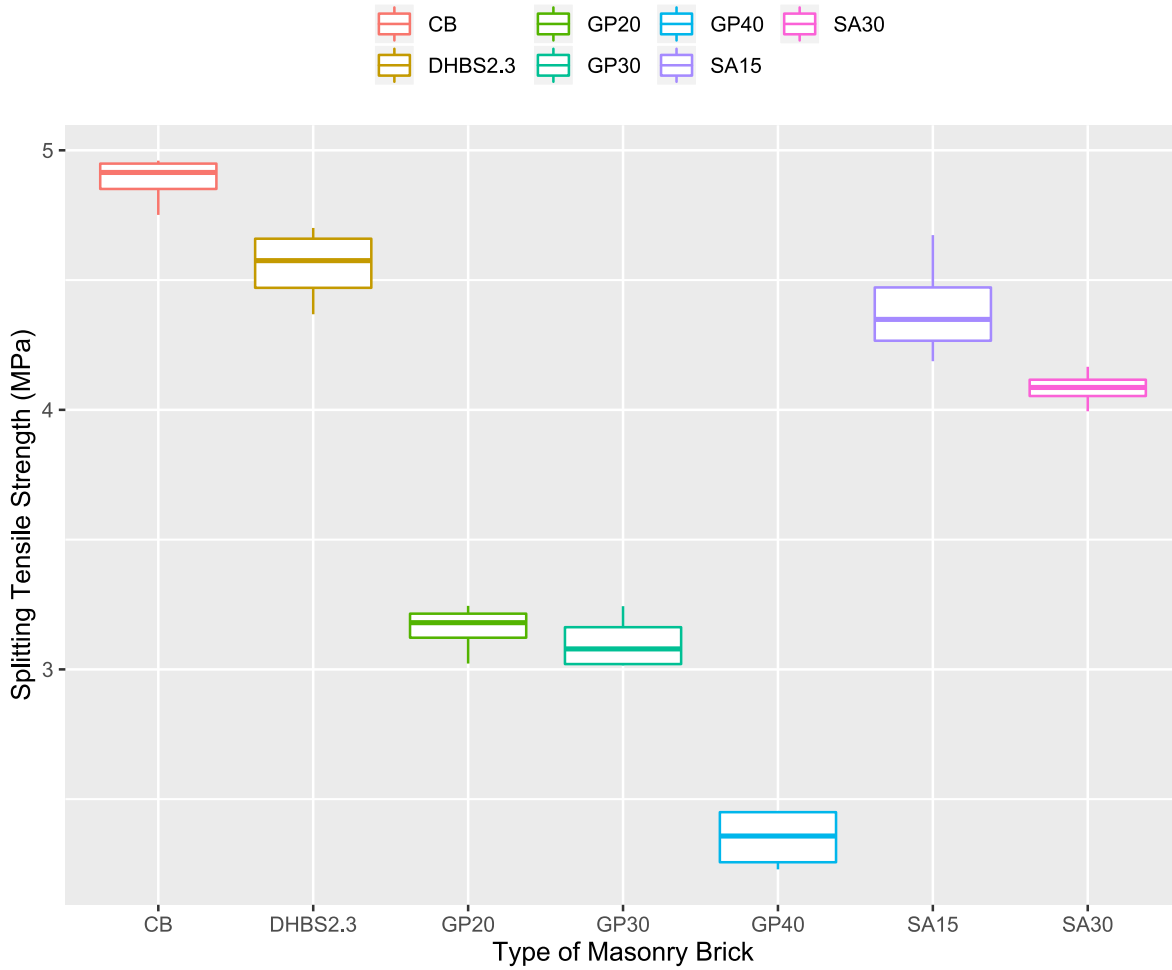
(b)

Figure 5-14 (a) :Average Splitting Tensile Strength of Bricks (b): Box plot for splitting tensile strength of all brick

5.1.2.2 Failure pattern

The Failure pattern observed for the control bricks as well as the hybrid bricks are shown in the figures below. The failure crack occurs near the mid point, where the two bearing rods were placed for all the categories of the bricks. The cracks extended in the transverse direction. Furthermore, all the failure modes were brittle as in the case of flexural strength test.

Figure 5-15 : Failure crack pattern of Control bricks (CB)   *Figure 5-16 : Failure crack pattern of DHBS*
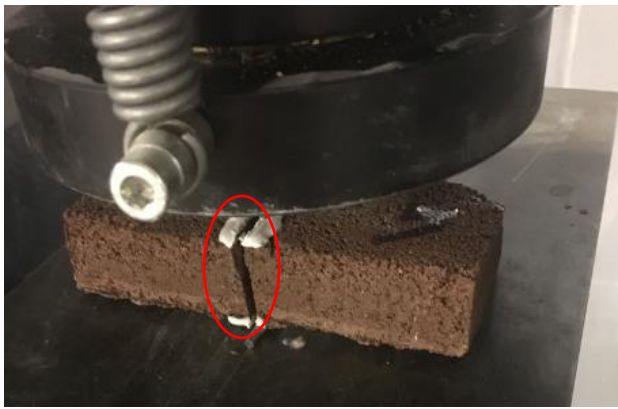
Figure 5-17: Failure crack pattern of GB-20   *Figure 5-18 : Failure crack pattern of GB-30*

Figure 5-19: Failure crack pattern of GB-40   *Figure 5-20: Failure crack pattern of SSAB-15*
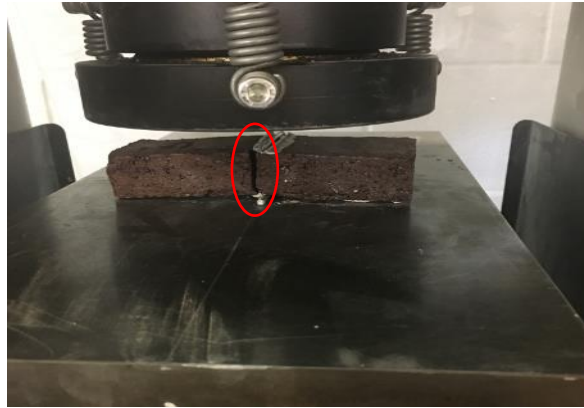
Figure 5-21: Failure crack pattern of SSAB-30

5.1.3 Compressive Strength Tests

To determine the resistance of the masonry units to compressive load, the compressive test was conducted as per ASTM C-67 Standard Test Methods for Sampling and Testing Brick and Structural Clay Tile, using the Controls Pilot testing machine and the test set up is as shown in Figure 5-22.

In order to carry out the compression test, five dry full bricks were used. Then, the bricks were cut in half so that each brick was dry half brick with half length, full height and full width of the actual brick. This has been done to conduct the compression test in horizontal and vertical orientations as described in the beginning of the chapter.

(a)   (b)
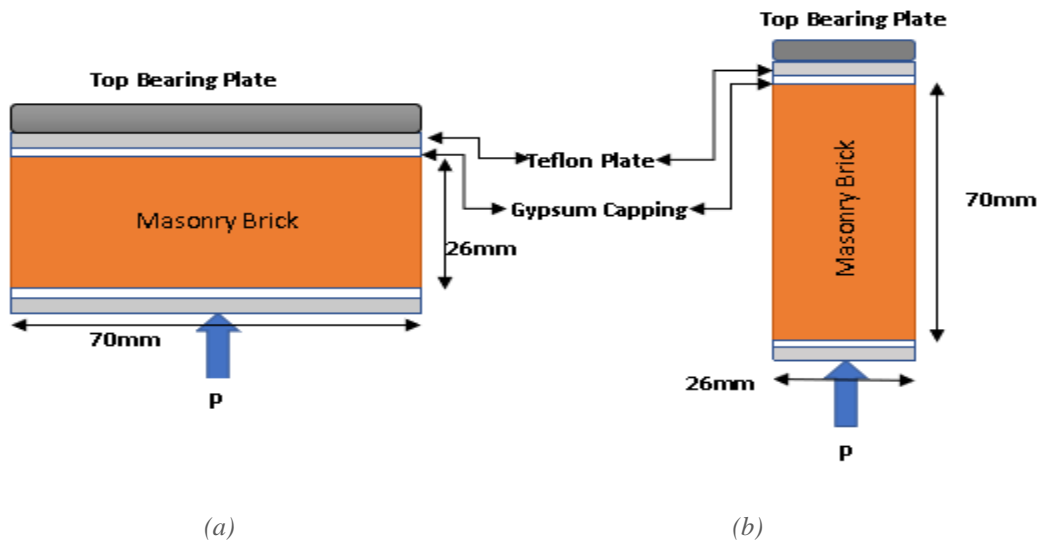
Figure 5-22: Set up and dimensions of the Compressive Load set up (a) Transverse Loading (b) Longitudinal Loading

[85]

(a)   *(b)*

Figure 5-23(a): Sawing machine used to cut the bricks in half (b): Brick Sawing in the Civil Engineering Laboratory

Figure 5- 24: Controls Pilot compression testing machine and the test set up (a) Transverse loading (b) Longitudinal Loading

5.1.3.1 Shellacking and Gypsum capping

The two opposite bearing surfaces of each brick was coated with a sealant (commercial name was "shellac") to prevent any water absorption of bricks during capping. The shellac coating was allowed to dry thoroughly for an hour. Then, the hydrostone gypsum capping was done on one of the dry shellacked surfaces of the brick by placing it on a levelled glass plate for the parallel smooth surfaces to avoid friction during the loading. The gypsum mix was prepared as described in section 5.1.1.When it was dried, the gypsum capping was done on the other surface as well using the same procedure; the thickness of the final layer was 2-4 mm. Figure 5-26 depicts the shellacking and capping of the masonry bricks.

Figure 5-25: Sealant used for Gypsum capping (Zinsser.com) Figure 5-26 : Shellacked bricks before the gypsum capping

Figure 5-27: The bricks arranged for the drying of gypsum
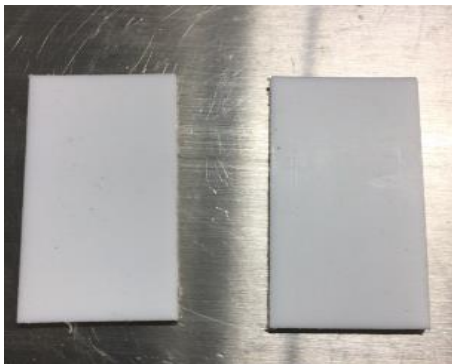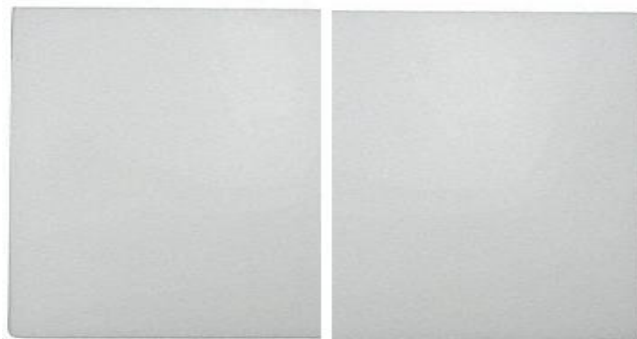
| (a) | (b) |

Figure 5-28: Teflon plates used for (a) Transverse loading (b) Longitudinal Loading

[88]

When the bricks were dried, they were subjected to compressive loading. Half of the individual bricks underwent the transverse loading and the other half of them underwent longitudinal loading. The compressive strength was calculated from Equation 5.3:

$$C = P / A \qquad\qquad (5.4)$$

where:

C = is the compressive strength of the brick in MPa,

P = is the maximum load in N indicated by the control pilot testing machine, and

A = is the area of the bearing surfaces of the bricks in mm^2

5.1.3.2 Compressive strength test - Transverse loading

The compressive strength test in transverse direction was done by placing the half brick in length-wise parallel to the bearing plate and the compressive load was applied at a uniform rate of 20N/s as per the standard. The size of the bricks were (70 mm ± 5 mm) x (58 mm ± 3 mm) x (26 mm ± 3 mm). The bearing sides were (70 mm ± 5 mm) x (58 mm ± 3 mm). To avoid friction, Teflon plates of size 70 x 60 x 3 mm were placed on the top and bottom bearing surfaces of the brick (see Figure. 5-28).

5.1.3.2.1 Peak Load and compressive strength Calculation

The peak compressive and the respective compressive strength calculations of transverse loading are shown in the following tables.

Table 5-15 Compressive strength of the Control Bricks (CB)

P (kN)	Area of the specimen, H (mm)	Compressive Strength (MPa)
118.80	3699.87	32.11
108.90	3649.55	29.84
110.40	3679.68	30.00
101.50	3670.73	27.65
113.50	3764.73	30.15
		29.95

Table 5-16 Compressive strength of the Dried High Biopolymer Bricks (DHBS)

P (kN)	Area of the specimen, H (mm)	Compressive Strength (MPa)
99.20	4015.31	24.71
99.10	4011.89	24.70
99.40	4025.59	24.69
99.30	4018.95	24.71
101.50	4010.83	25.31
		24.82

Table 5-17 Compressive strength of the Geopolymer Bricks (GB-20)

P (kN)	Area of the specimen, H (mm)	Compressive Strength (MPa)
77.30	4028.65	19.19
76.40	4026.20	18.98
75.80	4015.60	18.88
77.70	4018.75	19.33
76.80	4030.21	19.06
		18.80

Table 5-18 Compressive strength of the Geopolymer Bricks (GB-30)

P (kN)	Area of the specimen, H (mm)	Compressive Strength (MPa)
73.20	4012.30	18.24
72.50	4018.30	18.04
72.60	4010.85	18.10
74.80	4020.90	18.60
72.90	4023.60	18.12
		18.02

Table 5-19 Compressive strength of the Geopolymer Bricks (GB-40)

P (kN)	Area of the specimen, H (mm)	Compressive Strength (MPa)
61.20	4025.26	15.20
65.80	4015.23	16.39
61.70	4019.34	15.35
57.00	4016.70	14.19
63.90	4030.45	15.85
		15.07

Table 5-20 Compressive strength of the Sewage Sludge Ash Bricks (SSAB-30)

P (kN)	Area of the specimen, H (mm)	Compressive Strength (MPa)
98.20	3978.22	24.68
95.70	3940.68	24.29
94.40	3910.76	24.14
89.20	3901.00	22.87
94.30	3914.15	24.09
		24.12

Table 21 Compressive strength of the Sewage Sludge Ash Bricks (SSAB-30)

P (kN)	Area of the specimen, H (mm)	Compressive Strength (MPa)
89.40	3973.50	22.50
90.50	3974.07	22.77
89.15	3969.19	22.46
90.08	3942.50	22.85
91.30	3993.66	22.86
		22.69
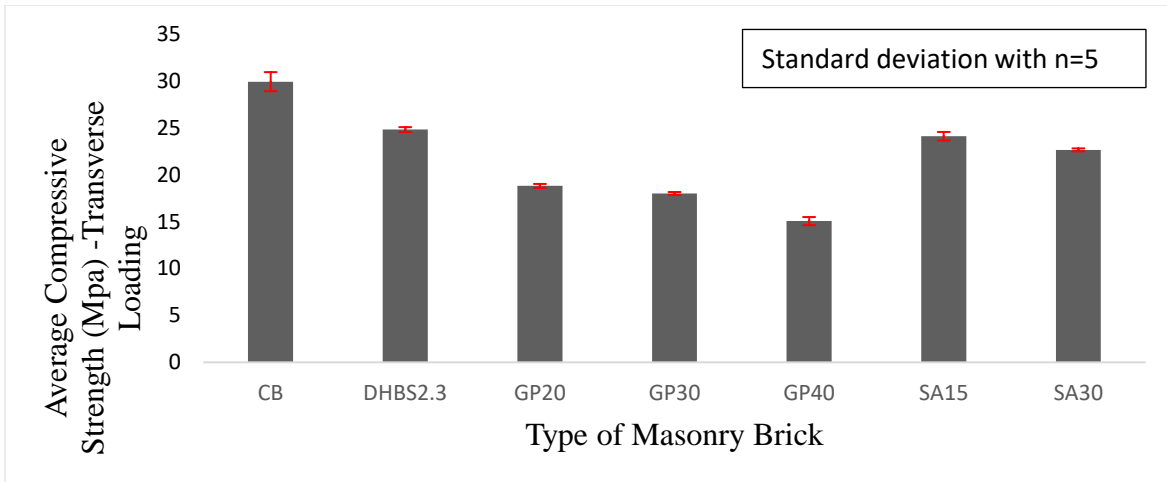
(a)
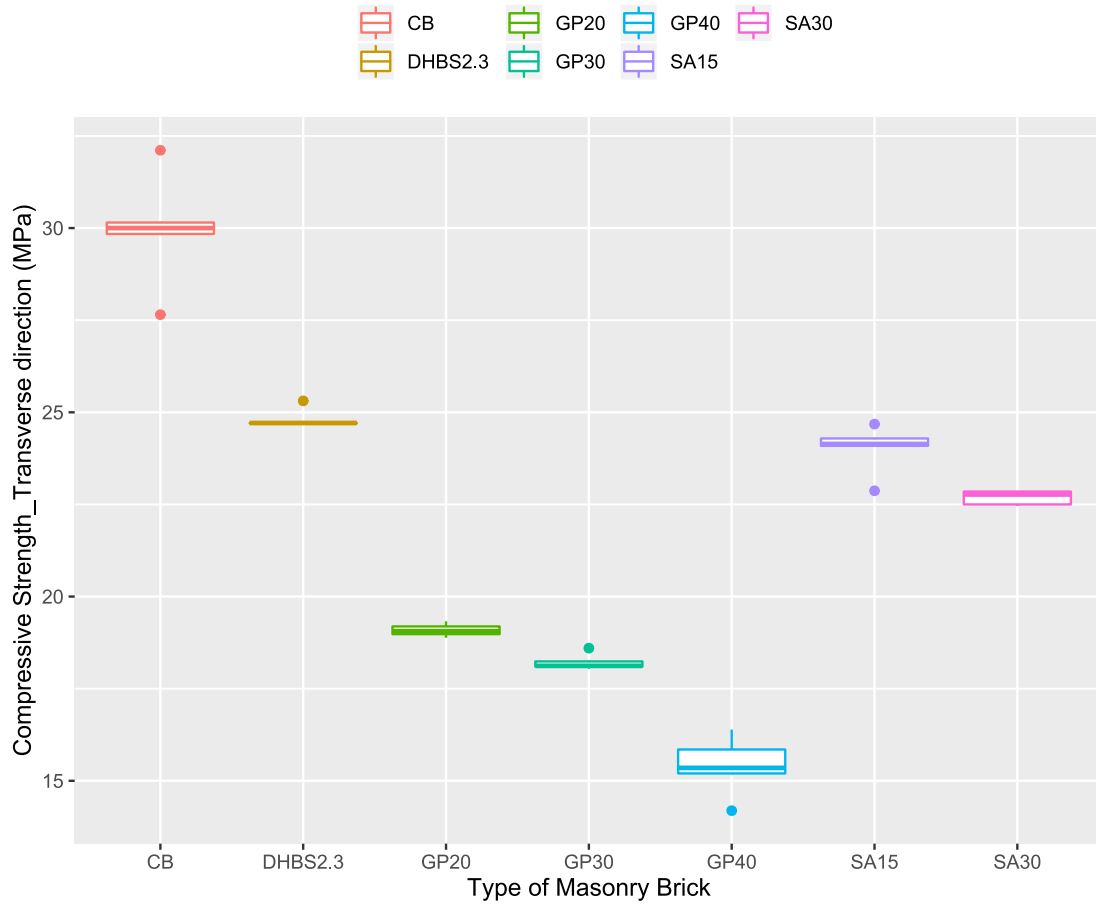
(b)

Figure 5-29(a): Average Compressive Strength (MPa)-Transverse Loading (b): Box plot for compressive strength_transverse of all bricks

5.1.3.2.2 Failure pattern

The Failure patterns observed for the control bricks as well as the hybrid bricks are shown in the figures below. A primary failure crack occurred in the form of shear cracks for all the bricks. The compressive strengths obtained are the strength corresponding to the load from the initial crack. Furthermore, all the failure modes were brittle as in the case of flexural and split tensile strength test.
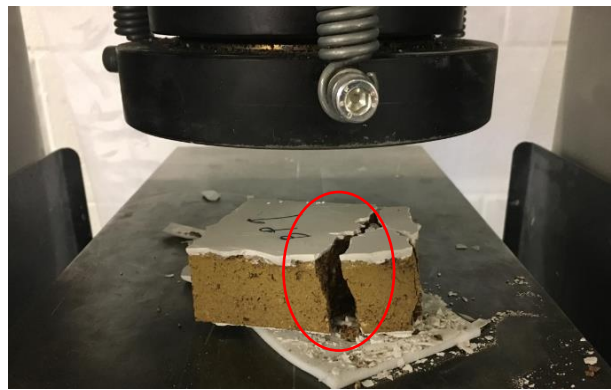
Figure 5-30: Failure crack pattern of Control bricks (CB)   *Figure 5-31: Failure crack pattern of DHBS*
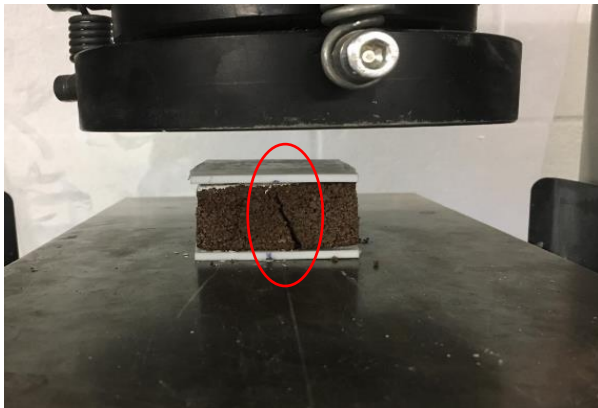
Figure 5-32: Failure crack pattern of GB-20   *Figure 5-33: Failure crack pattern of GB-30*

[93]
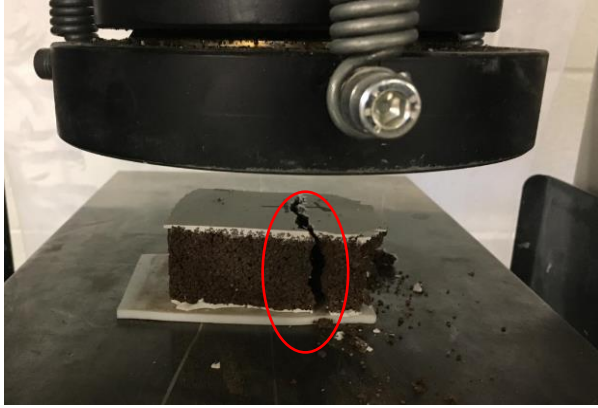
Figure 5-34: Failure crack pattern of GB-40   *Figure 5-35: Failure crack pattern of SSAB-15*
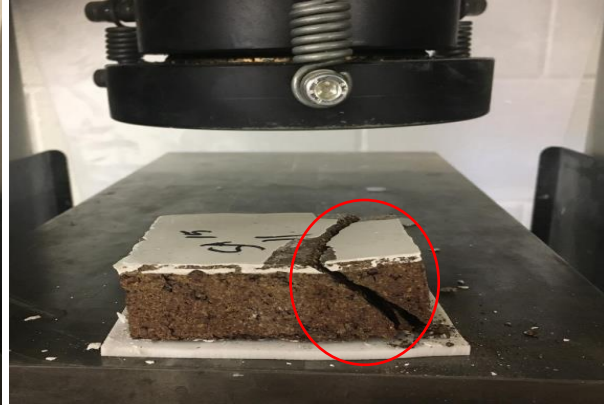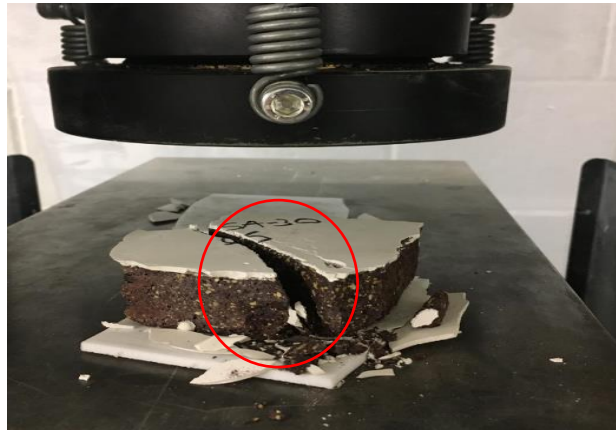
Figure 5-36: Failure crack pattern of SSAB-30

5.1.3.3 Compressive strength test-Longitudinal loading

The compressive strength test in longitudinal direction was performed by placing the half brick height-wise parallel to the bearing plate and the compressive load was applied at a uniform rate of 20N/s as per the standard. The sizes of the bricks were (70 mm ± 5 mm) x (58 mm ± 3 mm) x (26 mm ± 3 mm). The bearing sides were (58 mm ± 3 mm) x (26 mm ± 3 mm). To avoid friction, Teflon plates of size 60 x 30 x3 mm were placed on the top and bottom bearing surfaces of the brick.

5.1.3.3.1 Peak Load and compressive strength Calculation

The peak compressive and the respective compressive strength calculations of longitudinal loading are shown in the following tables.

Table 5-22 Compressive strength of the Control Bricks (CB)

P (kN)	Area of the specimen, H (mm)	Compressive Strength (MPa)
40.40	1465.87	27.56
42.25	1450.15	29.14
44.80	1426.57	31.40
41.30	1440.45	28.67
41.10	1506.52	27.28
		27.15

Table 5-23 Compressive strength of the Dried High Biopolymer Bricks (DHBS)

P (kN)	Area of the specimen, H (mm)	Compressive Strength (MPa)
43.70	1471.95	29.69
43.90	1445.73	30.37
43.80	1457.16	30.06
44.10	1503.85	29.32
42.20	1486.24	28.39
		29.57

Table 5-24 Compressive strength of the Geopolymer Bricks (GB-20)

P (kN)	Area of the specimen, H (mm)	Compressive Strength (MPa)
25.10	1464.49	17.14
24.50	1456.52	16.82
22.80	1501.30	15.19
25.40	1516.05	16.75
23.60	1454.76	16.22
		16.42

Table 5-25 Compressive strength of the Geopolymer Bricks (GB-30)

P (kN)	Area of the specimen, H (mm)	Compressive Strength (MPa)
22.40	1408.51	15.90
21.80	1458.78	14.94
21.30	1458.29	14.61
23.20	1477.91	15.70
23.10	1460.52	15.82
		15.39

Table 5-26 Compressive strength of the Geopolymer Bricks (GB-40)

P (kN)	Area of the specimen, H (mm)	Compressive Strength (MPa)
19.80	1462.76	13.54
18.60	1474.04	12.62
18.90	1469.43	12.86
19.10	1490.17	12.82
20.70	1476.04	14.02
		13.17

Table 5-27 Compressive strength of the Sewage Sludge Ash Bricks (SSAB-15)

P (kN)	Area of the specimen, H (mm)	Compressive Strength (MPa)
45.40	1506.30	30.14
46.80	1471.72	31.80
46.50	1467.14	31.69
44.50	1489.98	29.87
41.90	1504.09	27.86
		30.27

Table 5-28 Compressive strength of the Sewage Sludge Ash Bricks (SSAB-30)

P (kN)	Area of the specimen, H (mm)	Compressive Strength (MPa)
37.50	1486.51	25.23
36.40	1480.34	24.59
35.90	1451.04	24.74
36.80	1531.05	24.04
34.20	1467.30	23.31
		24.38
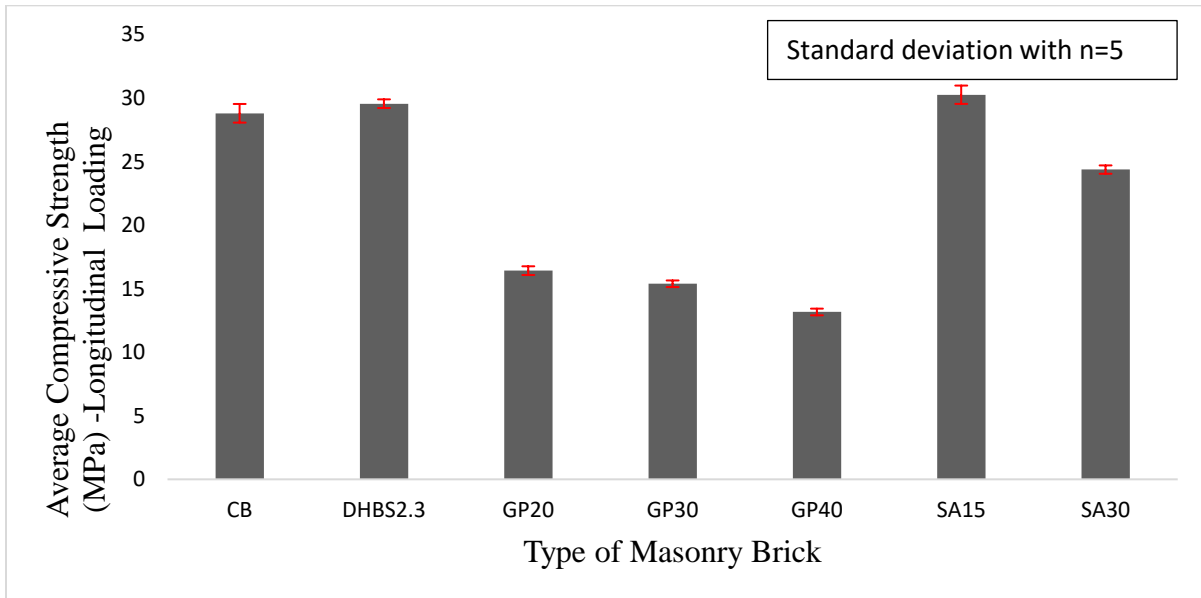
(a)
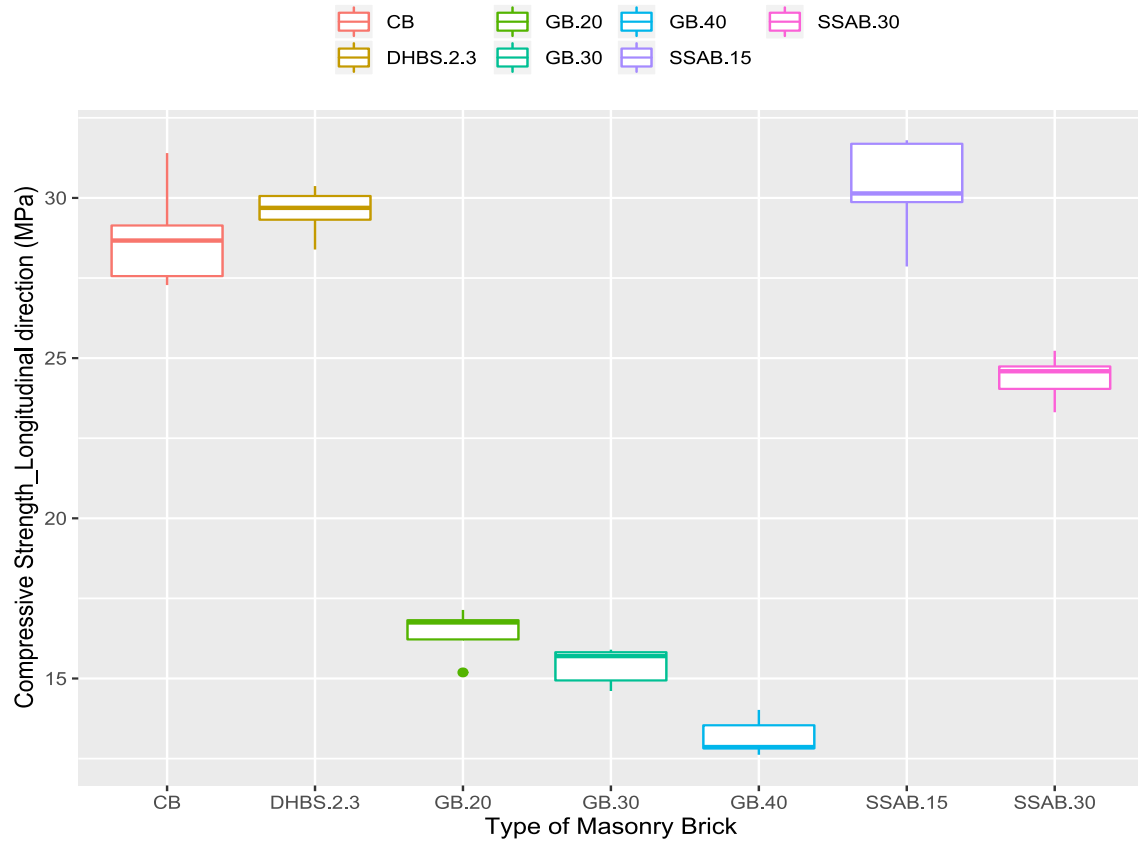
Figure 5-37 (a): Average Compressive Strength (MPa)- Longitudinal Loading (b): Box plot for compressive strength_longitudinal of all bricks

5.1.3.3.2 Failure pattern

The Failure pattern observed for all the brick types tested in the vertical direction under compression are depicted in the figures below. The failure crack occurred in the form of scaling of the outer layer of the brick followed by diagonal cracks for all the bricks. The compressive strength reported correspond to the load at the occurrence of the initial crack. Furthermore, all the failure modes were brittle as in the case of flexural and split tensile strength test.

Figure 5-38: Failure crack pattern of Control bricks (CB)

Figure 5-39: Failure crack pattern of DHBS

Figure 5-40: Failure crack pattern of GB-20

Figure 5-41 : Failure crack pattern of GB-30

Figure 5-42: Failure crack pattern of GB-40

Figure 5-43 :Failure crack pattern of SSAB-15

Figure 5-44: Failure crack pattern of SSAB-30

5.1.3.4 Comparison of Compressive strength in transverse and longitudinal loading

The compressive strength of the DHBS, SSAB-15 and SSAB-30 bricks was higher in the longitudinal direction than in the transverse directi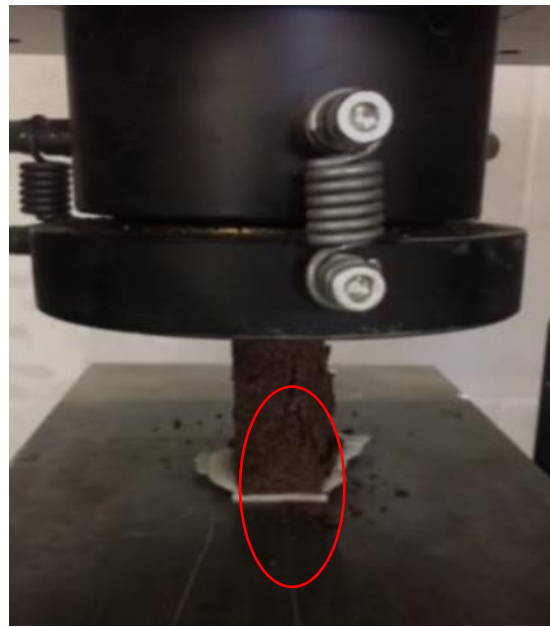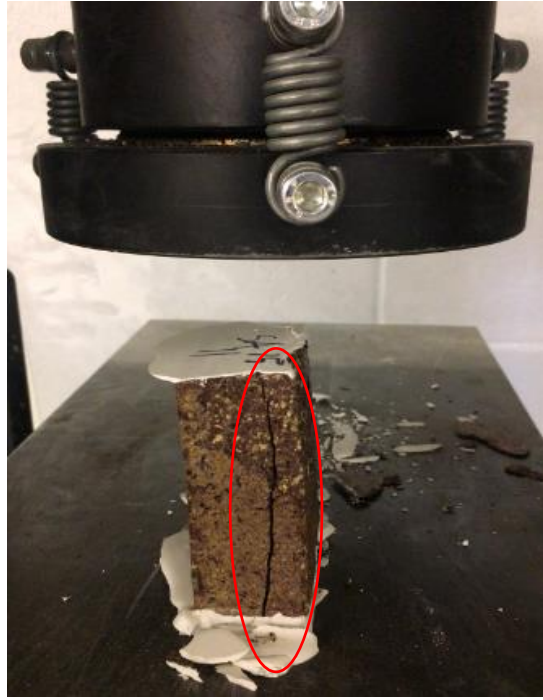on. For DHBS brick it was 19.04% higher in longitudinal direction, whereas in the case of SSAB-15 and SSAB-30 it was 25.4% and 7.5% higher, respectively. Similarly, for control brick and the GB bricks, the compressive strength in transverse direction is 20% less than the strength in longitudinal direction. For control bricks, the strength in longitudinal direction is 90.65% of the strength in transverse direction. Likewise, it's 87.2%, 85.4% and 87.39% for GB-20, GB-30, GB-40 respectively. Observing that the strength in the transverse direction may be expected t be twice as high as in the longitudinal direction, it is concluded that this might be due to brick orthotropy. In terms of the casting methodology, all the bricks are hand pressed with a plunger in transverse direction which makes the bricks denser in longitudinal axis and hence the commensurate compressive strength. The comparison of compressive strength in transverse and longitudinal loading is shown in Figure 5-44.
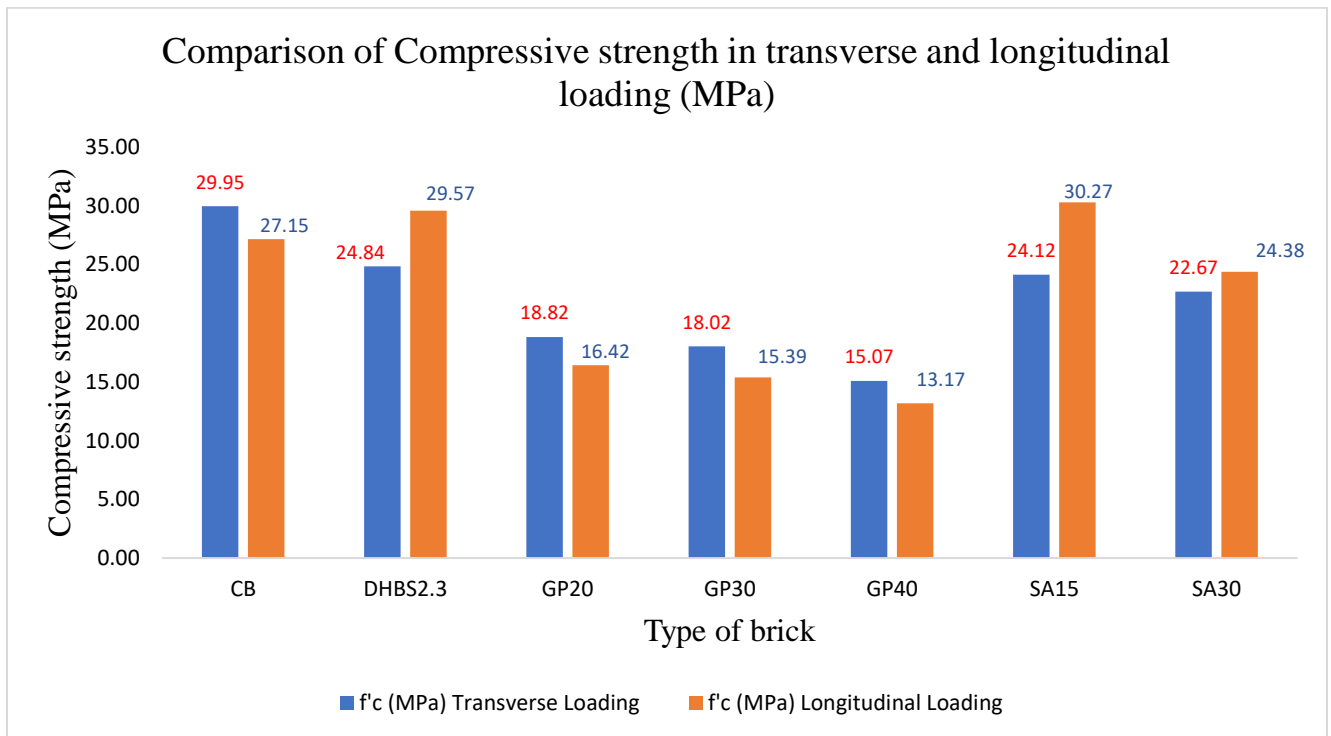

Figure 5-45: Comparison of compressive strengths in transverse and longitudinal loading.

5.2 Non-Destructive Tests

Prior to mechanical or physical testing, two non-destructive tests were conducted including Resonant Frequency Tests (RFT) and Ultrasonic Pulse Velocity Tests (UPV). Several researchers confirmed the suitability of the ultrasonic pulse velocity test and resonance frequency test methods for evaluating the degree of damage to the internal structure [e.g. Brozovsky et.al., 2017]. In the current research, the non-destructive tests were done for two reasons: (a) to determine the structure of defects if any in the bricks, and (b) to develop a database of test results that could be used to calibrate the destructive test results (mechanical properties) with the non-destructive measures.

5.2.1 Resonant Frequency Tests (RF)

Resonance frequency test measures the vibration of a structure that is exposed to dynamic loads. The resonant frequency test was done following the ASTM C215-Standard Test Method for Fundamental Transverse, Longitudinal, and Torsional Resonant Frequencies of Concrete Specimens. By initiating impacts at the midpoint of the specimen using a hammer, the accelerometer adhered on the specimen surface measures the frequency of the vibration. By changing the location of the impact, accelerometer allows testing for different modes of vibration. The accelerometer and the hammer is from The Dytran Dytranpulse™. The 7705 series accelerometer with advanced impulse sensing technology and the general purpose 5800 series hammer with a spherical striking end and a head weight of 100grams is used for the test. A typical test set up of the resonant frequency test in transverse mode is shown in Figure 5-45 [Giannini,2012]. In the current study, the transverse mode of vibration was excited.

The elastic dynamic modulus was obtained from the frequency or the measured velocity of stress waves passing through the material from the transverse mode of vibration. The signal from the accelerometer with the impact has been converted into the frequency by using a data acquisition software called CatmanAP DAQ V4.1.2. The evaluation of elastic dynamic mechanical properties can be very useful for the safety assessment of structures exposed to dynamic loading conditions. For the current test, two rubber strips are used to keep the brick simply supported. The distance to the support from the end of the brick was 0.122L as per ASTM C215.Also, in order to hold the accelerometer in position during the impact, an elastic band was used to tie it the specimen.
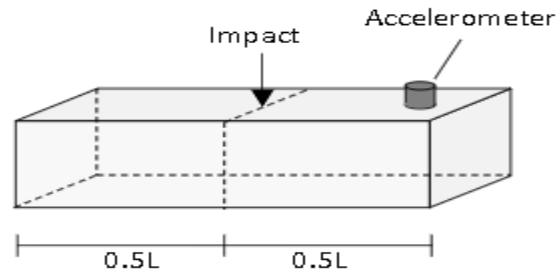
Figure 5-46:A representation of the resonant frequency test in transverse mode (Giannini, 2012).
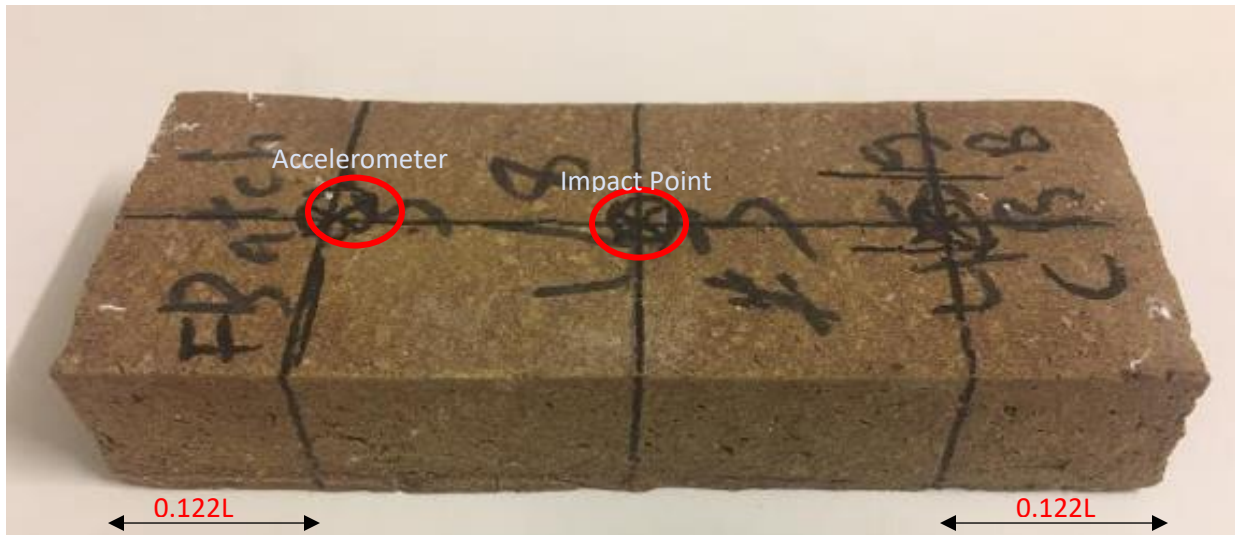
(a)

(b)

Figure 5-47 (a) (b) : A typical test set up of the resonant frequency test in transverse mode

The recorded response from the impact is in the form of acceleration versus time graph as shown in Figure 5-48(a.) The acceleration - fundamental frequency graph is then obtained from the acceleration-time graph as shown in Figure 5-48(b):
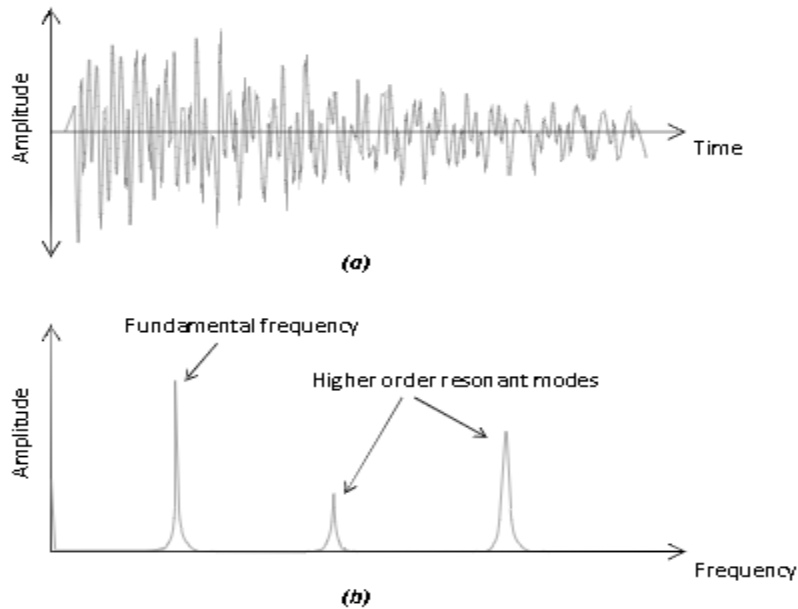
Figure 5-48: (a) acceleration-time graph; (b) acceleration- fundamental frequency graph (Kreitman 2011).

5.2.1.1 Calculation of transverse resonant frequency and Dynamic Modulus of Elasticity

Transverse resonant frequency has been calculated as per the standard on all fourteen bricks before carrying out any other tests. The sample Acceleration-time and Acceleration-frequency graphs for all categories of brick from the experiment are shown below.
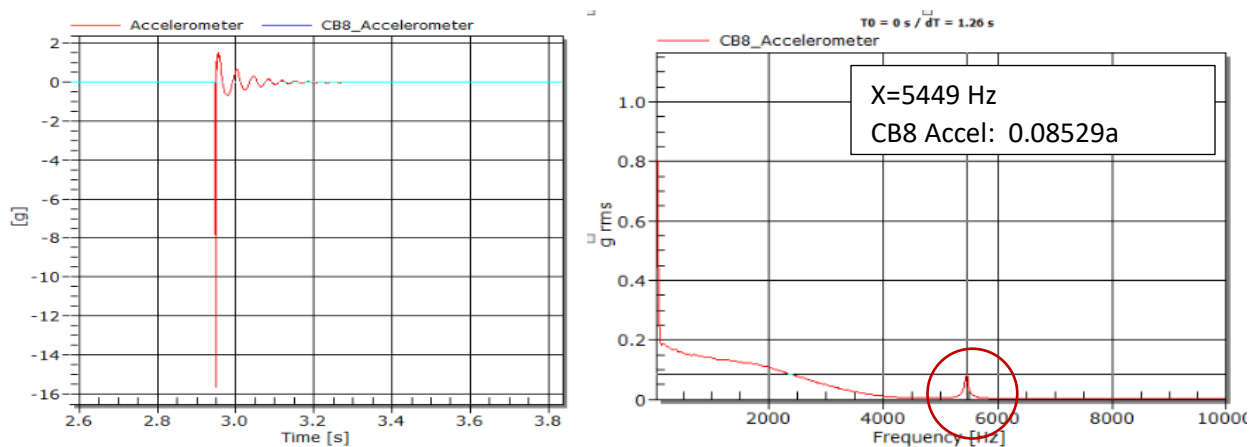
Figure 5-49: Transverse resonant frequency for Control Brick
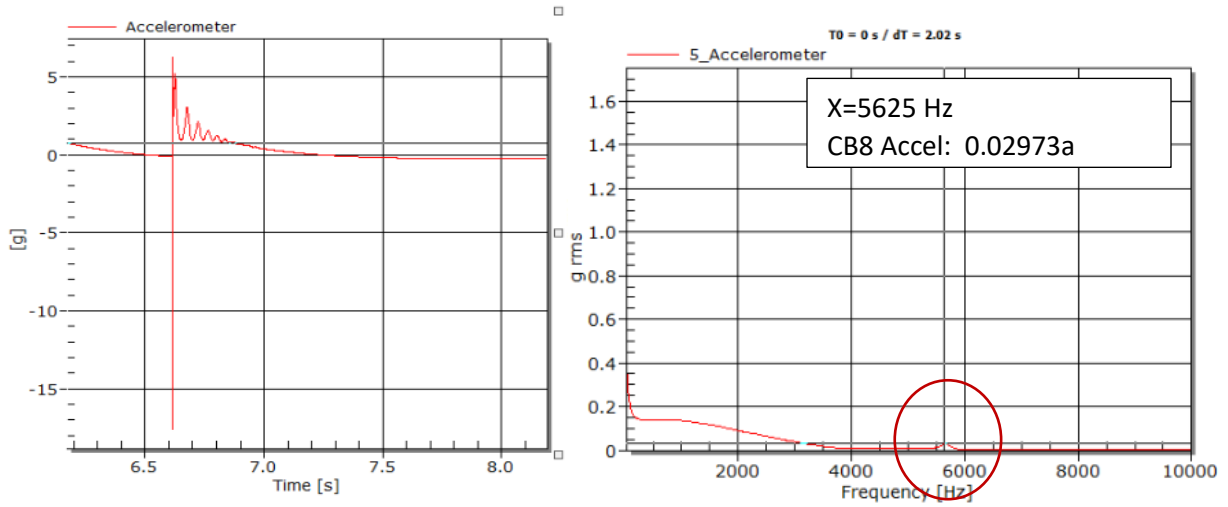
Figure 5-50: Transverse resonant frequency for Dried High Biopolymer Brick (DHBS)
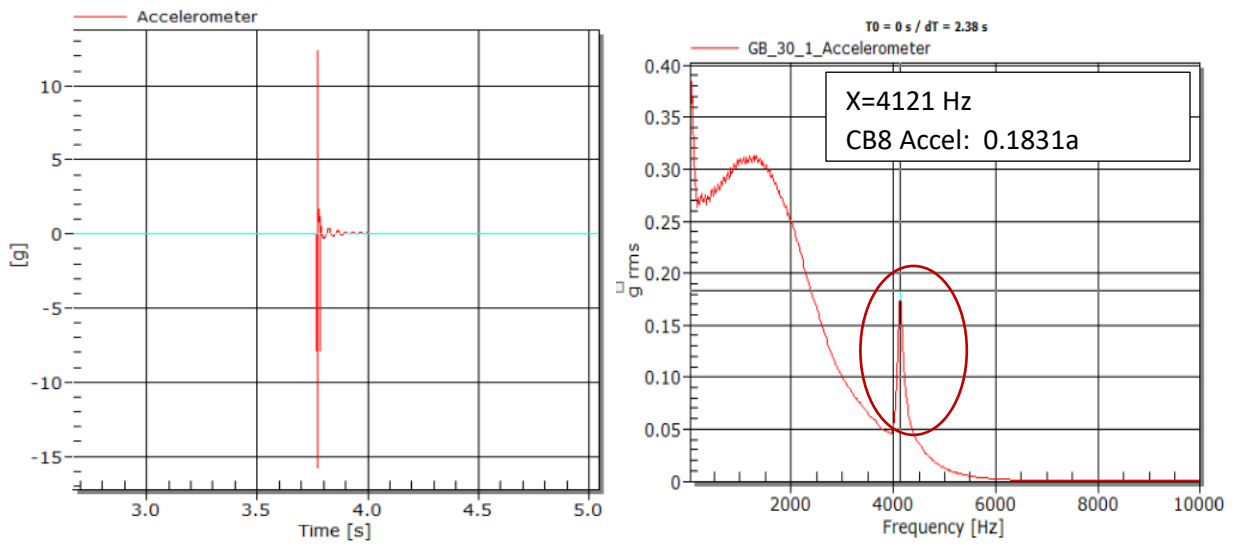
Figure 5-51:Transverse resonant frequency for Geopolymer(GB-20) Brick
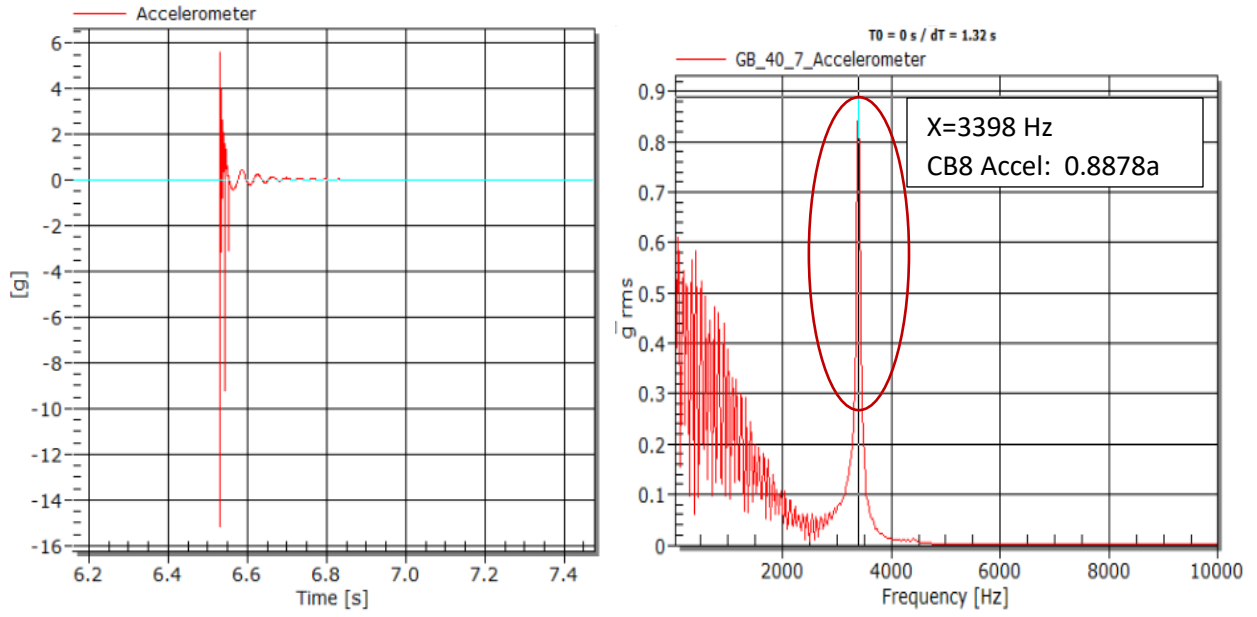
Figure 5-52: Transverse resonant frequency for Geopolymer(GB-30) Brick
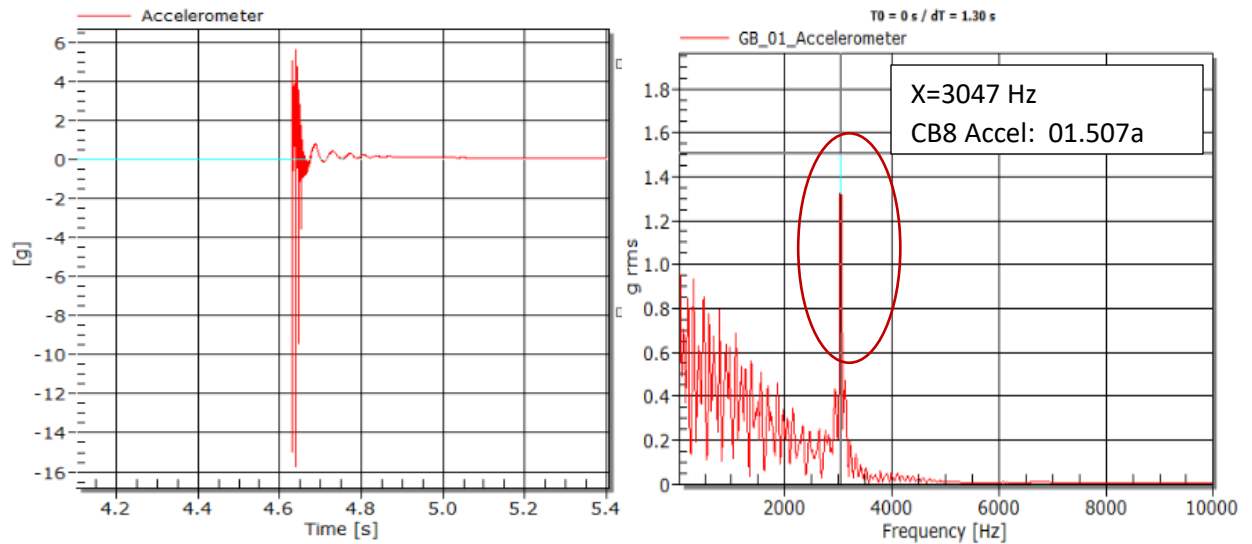
Figure 5-53: Transverse resonant frequency for Geopolymer(GB-40) Brick
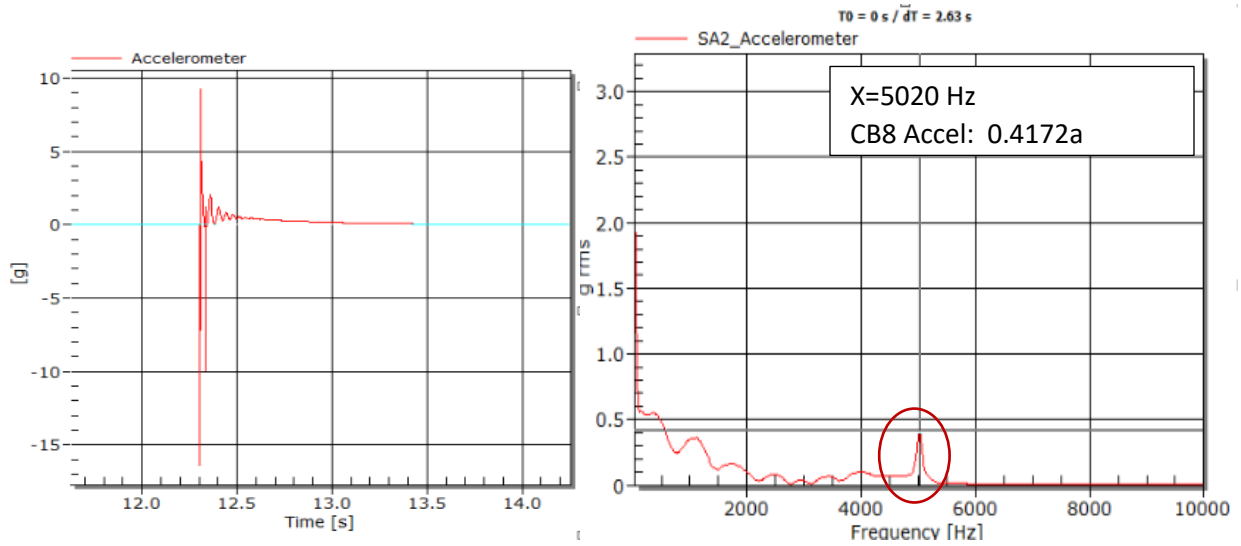
Figure 5-54: Transverse resonant frequency for Sewage Sludge Ash (SSAB-15) Brick
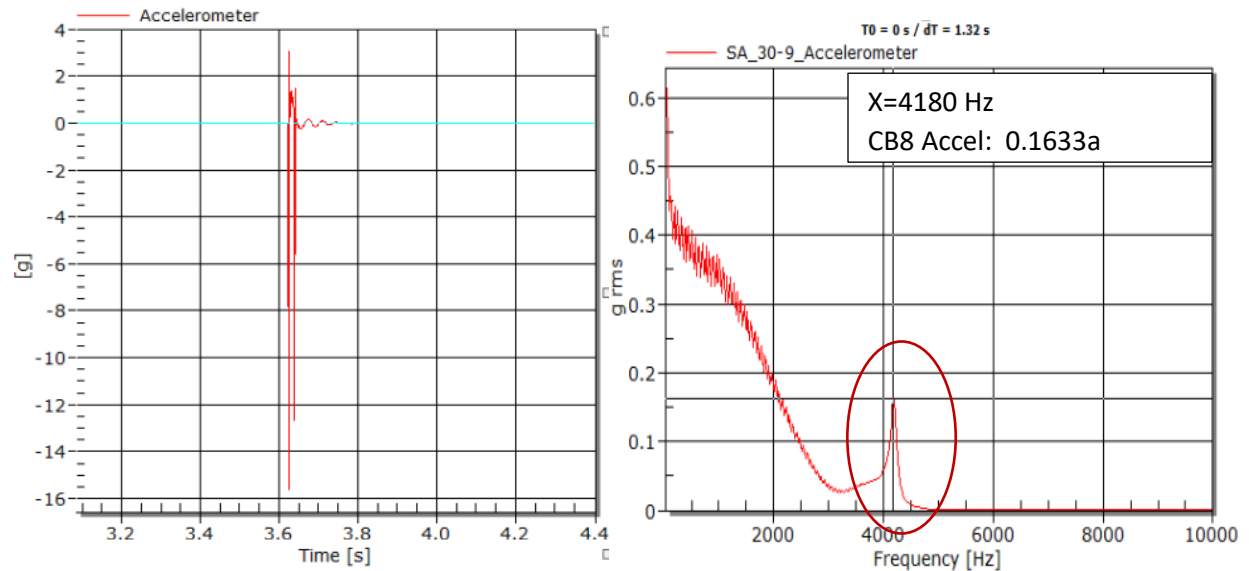
Figure 5- 55: Transverse resonant frequency for Sewage Sludge Ash (SSAB-30) Brick

The transverse resonant frequency test was done on each of the fourteen masonry units from all categories. The results from the transverse resonant frequency tests for each brick are shown in the Figure 5-56(a) and the average resonant frequency for all the categories of brick are given in Figure 56(b) below:
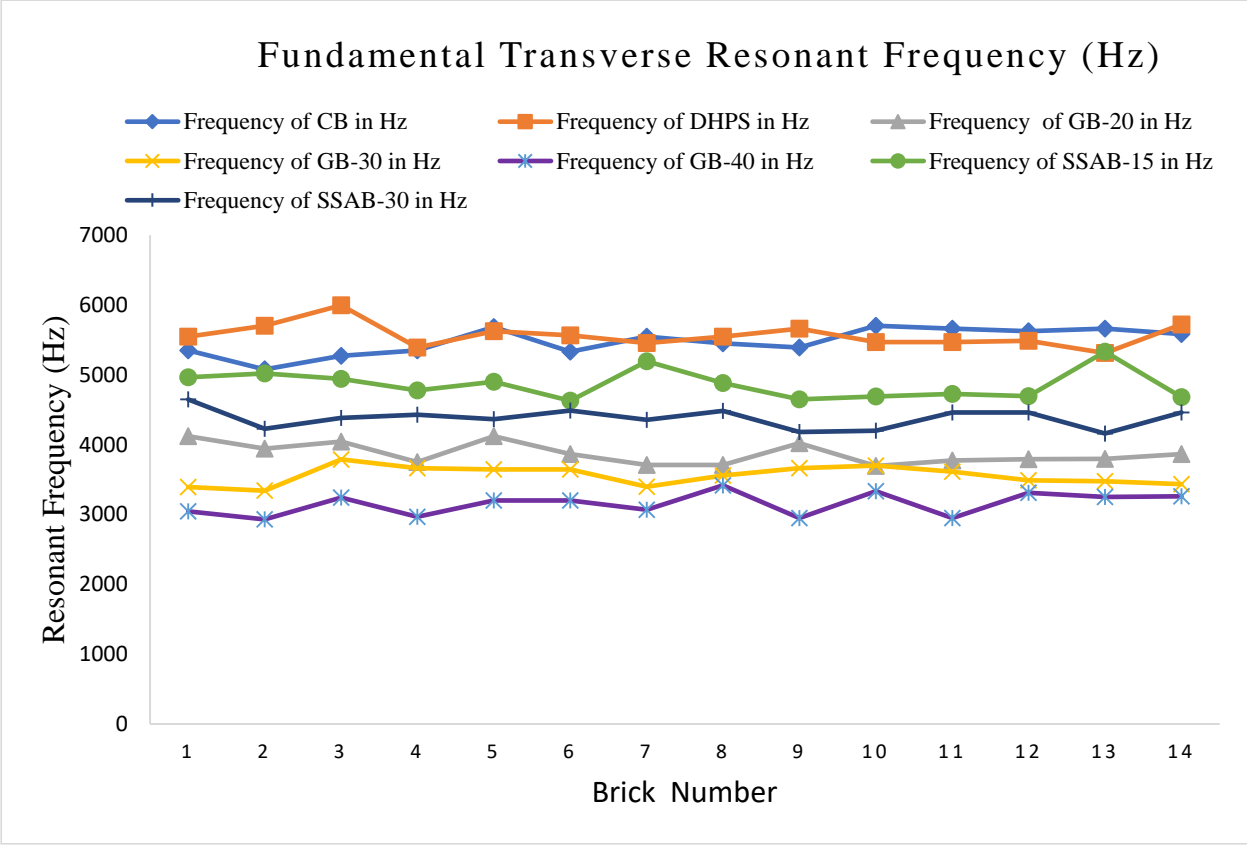
Figure 5-56(a): Fundamental Transverse Resonant Frequency for each brick tested (Hz)

(b)

[108]
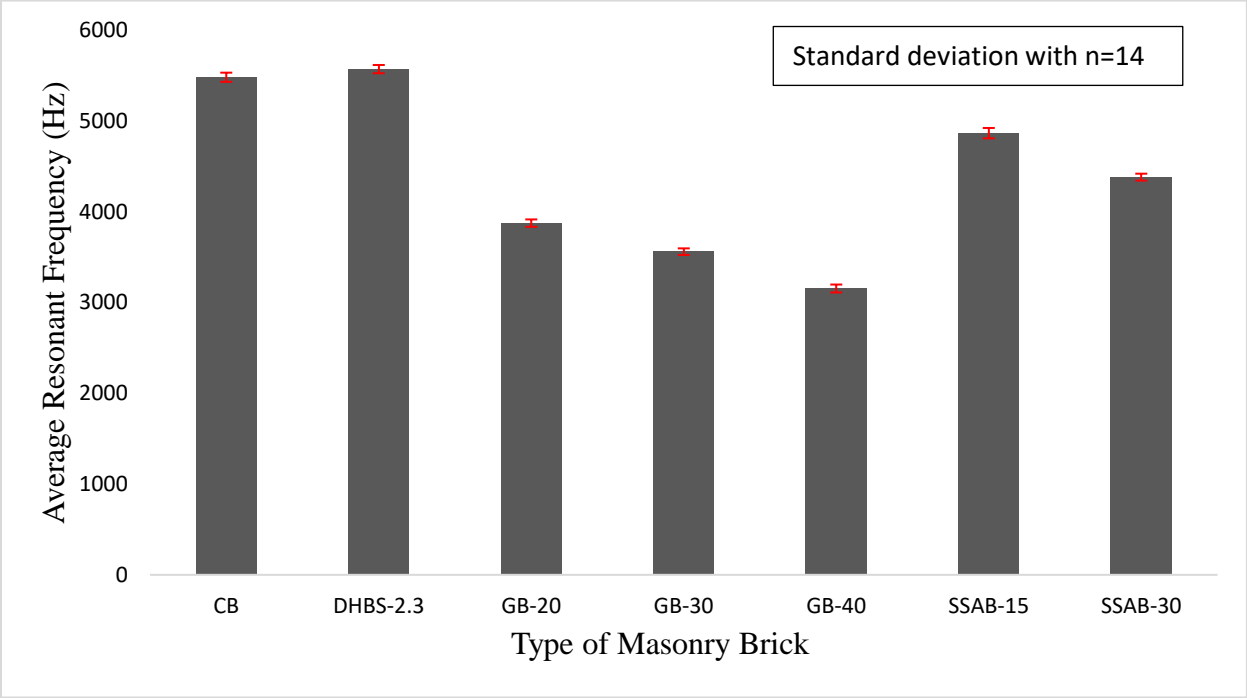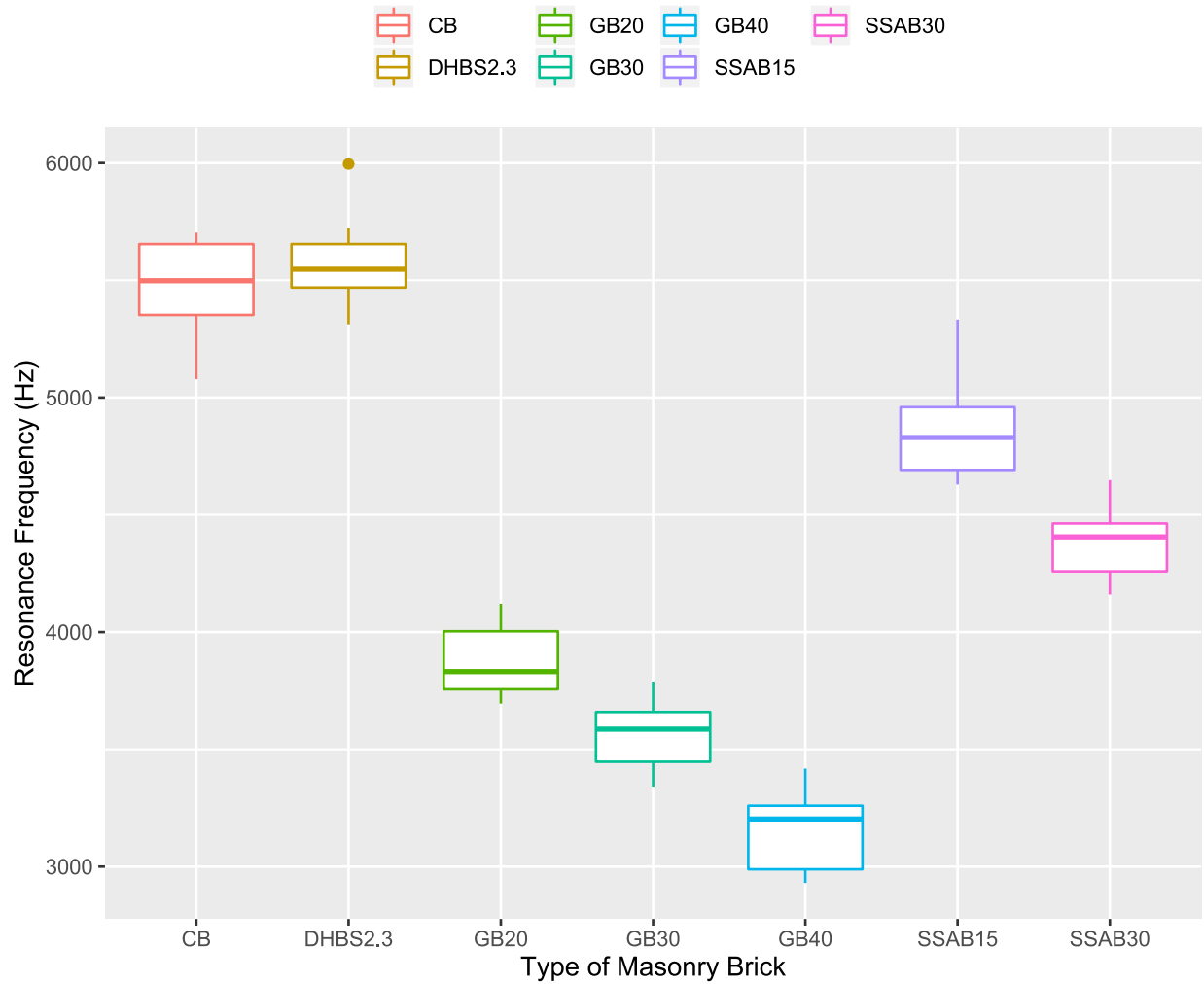
(c)

Figure 5-56(b): Average Fundamental Transverse Resonant Frequency (Hz) (c): Box plot for the RFT of individual brick

According with the relevant standard, the Elastic dynamic Young's modulus has been calculated from the fundamental transverse resonant frequency using the Equation (5.4):

$$Dynamic\ E = CMn^2 \qquad\qquad (5.4)$$

where:

M = is the Mass of specimen in kg,

n = is the Fundamental transverse frequency in Hz,

C= is a calibrated constant, equal to 0.9464 (L^3T/bt^3) in $N \cdot s^2$ for a prism,

L = is the Length of Brick, in m,

t, b = are the dimensions of cross section of Brick in m, t being measured in the direction in which the impact is driven, and

T = is a correction factor that depends on the ratio of the radius of gyration (K) to the length of the specimen, L, and on Poisson's ratio,

K = t/3.464. For bricks of the size tested in this program, it follows that K==0.026/3.464 =7.51m

Taking Poisson's ratio, μ =0.2, with the K/L =7.51/0.14 = 0.05, corresponding to μ, the correction factor T is obtained from Table 1 (Table 5-29) of ASTM C-215 as being equal to 1.2.

Table 5-29 Values of Correction Factor, T

K/L	Value of TA			
	μ=0.17	μ=0.20	μ=0.23	μ=0.26
0.00	1.00	1.00	1.00	1.00
0.01	1.01	1.01	1.01	1.01
0.02	1.03	1.03	1.03	1.03
0.03	1.07	1.07	1.07	1.07
0.04	1.13	1.13	1.13	1.14
0.05	1.2	1.2	1.21	1.21
0.06	1.28	1.28	1.29	1.29
0.07	1.38	1.38	1.39	1.39
0.08	1.48	1.49	1.49	1.5
0.09	1.6	1.61	1.61	1.62
0.1	1.73	1.74	1.75	1.76
0.12	2.03	2.04	2.05	2.07
0.14	2.36	2.38	2.39	2.41
0.16	2.73	2.75	2.77	2.8
0.18	3.14	3.17	3.19	3.22
0.2	3.58	3.61	3.65	3.69
0.25	4.78	4.84	4.89	4.96
0.3	6.07	6.15	6.24	6.34

The dynamic Young's modulus of elasticity has then been calculated for all the categories of brick. The average value of the Young's modulus of elasticity is given in Figure 5-57:
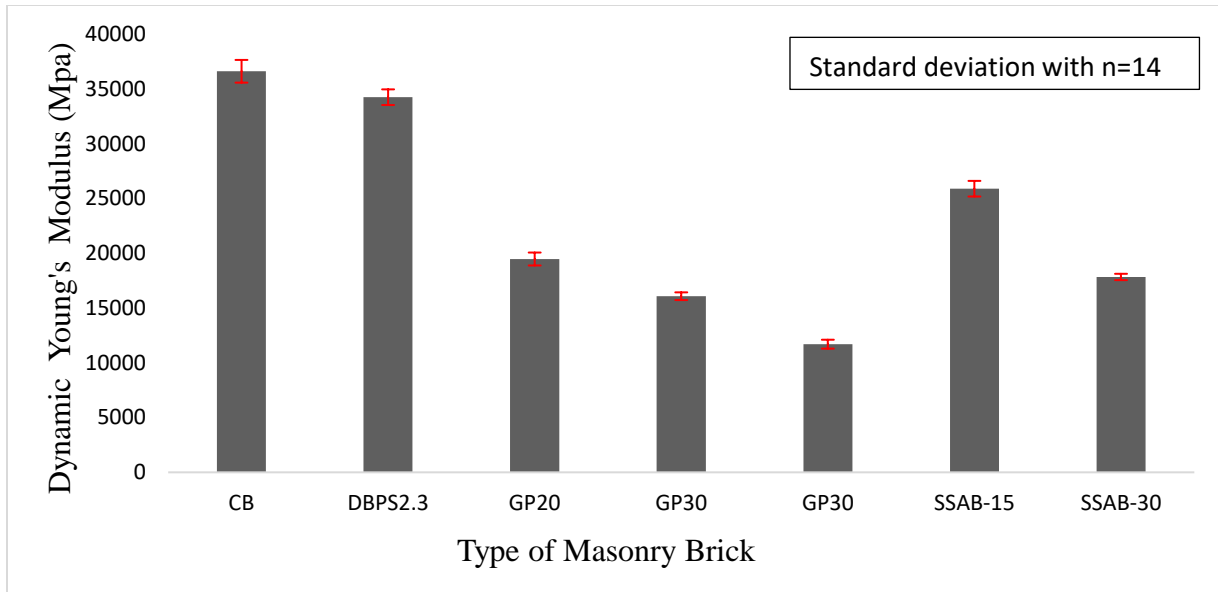
(a)
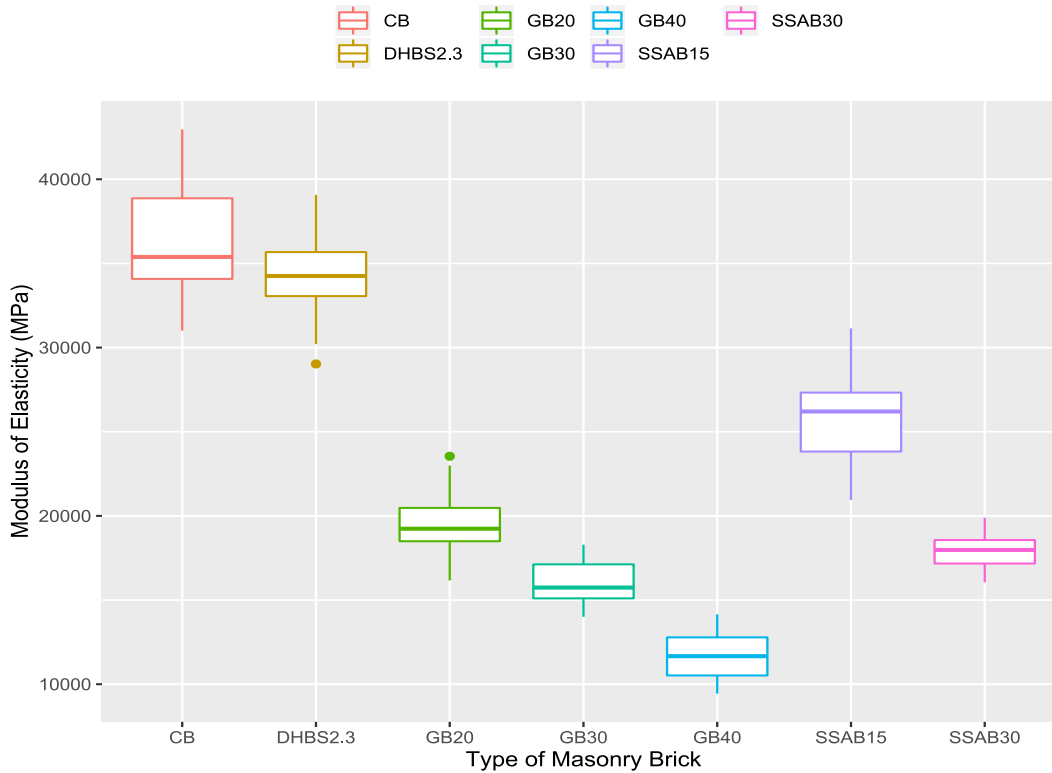
(b)

Figure 5-57(a): Dynamic Young's Modulus (MPa) of the masonry brick from transverse resonant frequency Test (b): Box plot for Dynamic Young's Modulus

5.2.2 Ultrasonic Pulse Velocity Test (UPV)

The second non-destructive test performed was the Ultrasonic Pulse Velocity Test (UPV) as per ASTM D2845-08, Standard Test Method for Laboratory Determination of Pulse Velocities and Ultrasonic Elastic Constants of Rock. The ultrasonic pulse velocity method is used for the determination of brick uniformity, cracks or voids' presence, and the changes in properties that occur with time. The working principle of this test is based on propagation of high-frequency sound wave through the brick. The pulse velocity of the brick depends on the density of the material. For a material with higher density, the pulse velocity would be higher because of the lowest transit time of the ultrasonic pulse through the material. Similarly, for a material with lower density, the pulse velocity would be smaller because of the longest transit time of the ultrasonic pulse through the material.

The experimental set up for this test consists of transmitting and receiving transducers of bandwidth 54 kHz and 50 mm x 46 mm diameter and length respectively, and the PUNDIT® PL-200 reading display unit from the manufacturer (Co mmercial name is Proceq). The PUNDIT® PL-200 instrument measures the ultrasonic pulse velocity from the transmitting transducer to the receiver transducer along the shortest path through the brick. For the accurate reading of pulse velocity from the device, a proper contact between the transducers and the brick surface is necessary. This has been achieved by the use of a couplant, i.e., a jelly liquid that helps to keep proper contact between the transducers and the brick surface.

The ultrasonic pulse velocity test has been conducted on all the bricks that were intended for being subsequently tested in compression. So, a total of five brick from each brick category has been tested for UPV. The test set up of UPV is shown in Figure 5-58. The test results are given in Figure 5-59.

(a)   (b)

Figure 5-58 (a): UPV set-up; (b) : Conducting UPV test in the Civil Egineering Highbay laboratory
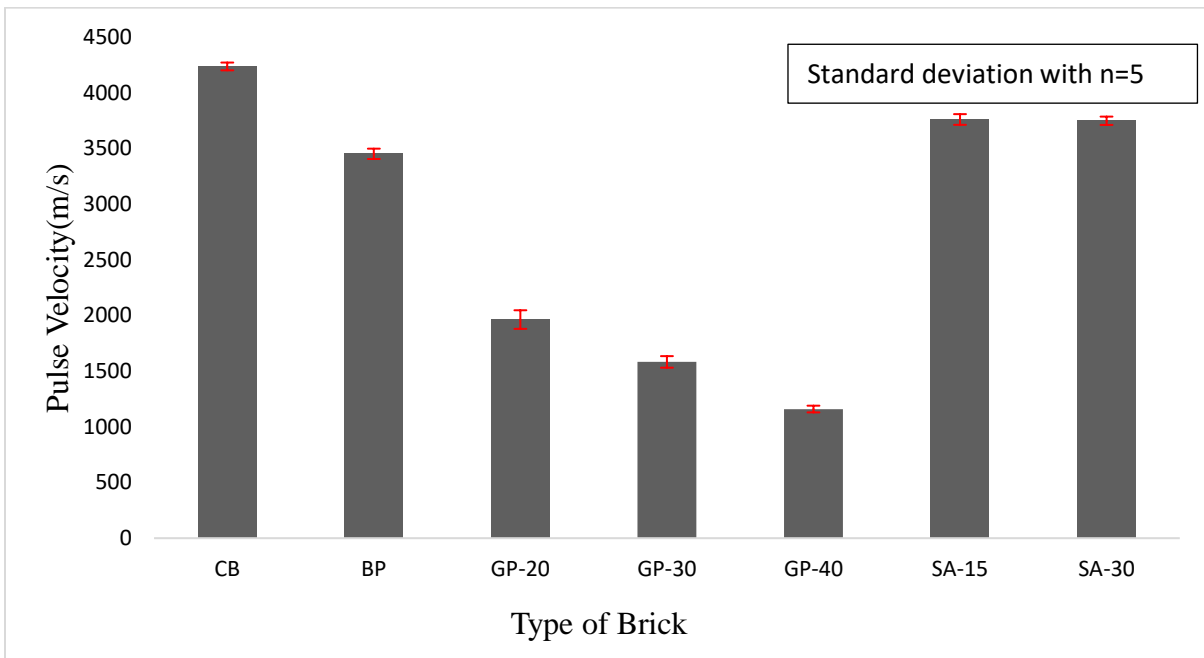
(a)
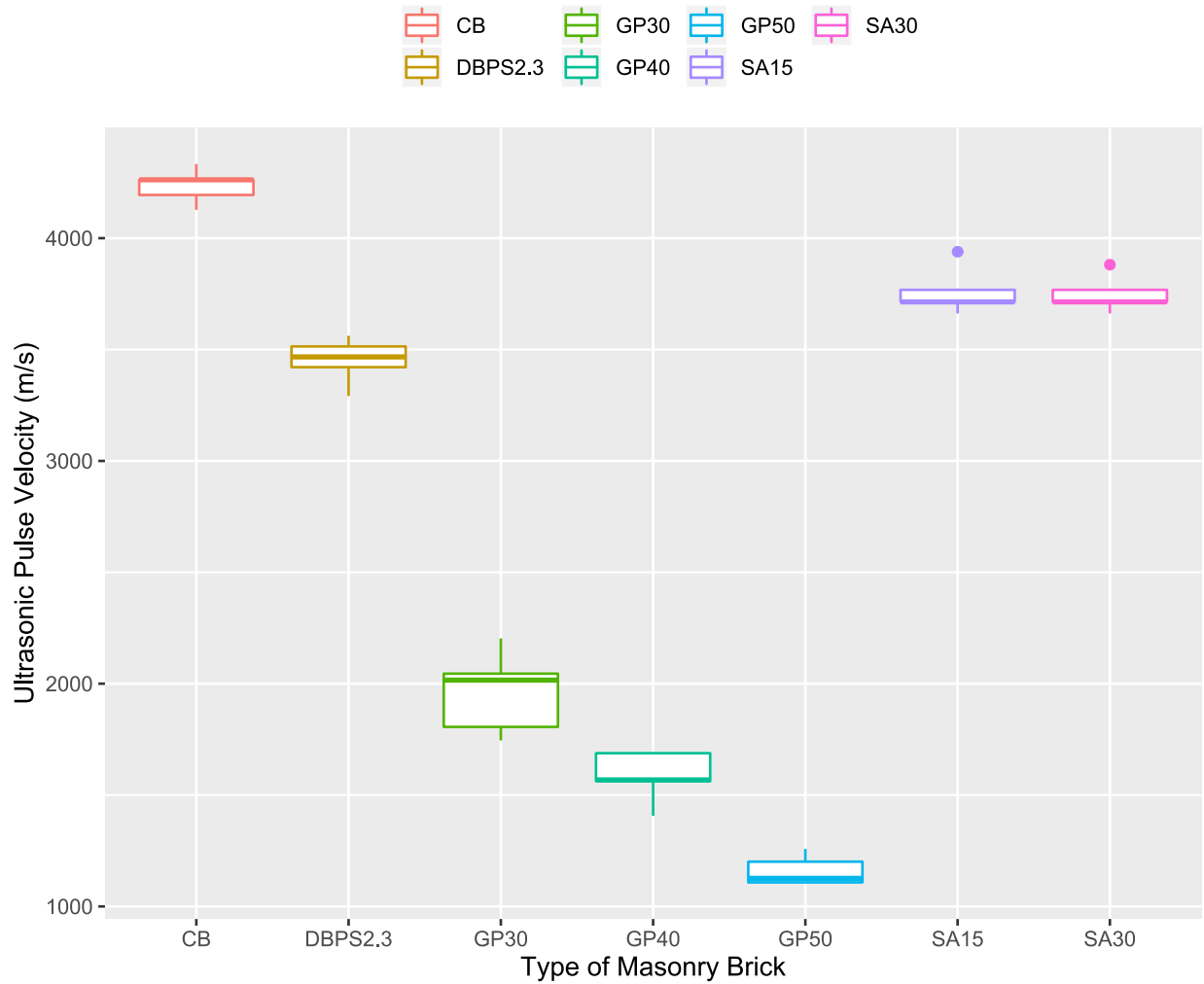
(b)

Figure 5-59 (a): Ultrasonic pulse velocity of masonry bricks (b) Box plot for the Ultrasonic pulse velocity of the brick

5.3 Water Absorption Tests

Water absorption is another important qualitative parameter that needs to be considered in the assessment of masonry bricks. Both cold-water absorption and hot-water absorption tests were performed as per ASTM C-67 Standard Test Methods for Sampling and Testing Brick and Structural Clay Tile. Further, both tests were done on five bricks that have undergone the split-tensile strength or the flexural strength test.

5.3.1 Cold-Water Absorption Tests

All the loose particles on the five bricks were ground off and were subjected to the cold-water absorption test after ensuring that they were crack free. Five half bricks from each category were used and all these bricks were weighed before test was commenced in order to obtain the dry weight of the specimen. For the saturation, these bricks were then submerged in distilled water at 24°C for 24 hours. Then the bricks were removed from the bath and the surface water was wiped off with a paper towel and the individual half brick was weighed within five minutes.

The cold-water absorption was calculated using Equation (5.5):

$$\text{Absorption, \%} = 100\,(W_s - W_d)\,/\,W_d \tag{5.5}$$

where:

W_d = Dry weight of the half brick in grams, and

W_s = Saturated weight of the half brick after submersion in cold water for 24 hours in grams.

The Figure 5-59 below shows the bricks under the cold-water absorption test whereas the Figure 5-60 below shows the average cold-water absorption of the bricks.

Figure 5-60: Cold-water absorption test
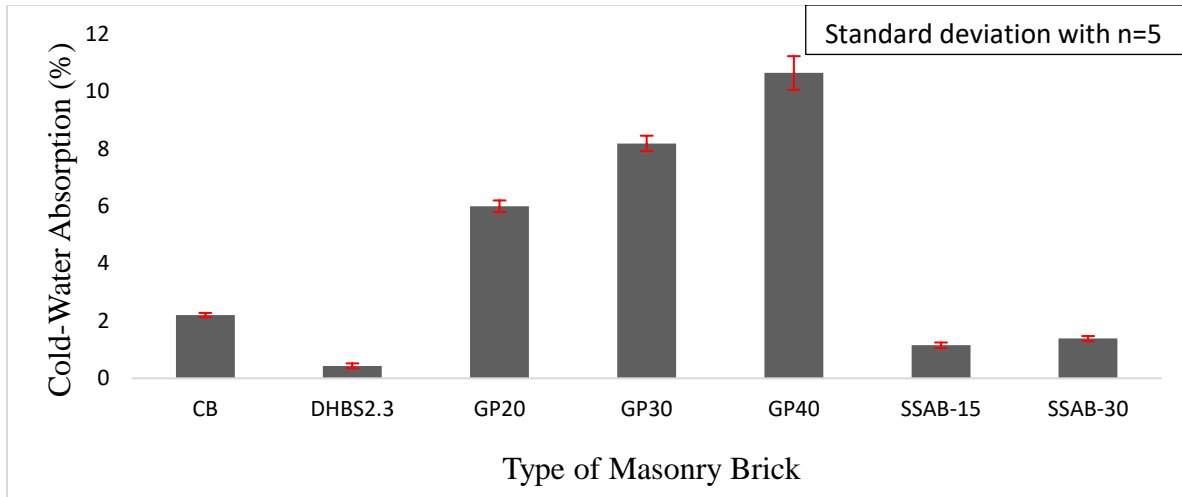
Figure 5-61: Cold water absorption of the masonry bricks

As per the CAN/ CSA A82– Material standards for Fired masonry brick made from clay or shale, the percentage of cold-water absorption should be less than 15% of the total weight of the brick for the first-class bricks. For all the bricks tested for the CWA, the percentage was less than 11% by the weight of the brick. It is noteworthy that the cold-water absorption test shows the opposite trends than the mechanical strength properties: where water absorption is lowest the strength is highest. This is an indication that connected capillary pores are related to the material mechanical performance. It is also worth noting that despite the low ratio of shale replacement by organic solids, the DHBS specimens we the most resilient to water absorption thereby indicating better durability prospects.

5.3.2 Hot-Water Absorption Tests

The hot-water absorption was done on the same bricks after completing the 24 hours cold water absorption test. With the existing saturation on the bricks, all of them again were submerged in distilled water and placed inside the oven to get the system boiled. The bricks were left in the oven at 100°C to boiling for an hour. They were then taken out of the oven after cooling by the natural loss of heat. Then the specimens was taken out of the water bath and the surface water was wiped off the with a paper towel. Specimens were weighed to obtain the hot water saturated weight of the bricks.

The hot-water absorption of the bricks was calculated using Equation (5.6):

$$\text{Absorption, } \% = 100(W_b - W_d) / W_d \qquad (5.6)$$

[116]

where:

W_d = is the dry weight of the half brick in grams, and

W_b = is the saturated weight of the half brick after submersion in boiling water for an hour in grams.

Figure 5-61 plots the average hot-water absorption of the bricks.
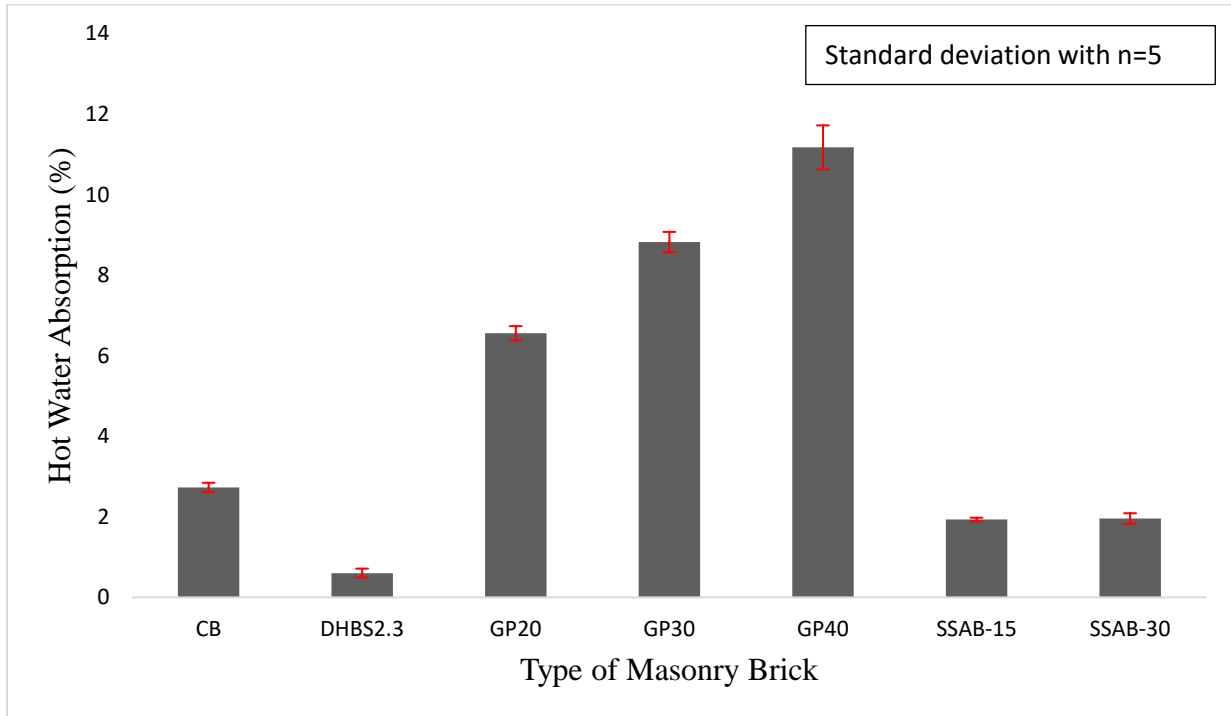
Figure 5-62: Hot-water absorption of the masonry bricks

As per the CAN/ CSA A82, the percentage of hot water absorption should be less than 17% of the total weight of the brick. For all the bricks tested for the HWA, the percentage was less than 12% by the weight of the brick.

5.3.3 Saturation Coefficient (SC)

Saturation coefficient is the ratio between the cold-water absorption and the hot water absorption. The SC has been calculated using Equation (5.7):

$$\text{Saturation coefficient} = (W_s^2 - W_d) / (W_b^5 - W_d) \tag{5.7}$$

Where,

[117]

W_d = dry weight of the half brick in grams**,**

W_s^2 = saturated weight of the half brick after 24 hours submersion in cold water, and

W_b^5 = saturated weight of the half brick after an hour submersion in boiling water.
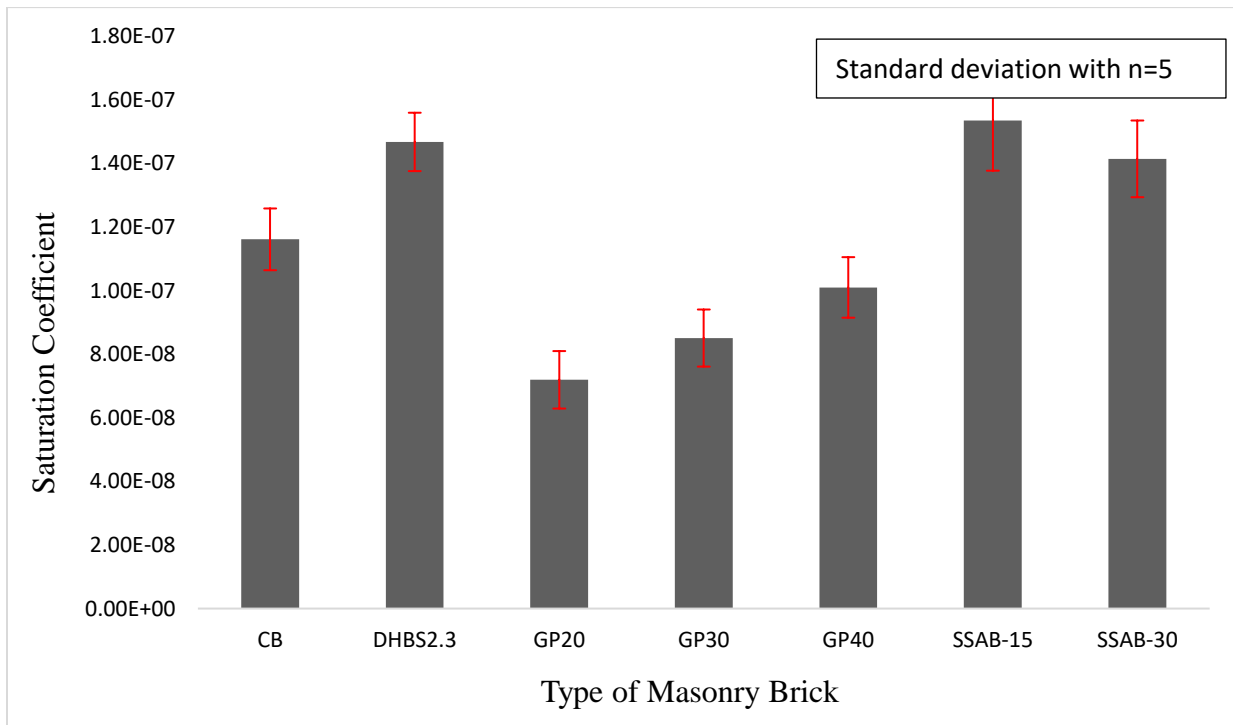
Figure 5-63: Saturation Coefficient of the masonry bricks

As per the CAN/ CSA A82, the value of saturation coefficient is not applicable for the bricks having the cold-water absorption less than 8% or if the SC value is less than 0.78. In the current research, for all the hybrid bricks except for the GB-30 and GB-40, the CWA value was found to be less than 8%. For the GB-30 and GB-40, the SC value was 8.2% and 10.7% respectively. However, the SC value was less than 0.78 even in these cases.

5.4 Efflorescence Test

The same bricks used for the water absorption tests were also used to test the efflorescence performance or the leaching out of salt from inside of the brick when exposed to water. In order to carry out this type of test as per ASTM C-67 Standard Test Methods for Sampling and Testing Brick and Structural Clay Tile, all the five bricks from each category were placed in an aluminium

tray of 50 mm depth with water depth of 25.4 mm, in a room with 24 °C for seven days. At the end of seven days, all the bricks were dried in the oven at 100°C. After drying, no sign of efflorescence was found for any of the bricks. Figure 5-64 shows the bricks placed in the setup for the efflorescence test and their appearance after the efflorescence test.

Figure 5-64 (a): The bricks placed in the tray for efflorescence test (b): Appearance of the bricks after the efflorescence test.

5.5 Freeze-Thaw Test

The few bricks from the splitting tensile strength test and the three cubes from each category were used to test for the freeze-thaw resistance as per ASTM C-67 Standard Test Methods for Sampling and Testing Brick and Structural Clay Tile. Five bricks from each category were placed in a thawing tank as shown in Figure 5-65 for 4 hours. Then the bricks were placed in a freezing chamber of -18±5°C in an aluminium tray with one of the ends in upwards position. The spacing between all the bricks was ensured to be 10±5 mm as shown in Figure 5-67. Water was then poured in the aluminium tray to a depth of 13 mm and kept in the freezing chamber for 20 ± 1 hours. After 20 ± 1 hours the bricks with the tray were immersed completely in the thawing tank for 4±0.5hours. So, a full cycle was 24 hours, and the tests continued for 50 cycles.

Figure 5-65 :   Bricks in the thawing tank

Figure 5-67: Bricks inside the freezing chamber

The Percent weight loss after 50 cycles of freeze-thaw for the SSAB and DHBS brick were much lower than the CB. However, for the GB brick, it was between 1.21 and 2.12% of the total weight of the brick.
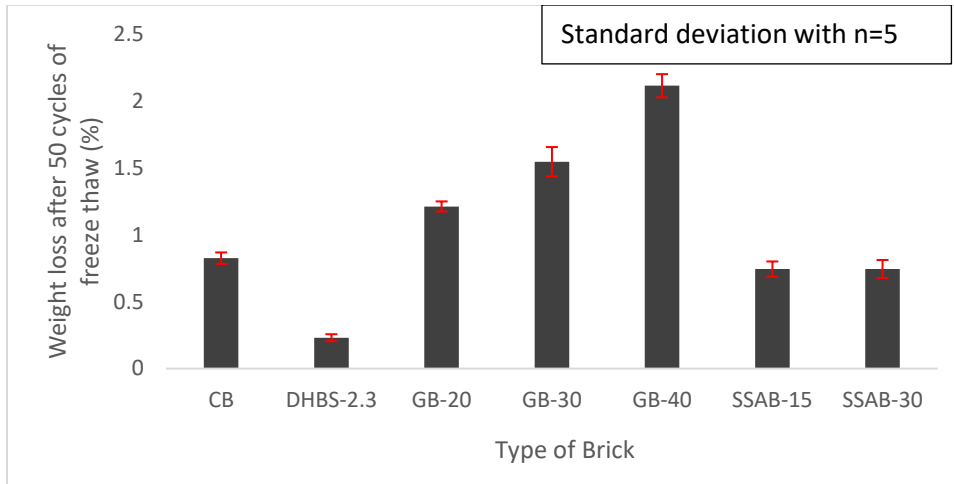
Figure 5-68: Average weight loss after 50 cycles of freeze-thaw

5.6 Weight of the Bricks

All the bricks were weighed before conducting any tests on them. The average weight of each category of the bricks are shown in Figure 5-68. The dried high biopolymer bricks and sewage sludge ash bricks with 15% and 30% shale replacement, were found lighter when compared with all other category of the bricks made.
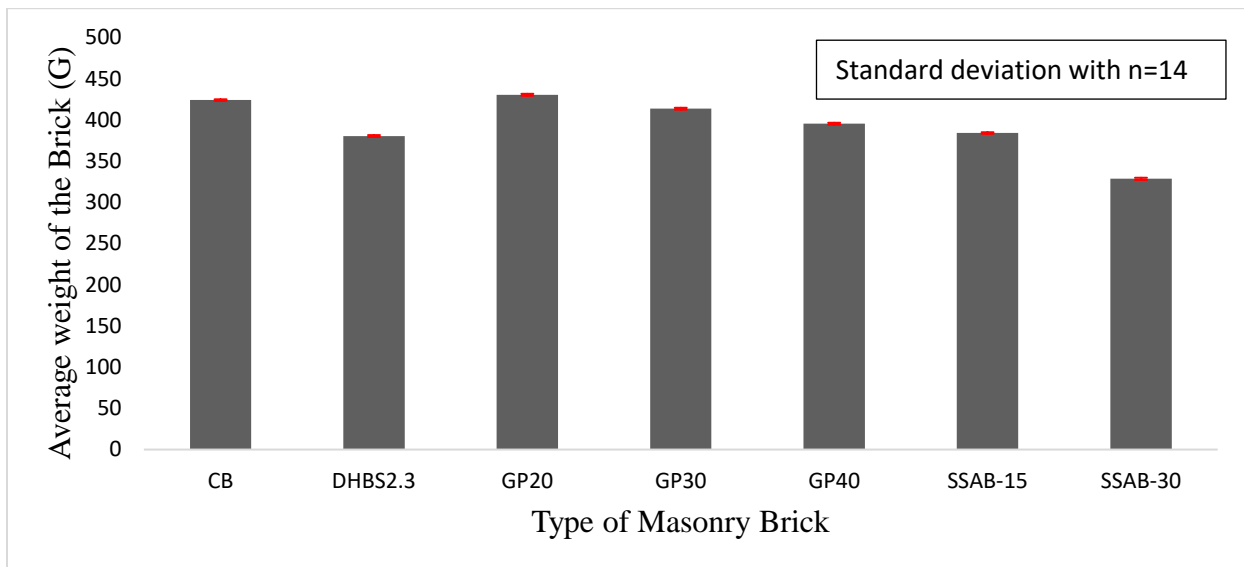

Figure 5-69: The average weight of the bricks

Chapter 6. Numerical Simulation for Inverse Analysis

6.1 Introduction

Numerical simulation is used in estimating the behaviour of the bricks under mechanical load with the help of a Finite Element software. This type of modeling approach is based on the principles of equilibrium, compatibility and stress-strain relationships. The degree of detail that can be obtained through numerical simulation allows for consideration of the interaction between the test setup and the specimen, including important variables such as aspect ratio, specimen size, and specimen support conditions. Today, there is a variety of software available to perform nonlinear finite element modeling of structures, such as Autodesk Simulation Multiphysics, Abaqus, ANSYS, COSMOS/M, GT-STRUDL, LS-DYNA, MARC, SAP2000, VecTor$^{©}$ suite; the latter option is a specialized Finite Element platform developed specifically for modelling concrete and is therefore endowed with an array of brittle and semi-brittle material constitutive models that can be adapted to the case of masonry materials.

In Finite Element Analysis (FEA), the structure is discretized into an equivalent mesh of finite elements. In convergent algorithms, a denser mesh generally leads to better accuracy. Elements could be 1D line springs or trusses, beam, pipe and so on, 2D plane element for membrane, plate, shell etc., or 3D volume elements that are more appropriate for generalized stress states, temperature, and flow velocity. Elements are interconnected at nodal points and along boundary lines. A finite element model of a typical masonry unit studied in this thesis under flexural testing is shown in Figure 6-1.
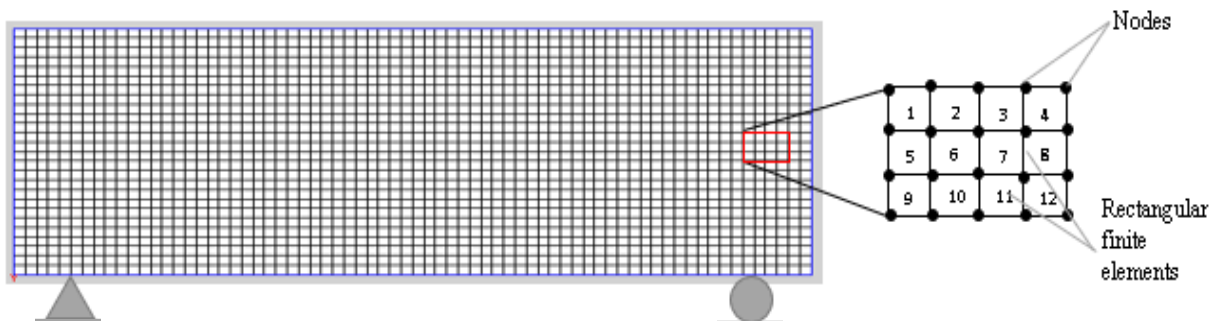

Figure 6-1: A finite element model of a masonry unit (VecTor2)

Establishing the boundary conditions is a crucial step in the FEA. The element properties are represented by the element stiffness matrices [k] that are obtained through approximations of the differential equation using a weak formulation of the Galerkin class, and the constitutive laws of the material [Yamaguchi, 2014].

Considering the displacements u and v of a point in the x,y domain of a 2-D plane stress analysis problem, which are here the field functions of the formulation, the weak form is intended to satisfy the following governing partial differential equations:

$$\frac{\partial^2 u}{\partial x^2} + \frac{\partial^2 u}{\partial y^2} - \frac{1+v}{2}\left[\frac{\partial^2 u}{\partial y^2} + \frac{\partial^2 v}{\partial x \partial y}\right] = 0 \qquad\qquad 6.1$$

$$\frac{\partial^2 v}{\partial x^2} + \frac{\partial^2 v}{\partial y^2} - \frac{1+v}{2}\left[\frac{\partial^2 v}{\partial y^2} + \frac{\partial^2 u}{\partial x \partial y}\right] = 0 \qquad\qquad 6.2$$

The element stiffness matrices [k] for all the elements are assembled into the global stiffness matrix [K]. Subsequently, the problem for the entire body is solved by formulating the equations of equilibrium for each nodal degree of freedom and combining them through statements of displacement compatibility in order to obtain the solution. For this, the product of [K] matrix by the vector of nodal displacements {u,v} is set equal to the value of the externally applied loads (F). Several parameters such as deformations and internal forces/stresses of the whole structure can be calculated using FEA which is considered today the most versatile method for solving mechanics problems.

6.2 VecTor 2-Non-Linear Finite Element Software

In the present investigation VecTor2 was used, being specially designed to analyze semi-brittle structures and materials. The program relies on two-dimensional non-linear finite element idealization of general two-dimensional reinforced or prestressed concrete structures. In the current research, the software has been used to compare the behaviour of the masonry bricks with the mechanical tests, with the objective to perform inverse analysis so as to decipher the true mechanical properties of the materials tested through matching of the experimental and analytical results. The particular interest lies with the true tensile strength of brittle and semi-brittle materials such as those tested in the present study where this property is obtained indirectly through flexural testing. Evidence from the few direct tests that have been conducted in the past [Thomas & O'Leary, 1966], conclusively shows that the tensile strength obtained from indirect testing is much higher unless inverse analysis is used to perform the strength identification through minimization

of the error between measured and calculated results. In the current study, this type of inverse, iterative analysis is conducted through F.E. simulation.

VecTor2 has two processors - Formwork and Augustus. Formwork [Wong, 2002] works as a preprocessor where the modelling, meshing, material property definition, support condition, loading and preliminary steps of the analysis are done on a graphical user interface method (GUI) whereas Augustus [Bentz, 1996] works as a post processor where the structural responses like load-deformation, stresses, strains, failure modes including cracks may be assessed.

6.3 Finite Element Modelling of the Masonry Brick

The finite element modelling of the masonry brick unit was carried out in VecTor2 by generating the skeleton-model of the structure using 'define and mesh structure'. The model was then discretized with plane-stress rectangular elements. Then the material properties and the boundary conditions were assigned accordingly to continue with the post processor.

In the current research, the mechanical tests modelled are, the compressive strength tests in longitudinal and transverse direction, flexural strength test as well as the split tensile strength test. The referent experimental results correlated through the study concerned all the different types of bricks made in the main phase of the investigation (i.e., control bricks, dried high biopolymer sludge bricks, geopolymer bricks with 20 %,30 % and 40 % replacement of shale with recycled crushed glass and sewage sludge ash brick with 15 % and 30 % replacement of shale by incinerated sewage sludge ash.) Tests modelled included the flexural strength test, compressive strength test and splitting tensile strength test with the objective to obtain the actual material properties by calibrating of analysis and test result.

6.3.1 Simulation of the Flexural Strength Test-Three-Point Bending

The finite element modelling of the flexural strength test set up was done for all the categories of bricks. All the bricks modelled were 140 mm in length, 58 mm in width and 26 mm in depth. The model consists of 3928 plane stress rectangular elements of size 1mm x 1mm with an aspect ratio of 1 and 4150 nodes.

Discrete reinforcement elements

In order to simulate the metallic plate used in the mechanical test, 2-noded truss-bar elements were placed at the top of the brick mesh for a length of 30mm. The truss element had width of 58mm

and depth of 6mm which is the exact dimension of the metallic plate. This type of element is provided in order to de-bond the brick and the metallic plate so as to simulate the failure crack observed in the actual mechanical test. All the brick models are simulated using a discrete reinforcing bar in the role of the bearing plate in order to effectively model the flexural strength test as shown in Figure 6-2(a).

Bond link element properties

All FE models were endowed with bond-link elements to connect the brick with the metallic plate as a part of a de-bonding mechanism. A total of 30 linkage elements in the form of an unbonded bar was used.

Support conditions

To model the supports, steel plates with high stiffness were provided to avoid local crushing at the bearing zones; the support condition at the bottom of the brick were assumed simple supports allowing translational movement only.

Loading protocol

To simulate the three-point bending test, a point load was applied at the mid length of the brick model, while loading was displacement controlled using 0.01 mm increments per load step.

Constitutive models utilized in VecTor2

The default models present in VecTor2 are appropriate to perform the nonlinear analysis. The same default models are utilized in the current numerical analysis to see the response of the of the brick specimens under the three-point bending test. The constitutive models used for the various aspects of material simulation are shown in the Table 6-1.

Table 6-1 Constitutive models utilized in VecTor2

Material Behavior	Constitutive Model
Concrete Compression Pre-Peak	Hognestad (Parabola)
Concrete Compression Post-Peak	Modified Park-Kent
Concrete Compression Softening	Vecchio 1992-A (e1/e2-Form)
Concrete Tension Stiffening	Modified Bentz 2003
Concrete Tension Softening	Linear
Concrete FRC Tension	SDEM-Monotonic
Concrete Confined Strength	Kupfer/Richart
Concrete Dilation	Variable-Isotropic
Concrete Cracking Criterion	Mohr-Coulomb (Stress)
Crack Stress Calculation	Basic
Concrete Crack Width Check	Agg/2.5 Max Crack Width
Slip Distortion	Walraven
Concrete Creep and Relaxation	Not Considered
Concrete Bond	Eligehausen
Concrete Hysteretic Response	Nonlinear w/ Plastic Offsets

6.3.1.1 Mechanical properties and failure patterns

 The mechanical properties of the masonry bricks were obtained from the experimental mechanical tests. For each type of bricks, the properties were different and are given below for each category of bricks. The finite element model of a brick under three-point bending is shown in Figure 6-2.
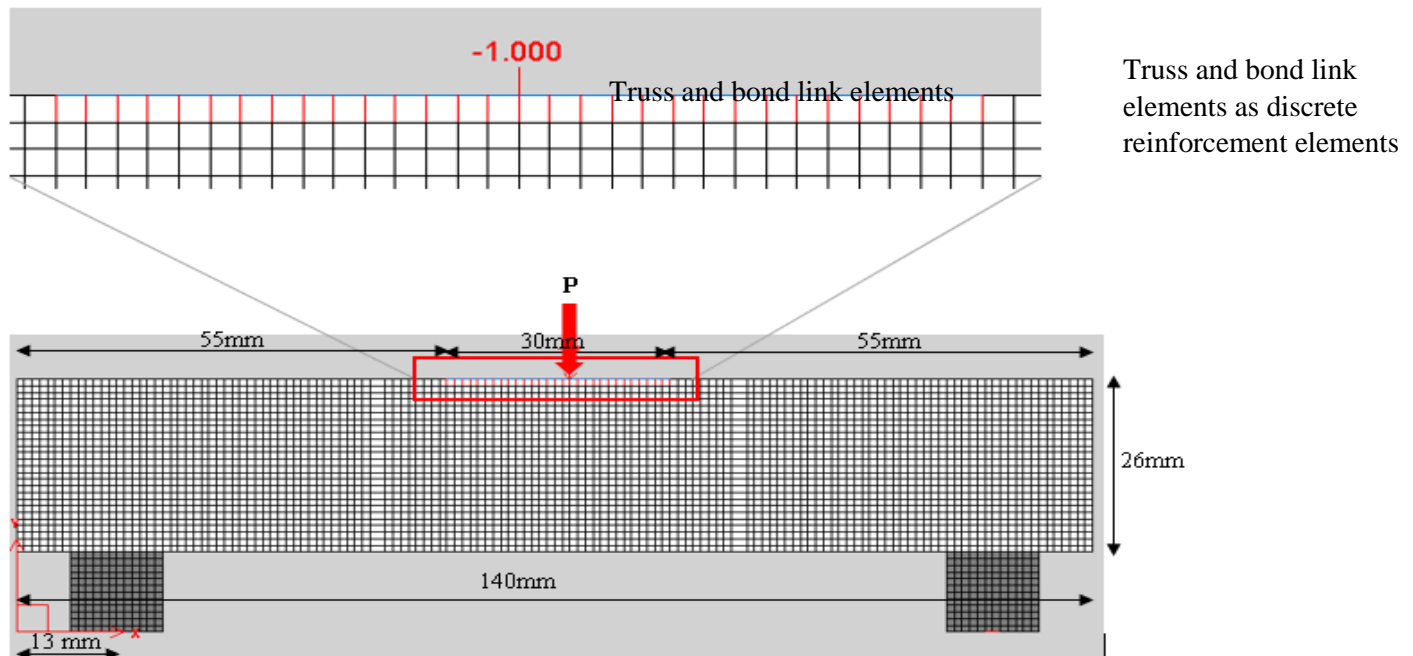

Figure 6-2: The finite element model of the control brick under three- point bending test

6.3.1.1.1 Control Brick (CB)

The material properties for the control brick were specified by selecting the reference material as the reinforced concrete in the FEM simulation of the flexural strength test. However, the values of the parameters including the compressive strength $f_c^{'}$, Modulus of elasticity E_c, and density ρ were 29.9 MPa, 36625 MPa, and 2008.3 kg/m^3 respectively as obtained from the Experimental tests. The value for the Poisson's ratio μ was assumed as 0.2. The tensile strength of the control brick that matched the tests was found to be 7.0 MPa. The indirect tensile strength values from the three-point bending test and the splitting tensile strength test were 15.3 MPa and 4.8 MPa respectively. The thickness of the control brick for modelling of the flexure test was 58 mm. Apart from reproducing the load-displacement curve, this analysis yielded the same failure pattern of the brick as observed during the experiment (see Figure 6-3(b)). The peak load and the maximum displacement at the midpoint of the brick at failure was 3.0 kN and 0.03 mm respectively. Figure 6-3(c) represents the analytical load-mid displacement response curve for the typical Control Brick. The peak load and mid displacement from the experimental analysis was 3.1 kN and 0.03 mm respectively and the peak load is represented as a dashed red line in the same response curve. The analysis produced a load strength that was very close to the experimental values; Acceptable tolerance for the type of test conducted lies within the magnitude of experimental error, i.e., in the range of 10% of the peak value (i.e., 0.3 kN).

(a)

(b)

[128]
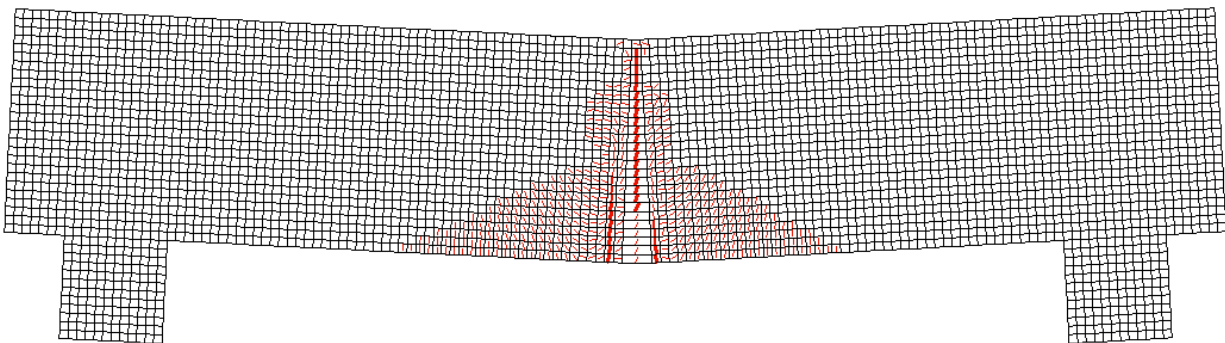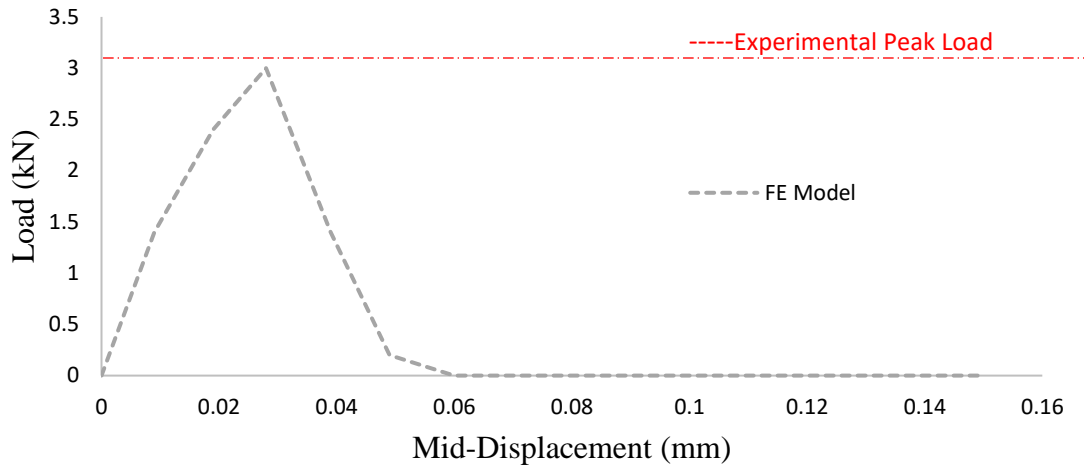
(c)

Figure 6-3 (a):Properties of the Control Brick used for the modelling in matching analysis with experiment ; (b): The failure pattern of control brick under flexural strength test; (c): Experimental and FEM response of the Control Brick

6.3.1.1.2 Dried High Biopolymer Sludge (DHBS) Brick

For the simulation of the flexural strength test in FEM for Dried High Biopolymer Sludge brick, the material properties used are shown in Figure 6-4(a).The tensile strength found was 7.0 MPa after several steps of iteration. The indirect tensile strength values from the three- point bending test and the splitting tensile strength test for the DHBS brick were 14.9 MPa and 4.6 MPa respectively. The failure pattern of the DHBS brick under the flexural test was within acceptable error (<10%) from the analysis, as shown in Figure 6-4(b). The peak load and the maximum displacement at the midpoint of the brick at failure was 2.8 kN and 0.03 mm respectively.

Figure 6-4(c) represent the analytical load- mid displacement response curve for DHBS brick. The peak load and mid displacement from the experimental analysis was 2.9 kN and 0.03 mm respectively. Also, the peak load is shown in a red dashed line for the comparison. The response was nearly the same from both the analyses.

(a)

(b)

[130]
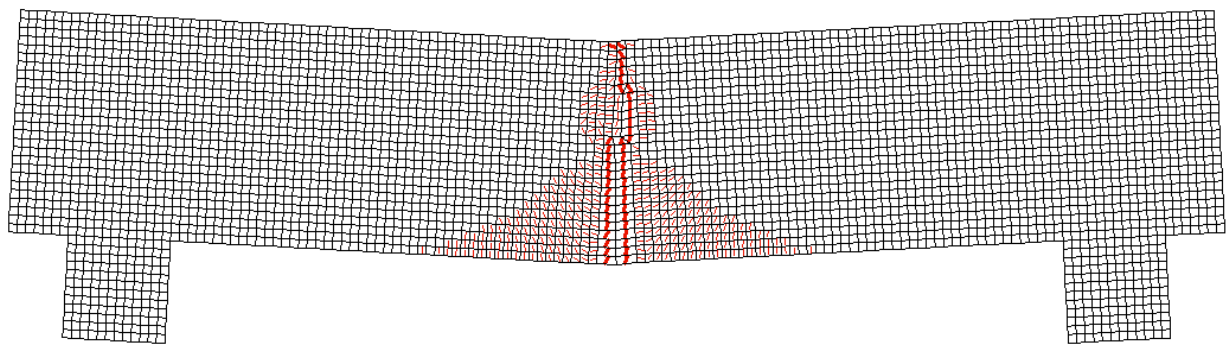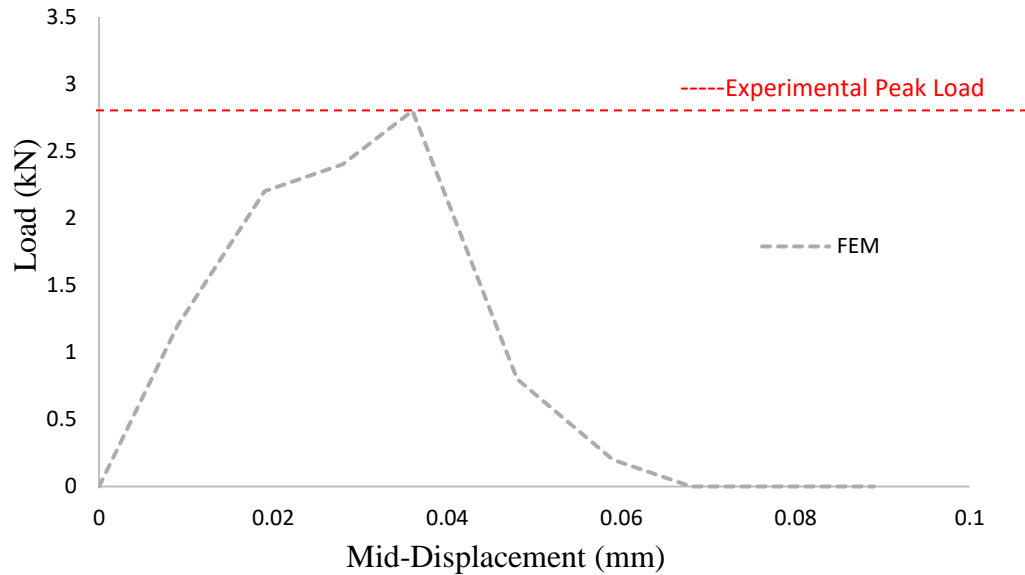
(c)

Figure 6-4 (a): Properties of the DHBS Brick used for the modelling in matching analysis with experiment (b):The failure pattern of DHBS brick under flexural strength test (c): Experimental and FEM response of the DHBS Brick

6.3.1.1.3 Geopolymer Brick (GB-20)

The material properties used for the Geopolymer (GB-20) brick in the FEM simulation of the flexural strength test is shown in Figure 6-5(a). After iteration, the tensile strength of the control brick was found to be 5.0 MPa. The indirect tensile strength values from the three- point bending test and the splitting tensile strength test for the GB-20 brick were 10.4 MPa and 3.2 MPa respectively. Likewise, the estimated failure pattern of the GB-20 brick under the flexural test successfully matched the actual test. The failure pattern is shown in Figure 6-5(b). The peak load and the maximum displacement at the midpoint of the brick at failure was 2.0 kN and 0.03 mm respectively.

(a)

(b)

[132]
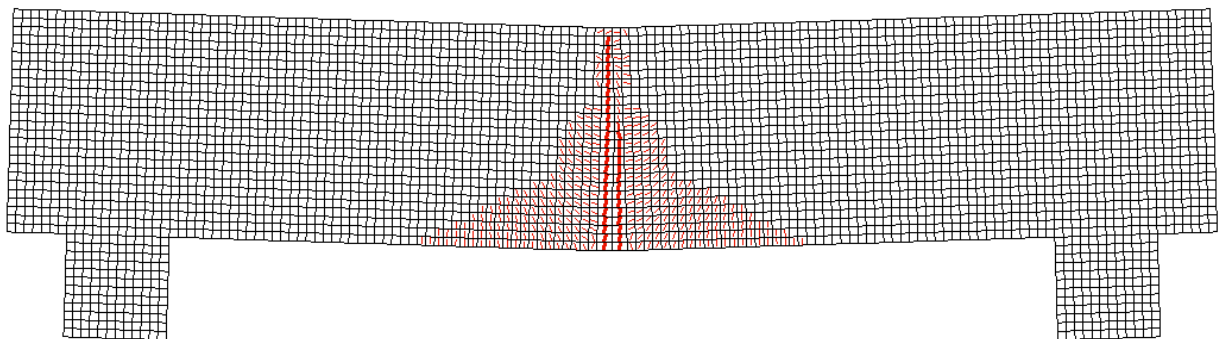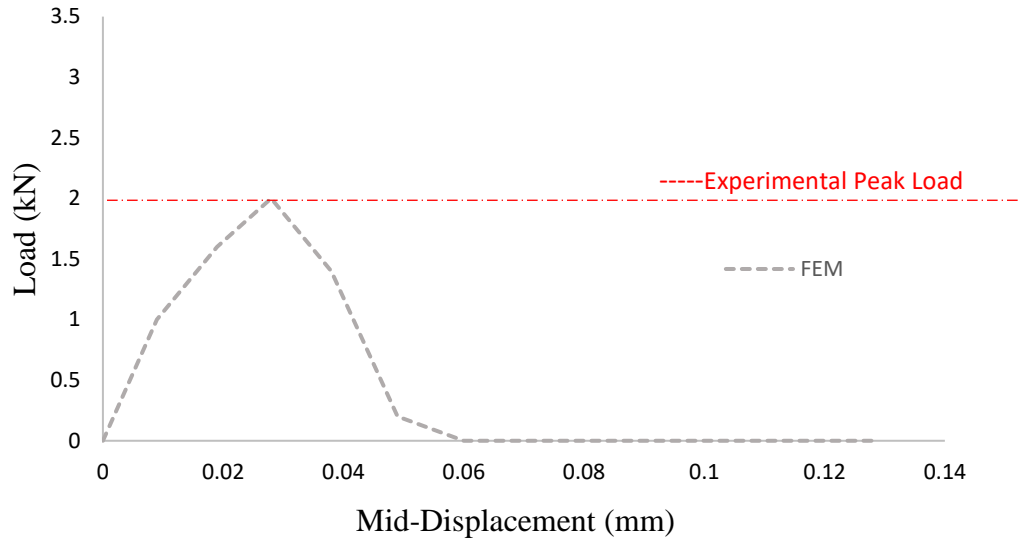
(c)

Figure 6-5 (a): Properties of the GB-20 used for the modelling in matching analysis with experiment (b): Failure

pattern of GB-20 brick under flexural strength test (c): Experimental and FEM response of the GB-20Brick

Figure 6-5(c) represents the analytical load- mid displacement response curve for the GB-20 brick. The peak load and mid displacement from the experimental analysis was 2.0 kN and 0.02 mm respectively. Although the peak load (red dashed line in Figure 6-5(c)) was the same from both analyses, the mid- displacement from the experimental analysis was only 84.4% of the FE estimation.

6.3.1.1.4 Geopolymer Brick (GB-30)

For the Geopolymer (GB-30) the properties depicted in Figure 6-6(a) were used for the FEM simulation of the flexural strength test. After iteration in matching the analysis and the experimental response curves it was determined that the tensile strength of GB-30 brick was 4 MPa. The indirect tensile strength values from the three- point bending test and the splitting tensile strength test for the GB-30 brick were 8.2 MPa and 3.1 MPa respectively. Comparably, the obtained direct tensile strength value from the FEM was found greater than the splitting tensile strength and lower than the flexural strength. The failure pattern of the GB-30 brick under flexural strength test was similar to the actual test as depicted in Figure 6.6(b).The peak load and the maximum displacement at the midpoint of the brick at failure was 1.8 kN and 0.03 mm respectively.

(a)

(b)

[134]
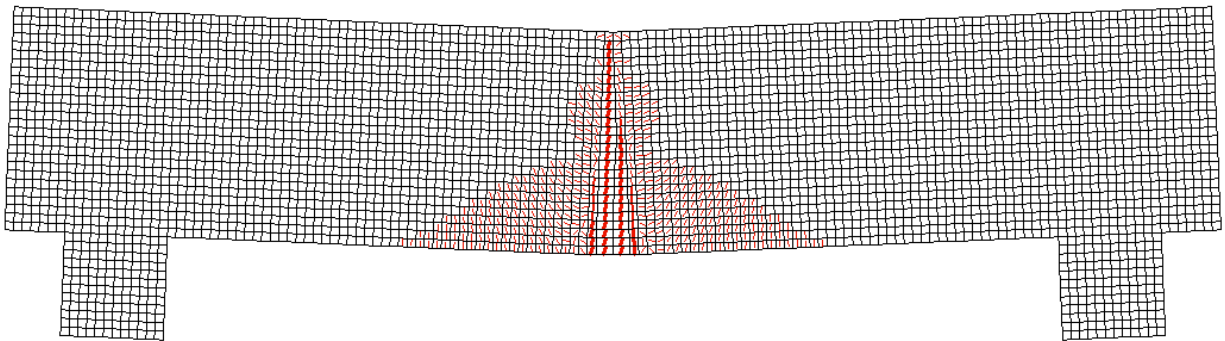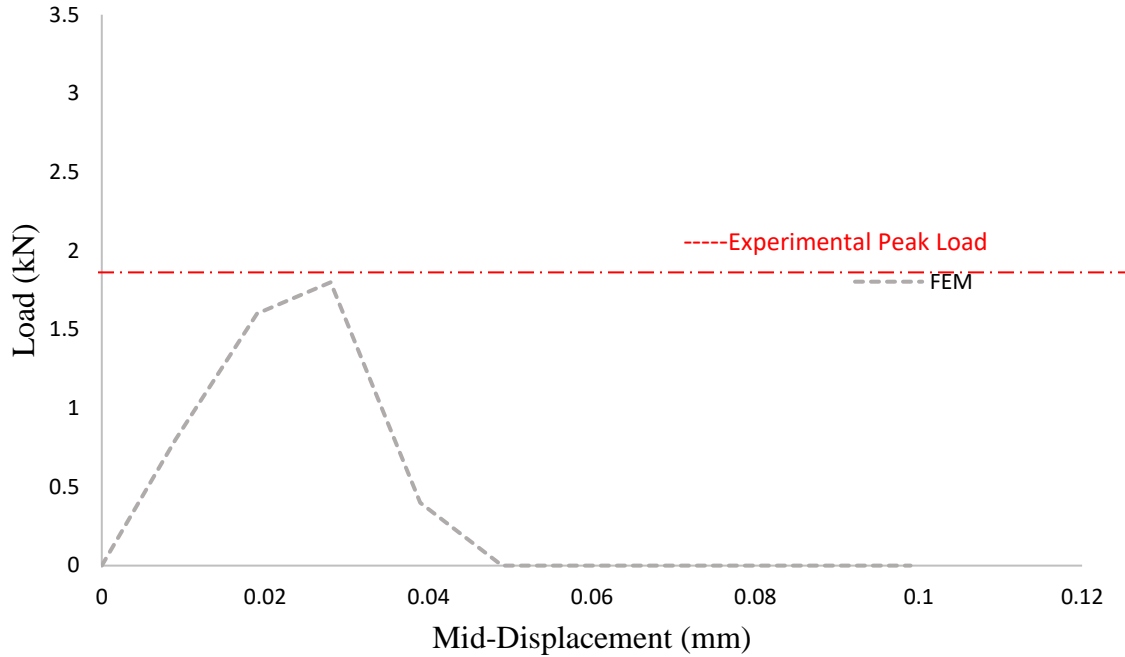
(c)

Figure 6-6 (a): Properties of the GB-30 used for the modelling in matching analysis with experiment (b): Failure pattern of GB-30 brick under flexural strength test (c): Experimental and FEM response of the GB-30 Brick

Figure 6-6(c) represents the analytical load- mid displacement response curve for GB-30 brick. The peak load and mid displacement from the experimental analysis was 1.7 kN and 0.02 mm respectively. The peak load is shown in a red dashed line in the response curve. Although the peak load was the same from both analyses, here as well, the mid- displacement from the experimental analysis was only 78.7% of the FE estimate.

6.3.1.1.5 Geopolymer Brick (GB-40)

The material properties used for the Geopolymer (GB-40) brick in the FEM simulation of the flexural strength are shown in Figure 6-7(a). Upon iteration for matching of the results, the tensile strength of the GB-40 brick was found to be 3.0 MPa. The indirect tensile strength values from the three- point bending test and the splitting tensile strength test for the GB-40 brick were 6.5 MPa and 2.4 MPa respectively. Here as well, the obtained direct tensile strength value from the FEM identified again that, values were within acceptable experimental error to the splitting tensile strength value and approximately half that of the flexural strength. The calculated failure pattern

[135]

of the GB-40 brick under flexural strength test was consistent to the actual test, as depicted in Figure 6-7(b). The peak load and the maximum displacement at the midpoint of the brick at failure was 1.2 kN and 0.02 mm respectively. The experimental peak load is highlighted as a red dashed line in the same response curve.

Material Properties

|	
Reference Type:	Reinforced Concrete
Thickness, T:	58 mm
Cylinder Compressive Strength, f'c:	15.07181 MPa
Tensile Strength, f't:	* 3 MPa
Initial Tangent Elastic Modulus, Ec:	* 11704.32 MPa
Cylinder Strain at f'c, eo:	* 1.28 me
Poisson's Ratio, Mu:	* 0.2
Thermal Expansion Coefficient, Cc:	* 1e-006 /°C
Maximum Aggregate Size, a:	* 0.1 mm
Density:	* 1872.895 kg/m3
Thermal Diffusivity, Kc:	* 0 mm2/s
Maximum Crack Spacing...	
perpendicular to x-reinforcement, Sx:	* 1000 mm
perpendicular to y-reinforcement, Sy:	* 1000 mm
Color	

(a)

(b)

[136]
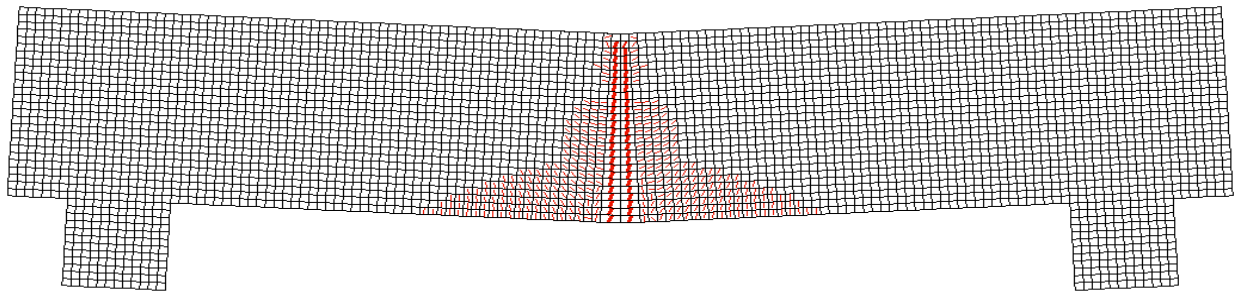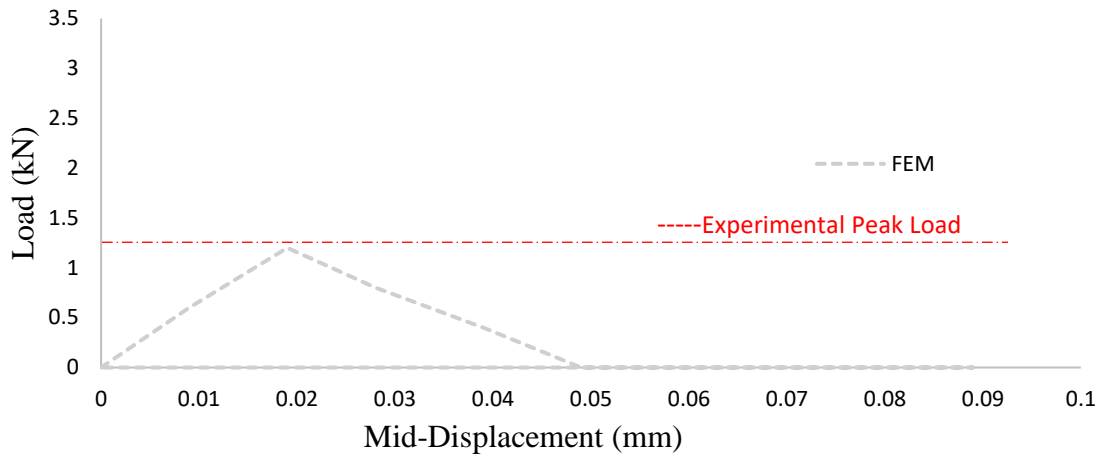
Figure 6-7 (a) Properties of the GB-40 used for the modelling in matching analysis with experiment (b): Failure pattern of GB-40 brick under flexural strength test (c) The experimental and analytical load- mid displacement response for GB-40 brick

Figure 6-7(c) represent the experimental and analytical load- mid displacement response for GB-40 brick. The peak load (red dashed line in the response curve) and mid displacement from the experimental analysis were 1.2 kN and 0.01 mm respectively. Athough the estimated strength was the same in both analyses, the mid- displacement from the experimental analysis was only 84.27% of the FE analysis (i.e. the stiffness was overestimated).

6.3.1.1.6 Sewage Sludge Ash Brick (SSAB-15)

For the simulation of the flexural strength test in FEM for SSAB-15 brick, the material properties used are shown in Figure 6-8(a).The tensile strength found was 7MPa after several steps of iteration. The indirect tensile strength values from the three- point bending test and the splitting tensile strength test for the SSAB-15 brick were, 14.2 MPa and 4.4 MPa respectively. Equivalently, the failure pattern of the SSAB-15 brick under the flexural strength test was consistent with the test values. The failure pattern is shown in Figure 6-8(b). The peak load and the maximum displacement at the midpoint of the brick at failure were 2.8 kN and 0.03 mm respectively.

The experimental and analytical load- mid displacement response for SSAB-15 brick is depicted in Figure 6-8(c). The peak load and mid displacement from the experimental analysis were, 2.7 kN and 0.03 mm respectively. The mid- displacement from the experimental analysis was 93.3% of the FEM. Nevertheless, the peak load was the same from both the analyses.

(a)
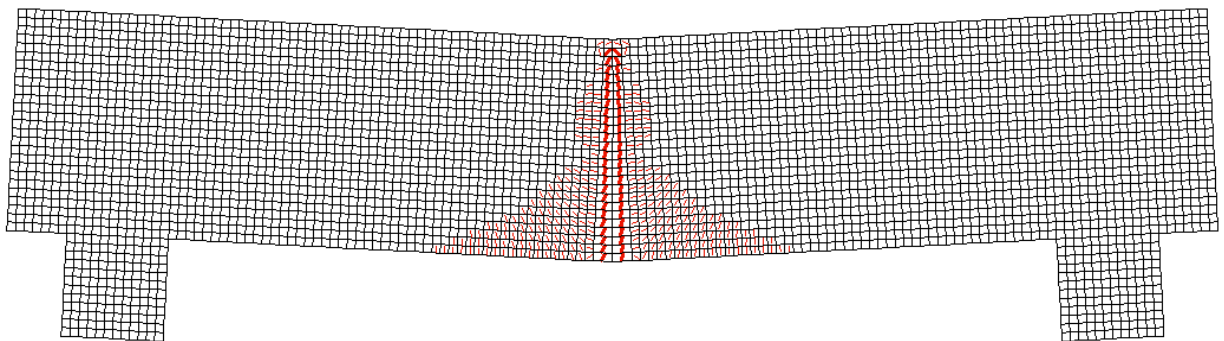
(b)
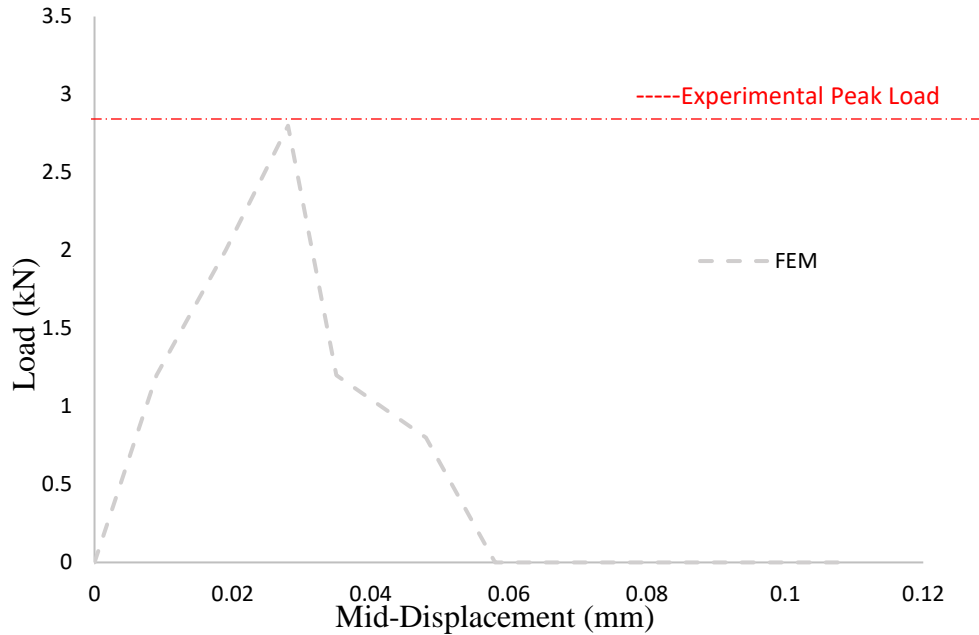
(c)

Figure 6-8 (a): Properties of the SSAB-15 used for the modelling in matching analysis with experiment (b):Failure pattern of SSAB-15 brick under flexural strength test (c): The experimental and analytical load- mid displacement response for SSAB-15 brick

6.3.1.1.7 Sewage Sludge Ash Brick (SSAB-30)

For the SSAB-30 brick, the properties depicted in Figure 6-9(a) was used for the FEM simulation of the flexural strength test. After iteration in matching the analysis and the experimental response curves it was determined that the tensile strength of SSAB-30 brick was 4.0 MPa. The indirect tensile strength values from the three- point bending test and the splitting tensile strength test for the SSAB-30 brick were, 12.8 MPa and 4.1 MPa respectively. Correspondingly, the direct tensile strength value from the FEM found approximately the same as the splitting tensile strength and consistent with the flexural strength. The failure pattern of the SSAB-30 brick under flexural strength test also reproduced successfully the experimentally observed failure. The failure pattern is shown in Figure 6-9(b).The peak load and the maximum displacement at the midpoint of the brick at failure was 2.6 kN and 0.03 mm respectively.

(a)
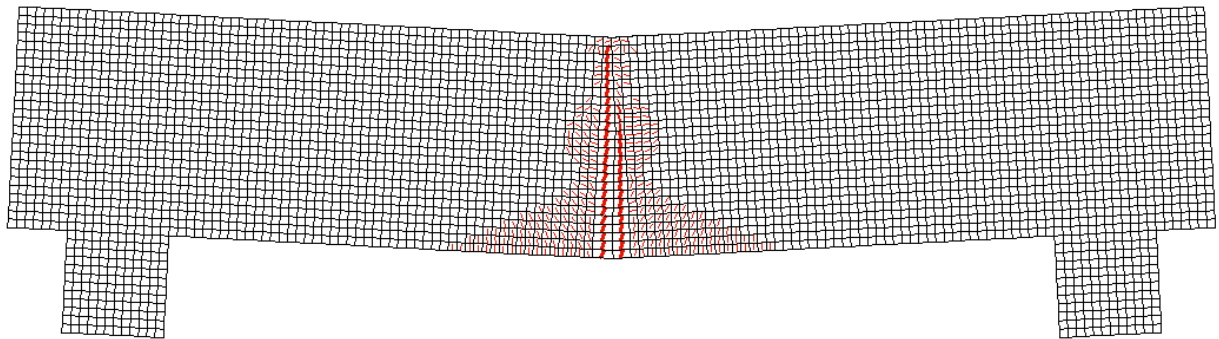
(b)
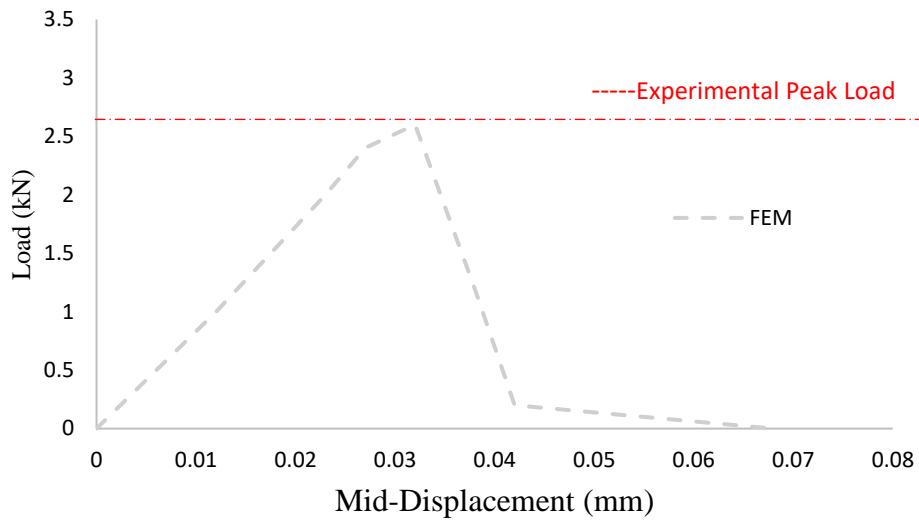
(c)

Figure 6-9(a): Properties of the SSAB-30 used for the modelling in matching analysis with experiment (b):Failure pattern of SSAB-30 brick under flexural strength test (c): The experimental and analytical load- mid displacement response for SSAB-30 brick

The experimental and analytical load- mid displacement response for SSAB-15 brick is presented in Figure 6-9(c). The peak load which is shown in red dashed line and mid displacement from the experimental analysis was 2.6 kN and 0.03 mm respectively. The mid- displacement and the peak load was almost the same from both the analyses.

6.3.1.2 Comparison of numerical and experimental Analysis

Results of the numerical and experimental analysis of peak load under the 3-point flexural test are compared in Figure 6-10(a). The dark grey bar represents the experimental result and the light grey represents the FE analysis result. The peak load P, from the experimental analysis is within the same range with the load P from the FE analysis. It was found that the crack pattern and response of all the bricks were for all practical purposes consistent. However, the tensile strength was overestimated for the control brick, DHBS, SSAB-15 and SSAB-30 bricks when compared to the experimental results.
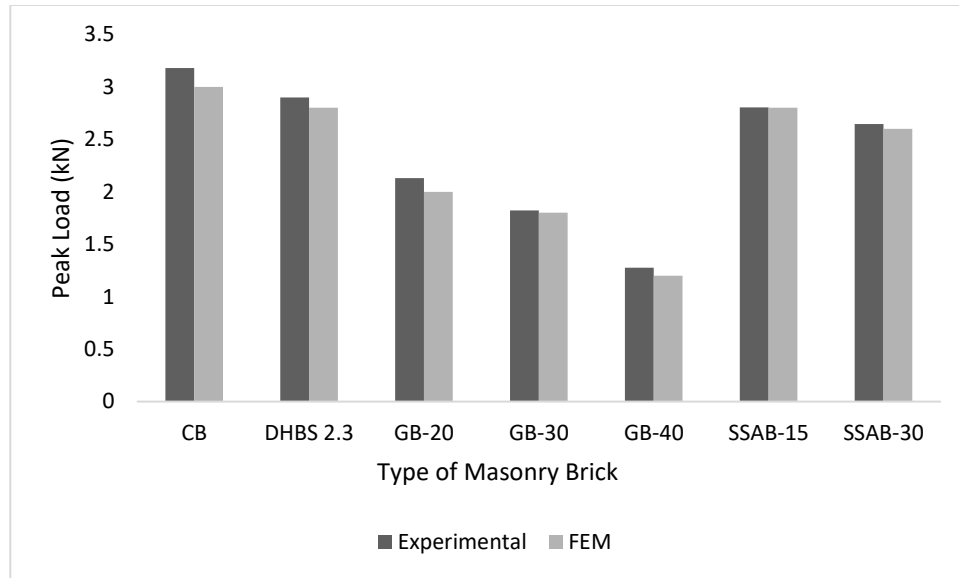
Figure 6.10: Numerical and experimental analysis of peak load under the flexural test

6.3.2 Simulation of the Splitting Tensile Strength Test

Finite element modelling of the splitting tensile strength test was also done for all the categories of bricks. The bricks modelled were of 140 mm in length and 26mm in depth. The model consists of 3672 plane stress rectangular elements of size 1mm x 1mm with an aspect ratio of 1 and 3847 nodes. The boundary conditions for the splitting tensile strength modelling were given as simple supports at the top centre. The default models present in VecTor2 described in Section 6.3.1 are used as constitutive models. To simulate the splitting tensile strength test, a point load was applied to the models at the bottom centre as quasi-static loading with 0.01 mm increments per load step, using a displacement-controlled approach. The finite element model of a brick under splitting tensile strength test is shown in Figure 6-11.
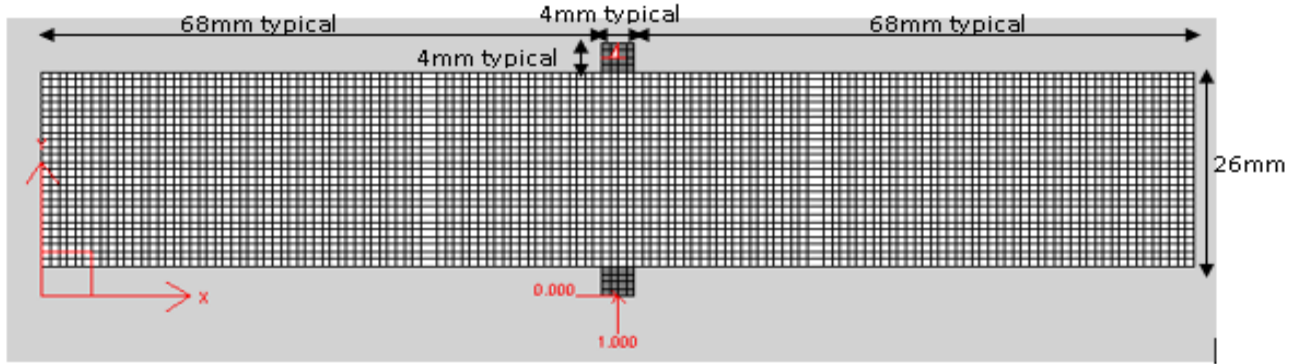
Figure 6-11 The finite element model of a brick under splitting tensile strength test

6.3.2.1 Mechanical properties and failure patterns

For the simulation of splitting tensile strength test, the mechanical properties of the masonry bricks were obtained from the Experimental mechanical tests. All the parameters - compressive strength f_c', Modulus of elasticity E_c, tensile strength, f_t , density ρ, and Poisson's ratio μ, were the same as in the case of three point bending or the flexural strength test.

6.3.2.1.1 Control Brick (CB)

The failure pattern of the control brick under the splitting tensile strength test matching the experimentally observed mode of failure (Figure 6-12(a)). The peak load and the maximum displacement at the midpoint of the control brick at failure was 11.2 kN and 0.01 mm respectively. The peak load from the experimental analysis was 11.3 kN which within the acceptable range of experimental error (<10%) from the FE analysis value. The analytical load- mid displacement response curve for the control brick is presented in Figure 6-12(b).

[143]
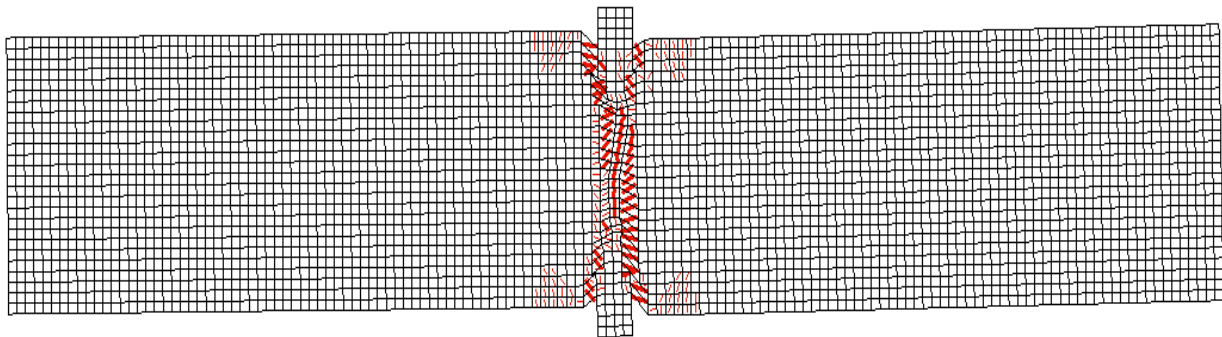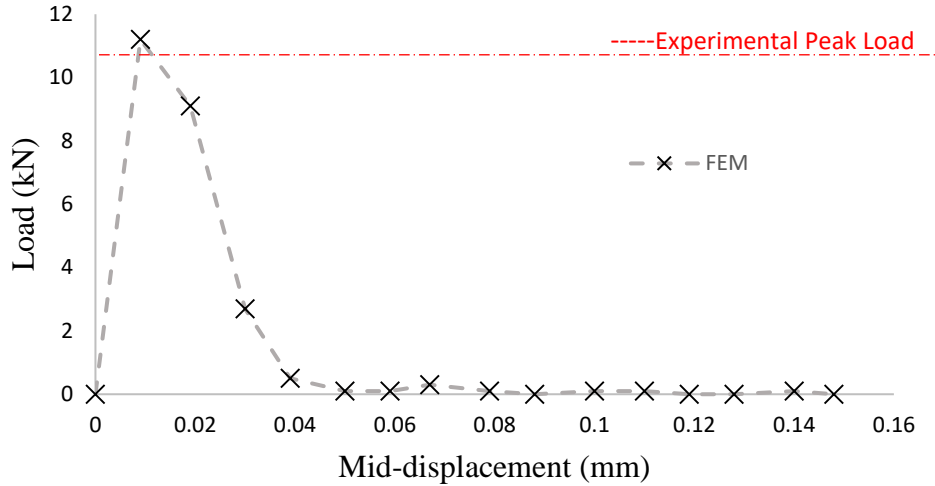
Figure 6-12(a): The failure pattern of the Control brick under Splitting Tensile Strength Test; (b):The analytical load- mid displacement response for control brick

6.3.2.1.2 Dried High Biopolymer Sludge (DHBS) Bricks

The response of the DHBS brick under splitting tensile strength test was consistent with the response of the actual mechanical test, as shown in Figure 6-13(a). The peak load and maximum displacement at the midpoint of the control brick at failure was 10.4 kN and 0.01 mm respectively. The peak load from the experimental analysis was 10.5 kN which is consistent with the FE estimation. The analytical load- mid displacement response curve for DHBS brick is illustrated in Figure 6-13(b).

(b)

Figure 6-13(a): The failure pattern of the DHBS brick under Splitting Tensile Strength Test; (b): The analytical
load- mid displacement response curve for DHBS brick

6.3.2.1.3 Geopolymer Bricks (GB-20)

The mode of failure of the GB-20 brick under the splitting tensile strength test is depicted in Figure 6-14(a). From the FE analysis, the peak load and the maximum displacement at the midpoint of the GB-20 brick at failure was 7.5 kN and 0.01 mm respectively. The peak load from the experimental analysis was 7.4 kN, almost the same for the FE analysis as well. The analytical load- mid displacement response curve for GB-20 brick is presented in Figure 6-14(b).

(a)

(b)

Figure 6-14(a): The failure pattern of the GB-20 brick under Splitting Tensile Strength Test (b): Analytical load-mid displacement response for the GB-20 brick

6.3.2.1.4 Geopolymer Bricks (GB-30)

The response of the GB-30 brick under the splitting tensile strength test was consistent with the experimentally observed failure. The failure pattern of the control brick under splitting is depicted in Figure 6-15(a).The peak load and the maximum displacement at the midpoint of the GB-30 brick at failure was 7.1 kN and 0.01 mm respectively. The peak load from the experimental analysis was 7.1 kN which conforms with the FE results. The analytical load- mid displacement response curve for GB-30 brick is given in Figure 6-15(b).
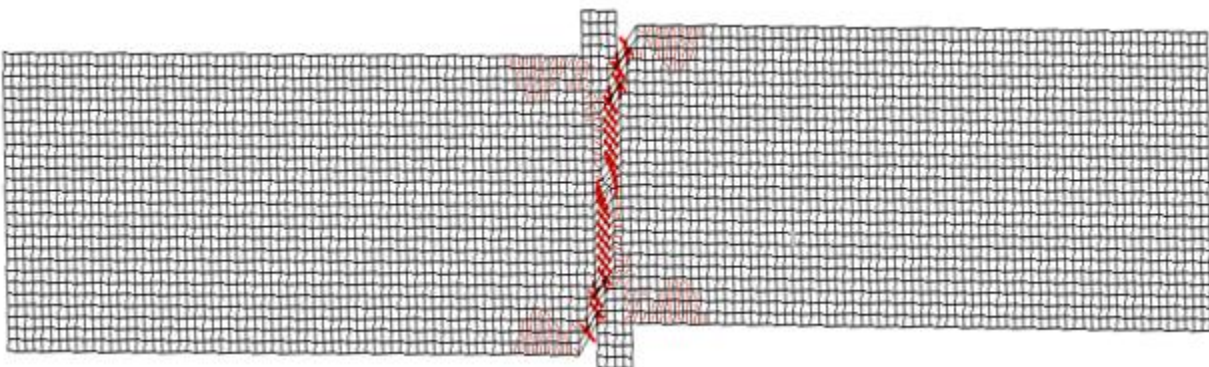

(a)

[146]

(b)

Figure 6-15(a): The failure pattern of the GB-30 brick under Splitting Tensile Strength Test (b): The analytical load- mid displacement response for GB-30 brick

6.3.2.1.5 Geopolymer Bricks (GB- 40)

The response of the GB-40 brick under splitting tensile strength test was consistent with the experimentally observed mode of failure, as depicted in Figure 6-16(a). The peak load and the maximum displacement at the midpoint of the GB-40 brick at failure was 5.5 kN and 0.01 mm respectively. The peak load from the experimental analysis was 5.5 kN which agrees with the FE analysis. The analytical load- mid displacement response curve for GB-40 brick is presented in Figure 6-16(b).
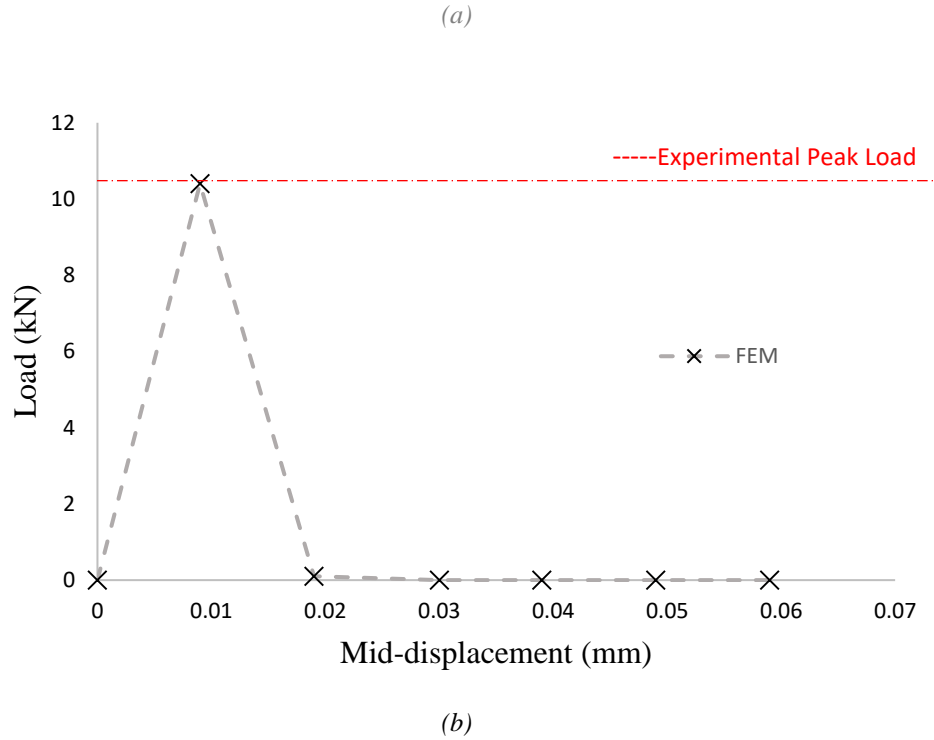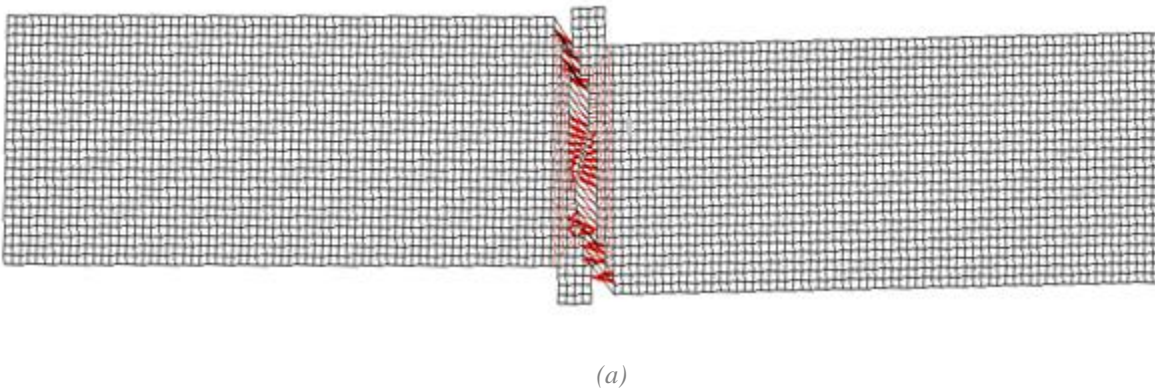

(a)

Figure 6-16(a): The failure pattern of the GB-40 brick under Splitting Tensile Strength Test (b): The analytical load- mid displacement response for GB-40 brick

6.3.2.1.6 Sewage Sludge Ash Brick (SSAB-15) Bricks

The failure pattern of the SSAB-15 brick under splitting tensile strength test was similar to the failure observed in the mechanical test, and here it is depicted in Figure 6-17(a).The peak load and the maximum displacement at the midpoint of the SSAB-15 brick at failure was 10.1 kN and 0.01 mm respectively. The peak load from the experimental analysis was 10.2 kN which is slightly greater than (approximately equal) the FEM response. The analytical load- mid displacement response curve for SSAB-15 brick is presented in Figure 6-17(b).
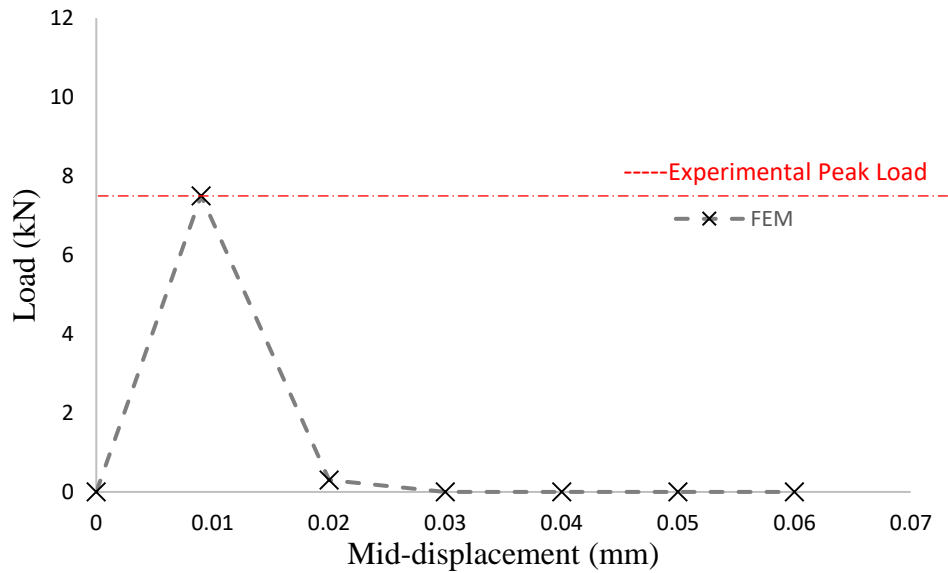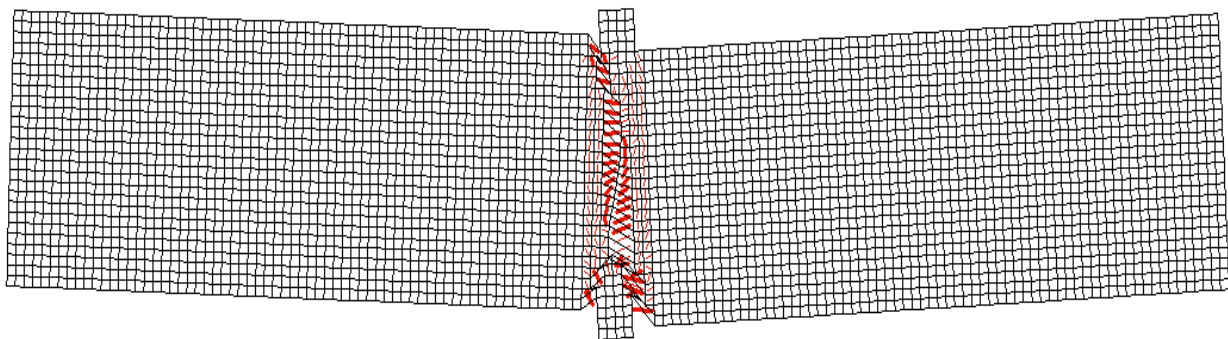

(a)
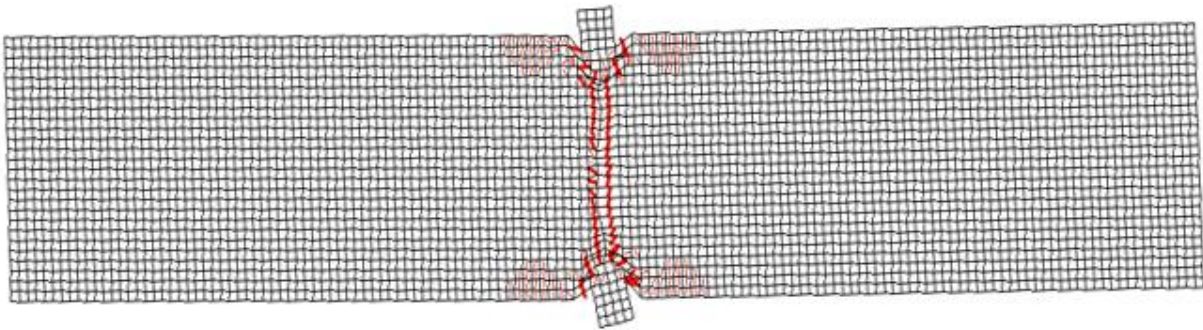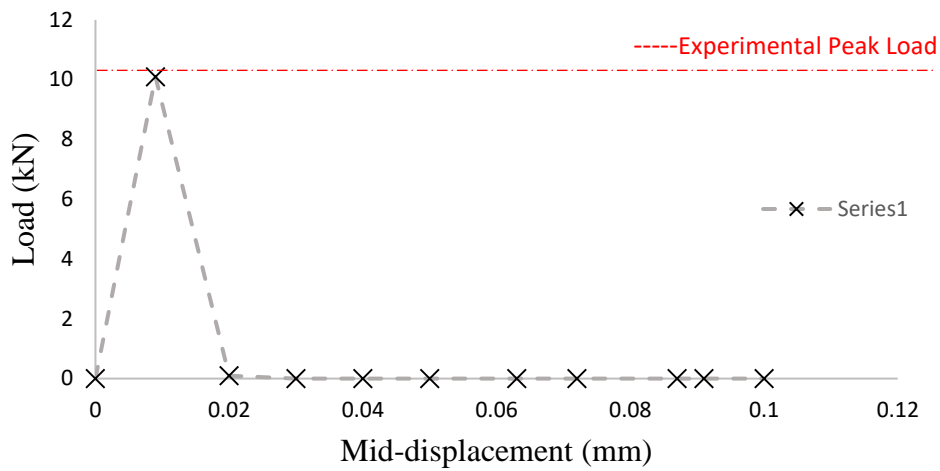
Figure 6-17(a): The failure pattern of the SSAB-15 brick under Splitting Tensile Strength Test; (b): The analytical load- mid displacement response for SSAB-15 brick

6.3.2.1.7 Sewage Sludge Ash Brick (SSAB-30) Bricks

As in the previous cases, the failure pattern of the SSAB-30 brick under splitting tensile strength test was consistent – within experimental error – with the experimental observations I as shown in Figure 6-18(a).The peak load and the maximum displacement at the midpoint of the SSAB-30 brick at failure was 9.6 kN and 0.01 mm respectively. From the experimental analysis, the peak load   was 9.5 kN which is within experimental error within the range of the FE results. The analytical load- mid displacement response curve for SSAB-30 brick is presented in Figure 6-18(b).
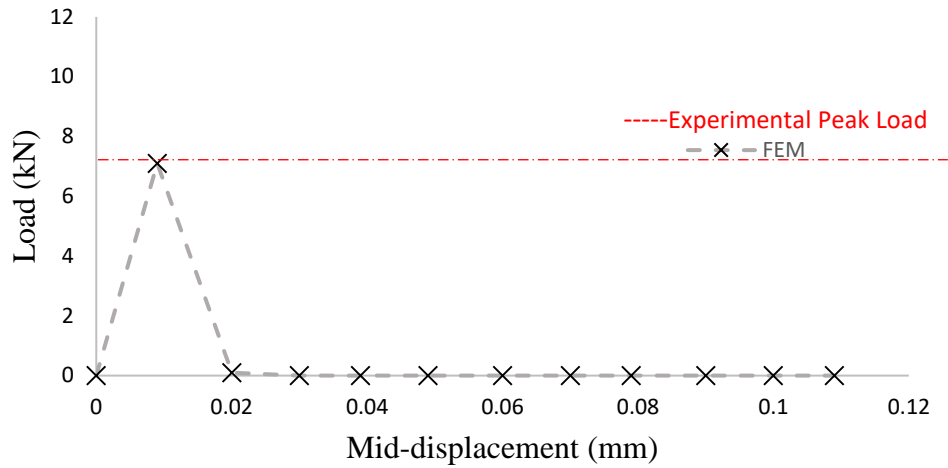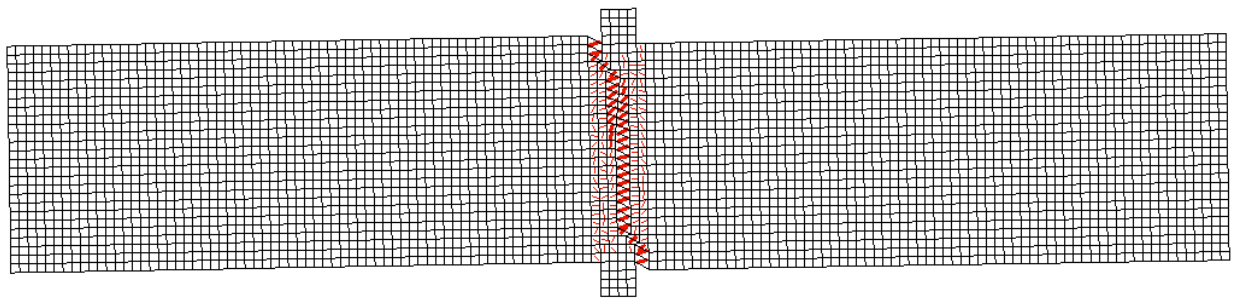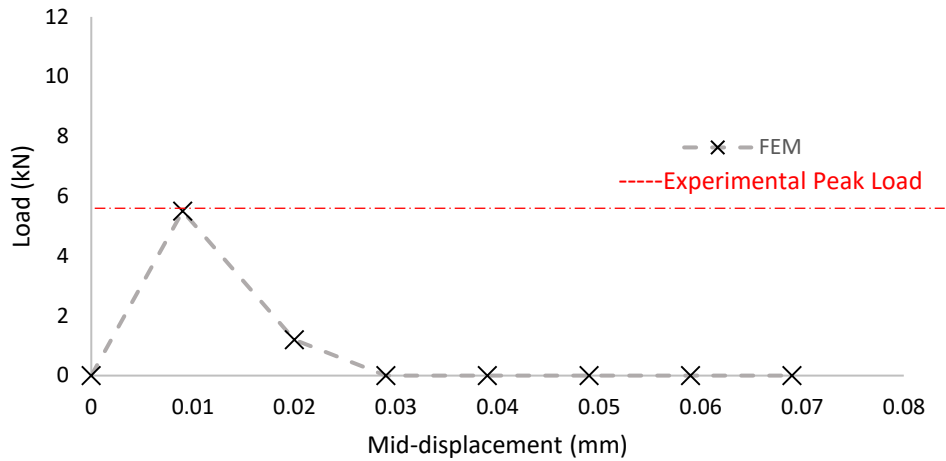

(a)

[149]
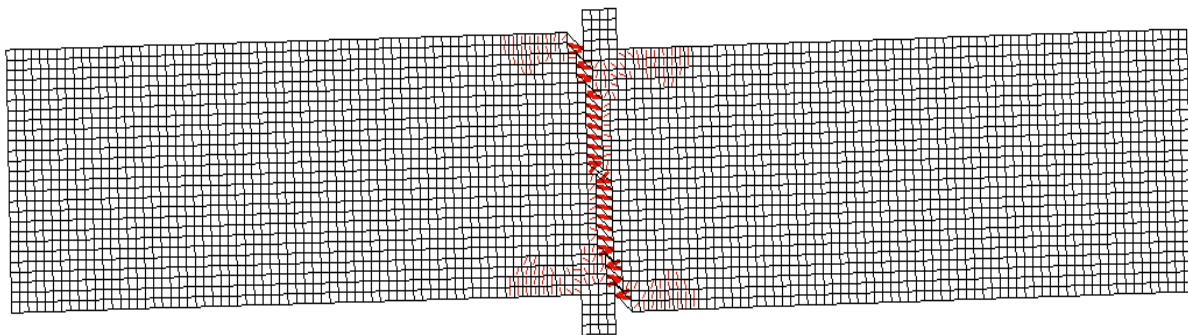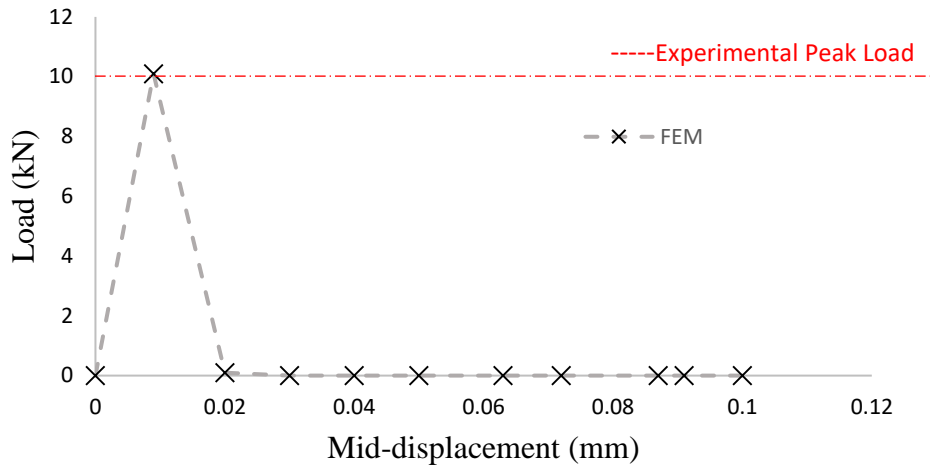
(b)

Figure 6-18(a): The failure pattern of SSAB-30 brick under Splitting Tensile Strength Test; (b): The analytical load-mid displacement response for SSAB-30 brick

6.3.2.2 Comparison of numerical and experimental Analysis

Figure 6-19 illustrates the comparison of results from the numerical and experimental analysis of peak load under splitting tensile strength test. The FEM model resulted in values that were practically the same as the reported peak load values; the same peak load for all the categories of bricks except for a slight overestimation in the case of GB 20, GB 30 and SSAB-30 bricks. However, the failure pattern was consistent throughout the analyses and samples considered.
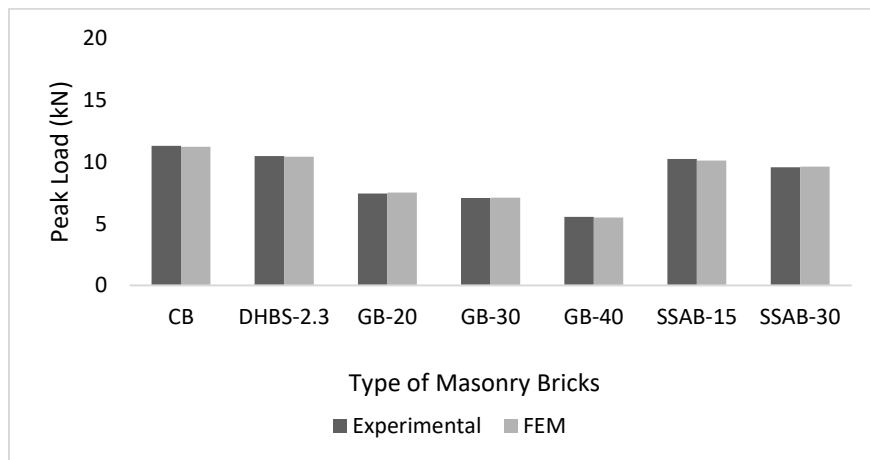
Figure 6-19: Numerical and experimental analysis of peak load under splitting tensile strength test

6.3.3 Simulation of the Compressive Strength Test-Transverse Direction

Finite element modelling of the test set up for the compressive strength of the hybrid masonry brick in the transverse axis was done for all the categories of bricks. Bricks modelled were 140mm in length by 26mm in depth. The model consisted of 875 plane stress rectangular elements of size 2mm x 2mm with an aspect ratio of 1, including the steel loading plates (noted by grey in Fig. 6-20). The mesh comprised 936 nodes in total. The boundary conditions for the compressive strength test in modelling the transverse direction testing were represented using simply supported nodes (i.e., unrestrained sliding in the horizontal direction due to Poisson's effects, but no translation in the vertical direction) at the top. The default models present in VecTor2 described in Section 6.3.1 is used as constitutive models. Regarding the loading protocol, to simulate the compressive strength test, a uniform load was applied at the bottom of the brick models as a quasi-static type of loading with 0.01 mm increments per load step using displacement control.
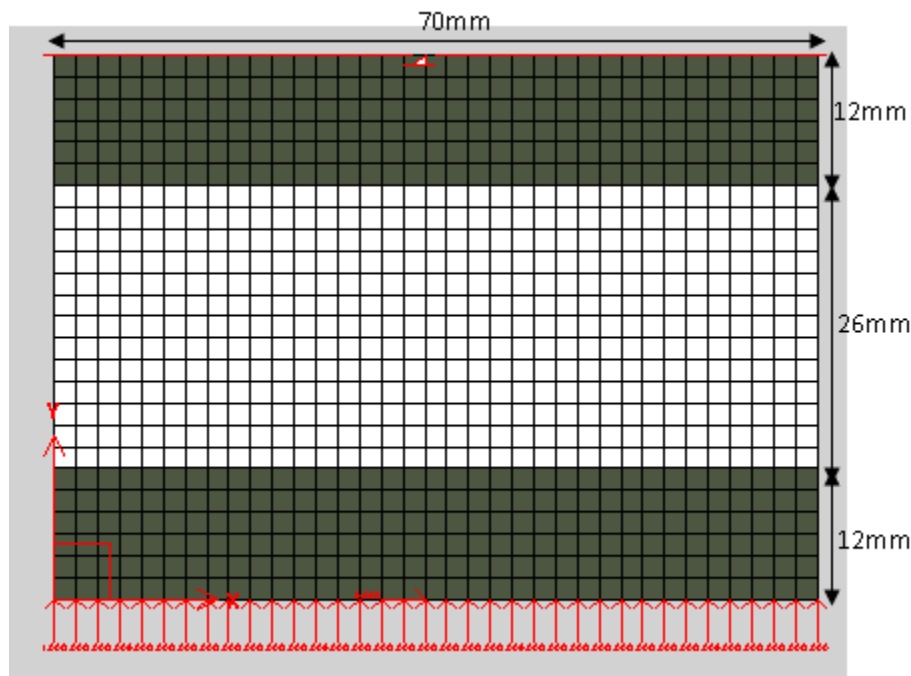
Figure 6-20 : The finite element model of a brick under compressive strength test in the transverse direction

6.3.3.1 Mechanical properties and failure patterns

For the simulation of compressive strength test in the transverse direction, the mechanical properties of the masonry bricks were obtained from the Experimental mechanical tests. All the

parameters- compressive strength f_c', Modulus of elasticity E_c, density $\boldsymbol{\rho}$, Poisson's ratio μ, were the same as in the case of three point bending or the flexural strength test.

6.3.3.1.1 Control Brick (CB)

The failure pattern of the control brick under the compressive strength test in the transverse direction consistently reproduced the failure patterns observed in the actual mechanical test, depicted here in Figure 6.21(a). The peak load and the maximum displacement at the midpoint of the control brick at failure was, 110.5 kN and 0.02 mm, respectively, which is close to the response of the mechanical analysis, which was 110.6 kN

The response of the control brick in terms of load and the mid displacement from FEA is shown in Figure 6.21(b).

(a)

[152]
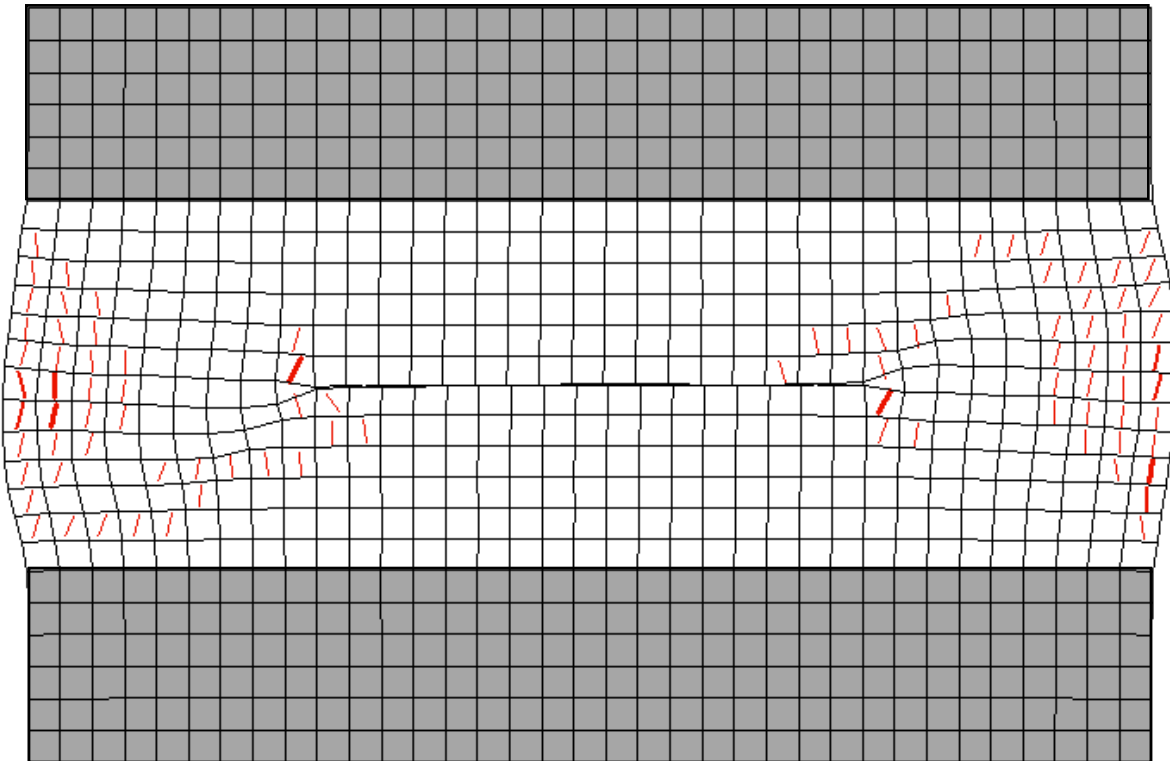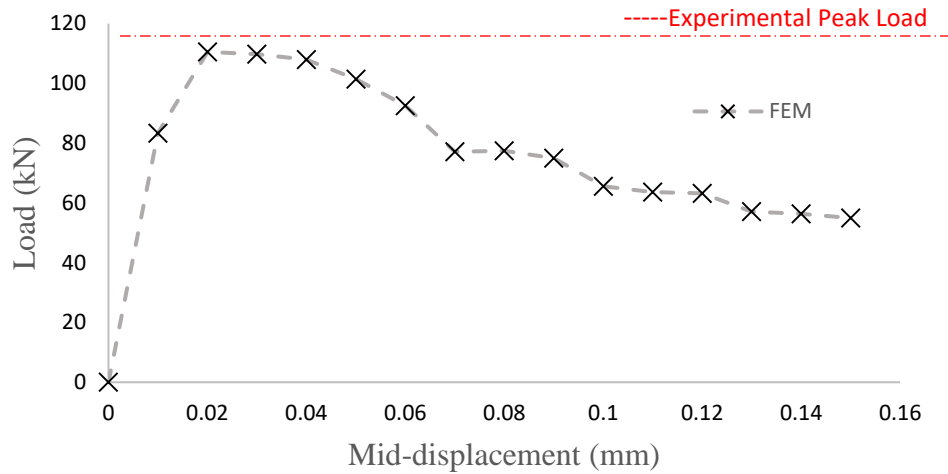
(b)

Figure 6-21(a): The failure pattern of the control brick under compressive strength test in the transverse direction;
(b): The analytical load- mid displacement response for control brick

6.3.3.1.2 Dried High Biopolymer (DHBS) Brick

The response of the DHBS brick under compressive strength test in the transverse direction reproduced the experimentally observed modes of failure. The failure pattern of the DHBS brick under compressive strength test in the transverse direction is presented in Figure 6-22(a).The peak load and the maximum displacement at the midpoint of the DHBS brick at failure was 101.8 kN and 0.02 mm respectively. Likewise, the peak load from the experimental analysis was 99.7 kN which is very close (within acceptable experimental error) to the peak load from the numerical analysis.

The load versus mid displacement response curve from the numerical analysis is illustrated in Figure 6-22(b).

[153]

(a)

(b)

Figure 6-22(a): The failure pattern of the DHBS brick under compressive strength test in the transverse direction;

(b): The analytical load- mid displacement response for DHBS brick

[154]

6.3.3.1.3 Geopolymer Brick (GB-20)

The failure pattern of the GB-20 brick under compressive strength test in the transverse direction was rather similar to the failure at the actual mechanical test. The failure pattern of the control brick under compressive strength test in the transverse direction is shown in Figure 6-23(a). The peak load and the maximum displacement at the midpoint of the GB-20 at failure was 77.0 kN and 0.02 mm respectively, as shown in Figure 6-23(b). From the mechanical test, the peak load for the GB-20 was 76.8 kN which complements the FE estimations.

(a)

(b)

Figure 6- 23(a): The failure pattern of the GB-20 brick under compressive strength test in the transverse direction

(b): The analytical load- mid displacement response for GB-20 brick

6.3.3.1.4 Geopolymer Brick (GB-30)

As in preceding case, again the GB-30 brick developed a failure pattern in the transverse direction when loaded under the compressive strength test that was entirely consistent with the failure observed at the actual mechanical test. A schematic of the observed failure pattern of the control brick under this type of tests is shown in Figure 6-24(a). The peak load and the maximum displacement at the midpoint of the GB-30 at failure was 73.6 kN and 0.02 mm respectively. Similarly, the peak load from the experimental analysis was 73.2 kN, whereas the displacement estimate is shown in Figure 6-24(b)

(a)
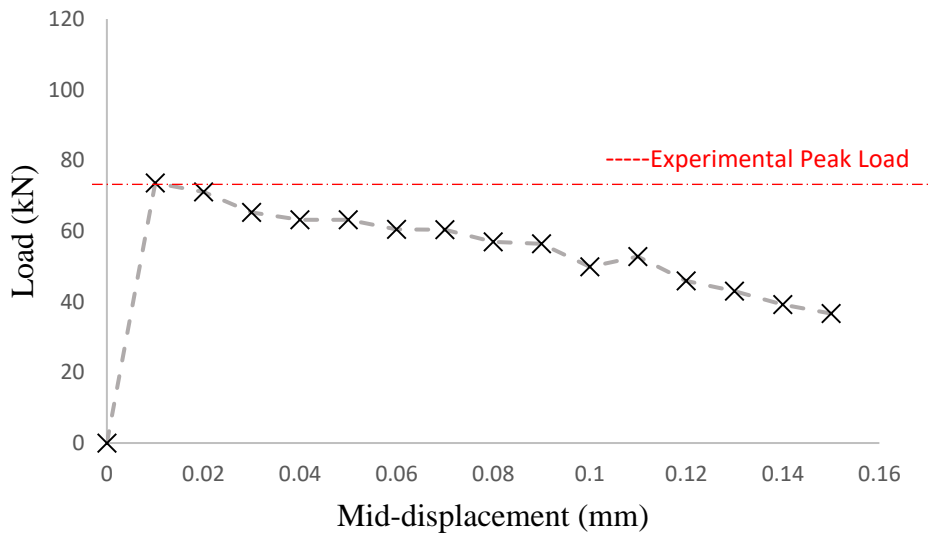
(b)

Figure 6-24(a): The failure pattern of the GB-30 brick under compressive strength test in the transverse direction

(b): The analytical load- mid displacement response for GB-30 brick

[157]

6.3.3.1.5 Geopolymer Brick (GB-40)

The response of the GB-40 brick under compressive strength test in the transverse direction was similar to the response at the actual mechanical test. The failure pattern of the control brick under the compressive test in the transverse direction is shown in Figure 6-25(a). The peak load and the maximum displacement at the midpoint of the GB-40   at failure was 62.7 kN and 0.02 mm respectively. Figure 6-25(b) shows the load -mid displacement curve from the FE analysis. The response from the FE analysis was consistent with the experimental response where the peak load was 61.9 kN, within acceptable experimental tolerance.
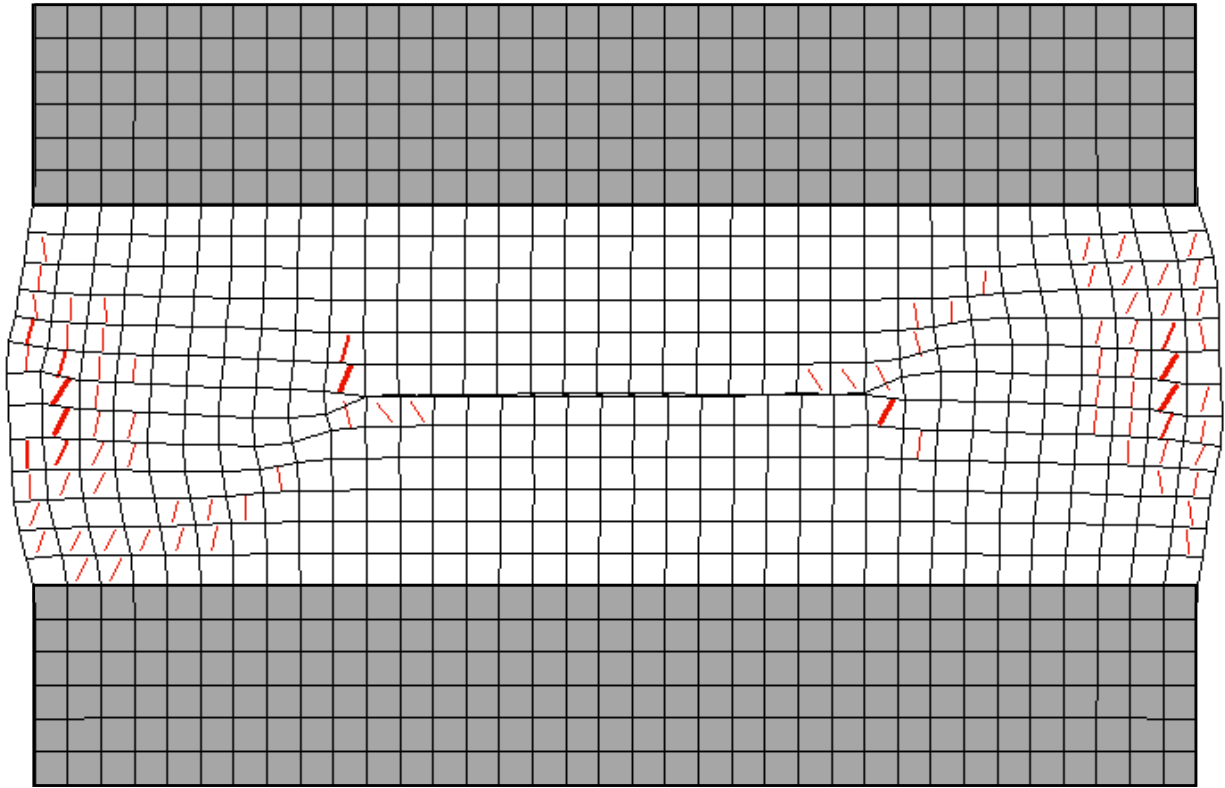

(a)

[158]
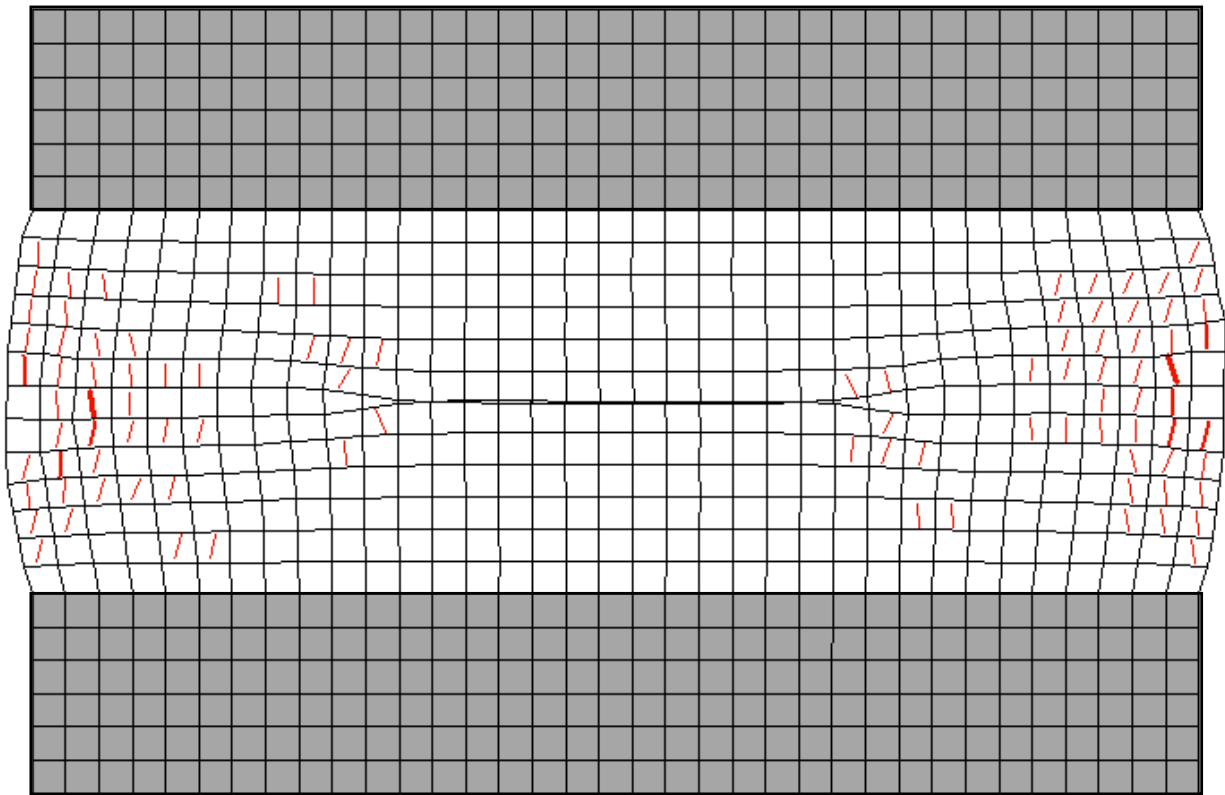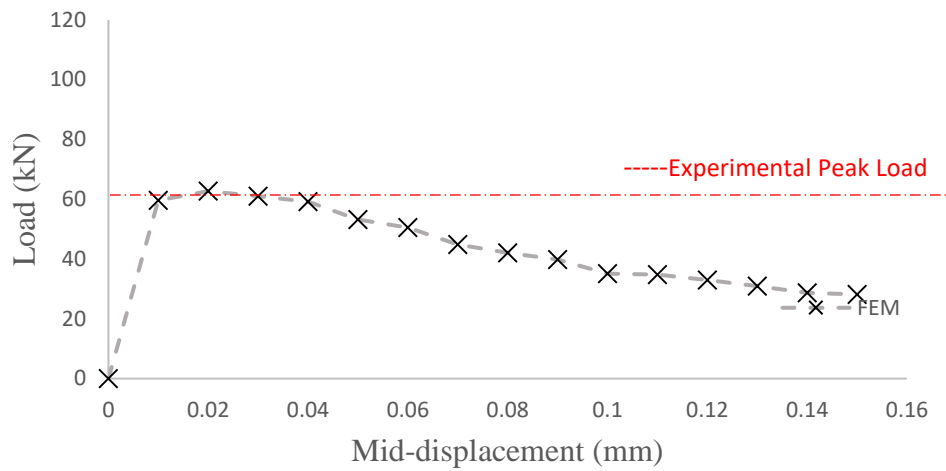
(b)

Figure 6-25(a): The failure pattern of the GB-40 brick under compressive strength test in the transverse direction

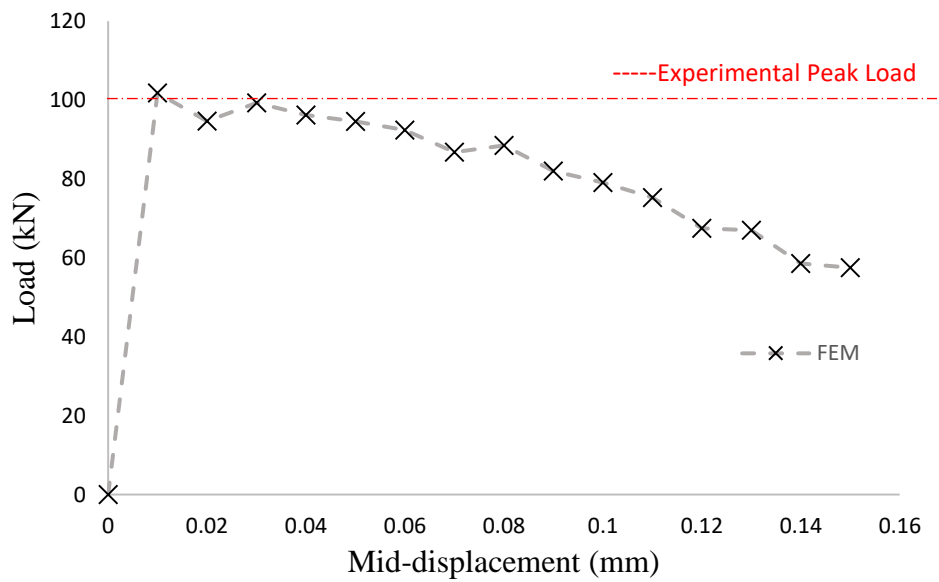*(b): The analytical load- mid displacement response for GB-40 brick*

6.3.3.1.6 Sewage Sludge Ash (SSAB-15)Brick

The failure pattern of the SSAB-15 brick under compressive strength test in the transverse direction matched the experimental observation. The failure pattern of the control brick under compressive strength test in the transverse direction is shown in Figure 6-26(a). The peak load and the maximum displacement at the midpoint of the SSAB-15 at failure was 94.2 kN and 0.02 mm respectively as depicted in Figure 6-26(b). From the experimental analysis the peak load was in close agreement with the peak load from the FE analysis which was 94.4 kN.
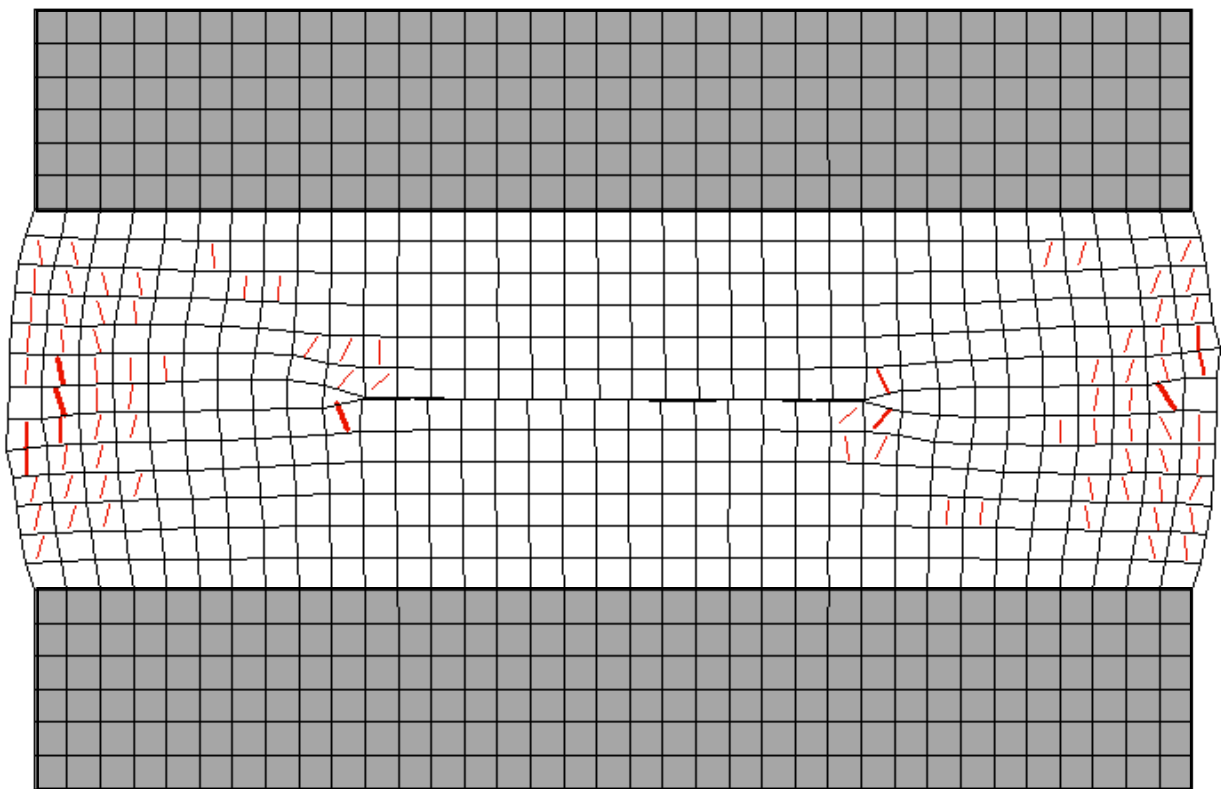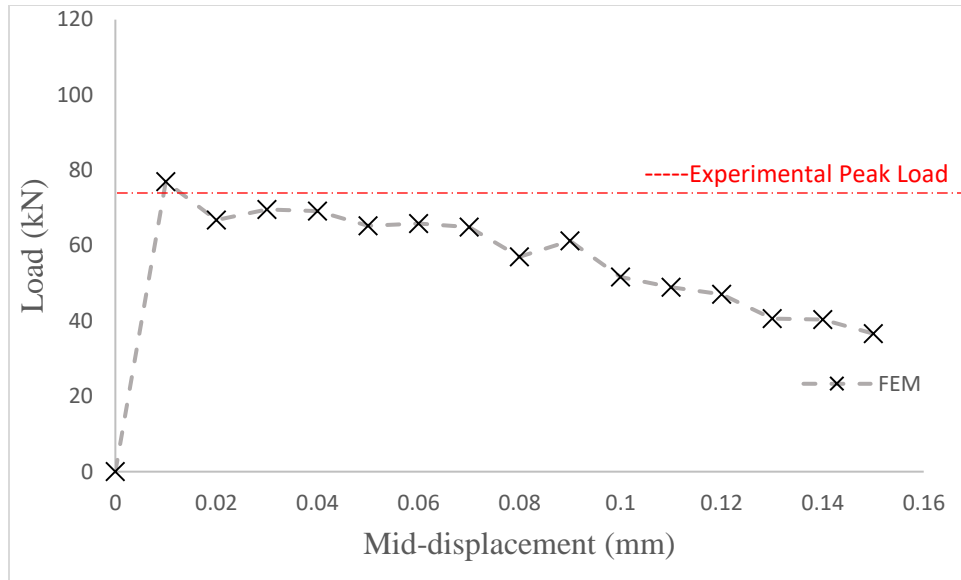
.
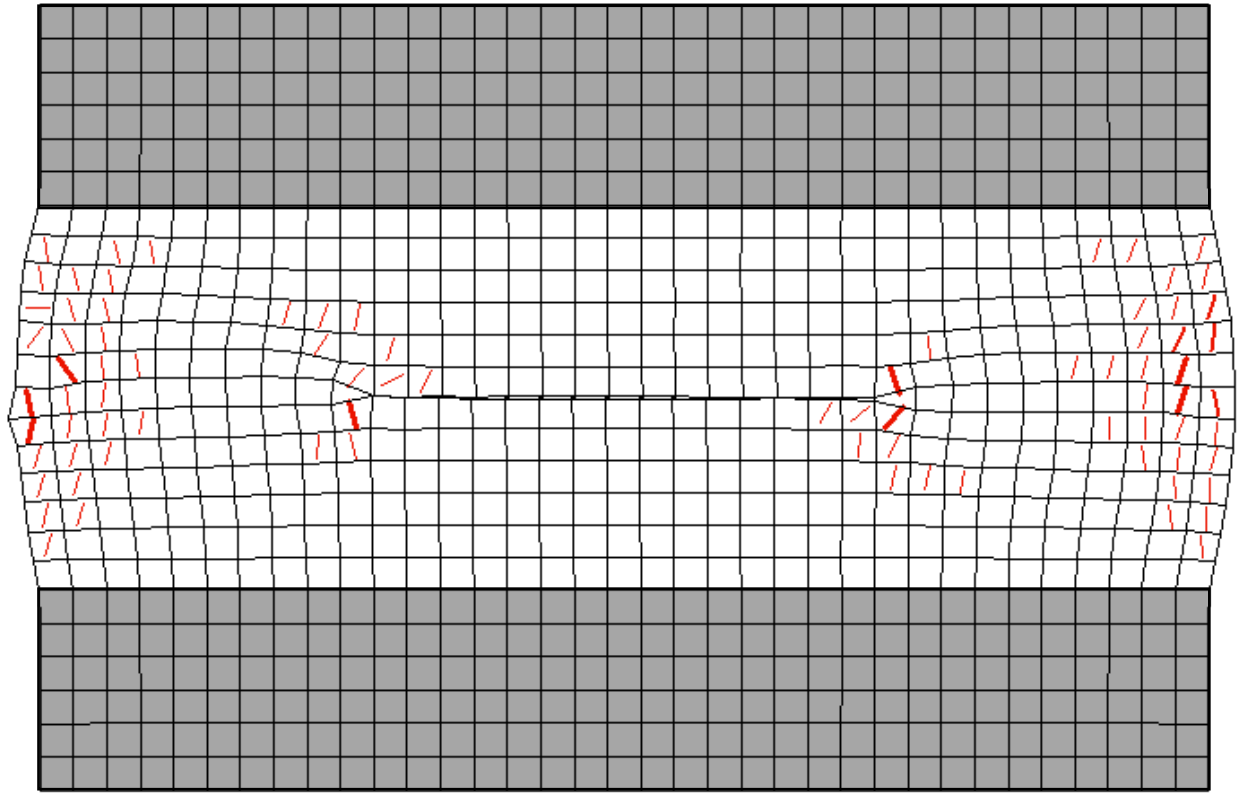
(a)
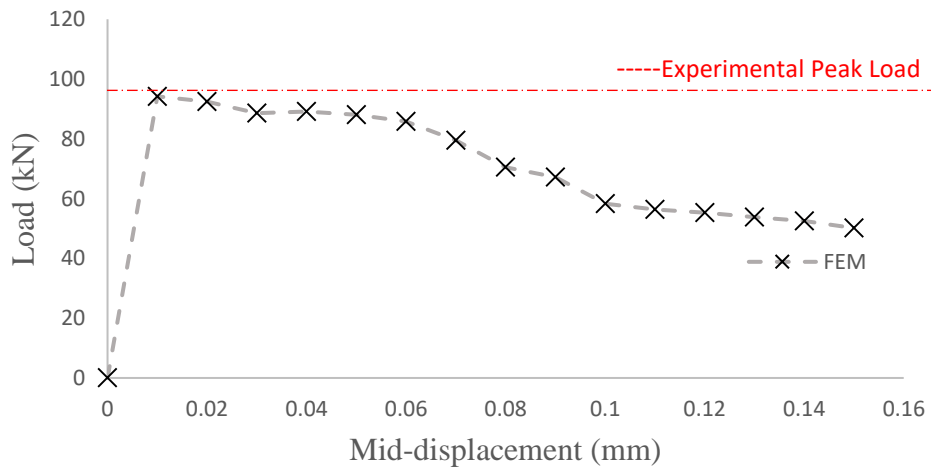
(b)

Figure 6- 26(a): The failure pattern of the SSAB-15 brick under compressive strength test in the transverse

direction (b): The analytical load- mid displacement response for SSAB-15 brick

6.3.3.1.7 Sewage Sludge Ash (SSAB-30)Brick

The failure pattern of the control brick under compressive strength test in the transverse direction is shown in Figure 6.27(a), consistent with the experimental observations. The peak load and the maximum displacement at the midpoint of the SSAB-30 at failure was 90.4 kN and 0.02 mm respectively. The FE analysis yielded the same response pattern at a peak load of 90.1 kN.
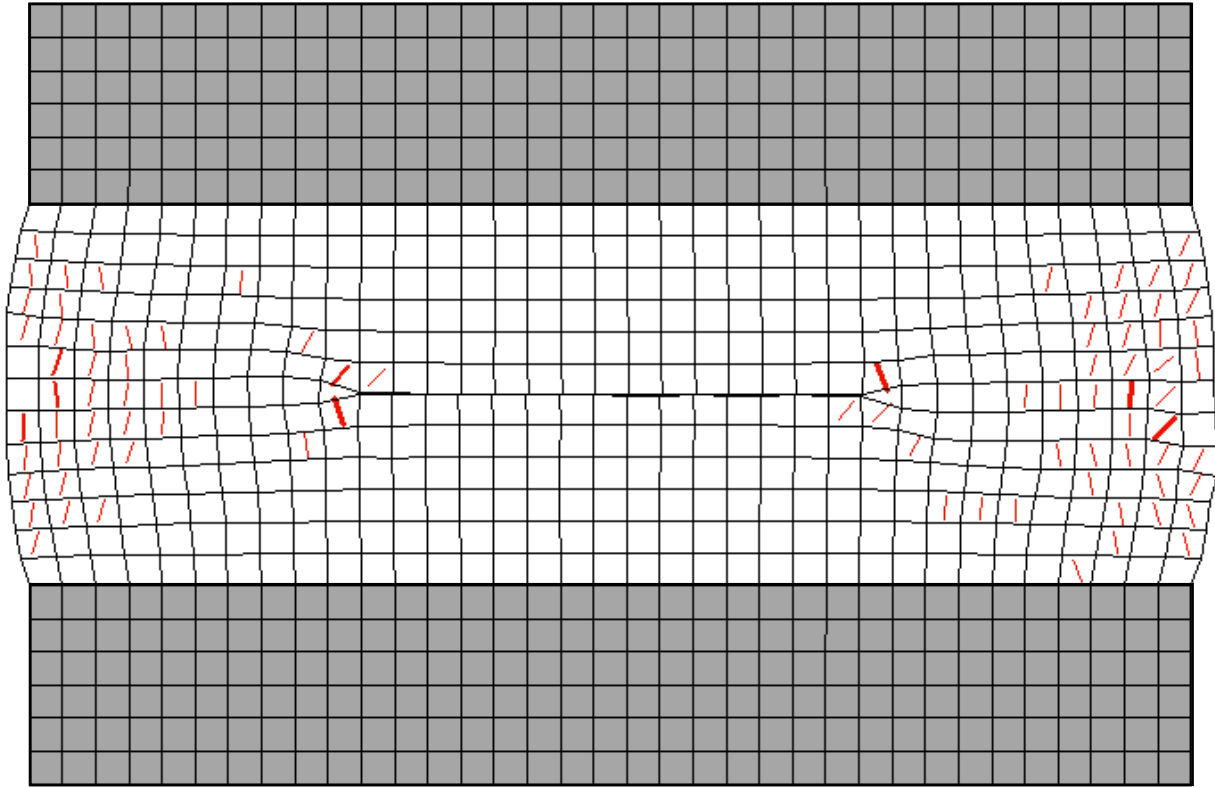

(a)

[161]
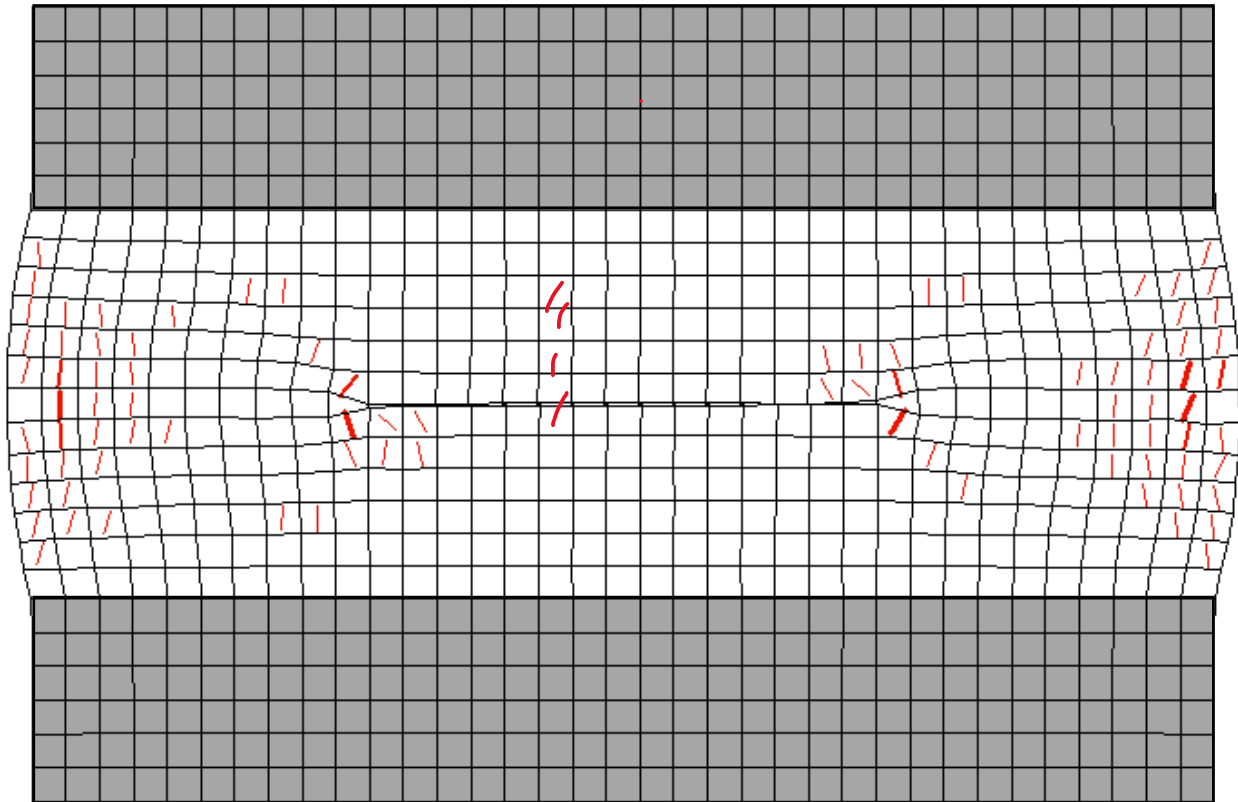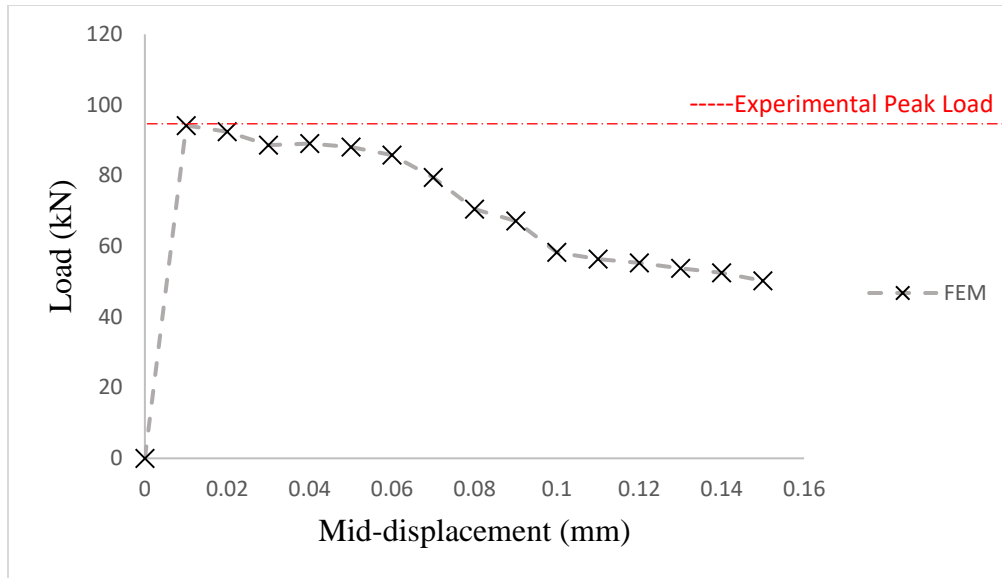
(b)

Figure 6-27(a): The failure pattern of the SSAB-30 brick under compressive strength test in the transverse direction (b): The analytical load- mid displacement response for SSAB-30 brick

6.3.3.2 Comparison of numerical and experimental analysis

Results from the from the numerical analysis and test values obtained for the peak load under compressive strength test in the transverse direction areshown in Figure 6-28. The response of the FE model for the all the brick specimens is within the range of the actual experimental values. However, there is a slight overestimation of peak load compared to the observed values. The percentage deviation between test and simulation was between 0.1 -2%, i.e., well below the tolerance for experimental error for this class of materials. Overall, the FE model was able to reproduce the response and the observed crack pattern as in the experimental analysis with consistency and accuracy.
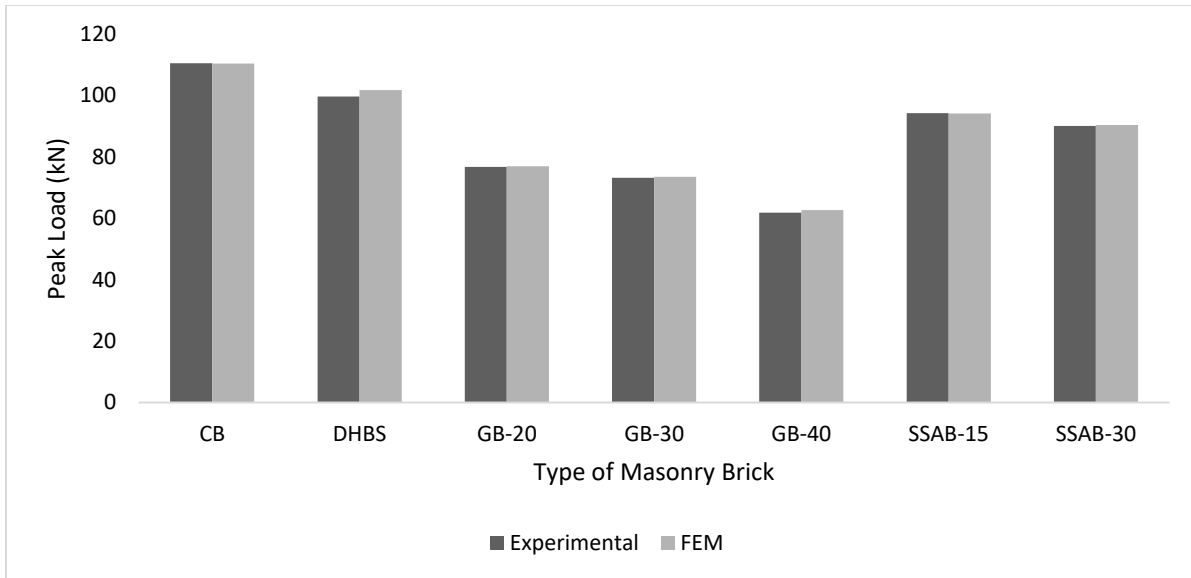
Figure 6-28: The numerical and experimental analysis of peak load under compressive strength test in the transverse direction

6.3.4 Simulation of the Compressive Strength Test-Longitudinal Direction

Finite element modelling of the test set up for the compressive strength of the hybrid masonry brick in the longitudinal axis was also conducted for all the categories of bricks. All the brick units modelled were, 70mm in length and 26mm in depth. The model consists of 611 plane stress rectangular elements of size 2mm x 2mm with an aspect ratio of 1 and 672 nodes; included in the model are the mechanical hardware (steel plates, Teflon layer). The default models present in VecTor2 described in Section 6.3.1 are used as constitutive models. The boundary conditions and the loading protocol for the compressive strength test in longitudinal direction was also same as the compressive strength test simulation in the transverse direction.
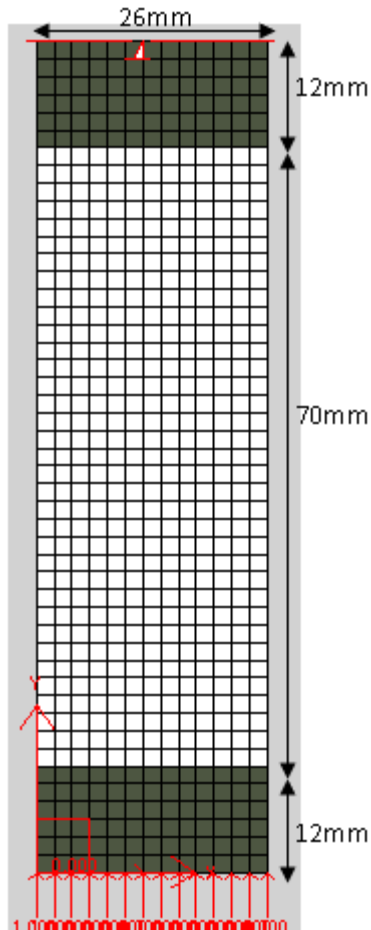
Figure 6-29 The finite element model of a brick under compressive strength test in the longitudinal direction

6.3.4.1 Mechanical properties and failure patterns

The mechanical properties of the masonry bricks were obtained from the characterization experiments described earlier. Using the Finite Element model and the input obtained earlier from these tests the response of the discretized body depicted in Figure 6-29 is calculated and correlated with this specific type of experiment so as to reduce from this comparison the true uniaxial strength of the brick in compression. The results are described in detail below.

6.3.4.1.1 Control Brick (CB)

The material properties for the control brick were as follows: the compressive strength of the hybrid masonry brick in the longitudinal axis, f_c'=27.15 MPa, E_c=36625 MPa, and ρ=2008.3 kg/m^3 respectively, as obtained from the Experimental tests. The tensile strength of the control brick in the longitudinal direction was determined at 6.0 MPa after several steps of iteration. Using the thickness of the control brick as 58mm the total load of the experiment was matched with that of

the analysis, confirming the compressive strength estimation; estimated failure pattern is shown in Figure 6-30(b).The peak load and the maximum displacement at the midpoint of the brick at failure was 42.6 kN and 0.04 mm respectively as shown in Figure 630(c). From the FE analysis, the peak load was 41.9 kN.

(a)
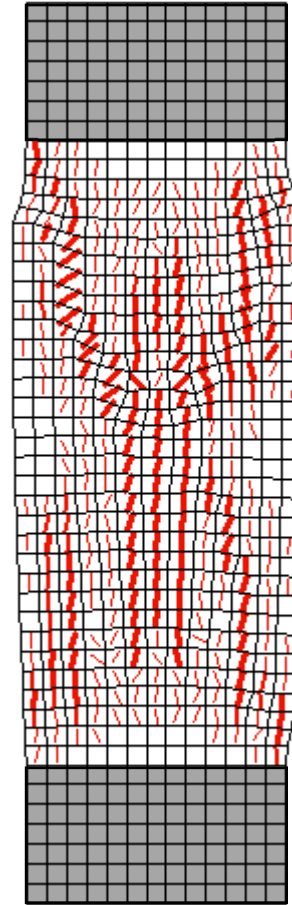
(b)
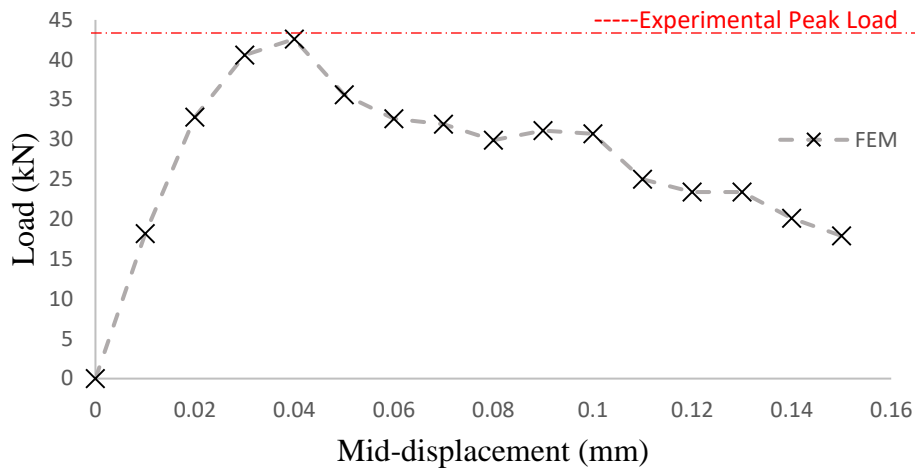
(c)

Figure 6-30 Properties of the CB used for the modelling in matching analysis with experiment; (b):Failure pattern of CB brick under Compressive Strength test in longitudinal direction; (c): The FEM response for CB

6.3.4.1.2 Dried High Biopolymer Sludge (DHBS) Bricks

The material properties for the DHBS brick used in the FEM simulation of the compressive strength of the hybrid masonry brick in the longitudinal axis were, the compressive strength $f_c^{'}$, Modulus of Elasticity E_c, density ρ, as 29.5 MPa, 34259 MPa, and 1802 kg/m^3 respectively, as obtained from the experimental test series. The value for the Poisson's ratio, μ was taken as 0.2. The tensile strength of the DHBS brick that matched the tests was found to be 7.0 MPa. The thickness of the control brick for the modelling of the compressive strength test was 58mm. The failure pattern of the brick under longitudinal compressive strength test was consistent with the experimental observation; the failure pattern is shown in Figure 6-30(b). The peak load and the maximum displacement at the midpoint of the brick at failure was 44.2 kN and 0.06 mm respectively. The experimental peak load was 43.8 kN which is almost equal to the FE estimation. The response of the analytical load- mid displacement response curve for DHBS brick is shown in Figure 6-30(c).

[166]
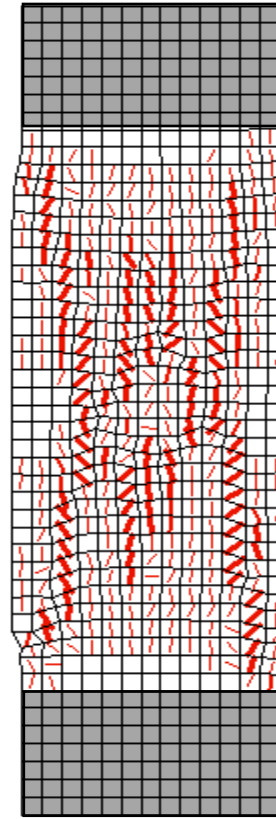
(a)   (b)
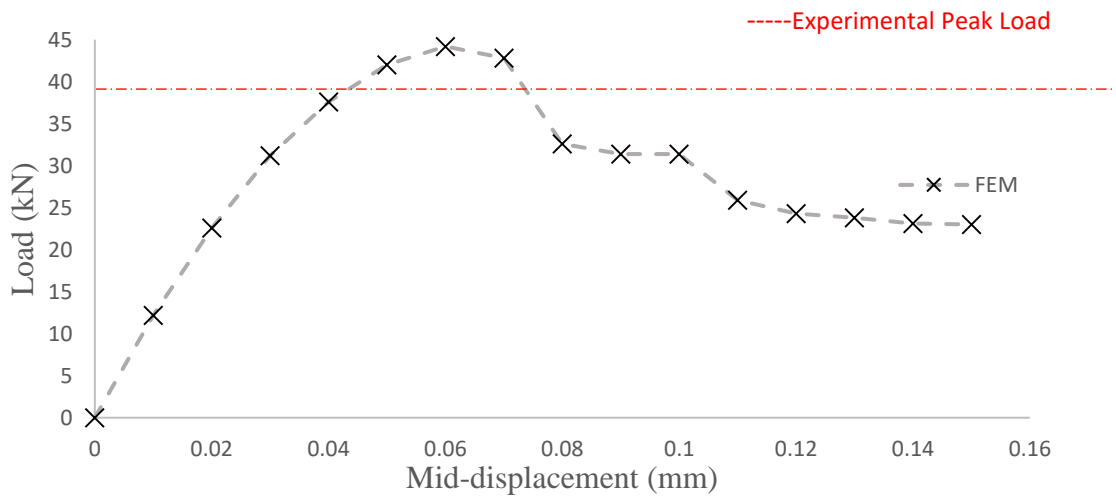
(c)

Figure 6-31(a): Properties of the DHBS brick used for the modelling in matching analysis with experiment

(b):Failure pattern of DHBS brick under Compressive Strength test in longitudinal direction (c): The FEM

response for DHBS brick

[167]

6.3.4.1.3 Geopolymer Bricks (GB-20)

For the FEM simulation of the mechanical test, the value of the parameters including the compressive strength f_c', Modulus of Elasticity E_c, and density were 16.4 MPa, 19482 MPa, and 2039.301 kg/m^3 respectively, were obtained from the experimental tests. The value for the Poisson's ratio was taken as 0.2. After iteration in matching the analysis and the experimental response curves it was determined that the tensile strength of GB-30 brick was 3.0 MPa. The thickness of the control brick for the modelling of compressive strength test was 58mm. The failure pattern of the brick under the longitudinal compressive test was cosnistenth with the experimental observation; the failure pattern is shown in Figure 6-3(b). Peak load and maximum displacement at the midpoint of brick failure was 24.8 kN and 0.06 mm respectively as depicted in the response curve (Figure 6-3(c)). The peak load from the experimental test was 24.3 kN which is a proof of relevance for the FE estimation.

(a)   (b)

(c)

Figure 6-32(a): Properties of the GB-20 used for the modelling in matching analysis with experiment (b):Failure pattern of GB-20 brick under Compressive Strength test in longitudinal direction (c): The FEM response for GB-20

6.3.4.1.4 Geopolymer Bricks (GB-30)

Compressive strength f_c', Modulus of Elasticity E_c, and density were taken from the experimental results as 15.4 MPa, 16089 MPa, and 1959 kg/m³ respectively. Poisson's ratio was taken as 0.2. The thickness of the GB-30 for the modelling of compressive strength test was taken as 58 mm. The tensile strength of the GB-30 brick was found to be 3.0 MPa after several iterations. The failure pattern of the brick under compressive strength in longitudinal axis was consistent with the experimental observations . The failure pattern is shown in Figure 6-3(b). Peak load and maximum displacement at the midpoint of the brick at failure were, 23.4 kN and 0.07 mm respectively, as depicted in Figure 6-3(c).

Material Properties

Reference Type:	Reinforced Concrete	
Thickness, T:	58	mm
Cylinder Compressive Strength, f'c:	15.39	MPa
Tensile Strength, f't:	* 2	MPa
Initial Tangent Elastic Modulus, Ec:	* 16085	MPa
Cylinder Strain at f'c, eo:	* 0.957	me
Poisson's Ratio, Mu:	* 0.2	
Thermal Expansion Coefficient, Cc:	* 1e-006	/°C
Maximum Aggregate Size, a:	* 0.1	mm
Density:	* 1959.187	kg/m3
Thermal Diffusivity, Kc:	* 0	mm2/s
Maximum Crack Spacing...		
perpendicular to x-reinforcement, Sx:	* 1000	mm
perpendicular to y-reinforcement, Sy:	* 1000	mm

Color
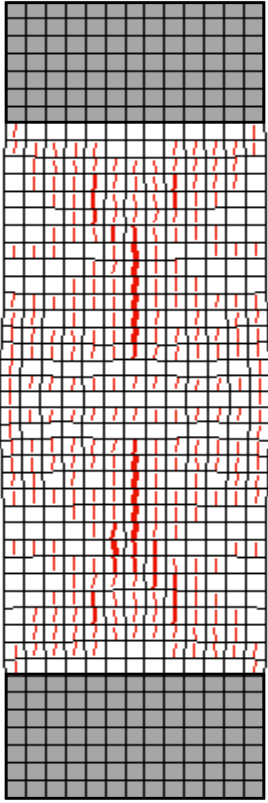
(a)

(b)
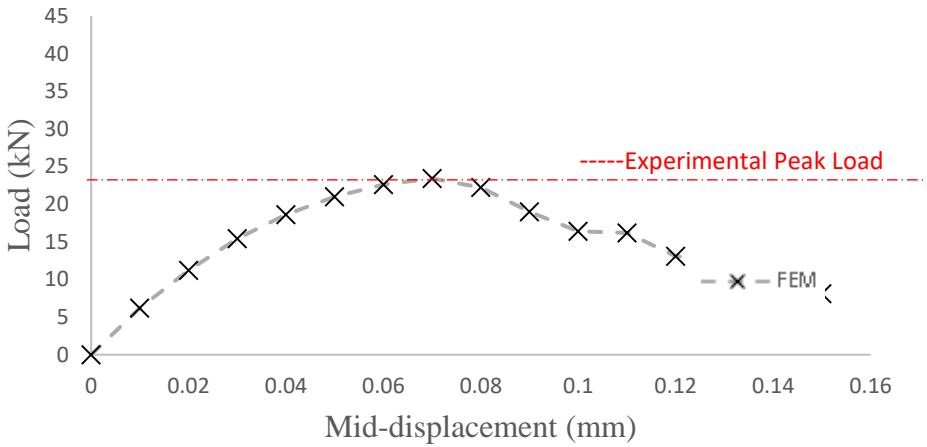
(c)

Figure 6-33(a): Properties of the GB-30 used for the modelling in matching analysis with experiment (b):Failure pattern of GB-30 brick under Compressive Strength test in longitudinal direction (c): FEM response for GB-30 brick

[170]

6.3.4.1.5 Geopolymer Bricks (GB-40)

As previously, the essential input parameters obtained from the experiments were, f'_c=13.17 MPa, E_c=11704 MPa, and ρ =1872.896kg/m^3 respectively.The value for the Poisson's ratio μ, was taken as 0.2. A tensile strength of 2.0 MPa was determined after matching with the experimental data. The thickness of the GB-40 for the modelling of compressive strength test was 58 mm. Failure pattern of the brick under compressive strength in longitudinal direction was consistent with the experimental observation, as shown in Figure 6-3(b). Peak load and maximum displacement at the midpoint of the brick at failure was 19.8 kN and 0.08 mm respectively (Figure 6-3(c)). The experimental peak load value was 19.4 kN.

(a)

(b)

(c)

Figure 6-34 : Properties of the GB-40 used for the modelling in matching analysis with experiment (b):Failure pattern of GB-40 brick under Compressive Strength test in longitudinal direction (c): The FEM response forGB-40 brick

6.3.4.1.6 Sewage Sludge Ash (SSAB-15) Bricks

For the FEM simulation of the compressive strength of the hybrid masonry brick in the longitudinal axis the material properties used are obtained from t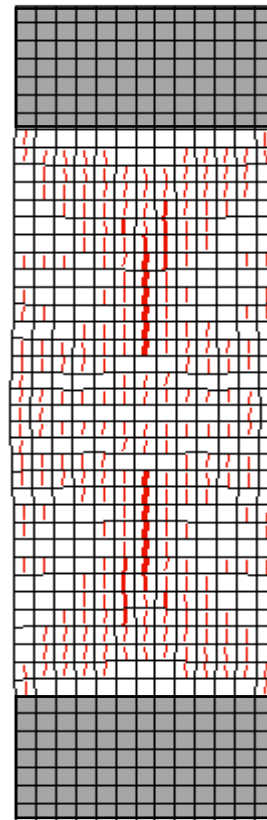he experimental program as follows: compressive strength $f_c{}'$, Modulus of Elasticity E_c, density ρ, were, 30.3 MPa, 25901 MPa, and 1819 kg/m^3 respectively. The value for the Poisson's ratio μ, was taken as 0.2. The tensile strength of the SSAB-15 brick was found to be 6 MPa from several iterations until the difference between measured and estimated load was within the experimental tolerance. The thickness of the SSAB-15 for the modelling of compressive strength test was taken as 58 mm. The failure pattern of the brick under flexural strength test was similar to the actual test. The failure pattern is shown in Figure 6-31(b). The peak load and the maximum displacement at the midpoint of the brick at failure was 45.0 kN and 0.08 mm respectively as shown in the response curve (Figure 6-31(c)). The experimental peak load was 45.0 kN.
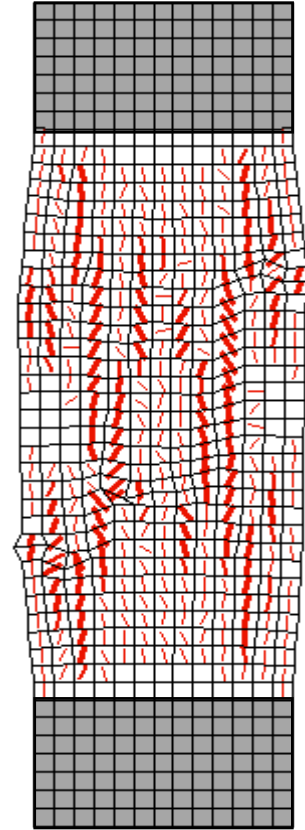
(a)   (b)

(c)

Figure 6-35(a): Properties of the SSAB-15 used for the modelling in matching analysis with experiment(b): Failure

pattern of SSAB-15 brick under Compressive Strength test in longitudinal direction (c): The FEM response for

SAB-15 brick

[173]

6.3.4.1.7 Sewage Sludge Ash (SSAB-30) Bricks

The compressive strength $f_c^{'}$, Modulus of Elasticity E_c, and density used were obtained from the experiments as 24.4 MPa, 17843 MPa, and 1556 kg/m^3 respectively. Again, Poisson's ratio was taken as 0.2. Upon several iterations, the tensile strength of the SSAB-30 brick was found to be 6 MPa. Here as well, the thickness of the SSAB-30 for the modelling of compressive strength test was taken as 58mm.The failure pattern of the brick under the flexural strength test was consistent with the experimental observation. The failure pattern is depicted in Figure 6-32(b).The peak load and the maximum displacement at the midpoint of the brick at failure was 36.6 kN and 0.1mm respectively is depicted in Figure 6-32(c). The actual experimental peak load was 36.2 kN which is close to the peak load from FE analysis.
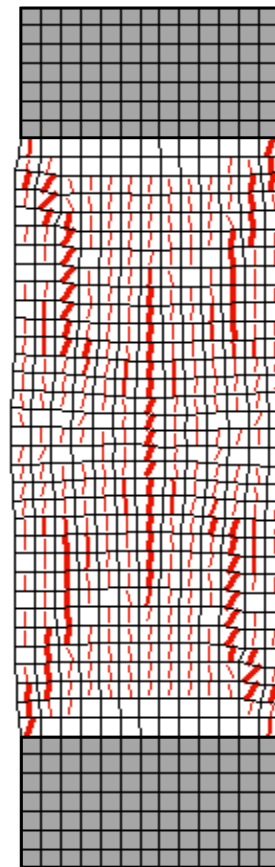
(a)   *(b)*
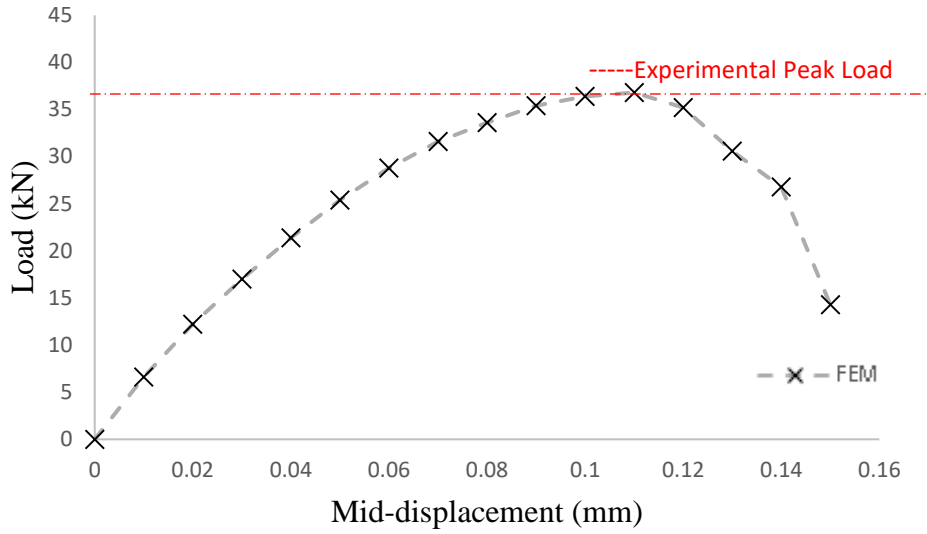
(c)

Figure 6-36:Properties of the SSAB-30 used for the modelling in matching analysis with experiment (b):Failure pattern of SSAB-30 brick under Compressive Strength test in longitudinal direction (c): The FEM response for SSAB-30 brick

6.3.4.2 Comparison of numerical and experimental Analysis
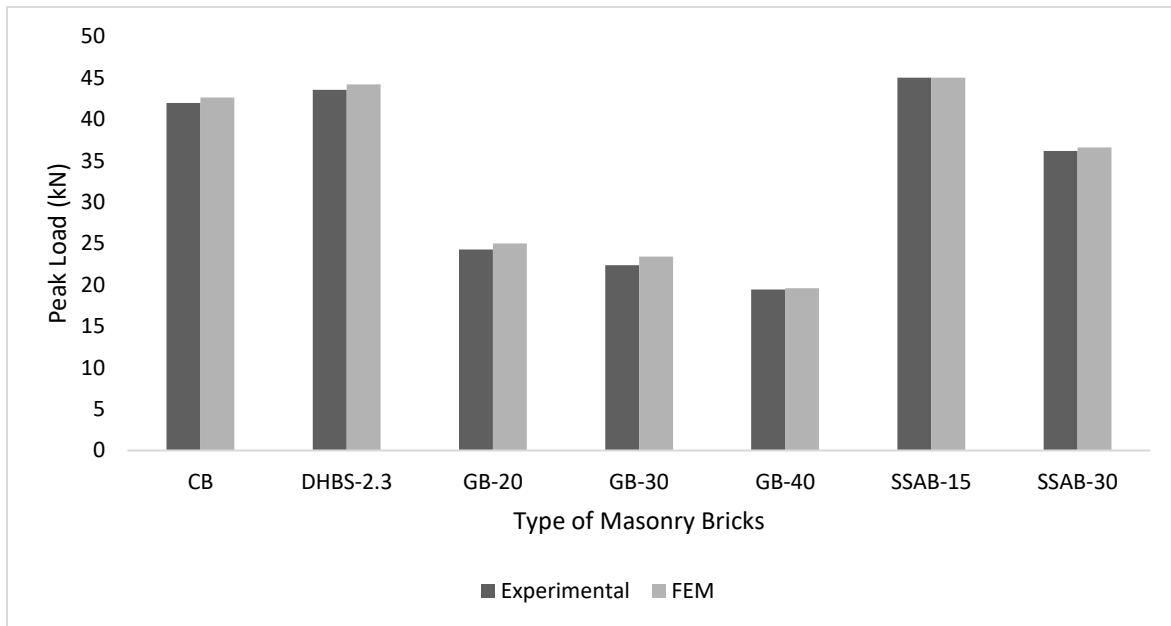
Figure 6-37 : The numerical and experimental analysis of peak load under compressive strength test in the longitudinal direction

[175]

Results from the numerical analysis and the experiments for the peak load obtained from the compressive test in the longitudinal direction are compared in Figure 6.37. Load responses were reproduced with sufficient accuracy with the difference between analytical and experimental values being in the range from 0.04% to 4.4 %.

6.3.5 Tensile strength in transverse and longitudinal direction
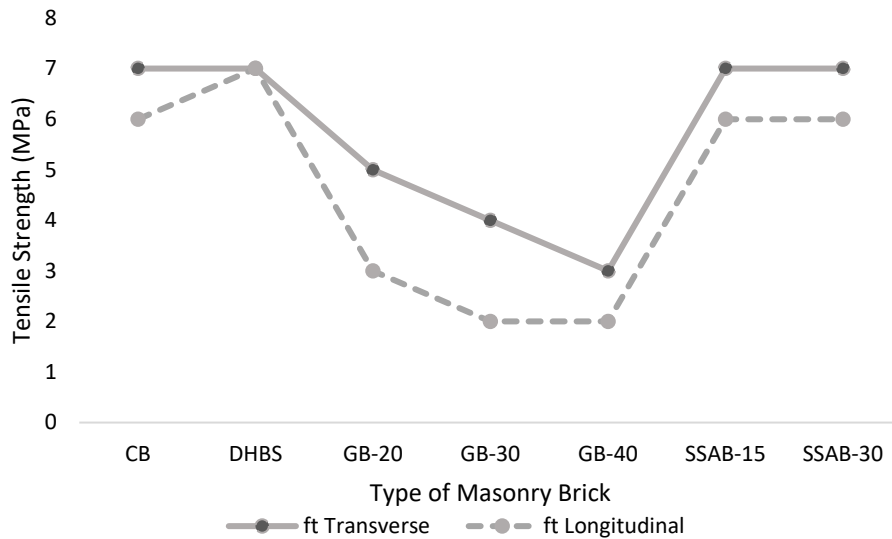
From the iterative inverse analysis by matching within acceptable tolerance (less than the experimental error in the range of 10%) of the numerical load-displacement response curve with its experimental counterpart, the actual tensile strength was obtained for all the categories of brick in the transverse and longitudinal direction. The tensile strength for DHBS brick found the same for both directions of testing. However, for all other brick the tensile strength in the longitudinal direction was in the range of 60-85% of the tensile strength measured when applying compression in the transverse direction.

6.3.6 Summary

The numerical responses obtained are consistent with the responses obtained from the tests for all categories of brick developing practically the same peak load and failure pattern. This enables accepting the resulting values for the explored mechanical properties through the inverse analysis for quality control of the bricks, for qualification of the acceptance criteria set by the Industry and codes, and for the next phase of the investigation presented in Chapter 7 which explores

correlations and inter-relationships between values obtained from non-destructive qualifiers and destructive tests of the fabricated bricks.

Chapter 7. Correlation Analysis

Through this research, various parameters associated with the properties of masonry brick have been studied through several laboratory tests as well as numerical analysis. Correlation of various physical and mechanical response indices based on the experimental results is pursued in this chapter. Correlation analysis is used in order to identify and establish relationships between mechanical properties including compressive strength, tensile strength, flexural strength, splitting tensile strength, Young's Modulus and physical properties including water absorption, resonance frequency, ultrasonic pulse velocity of masonry bricks which are mostly obtained from non-destructive tests and could then be used as calibrated predictors of mechanical properties all of which are measured with destructive tests. The coefficient of determination R^2 shows the percent variation of the parameter in Y axis, which is explained by all the X variables together. Similarly, another term that shows degree of relationship between the variables in X and Y axis in a range of -1 to +1 called Coefficient of correlation or Pearson Correlation Coefficient (R) is used.

The correlation between the several parameters studied for brick types CB, DHBS, GB-20, GB-30, GB-40, SSAB-15, and SSAB-30 are illustrated in the following figures.

7.1 Correlation between the square root of Compressive Strength in Transverse Direction and Tensile Strength.
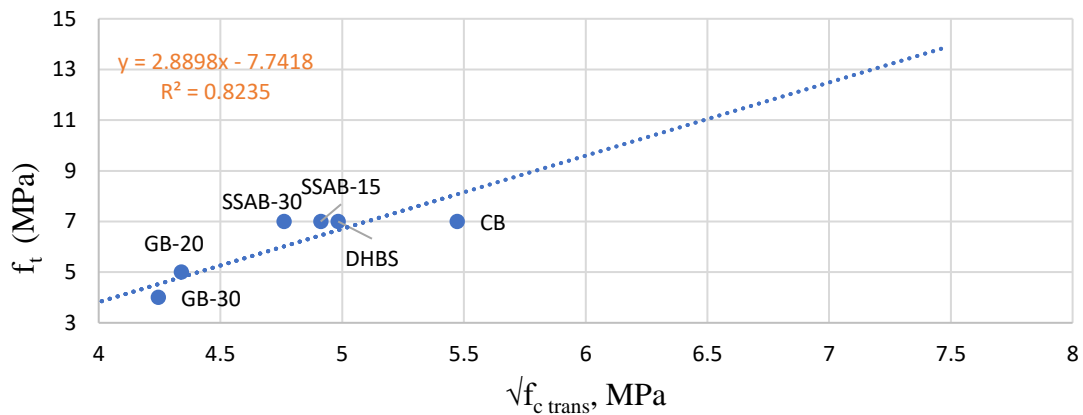
Figure 7-1: Correlation between the square root of Compressive Strength in Transverse Direction and Tensile Strength

The square root of the compressive strength is a standard point of reference in brittle and semi-brittle materials as most tensile phenomena and strength indices are expressed as multiples of this

parameter. The correlation between the square root of compressive strength of the masonry bricks in the transverse direction and the tensile strength obtained after F.E. calibration is shown in Figure 7-1. The coefficient of determination or the percentage variation of the compressive strength with respect to the tensile strength is 82.3%. It is clear from the plot that there is a good correlation between the compressive strength of the masonry bricks in the transverse direction and the tensile strength, a finding that underlines the similarity in response of masonry with that of concrete and other brittle materials.

7.2 Correlation between the Square Root of Compressive Strength in Longitudinal direction and Tensile Strength.
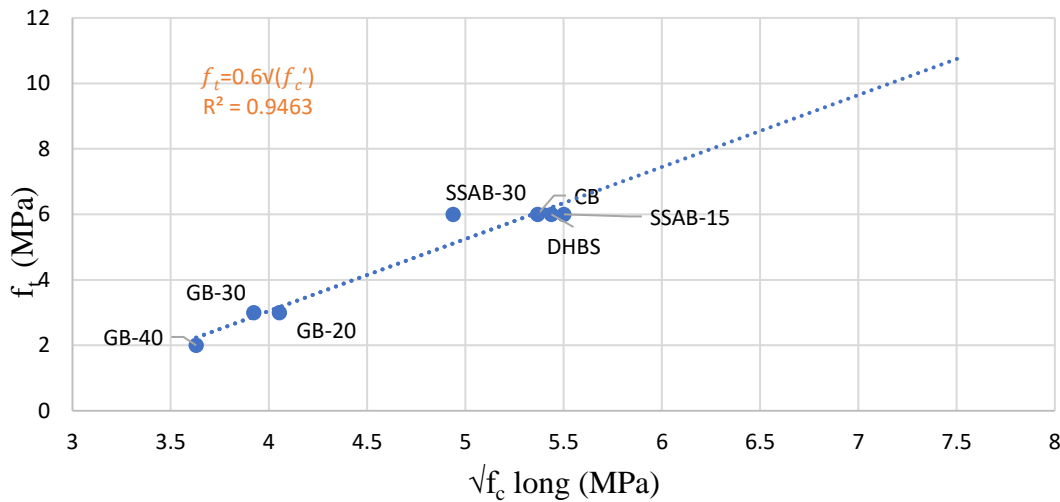
Figure 7-2: Correlation between the square root of Compressive Strength in Longitudinal direction and Tensile Strength

The coefficient of determination or the percentage variation of the square root of the compressive strength in the longitudinal direction with respect to the tensile strength obtained after F.E. matching of the experimental results, is 94.36%. Here it was shown that the tensile strength may be obtained from the compressive strength using the expression below, which is consistent with the established practice for masonry (from the Industry):

$$f_t = 0.6\sqrt{f_c'} \qquad\qquad (7.1)$$

7.3 Correlation between the Square Root of Compressive Strength in transverse Direction and Flexural Strength

Figure 7.3 plots the square root of compressive strength against the equivalent tensile strength value obtained from the flexural tests; the latter is calculated from the total load, W, carried by the brick under three-point loading, as $f_{t\ flex} = \frac{3W(L/2-x)}{bd^2}$. Correlation is satisfactory with coefficient of determination equal to 91.67% leading to a relationship:

$$f_{flex} = 2.9\sqrt{f_c'} \tag{7.2}$$
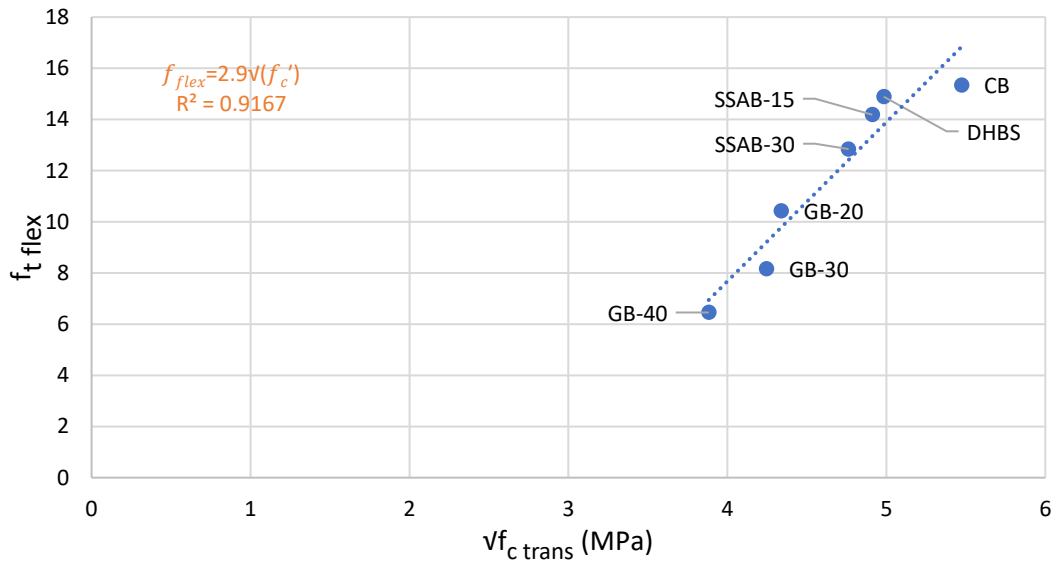
Figure 7.3: Correlation between the square root of Compressive Strength in Longitudinal Direction and Flexural Strength

7.4 Correlation between the Square Root of Compressive Strength in Transverse Direction and Splitting Tensile Strength

The coefficient of determination of the square root of compressive strength in transverse direction with respect to the splitting tensile strength, the latter being an alternative measure of tensile resistance is found to be 56.38%. Therefore, the correlation between compressive strength with splitting tensile strength is less evident and unreliable.
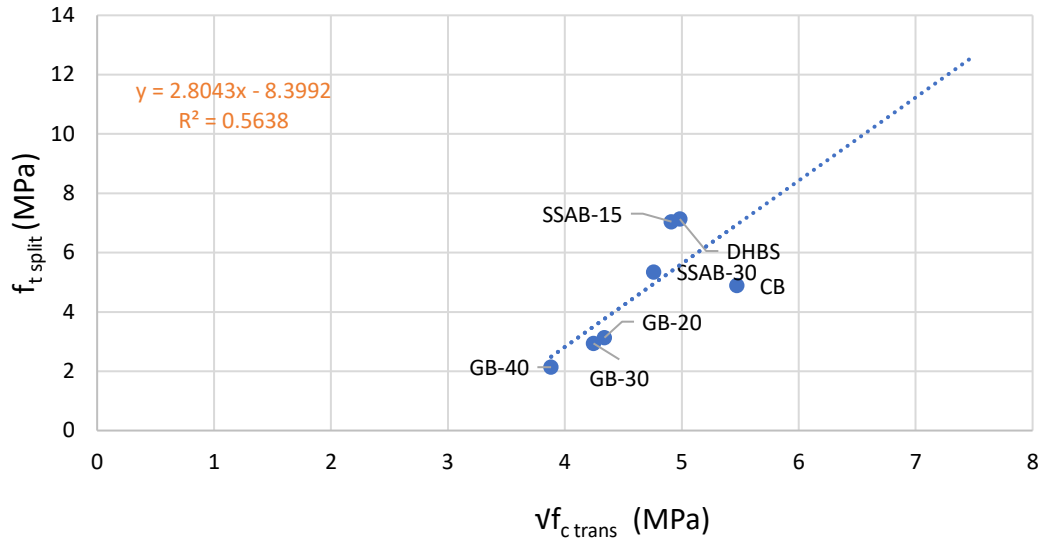
Figure 7-4: Correlation between Compressive Strength in Transverse Direction versus Splitting Tensile Strength

7.5 Correlation between Splitting Tensile Strength and Flexural Strength
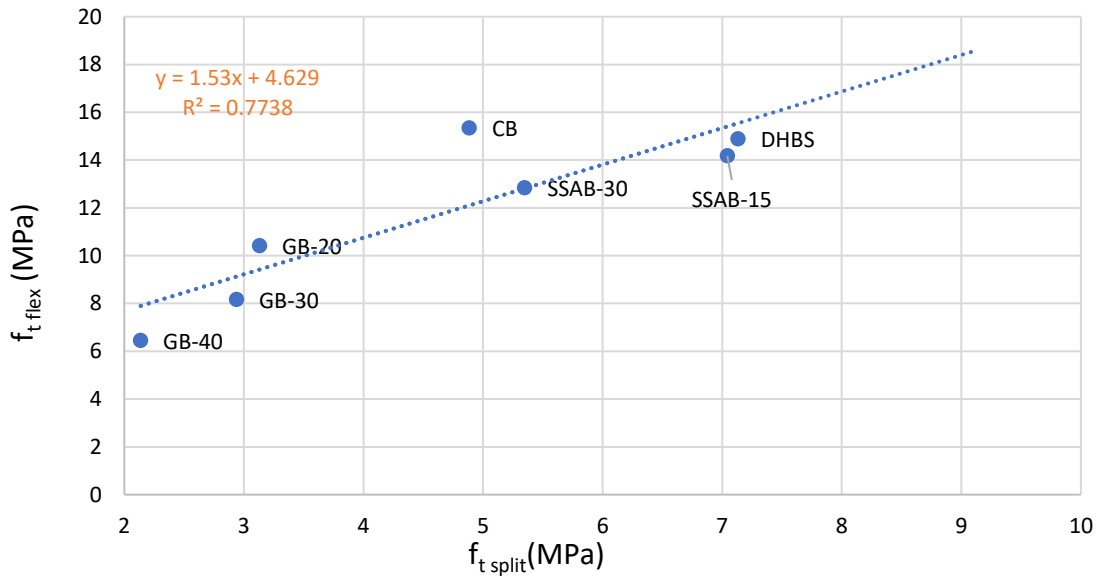
Figure 7-5: Correlation between Splitting Tensile Strength and Flexural Strength

Figure 7-5 shows a positive correlation between the Splitting Tensile Strength and the Flexural Strength of the masonry bricks. The coefficient of determination is found to be 77.38%.

7.6 Correlation between the Square Root of Compressive Strength in Transverse Direction and Ultrasonic Pulse Velocity
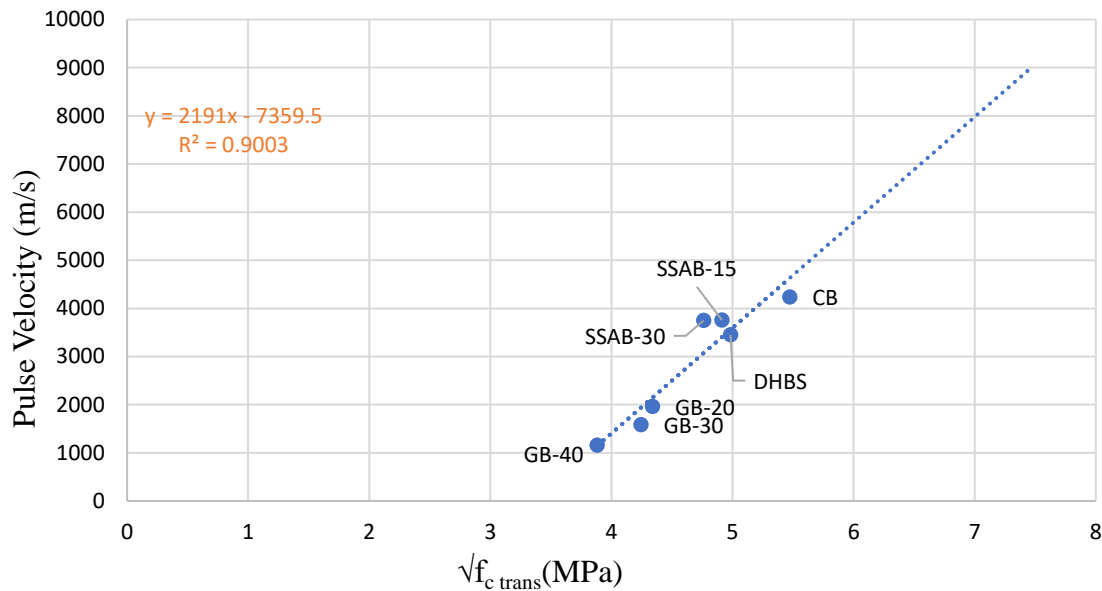
Figure 7-6: Correlation between the square root of the Compressive Strength in transverse direction and Ultrasonic Pulse Velocity

In terms of as the prospects of using non-destructive evaluation tools to assess quality and strength, the square root of the compressive strength of the bricks in transverse direction is correlated with the ultra sonic pulse velocity obtained prior to mechanical testing, as shown in Figure 7.6. Note that the UPV test is a standard quality control test in brick manufacturing. The coefficient of determination or the percentage variation of the compressive strength with respect to the ultra sonic pulse velocity is 90.03% indicating a strong dependence between the two parameters.

7.7 Correlation between Compressive Strength in Transverse Direction and Resonance Frequency

Another type of non-destructive evaluation method is the transverse resonant frequency test which is used routinely in assessment of freeze thaw damage of structural materials. Here results for compressive strength are plotted against the resonant frequency value in Figure 7-7. With a coefficient of determination equal to 88.72%, resonant frequency appears to be a very effective non-destructive means of projection of brick strength.
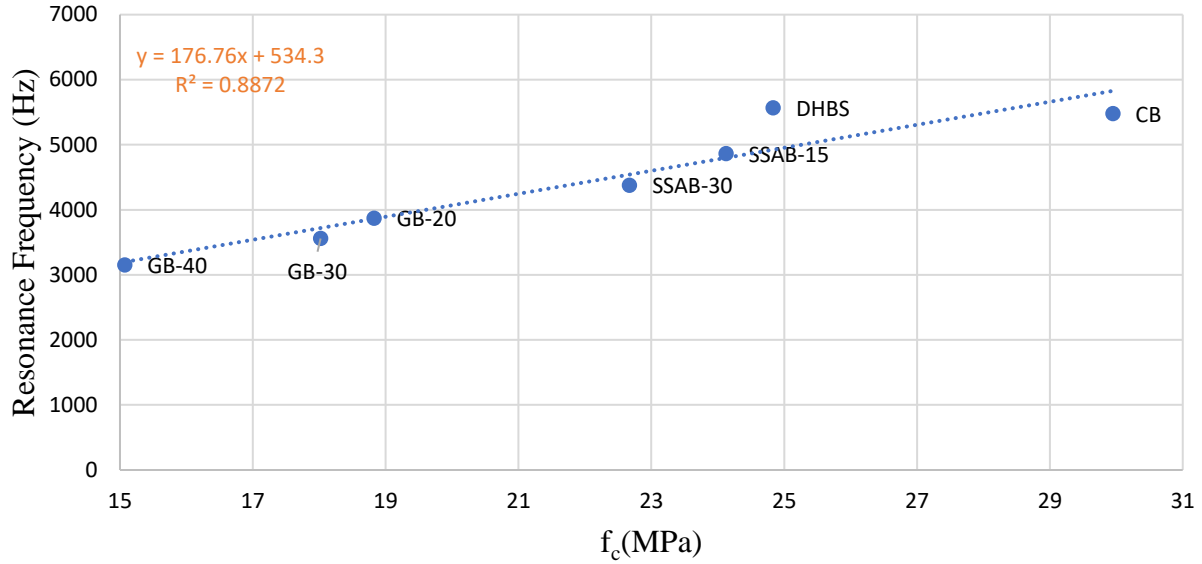
Figure 7-7: Correlation between Compressive Strength and Resonance Frequency

7.8 Correlation between Compressive Strength in Transverse Direction and Modulus of Elasticity
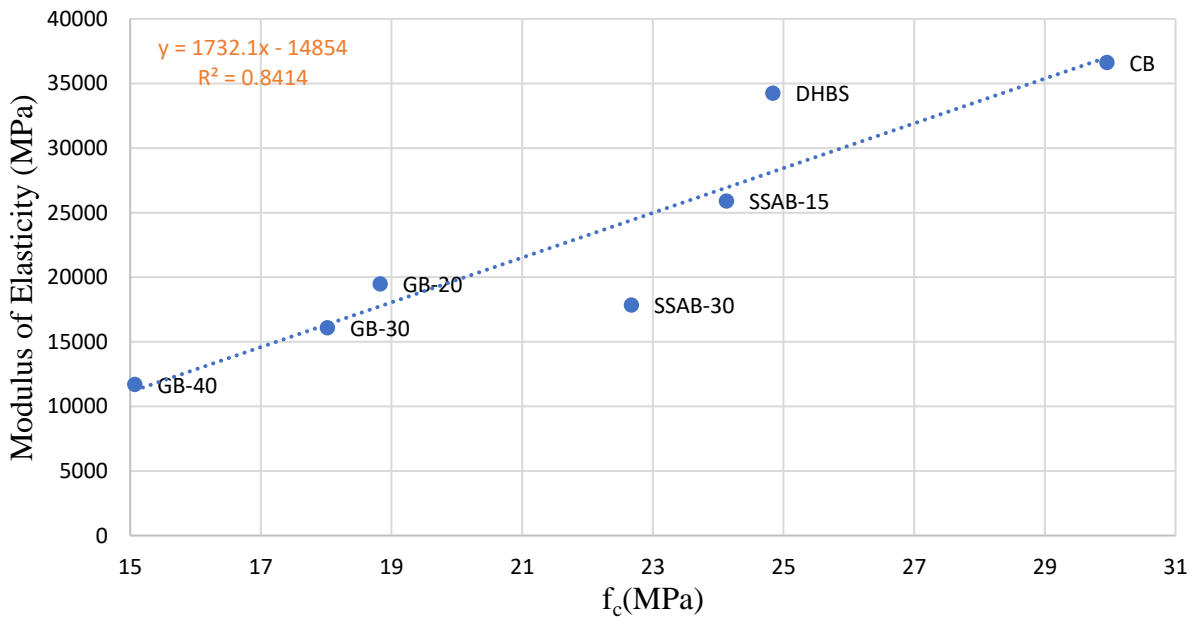
Figure 7.8: Correlation between Compressive Strength and modulus of elasticity

Modulus of elasticity is considered to be in linear correlation with the Resonant Frequency; the value considered in the correlation is the calibrated value obtained after matching the response

[183]

curves of the FE model of the specimens with the actual experimental envelopes. The percentage variation of the compressive strength with respect to the modulus of elasticity is 84.14%; as depicted in Figure 7-8, there is almost a linear relationship between the sets of values of the two parameters.

7.9 Correlation between Density and Compressive Strength in transverse direction
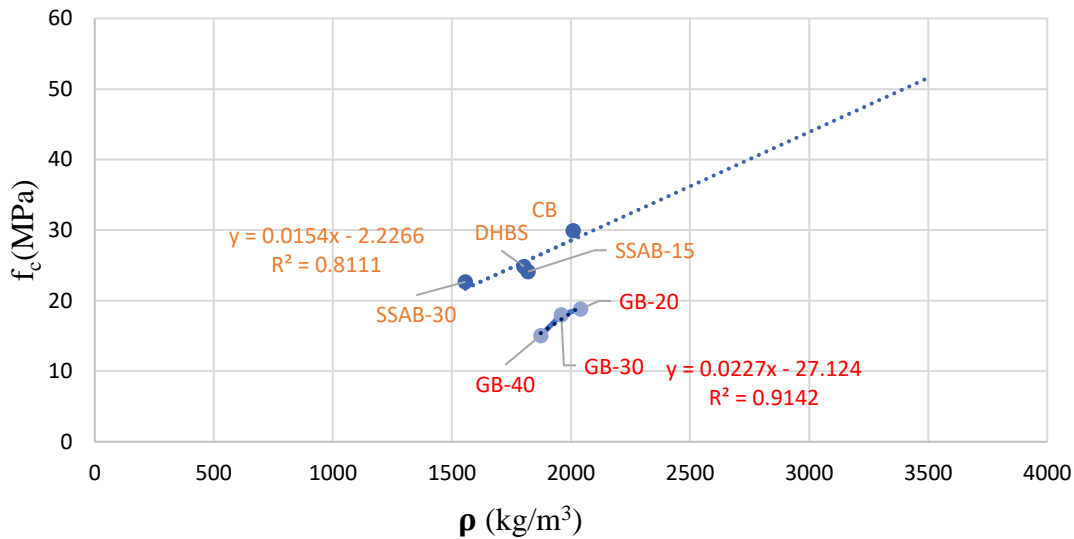
Figure 7-9: Correlation between Density and Compressive Strength

The coefficient of determination of the density with respect to the compressive strength for geopolymer bricks is 91.4% whereas in the case of CB, DHBS and SSAB bricks it's 81.11% indicating a linear and strong dependence between the two parameters as shown in Figure 7-9. An improved correlation is obtained when the Geopolymer bricks are grouped separately

7.10 Correlation between Density and Modulus of Elasticity

Similarly, the correlation between the density and modulus of elasticity of the geopolymer bricks is 99.74% whereas for the CB, DHBS and SSAB bricks, it's only 79.98%.Correlation is improved if Geopolymer bricks are grouped separately as presented in Figure 7.10.
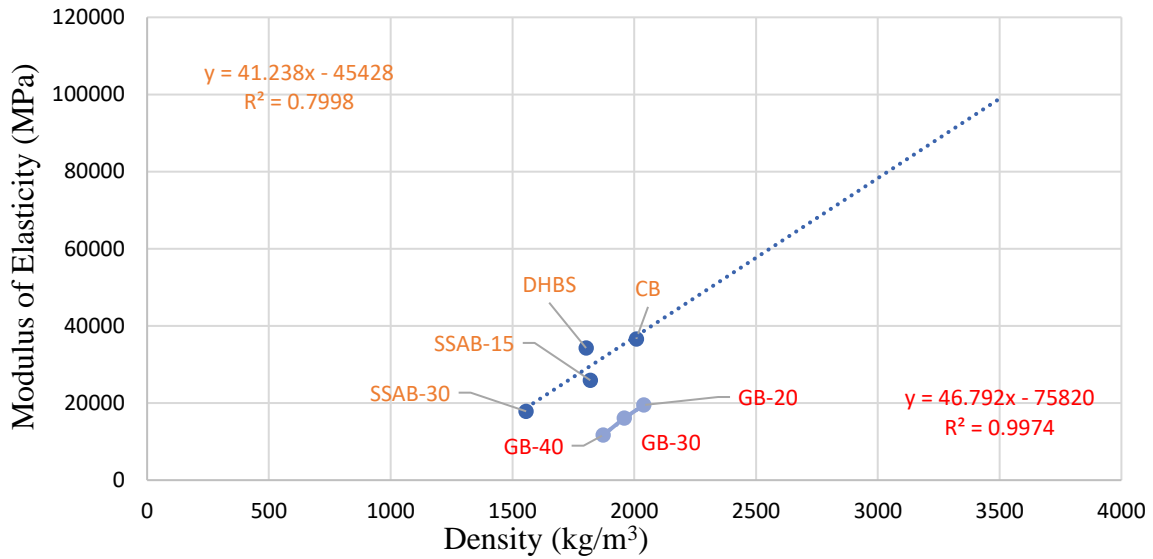
Figure 7-10 : Correlation between Density and Modulus of Elasticity

7.11 Correlation between Cold-Water Absorption and Ultrasonic Pulse Velocity
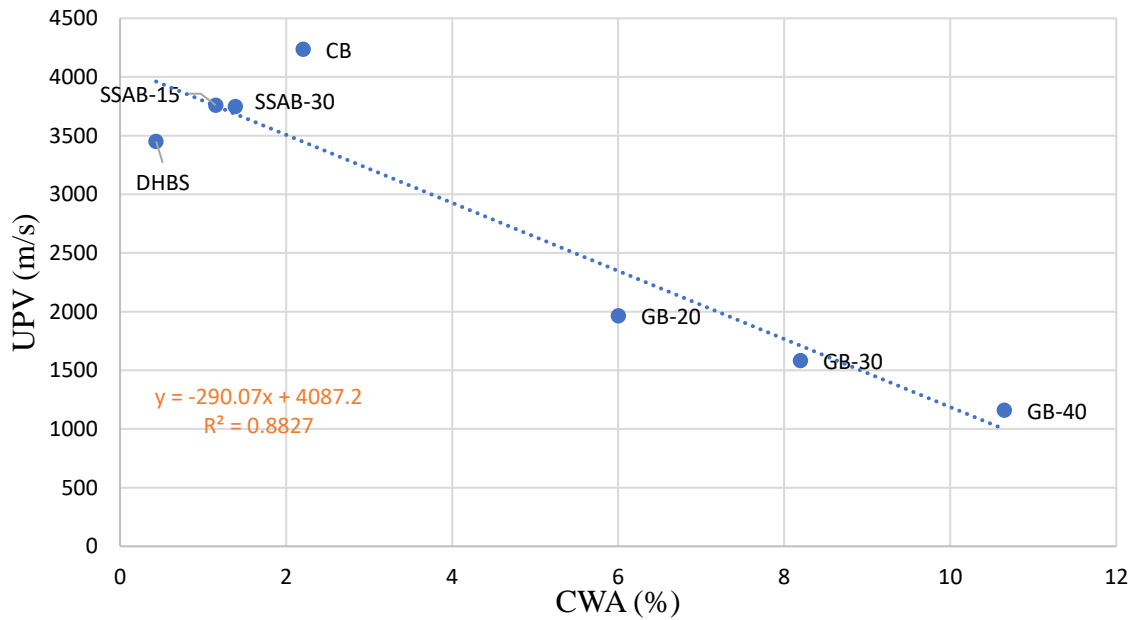
Figure 7-11: Correlation between Cold-Water Absorption and Ultrasonic Pulse Velocity

Motivated by the same concepts as in the preceding section the correlation between CWA and UPV is explored in Fig. 7-11. Clearly, there is a strong relationship between the two variables,

with the CWA reducing with increasing UPV value. The coefficient of determination was found to be 88.27 %.

7.12 Correlation between Hot-Water Absorption and Ultrasonic Pulse Velocity
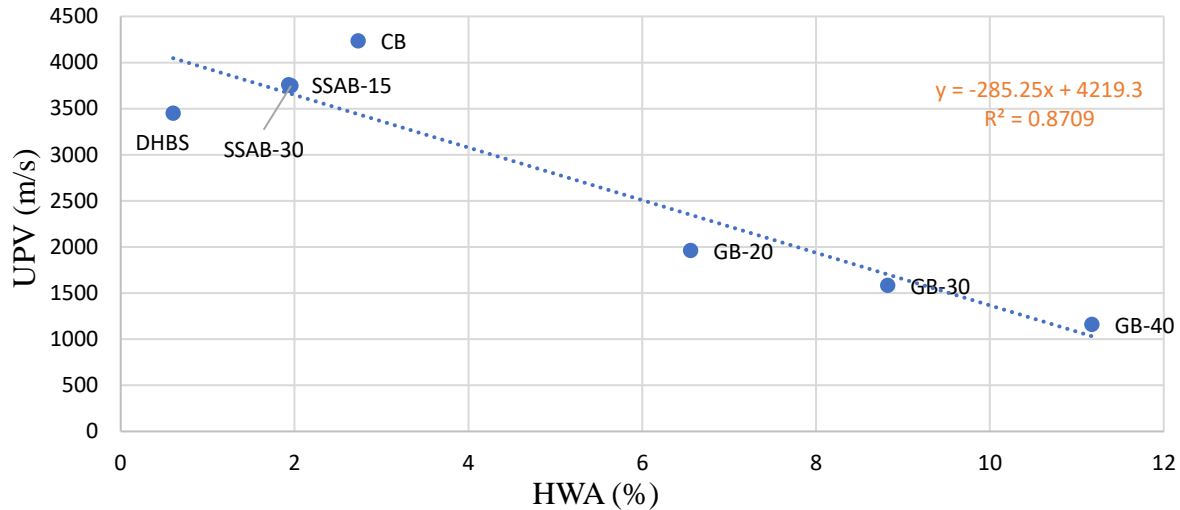
Figure 7-12: Correlation between Hot -Water Absorption and Ultrasonic Pulse Velocity

The same trend is also seen when relating the UPV with the HWA, which is an indicator of the total porosity in the material structure (i.e. both capillaries and fine pores where only gas form of water can penetrate). The coefficient of determination is found to be 87.09 % with an inverse proportionality between the two examined variables.

7.13 Correlation between Cold-Water Absorption and Resonance Frequency

Cold water absorption is an indirect measure of the connected capillary porosity having a minimum size that can overcome the tension forces of the meniscus formed by water molecules. That means that the true porosity is higher, however the additional amount comprises fine pore sizes that cannot be filled with water. Resonant frequency increases with density of the material and is therefore inversely proportional to any measure of porosity – CWA in this section, and HWA in the following section. Correlation is depicted in Figure 7-13, in the range of 80.87%, indicating a strong relation between the two variables as expected from a theoretical viewpoint.
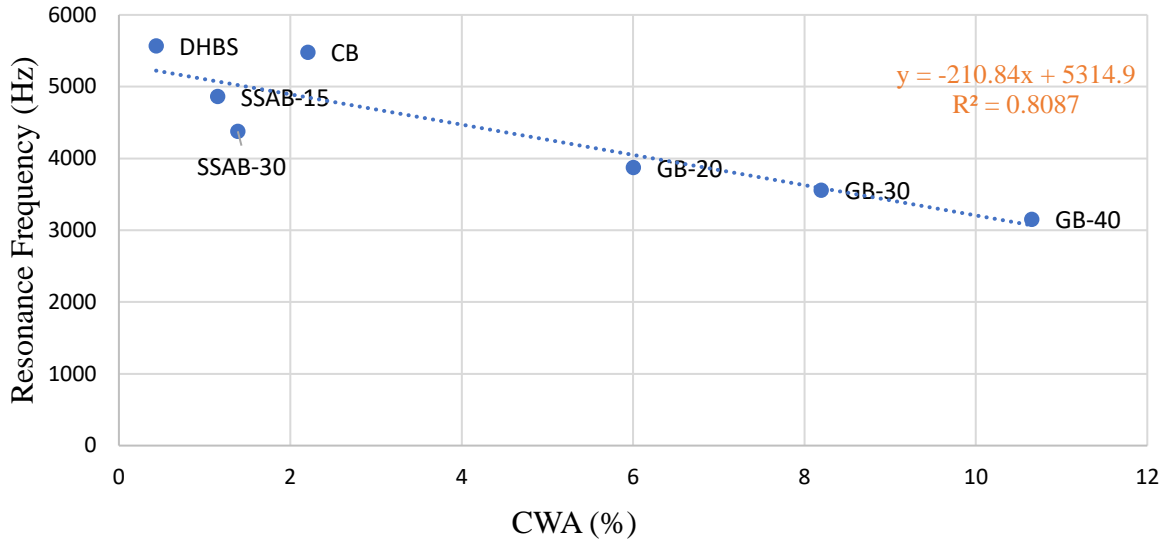
Figure 7-13: Correlation between Cold-Water Absorption and Resonance Frequency

7.14 Correlation between Hot-Water Absorption and Resonance Frequency
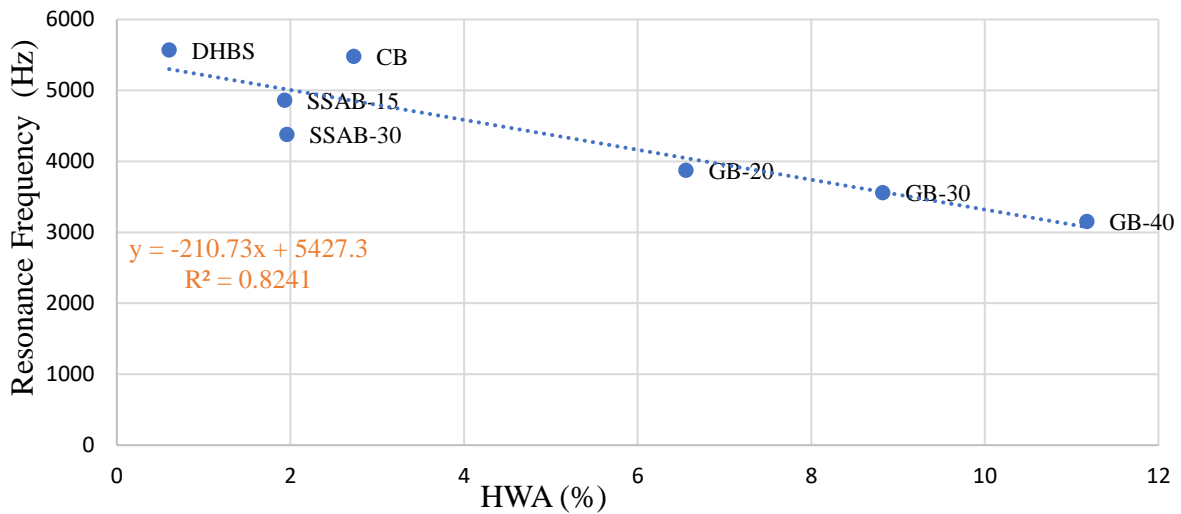
Figure 7-14: Correlation between Hot-Water Absorption and Resonance Frequency

Resonant frequency is correlated to the hot-water absorption capacity; the former is an indication of material stiffness (and therefore density) whereas the latter is an indication of the connected pore structure including the micropores which can be occupied by steam instead of water; coefficient of determination of a descending linear trend is 82.41%; the higher the value of HWA the lower the value of RFT.

[187]

7.15 Correlation between Pulse Velocity and Resonance Frequency

$y = 0.6812x + 2474$
$R^2 = 0.8046$
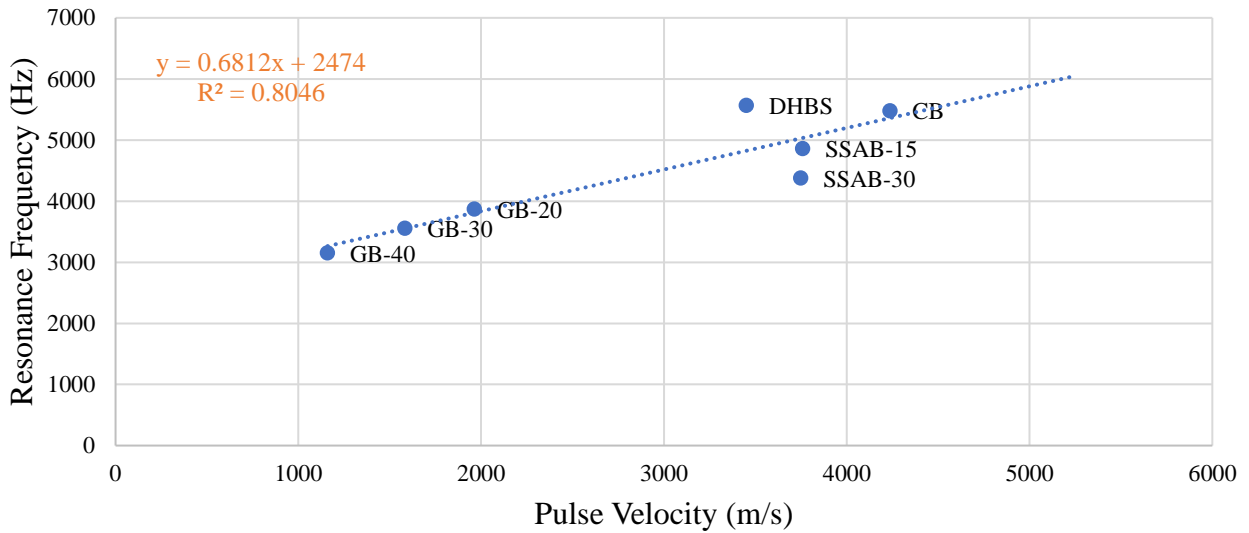
Figure 7-15: Correlation between Pulse Velocity and Resonance Frequency

Figure 7-15 explores the degree of correlation between the values obtained from the two non-destructive procedures considered in the present study. Both variables increase proportionately at a constant rate. With a percent variation of the Ultra Sonic Pulse Velocity with respect to the resonant frequency found to be 80.46% it is expected that either of the two equipment may be used in the role of quality control predictor in practice.

7.16 Correlation between Mechanical and Physical Properties of Masonry Bricks

Table 7.1 shows the correlation between mechanical and physical properties of masonry bricks obtained from several experimental and the numerical analysis. The objective of the correlation analysis is to use the correlation factors as calibrated presages. The parameters presented in Table 7.1 are plotted as correlation charts in the above sections. Also, the empirical relations between the indirect and direct tensile strength with the compressive strength of the masonry brick unit are also calculated.

Table 7.1 Correlation analysis between the parameters studied

Parameters	Coefficient of Determination (R^2)	Empirical Relation	Type of relation
$\sqrt{f_{c\ trans}}$ versus f_t	0.82	$f_t = 3\sqrt{f_{c\ trans}} - 8$	Linear Correlation
$\sqrt{f_{c\ long}}$ versus f_t	0.94	$f_t = 2\sqrt{f_{c\ trans}} - 5$	Linear Correlation
$\sqrt{f_{c\ trans}}$ versus $f_{t\ flex}$	0.91	$f_t = 6\sqrt{f_{c\ trans}} - 17$	Linear Correlation
$f_{c\ split}$ versus $f_{t\ flex}$	0.77	$f_{t\ flex} = 1.5\ f_{t\ split} - 4.5$	Linear Correlation
$\sqrt{f_{c\ trans}}$ versus UPV	0.90	$UPV = 2200\sqrt{f_{c\ trans}} - 7350$	Linear Correlation
$f_{c\ trans}$ versus RFT	0.88	$RF = 175 f_{c\ trans} + 530$	Linear Correlation
$f_{c\ trans}$ versus E	0.84	$E = 1700\ f_{c\ trans} - 14800$	Linear Correlation
CWA versus UPV	0.88	$UPV = -290\ CWA + 4000$	Inverse- Linear Correlation
HWA versus UPV	0.87	$UPV = -280\ HWA + 4200$	Inverse- Linear Correlation
CWA versus RFT	0.80	$RFT = -210\ CWA + 5300$	Inverse- Linear Correlation
HWA versus RFT	0.82	$RFT = -210\ HWA + 5400$	Inverse- Linear Correlation
UPV versus RFT	0.80	$RFT = 0.6\ UPV + 2450$	Linear Correlation

Chapter 8. Summary and Conclusions

The research presented in this thesis aimed to develop a new class of hybrid masonry bricks that would potentially meet modern sustainability objectives in future construction. Motivating principles for the research was the quest for a solution that would, if fully exploited in practice, contribute towards the reduction in the use of quarried materials in while at the same time facilitating the disposal of non-pathogenic wastes produced from the wastewater treatment facilities as well as other wastes (such as crushed glass) to embed in the final products significant added value. The latter objective has several tangible and intangible benefits, ranging from the ongoing depletion of shales used in clay production, the management of large volumes of sludge that is inappropriate as fertilizer, the opportunity for the wastewater treatment facilities to better manage the fate of the sludge produced, and the introduction in useful products of industrial wastes such as crushed recycled glass that would otherwise end up in landfills. To achieve these objectives, an extensive experimental campaign has been undertaken which focussed on the development of manufacturing methods and characterization techniques necessary for innovative replacement of shale and clay with the proposed solid or liquid wastes without impairing the structural and physical properties of masonry bricks.

Source shale material was provided by a major brick manufacturer in Canada, to be used as the control raw ingredient in the brick manufacturing. Control bricks (CB) fabricated according to the mix design and procedures followed in the field, were made for benchmarking of all other trials. The experimental development of the work occurred in two phases, namely the preliminary phase and the main phase of the research.

In the preliminary phase, the effects of several waste replacement options on the important performance indicators like uniaxial (transverse) Compressive Strength and water absorption were studied so as to determine the feasibility of the endeavor and to also resolve practical issues that could hinder the realization of the project's objectives. In this regard, hybrid bricks with varying shale replacement rates were fabricated and tested using several waste materials that included Geopolymer bricks including Recycled Crushed Glass (RCG), Dried High Bio-polymer derived from sewage sludge, and Incinerated Sewage Sludge Ash (SSA) provided by the Municipal

wastewater treatment facilities. The following sections summarize the main findings of the study and conclusions drawn from the experimental and numerical observations.

8.1 Mechanical Properties of Hybrid Bricks

In the main phase of the research, five categories of the waste-shale combinations that were deemed most promising performers while still the first phase of the tests were studied in greater detail. Thus, a series of hybrid brick specimens were developed through the research, with different ingredients in terms of partial shale replacement (i.e., Dried High Biopolymer Sludge – DHBS; Sludge Ash Bricks – SSAB; Geopolymer Bricks – GB). In order to evaluate the parameters that decide the quality of the masonry bricks, a total of 119 masonry units were made. Among them, 98 units were whole units of size 140 mm x 58 mm x 26 mm and 21 units were cubes of size 50 mm. All of these bricks underwent several mechanical and durability tests- such as, compressive strength tests, flexural strength tests, splitting tensile tests, resonance frequency tests, ultrasonic pulse velocity tests, water absorption tests, efflorescence tests and the resistance to freeze- thaw. The observations of the experimental campaign are summarized below:

➢ The compressive strengths (in the transverse direction or perpendicular to the bed joint) of the DHBS and SSAB-15 brick were almost the same, equal to 24.8 MPa and 24.1 MPa respectively, i.e., 82.9% and 80.6% of the reference control brick (CB). Also, the compressive strength value of the SSAB-30 brick, with 30% replacement of sludge, was 22.6 MPa, i.e., 75.7% of the control brick. Similarly, the compressive strength for the GB-20, GB-30, and GB-40 were, 18.8 MPa, 18.0 MPa, and 15.1 MPa respectively, which is 62.9%, 60.2% and 50.3% of the control brick values. However, all of the brick types fabricated were within the acceptable range of brick performance as per *CSA A82-14: Fired masonry brick made from clay or shale.*

➢ The compressive strength of the masonry units (longitudinal direction or parallel to the bed joint) was higher than the compressive strength in transverse direction for all the categories except the GB bricks. The compressive strength for the reference CB was 28.8 MPa. Interestingly, for the DHBS and SSAB-15, the compressive strength was 8.9% and 11.5% higher than the CB. For SSAB-30 brick, the strength was 89.8 % of the CB. These are

believed to be closest to the true intrinsic values of the compressive strength of the brick by minimizing the effect of friction through the use of Teflon plates during the test. Overall, the compressive strength of the masonry units was satisfactory, especially for the SSAB and DHBS bricks.

➢ As one of the indirect tensile strength determination methods, the flexural strength of the hybrid bricks was calculated by three point bending tests. For the CB flexural strength was 15.3 MPa. The corresponding values for the DHBS and SSAB bricks were very near to this upper limit (97.1%, 92.5% and 83.7% of flexural strength of CB for DHBS, SSAB-15 and SSAB-30 bricks respectively.)

➢ The other method to calculate the indirect tensile strength was through the splitting tensile tests. Strength values were, 4.8 MPa for the reference CB, and 93.2%, 64.6%, 63.5%, 48.1%, 89.9% and 83.6% of this value for DHBS, GB-10, GB-20, GB-30, SSAB-15, and SSAB-30, respectively. Clearly, all the DHBS and SSAB bricks have shown a consistent tensile performance very close to that of the CB.

➢ One of the non destructive tests conducted on the bricks was the resonance frequency test which measures the vibration of a structure that is exposed to dynamic loads. The test also estimates the dynamic modulus of elasticity of the brick. The resonance frequency of the CB was 5479 Hz. In fact, DHBS brick had 1.6% higher resonance frequency than the CB, at 5568 Hz. For all other hybrid bricks the RF was between 57.5% and 88.8% of the control brick. Dynamic modulus of elasticity of DHBS brick, SSAB-15 and SSAB-30 bricks were pretty close to that of CB. For the CB, it was 36626 MPa whereas for all other bricks the dynamic modulus of elasticity was in the range of 93.5% to 32% of the CB values with DHBS and SSAB being highest.

8.2 Physical Properties and Durability of Hybrid Bricks

The durability and other physical properties of the brick were also evaluated from a number of pertinent tests, such as the measurement of the Ultrasonic Pulse Velocity (UPV), the Water Absorption Capacity (both to cold and to hot-water), freeze-thaw and efflorescence performance.

➤ The ultrasonic pulse velocity test is routinely used to determine the quality of the brick units in the industry; this concept is extended to the present study, on the basis that the higher the pulse velocity, the denser the microstructure of the material and the better the quality of the bricks. The pulse velocity for the CB was 4235.6m/s. Similarly, for DHBS, GB-20, GB-30, GB-40, SSAB-15, SSAB-30, were 3451 m/s, 1963 m/s, 1583 m/s, 1160 m/s, 3759 m/s and 3748 m/s respectively. From the pulse velocity, with an upper limit of greater than 3500 m/s and a lower limit of less than 1000 m/s may be considered as a durable brick [Koroth, Fasio & Feldman, 1998]. All of the hybrid bricks were found to pass the UPV quality tests especially the SSAB and DHBS bricks. With the exception of the GB category which had UPV values lower than 2000 m/s, however, well within the lower limit range of durability, i.e.,1000 m/s.

➤ The cold and hot water absorption tests are indicators of porosity of the brick (the cold-water test refers to the larger pores that can hold water whereas the hot water test measures the finer set of connected pores that can only store water in the form of steam). These variables were 2.2% and 2.7% respectively, for the CB. However, for DHBS bricks, the biopolymers inside the brick get burned during the firing process thereby creating fine pores inside the brick which are evidenced in the lighter weight of the brick; however, evidently these fine pores resulting from this process are not connected to the brick capillary network and as a result, the DHBS bricks has lower water absorption apparently owing to a better distribution of fine pores. All other bricks showed similar or less water absorption than the CB which improves their prospects in terms of durability resilience.

➤ From the freeze thaw tests the Percent weight loss for the SSAB and DHBS brick were much lower than the CB which was 0.83% of the weight of the brick. However, for the GB brick, it was between 1.21% and 2.12% of the total weight of the brick.

➤ Efflorescence was another physical property of the bricks studied. None of the hybrid bricks showed any sign of efflorescence.

The results from the study of the Geo-polymer bricks indicated that this research field presents an opportunity for development of an economical building construction material with great added value that could find use in many applications particularly in masonry construction or as infills; some of the brick types developed have the advantage of being fabricated with a low firing temperature, therefore leaving a reduced carbon footprint and requiring less firing energy than conventional bricks. In fact, the geopolymer bricks utilized only 40% of the firing energy used for the control bricks, yet, the process yielded a high-quality brick with excellent mechanical and durability properties.

From the study, it was evident that all the types of the prototype hybrid bricks developed in the main phase of the research were able to meet the objective of reducing the level of natural resources quarried for brick manufacturing with no compromise in durability and tensile strength (which are the key variables in the industry) with a minor up to moderate effect on compressive strength (which is not likely to control the design strength of masonry walls on account of the prevailing effect of the mortar in structural performance under compression). The hybrid bricks illustrated that it is possible, when scaled up to become an industrial product, the could also met the sustainability objective of the research, either by means of serving as host to industrial / sanitary wastes that would otherwise be landfilled, or by reducing the firing energy requirements for their manufacture.

8.3 Numerical Study of Hybrid Bricks

Characterization of the mechanical properties of the bricks required inverse analysis of the mechanical tests conducted. To this end, all the experiments of the main phase were modelled in VecTor2$^{©}$, an advanced nonlinear finite element analysis software with the intent to match – through sensitivity analysis the output response of the simulation with the corresponding experimental response curve; the unknowns of the study were the true compressive and tensile strengths of the materials considered; the input data included the assumed shape of the stress-strain response of the brick in compression (similar to that of plain concrete according to the Masonry Design Code (CSA S304-14 – Design of masonry structures) scaled to a peak strength that was to be determined through the inverse analysis; also input were the material density (experimental value) and the dynamic modulus of elasticity (from the transverse resonant

frequency tests). Through this process, and after obtaining the tensile strength from the flexural tests, and the compressive strength from the longitudinal compression brick tests, it was possible to reproduce the strength values for all other mechanical tests that were not used in the sensitivity-matching analysis; simulation was also successful in reproducing the behavioral patterns of these experiments including the form and distribution of the ultimate cracking at failure.

8.4 Correlation Analysis

Several parameters studied in the experimental part of the research were correlated to each other in an attempt to obtain simple tools that could be used as predictors of performance in future investigations without the necessity of destructive testing. Strong correlation (with a coefficient of variation over 80%) was found between the following pairs of parameters: $\sqrt{f_{c\ trans}}$ and f_t, $\sqrt{f_{c\ long}}$ and f_t, $\sqrt{f_{c\ trans}}$ and $f_{t\ flex}$, $f_{c\ split}$ and $f_{t\ flex}$, $\sqrt{f_{c\ trans}}$ and UPV, $f_{c\ trans}$ and RFT, CWA and UPV, HWA and UPV, CWA and RFT, HWA and RFT and UPV and RFT.

8.4 Discussion for Further Development of the Research

In the current research, for DHBS bricks, the percentage of shale replacement was just 2.3% by weight because of several constraints discussed in Section 3.1.2.6. With this amount of shale replacement, all the parameters studied were very satisfactory with regards to the standards of the masonry industry and improved in certain aspects owing to the water tightness, and low weight of these bricks. An improved version of DHBS bricks, by incorporating higher concentrations of high biopolymer sludge contents, should be a priority in the future once it is possible to achieve high concentration of solids in HBS in practice.

The SSAB bricks were found to be the most promising in terms of mechanical performance, and rather a sustainable hybrid masonry brick. Several studies could be done by constructing masonry walls or wallettes with SSAB bricks and mortar to assess their behaviour in actual structural components. All hybrid bricks considered demonstrated a superior durability performance, indicating that this is a promising direction of growth for a sustainable masonry industry.

Shale-Poraver®- Na_2SiO_3 Bricks was another promising brick, which developed exceptional strength and solid structure. However, further study would be required to identify the classification temperature so that the shape effects of the bricks could be also addressed.

Bibliography

Abdel-Ghani, N. T., Elsayed, H. A., & Abdelmoied, S. (2018). Geopolymer synthesis by the alkali-activation of blast furnace steel slag and its fire-resistance. HBRC Journal, 14(2), 159-164.

Adyela. T.M .,Rahmanb. S.H., Islamb. S.M.N., Hossain .M. Sayemc, Khand.M & Gafur.A.M.D.(2012). Characterization of Brick Making Soil: Geo-engineering, Elemental and Thermal Aspects, Jahangirnagar University Journal of Science Vol. 35, No.1, pp. 109-118.

Ajam, H., Gómez-Meijide, B., Artamendi, I., & Garcia, A. (2018). Mechanical and healing properties of asphalt mixes reinforced with different types of waste and commercial metal particles. Journal of Cleaner Production, 192, 138–150.

Akhtar, A.& Sarmah, A.K. (2018). Construction and demolition waste generation and properties of recycled aggregate concrete: a global perspective J. Clean. Prod., 186 , pp. 262-281.

Akinshipe O & Kornelius G (2017) Chemical and Thermodynamic Processes in Clay Brick Firing Technologies and Associated Atmospheric Emissions Metrics-A Review. J Pollut Eff Cont 5: 190.

Akkarapongtrakul, A., Julphunthong, P.& Thanongsak, N. (2017). Setting time and microstructure of Portland cement-bottom ash–sugarcane bagasse ash pastes. Monatsh. Chem. 148, 1355–1362.

Archibald, J. F., DeGagne´, D. O., Lausch, P., & De Souza, E. M. (1995). Ground waste glass as a pozzolanic consolidation agent for mine backfill. CIM Bull., 88(995), 80–87.

Arulrajah, T.-A. Kua, S. Horpibulsuk, C. Phetchuay, C. Suksiripattanapong, &Y.-J. Du.(2016). Strength and microstructure evaluation of recycled glass-fly ash geopolymer as low carbon masonry units, Constr. Build. Mater. 114 .400–406.

ASTM C1006 (2019). Standard test method for splitting tensile strength of masonry units, astm international, west conshohocken, pa, 2019.

ASTM C125-16. (2016). Standard terminology relating to concrete and concrete aggregates. ASTM International.

ASTM C125-19. Standard terminology relating to concrete and concrete aggregates, astm international, west conshohocken, pa, 2019.

ASTM C215 (2014). Standard test method for fundamental transverse, longitudinal, and torsional resonant frequencies of concrete specimens, astm international, west conshohocken, pa, 2014.

ASTM C597 (2016).Standard test method for pulse velocity through concrete, astm international, west conshohocken, PA, 2016.

ASTM C67 (2019). Standard test methods for sampling and testing brick and structural clay tile, astm international, west conshohocken, pa, 2019.

ASTM D2845 (2008). Standard test method for laboratory determination of pulse velocities and ultrasonic elastic constants of rock (withdrawn 2017), astm international, west conshohocken, pa, 2008.

ASTM D4318 (2017).Standard test methods for liquid limit, plastic limit, and plasticity index of soils, astm international, west conshohocken, pa, 2017.

ASTM D6913 / D6913M-17, Standard Test Methods for Particle-Size Distribution (Gradation) of Soils Using Sieve Analysis, ASTM International, West Conshohocken, Pa, 2017.

ASTM D698 (2012).Standard test methods for laboratory compaction characteristics of soil using standard effort (12 400 ft-lbf/ft^3 (600 kn-m/m^3)), astm international, west conshohocken, pa, 2012.

ASTM D7928 (2017).Standard test method for particle-size distribution (gradation) of fine-grained soils using the sedimentation (hydrometer) analysis, astm international, west conshohocken, pa 2017.

Atkinson R.H., Noland J.L.& Kingsley G.R. (1990) Application of NDE to Masonry Structures; Current Technology and Future Needs. In: Thompson D.O., Chimenti D.E. (eds) Review of Progress in Quantitative Non-destructive Evaluation. Review of Progress in Quantitative Non-destructive Evaluation. Springer, Boston, MA,

Auta, S. M.,Uthman,A., Sadiku,S., & Shiwua, A.J.(2016). Flexural strength of reinforced revibrated concrete beam with sawdust ash as a partial replacement for cement.Constr. of Unique Build. and Struct. 5 31-45.

Barbara C. L (2007). BEES 4.0: Building for Environmental and Economic Sustainability, National Institute of Standards and Technology (NIST).

Basegio, F. Berutti, A. Bernardes, C.P.   & Bergmann (2002). Environmental and technical aspects of the utilisation of tannery sludge as a raw material for clay products, J. Eur. Ceram. Soc. 22 (13) 2251–2259. s0955-2219(02) 00024-9

Bashar, T.& Ghassan, N. (2009). Utilizing Waste Recycled Glass as Sand/Cement Replacement in Concrete. Journal of Materials in Civil Engineering, 21(12), 709–721.

Bhushan, C., Basu, D.D., Yadav, N.K. & Kumar, R. (2016). National Brick Mission—A Scoping Paper. Roadmap for Brick Kiln Sector: Challenges and Opportunities. Centre for Science and Environment, New Delhi.

Brozovsky, J. & Russ J.,(2017). Ultrasonic pulse and resonance method–evaluation of the degree of damage to the internal structure of repair mortars caused by exposure to high temperatures, Russian Journal of Non-destructive Testing.

Buchholz , FL & Graham, AT - Modern Superabsorbent Polymer Technology John Wiley & Sons, November 1997, 0471194115

C. Thormark (2002). A low energy building in a life cycle—its embodied energy, energy need for operation and recycling potential. Build Environ, pp. 429-435

Cabrera-Covarrubias, F. G., Gomez-Soberon, J. M., Almaral-Sanchez, J. L., Arredondo-Rea, S. P., & Mendivil-Escalante, J. M. (2018). Mechanical and basic deformation properties of mortar with recycled glass as a fine aggregate replacement. International Journal of Civil Engineering, 16(1), 107-121.

Campbell, J. W. & Pryce, W. (2003). Brick: a world history. London: Thames and Hudson.

Chandra Paul, S., Šavija, B., & Babafemi, A. J. (2018). A comprehensive review on mechanical and durability properties of cement-based materials containing waste recycled glass. Journal of Cleaner Production, 198, 891-906.

Chidiac, S. E., & Federico, L. M. (2007). Effects of waste glass additions on the properties and durability of fired clay brick. Canadian Journal of Civil Engineering, 34(11), 1458-1466.

China Coal Information Institute (2015), China Statistic Yearbook of Coal Industry, Coal Industry Press, Beijing.

Chindaprasirt, P.& Rukzon, S. (2015). Strength and chloride resistance of the blended Portland cement mortar containing rice husk ash and ground river sand. Mater. Struct. 48(11), 3771–3777.

Conti J. (2011) Emission of greenhouse gases in the united states ,2009, US Energy Information Administration, U.S. department of energy, Washington, Available at : https://www.eia.gov/ environment/emissions/ ghg_report/ pdf /0 573%282009%29

CSA Standard S304.1-04. (2004) Design of masonry structures, ISBN 1-55397-402-6 © Canadian Standards Association — 2004

de Figueirêdo Lopes Lucena, L. C., Thomé Juca, J. F., Soares, J. B., & Portela, M. G. (2014). Potential Uses of Sewage Sludge in Highway Construction. Journal of Materials in Civil Engineering, 26(9), 04014051.

Demir, I. (2009). Reuse of waste glass in building brick production. Waste Management and Research, 27(6), 572-577.

Dixon, W. (2010). The Impacts of Construction and the Built Environment, Briefing Notes, Willmott-dixon Group.

Dondi, M., Guarini, G., Raimondo, M., & Zanelli, C. (2009). Recycling PC and TV waste glass in clay bricks and roof tiles. Waste Management, 29(6), 1945-1951.

Dove, C. A., Bradley, F. F., & Patwardhan, S. V. (2016). Seaweed biopolymers as additives for unfired clay bricks. Materials and Structures, 49(11), 4463–4482.

Dyer, T. D., & Dhir, R. K. (2001). Chemical reactions of glass cullet used as cement component. Journal of Materials in Civil Engineering, 13(6), 412-417.

Dyer, T.D.& Dhir, R.K. (2001). Chemical reactions of glass cullet used as cement component. J Mater Civ Eng, 13 (6) (2001), pp. 412-417.

Emrullahoglu Abi, C. B. (2014). Effect of borogypsum on brick properties. Construction and Building Materials, 59, 195–203.

Environmental Engineering Laboratory, York University, http://civil.lassonde.yorku.ca/graduate-facilities/

Eo, S.-H., & Yi, S.-T. (2015). Effect of oyster shell as an aggregate replacement on the characteristics of concrete. Magazine of Concrete Research, 67(15), 833–842.

European Environment Agency (EEA). Greenhouse gas emission trends and projections in Europe 2011: tracking progress towards Kyoto and 2020 Targets. Copenhagen: EEA; 2011.

Fay, R., Treloar, G. & Iyer-Raniga, U. (2000), Life-cycle energy analysis of buildings: a case study, Building Research & Information, Vol. 28 No. 1, pp. 31-41.

Fernandes F.M., Lourenço P.B.& Castro F. (2010) Ancient Clay Bricks: Manufacture and Properties. In: Dan M.B., Přikryl R., Török Á. (eds) Materials, Technologies and Practice in Historic Heritage Structures. Springer, Dordrecht.

Ferone. C. et al.,(2015) Thermally treated clay sediments as geopolymer source material, Appl. Clay Sci. 107 195–204

Garg, M., & Pundir, A. (2014). Utilization of Brine Sludge in Non-structural Building Components: A Sustainable Approach. Journal of Waste Management, 2014, 1–7.

Giannini. E.R. (2012) .Evaluation of Concrete Structures Affected by Alkali-Silica Reaction and Delayed Ettringite Formation., Construction and Building Materials 202:814-824,

Giugliano, M., & Paggi, A. (1985). Use of Tannery Sludge in Brick Production. Waste Management & Research, 3(1), 361–368.

Goel, G., & Kalamdhad, A. S. (2017). An investigation on use of paper mill sludge in brick manufacturing.Construction and Building Materials, 148, 334–343.

Hasan, N. M. S., Sobuz, H. R., Sayed, M. S., & Islam, M. S. (2012). The use of coconut fibre in the production of structural lightweight concrete. Journal of Applied Sciences, 12(9), 831-839.

Heindl, R.A. & Pendergast, W.L.(1929). A book on Progress Report on investigation of Fireclay Bricks and the Clays used in their preparation, J. Am. Ceram. Soc., 12 (10) (October 1929), pp. 640-675.

Hossain, S. S., Mathur, L., Majhi, M. R., & Roy, P. K. (2018). Manufacturing of green building brick: recycling of waste for construction purpose. Journal of Material Cycles and Waste Management.

Hu, C., Lin, W., Partl, M., Wang, D., Yu, H., & Zhang, Z. (2018). Waste packaging tape as a novel bitumen modifier for hot-mix asphalt. Construction and Building Materials, 193, 23-31.

Huang, P., Lv, L., Liao, W., Lu, C., & Xu, Z. (2018). Microstructural Properties of Cement Paste and Mortar Modified by Low Cost Nanoplatelets Sourced from Natural Materials. Materials, 11(5), 783.

Iwuagwu, J. O., & Ugwuanyi, J. O. (2014). Treatment and Valorization of Palm Oil Mill Effluent through Production of Food Grade Yeast Biomass. Journal of Waste Management, 2014, 1–9.

Jain, N., Garg, M., & Minocha, A. K. (2015). Green Concrete from Sustainable Recycled Coarse Aggregates: Mechanical and Durability Properties. Journal of Waste Management, 2015, 1–8.

Jiménez-Quero, V., Maza-Ignacio, O. T., Guerrero-Paz, J., & Campos-Venegas, K. (2017). Industrial wastes as alternative raw materials to produce eco-friendly fired bricks. Journal of Physics: Conference Series, 792, 012065.

Joo-Hwa, J., Sze-Yunn, H., & Kuan-Yeow, S. (2000). Reuse of Industrial Sludge as Pelletized Aggregate for Concrete. Journal of Environmental Engineering, 126(3), 279–287.

Joshua, O., Olusola, K. O., Ogunde, A. O., Ede, A. N., Olofinnade, R. M., & Nduka, D. O. (2017). Investigating for pozzolanic activity in palm kernel nut waste ash (PKNWA) with cement towards a sustainable construction. International Journal of Applied Engineering Research, 12(23), 13559-13565.

Kadir A.A.& A. Mohajerani, (2011). Bricks: an excellent building material for recycling wastes–a review.

Kamal. I, Sherwani. A, Ali. A, Khalid .A, Saadi .I & Harbi. A .(2017) Walnut Shell for Partial Replacement of Fine Aggregate in Concrete: Modeling and Optimization J. of Civ. Eng. Res. 4 109-119.

Kaza, S., Yao, L. C., Bhada-Tata, P., & Van Woerden, F. (2018). What a Waste 2.0: A Global Snapshot of Solid Waste Management to 2050 (No. 132827; pp. 1–295). Retrieved from The World Bank website: http://documents. worldbank.org/curated/en/ 697271544470229584/ What-a-Waste-2-0-A-Global-Snapshot-of-Solid-Waste-Management-to-2050

Kazmi, S. M. S., Abbas, S., Nehdi, M. L., Saleem, M. A., & Munir, M. J. (2017). Feasibility of Using Waste Glass Sludge in Production of Ecofriendly Clay Bricks. Journal of Materials in Civil Engineering, 29(8), 04017056.

Khankhaje,E., Salim, M.R., Mirza, J., Hussin, M.W. & Rafieizonooz, M.(2016).Properties of sustainable lightweight pervious concrete containing oil palm kernel shell as coarse aggregate Construction and Building Materials 126 1054-1065.

Kim, I. S., Choi, S. Y., & Yang, E. I. (2018). Evaluation of durability of concrete substituted heavyweight waste glass as fine aggregate. Construction and Building Materials, 184, 269-277. doi:10.1016/j.conbuildmat.2018.06.221.

Koroth, S.R., Fazio, P., & Feldman, D. (1998). Evaluation of Clay Brick Durability Using Ultrasonic Pulse Velocity. Journal of Architectural Engineering,Vol. 4, Issue 4 doi: 10.1061 /(asce) 1076- 0431(1998)4:4(142).

Kumar.D, Singh.S, Kumar.N & Gupta.A. (2014) Low Cost Construction Material for Concrete as Sawdust Int. J. of Current Engineering and Technology 4 3428-3430.

Kumutha, R., Vijai, K. & Vijayragavan, S. (2018). Mechanical properties of concrete using coconut shells as coarse aggregates. ARPN Journal of Engineering and Applied Sciences, 13(20), 8236-8242.

Lamrani, M., Laaroussi, N., Khabbazi, A., Khalfaoui, M., Garoum, M., & Feiz, A. (2017). Experimental study of thermal properties of a new ecological building material based on peanut shells and plaster. Case Studies in Construction Materials, 7, 294–304.

Lee, J., Yoo, H., Park, S., Cho, S., & Seo, Y. (2016). Recycling of cathode ray tube panel glasses as aggregates of concrete blocks and clay bricks. Journal of Material Cycles and Waste Management, 18(3), 552-562.

Lin, D.-F., & Weng, C.-H. (2001). Use of Sewage Sludge Ash as Brick Material. Journal of Environmental Engineering, 127(10), 922–927

Lin, K., Huang, L., Shie, J., Cheng, C., Lee, C., & Chang, T. (2012). Elucidating the effects of solar panel waste glass substitution on the physical and mechanical characteristics of clay bricks. Environmental Technology, 1, 1-10.

Liu, S., Peng, A., Wu, J., & Zhou, S. B. (2018). Waste engine oil influences on chemical and rheological properties of different asphalt binders. Construction and Building Materials, 191, 1210–1220.

Lutfi, M., Yamin, M., Rahman, M., & Ginsel Popang, E. (2018). A comparative analysis of the quality of concrete blocks produced from coconut fibre, oil palm empty fruit bunch, and rice husk as filler material (Vol. 195). Presented at the MATEC Web of Conferences.

Malhotra, V. M., & Carino, N. J. (1991). CRC Handbook on Nondestructive Testing of Concrete. Boca Raton: CRC Press.

Malhotra, V. M., & Mehta, P. K. (1994). Concrete Technology: Past, Present, and Future: Proceedings of V. Mohan Malhotra Symposium. Detroit, Michigan:American Concrete Institute.

Manoj.A., Dhanya.P., Ganapathy.R., Dhanasekar.R., & Sevugamoorthy.(2017). An experimental study of self healing of cracks in concrete using sodium silicate capsule, Journal of Chemistry 10(2):577-583.

Markus Schilling & Lichun Chiang. (2009). The depletion of non-renewable resources for non-sustainable externalities as an economic development policy cpsa annual conference (Canadian Political Science Association), Available at : https://www.cpsa-acsp.ca/papers-2009/Schilling.pdf

Martínez-García, C., González-Fonteboa, B., Martínez-Abella, F., & Carro- López, D. (2017). Performance of mussel shell as aggregate in plain concrete. Construction and Building Materials, 139, 570–583.

Maschio, S., Tonello, G., & Furlani, E. (2013). Recycling Glass Cullet from Waste CRTs for the Production of High Strength Mortars. Journal of Waste Management, 2013, 1–8.

Mehta, A., & Siddique, R. (2018). Sustainable geopolymer concrete using ground granulated blast furnace slag and rice husk ash: Strength and permeability properties. Journal of Cleaner Production, 205, 49–57.

Michel, A. T., Srubar, III W. V., & Billington, S. L. (2014). Biobased Materials for Sustainable Temporary Disaster-Relief Housing. Proceedings of the 3rd International Conference on Urban Disaster Reduction, Earthquake Engineering Research Institute, Boulder, CO, USA, 2014.

Mirza S .H., Anwar.A., Samarul H & Mohd .A.(2017). Cost Optimization of concrete by replacing fine aggregate with walnut shell powder Int. J. of Civil Engineering and Technology 8 82-89.

Mobili, A., Giosuè, C., & Tittarelli, F. (2018). Valorisation of GRP Dust Waste in Fired Clay Bricks. Advances in Civil Engineering, 2018, 1–9.

Moedinger Fritz (2003). Sustainable clay brick production – a case study.The 2005 World Sustainable   Building Conference, Tokyo, 27-29 September   2005 (SB05Tokyo)

Mondal, A., Das, S., Sah, R. K., Bhattacharyya, P., & Bhattacharya, S. S. (2017). Environmental footprints of brick kiln bottom ashes: Geostatistical approach for assessment of metal toxicity. Science of the Total Environment, 609, 215-224.

Mozo Moreno, W. R & Gómez, A.(2016). Biosolids and Biosolid Ashes as Input for Producing Brick-like Construction Materials, TECCIENCIA, Vol. 12 No. 21, 45-51.

Mozo Moreno, W. R. & Gómez, A.(2016). Biosolids and Biosolid Ashes as Input for Producing Brick-like Construction Materials, TECCIENCIA, Vol. 12 No. 21, 45-51, 2016.

Munir, M. J., Abbas, S., Nehdi, M. L., Kazmi, S. M. S., & Khitab, A. (2018). Development of Eco-Friendly Fired Clay Bricks Incorporating Recycled Marble Powder. Journal of Materials in Civil Engineering, 30(5), 04018069.

Naganathan., A.Y.O. Mohamed. & K.N. Mustapha.(2015). Performance of bricks made sing fly ash and bottom ash, Constr. Build. Mater. 576–580.

Okuno, N., & Takahashi, S. (1997). Full scale application of manufacturing bricks from sewage. Water Science and Technology, 36(11), 243-250.

Olutoge, F.A., Buari,T.A. & Adeleke, J.S.(2013).Characteristics Strength and Durability of Groundnut Shell Ash (GSA) Blended Cement Concrete in Sulphate Environment. International Journal of Scientific & Engineering Research 4 2122-134.

Owusu, P. A., & Asumadu-Sarkodie, S. (2016). A review of renewable energy sources, sustainability issues and climate change mitigation. Cogent Engineering, 3(1), 1167990.

Pardalopoulos, S. I., Karantoni, F. V., & Pantazopoulou, S. J. (2019). Practical assessment of the seismic behavior of a confined masonry system. Soil Dynamics and Earthquake Engineering, 127, 105831.

Pinarli, V., & Kaymal, G. (1994). An innovative sludge disposal option-reuse of sludge ash by incorporation in construction materials. Environmental Technology, 15(9), 843–852.

Priyadharshini, P., Ramamurthy, K., & Robinson, R. G. (2018). Reuse potential of stabilized excavation soil as fine aggregate in cement mortar. Construction and Building Materials, 192, 141–152.

Qudoos, A., Kim, H. G., Atta-ur-Rehman, & Ryou, J.-S. (2018). Effect of mechanical processing on the pozzolanic efficiency and the microstructure development of wheat straw ash blended cement composites. Construction and Building Materials, 193, 481–490.

Raheem, A. A., Adedokun, S. I., Adeyinka, E. A., & Adewole, B. V. (2017). Application of corn stalk ash as partial replacement for cement in the production of interlocking paving stones. International Journal of Engineering Research in Africa, 30, 85-93.

Ram, S., & Ralegaonkar, R. V. (2018). Development of low thermal conductivity walling material using industrial by-product. Journal of Cleaner Production, 204, 767–777.

Reddy Babu, G.& Venkata Ramana, N. (2013). Durability of Bricks Cast with Industrial Sludge. IOSR Journal of Mechanical and Civil Engineering, 6(4), 43–46.

Reddy, B.V.V. (2004). Sustainable building technologies. Curr. Sci., 87 (7) (2004), pp. 899-907.

Robert B. Gibson, Karine Péloffy, Daniel Horen Greenford, Meinhard Doelle, H. Damon Matthews, Christian Holz, Kiri Staples, Bradley Wiseman & Frédérique Grenier. (2019). From Paris to Projects Clarifying the implications of Canada's climate change mitigation commitments for the planning and assessment of projects and strategic undertakings, Available at :https://uwaterloo.ca/paris -to-projects/ sites/ca.paris- to-projects/files /uploads/files/p2p_ full_report_23jan19.pdf.

S. Lemmet. (2009). Buildings and climate change: Summary for decision-makers: United Nations Environment Programme (UNEP) (2009), pp. 1-56.

Sachs, J.& Warner, A. (1995). Natural resource abundance and economic growth. Harvard Institute for International Development, Cambridge (MA).

Sada,B. H., Amartey,Y. D., Bako,S. & Nigeria. (2013). An investigation into the use of groundnut shell as fine aggregate replacement Nigerian Journal of Technology 32 54-60.

Samadikun, B. P., Rukayah, S., Priyambada, I. B., Lumbantobing, S. T. R., & Budihardjo, M. A. (2018). Potential utilization of SSA from water treatment plant as brick material. Paper presented at the E3S Web of Conferences, , 73.

Sasikumar C.R (2010). Building from debris, Indianexpress.com, available at: https://indianexpress.com/article/opinion/columns/building-from-debris/

Shafy Hussein Abdel-Shafy & Mona S. M. Mansour. (2018). Solid waste issue: Sources, composition, disposal, recycling, and valorization, Egyptian Journal of Petroleum 27(4):1275-1290.

Smith S.R. (2008). A critical review of the bioavailability and impacts of heavy metals in municipal solid waste composts compared to sewage sludge. Environ Int. 2009 Jan;35(1):142-56.

Smith, A. S. (2004). Recycled glass as a brick fluxing agent. Paper presented at the Proceedings of the International Conference on Sustainable Waste Management and Recycling: Glass Waste, 149-165.

Sowers, G. F., (1979), Introductory soil Mechanics and foundations: geotechnical engineering, 4th edition,copyright, Macmilan Publising Co., Inc., New-York,

Statistics Canada 2018 : www150.statcan.gc.ca/n1/daily-quotidien/180615/dq180615d-eng.html

Thakkar. Krishan (2017): https://www.slideshare.net/KishanThakkar7/demolished-waste-as-coarse-aggregate.

U. Rajarathnam, V. Athalye, S. Ragavan, S. Maithel, D. Lalchandani, S. Kumar, E. Baum, C. & Weyant, T. Bond. Assessment of air pollutant emissions from brick kilns. Atmos. Environ., 98 (2014), pp. 549-553.

U.S. Department of State (DOS). U.S. climate action report 2010: fifth national communication of the United States of America under the United Nations Framework Convention on Climate Change. Washington, DC: DOS; 2010.

Ukwatta, A. Mohajerani, S. Setunge, & N. Eshtiaghi. (2015).Possible use of biosolids in fired-clay bricks, Constr. Build. Mater. 91. 86–93.

Wentao, Z., & Jason, M.I. (2010). Using Recycled Concrete Aggregates in New Zealand Ready-Mix Concrete Production. Journal of Materials in Civil Engineering, 22(5), 443–450.

Wiebusch, & C.F. Seyfried,(1997). Utilization of sewage sludge ashes in the brick and tile industry, Water Sci. Technol. 36 (11) 251–258

Wiebusch, B., & Seyfried, C. F. (1997). Utilization of SSA in the brick and tile industry. Water Science and Technology, 36(11), 251-258.

World Economic Forum (2019) Making Affordable Housing – A reality in cities report , Available at http://www3.weforum.org/docs/

World Energy Council (WEC). 2013 Survey of World Energy Resources. London: WEC; 2013.

Xu, W., Wen, X., Wei, J., Xu, P., Zhang, B., Yu, Q., & Ma, H. (2018). Feasibility of kaolin tailing sand to be as an environmentally friendly alternative to river sand in construction applications. Journal of Cleaner Production, 205, 1114–1126.

Xu, N.N. (2010), Destruction of solid clay brick on land resources and the countermeasures-case study of Guizhou province, Journal of the Henan University of Urban Construction, Vol. 19 No. 3, pp. 16-17.

Yamaguchi, E. (2014). Finite element method, in Bridge Engineering Handbook: Fundamentals, Second Edition.

Záleská, M., Pavlíková, M., Pokorný, J., Jankovský, O., Pavlík, Z., & Černý, R. (2018). Structural, mechanical and hygrothermal properties of lightweight concrete based on the application of waste plastics. Construction and Building Materials, 180, 1–11.

Zhang, L. (2013). Production of bricks from waste materials – a review. Constr. Build. Mater., 47 (2013),pp.643-655

Appendices

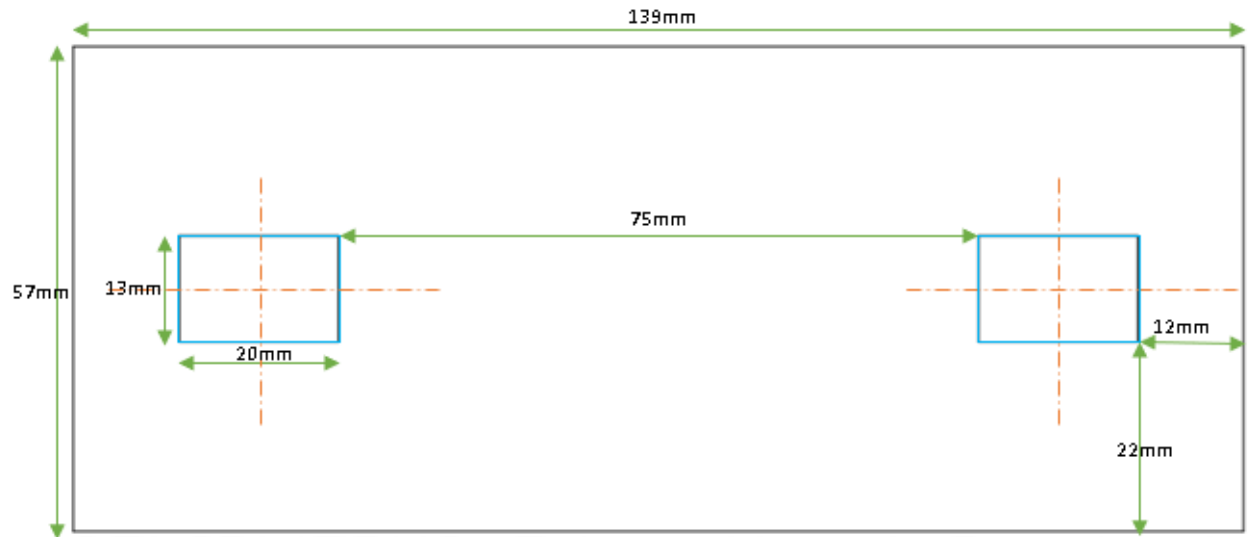## Appendix A: Drawings and detailing of the Acrylic Plastic Mold
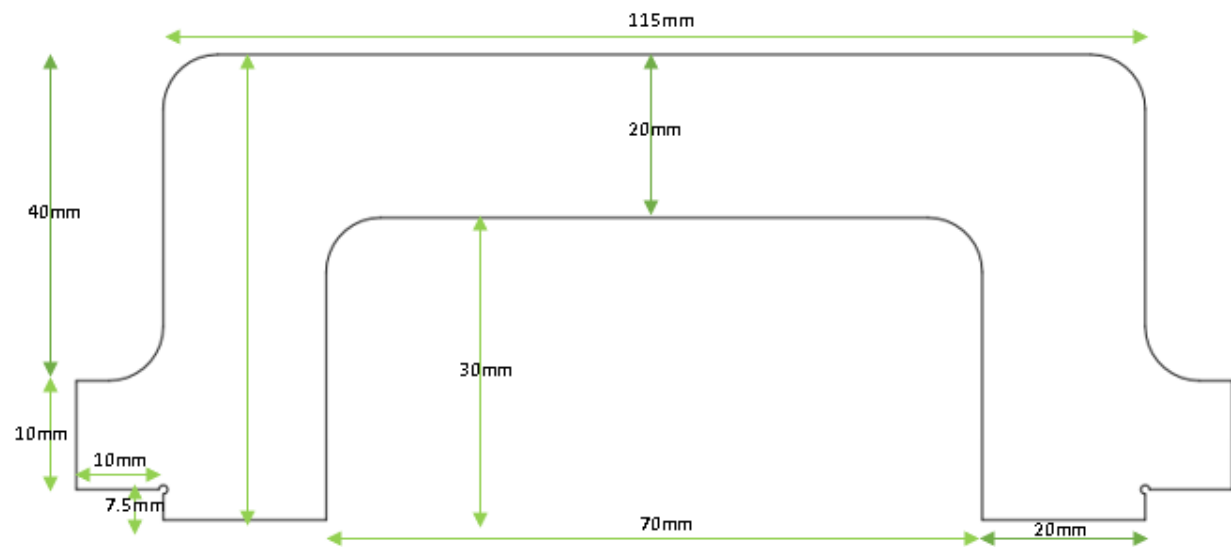

FigureA-1 Bottom Plate of the Plunger
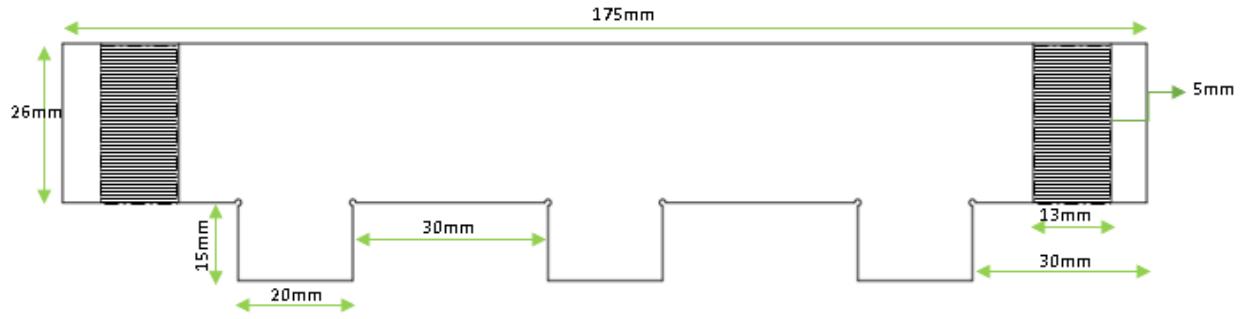

Figure A-2 Handle for Plunger

Figure A-3 Side 1 of the Acrylic Brick Mold
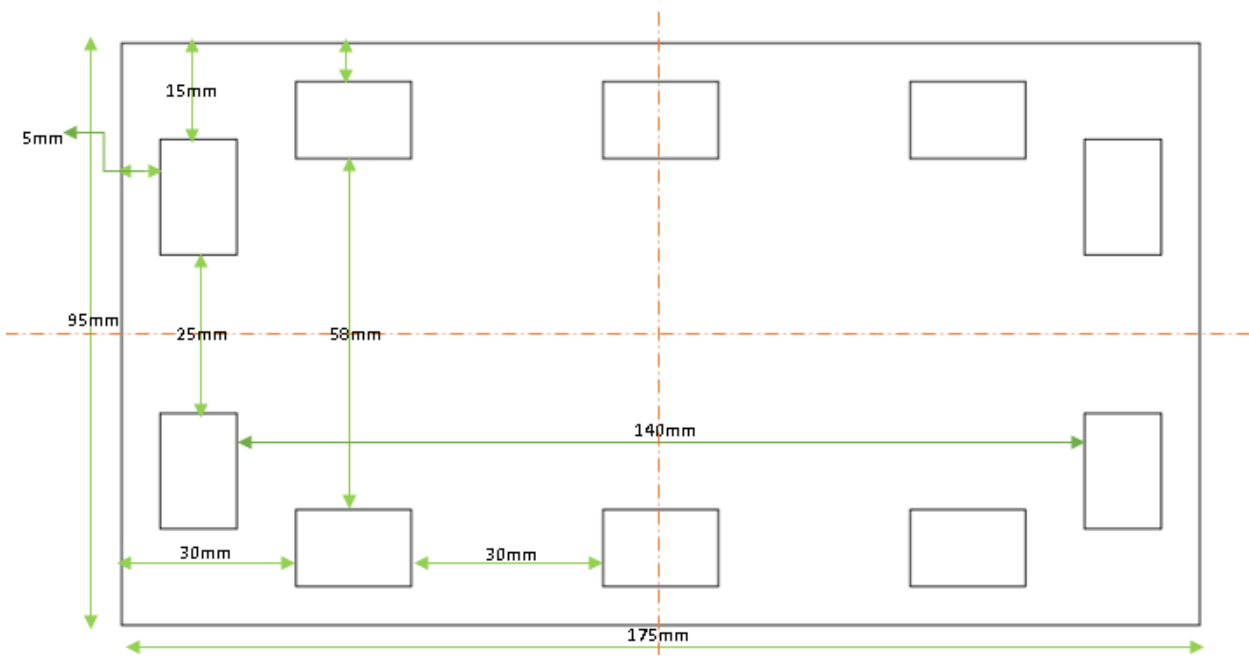

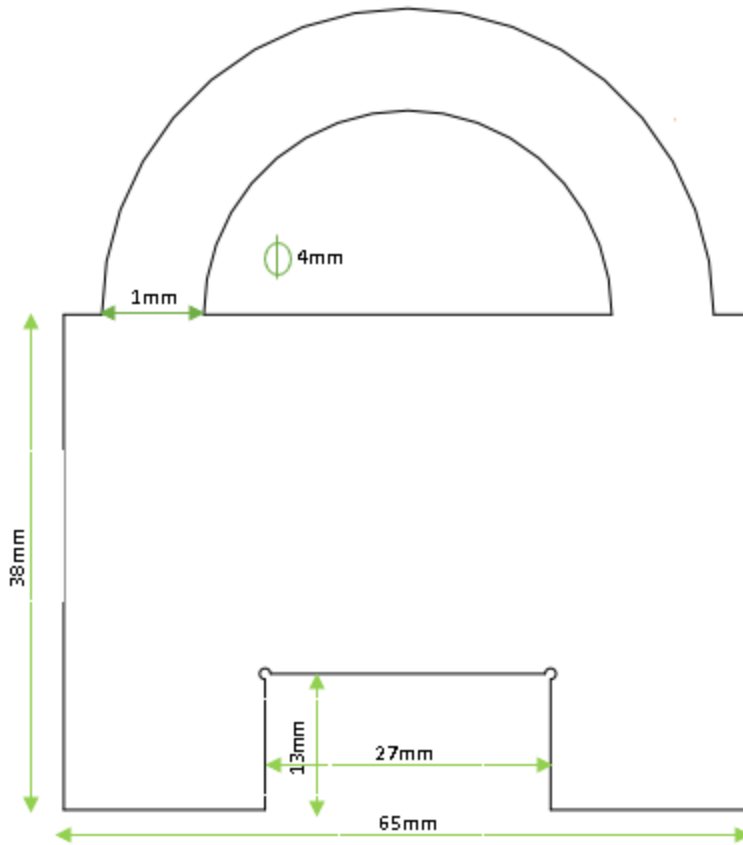*Figure A-4 Bottom Plate of Acrylic Brick Mold*

[211]

Figure A-5 Side 2 of the Acrylic Brick Mold

Appendix B: Mineral Analysis of Shale, Sewage Sludge Ash and RCG

SAMPLE	SHALE	SEWAGE SLUDGE ASH	RCG
SiO_2- Silicon dioxide	47.5	27.9	73.58
Al_2O_3- Aluminum oxide	12.95	6.37	0.86
Fe_2O_3- Iron Oxide	5.53	21.6	0.42
CaO-Calcium Oxide	11.35	14.8	9.54
MgO-Magnesium Oxide	3.36	3.46	2.97
Na_2O-Sodium Oxide	0.26	1.08	11.79
K_2O-Pottassium Oxide	3.98	1.32	0.29
Cr_2O_3- Chromium oxide	0.01	0.025	0
TiO_2-Titanium dioxide	0.7	0.84	0.23
MnO- manganese oxide	0.12	0.13	0.03
P_2O_5- Phosphorus pentoxide	0.14	19.5	0.17
SrO - Strontium oxide	0.02	0.08	0
BaO-Barium Oxide	0.05	0.14	0

Appendix C: Equipment used in the research

Standard Sieve Set

- Dual manufacturing company, IL USA-Geotechnical Engineering lab, York University.
- The sieve numbers are 4 (4.75mm) ,8 (2.36mm) ,10(2mm) ,16 (1.18mm),30(600μm), 40(425μm), 60(300μm), 100(150μm, (75μm), and pan arranged from top to bottom respectively

Washing Sieve

- Dual manufacturing company, IL USA-Geotechnical Engineering lab, York University.
- Size of the Sieve is No. 200 (75-μm).

Mechanical Sieve Shaker

- Hoskin scientific Ltd., The Rotary Lab Sifter-Geotechnical Engineering lab, York University.
- Sieve stack 200mm diameter, 10 full-height sieves plus pan.

Digital Balance

- Mettler Toledo digital balance.
- Large precision balance for heavy loads: 16200 g capacity,
- Easy readability,
- Large platform,
- Strong overload protection
- Chemical resistance.

[214]

Washing Sink with Spray Nozzle

- Geotechnical Engineering lab, York University.

Drying Oven

- Heratherm Large Capacity Ovens for drying by Thermo Fisher Scientific.
- Temperature ranges from 50-300°C(122-572°F) and electrical parameters 400V, 50/60Hz.

Sieving Containers and Specimen Containers

- Stainless Steel smooth walled containers.

Sieve Brushes

D2- Sieve Brush, Fine Mesh, Horsehair, 10.5" (267 mm)
D3-Sieve Brush, Oval Shaped,Horsehair,10.5" (267 mm)
D4- Sieve Brush, Fine Mesh, Horsehair ,5.25" (133 mm)
D5- Mold Cleaning Brush, Brass Wire, 10.25" (360 mm)
D6-General Cleaning Brush, Palmyra Barbs, 8.25" (210 mm)
D8-Table Brush, Horsehair, 13.5" (343 mm)

Soil Dispersion Mixer

- Soil Dispersion Mixer used for hydrometer analysis of soil.
- Manufacturer Hamilton Beach 115V/60Hz
- Provides thorough mixing of soil samples using a special mixing blade and a baffled dispersion cup

Hydrometer and cylinder

- Made from heavy-walled, annealed tubing for maximum strength by Thomas Scientific ltd.
- Built-in non-mercury thermometer
- Lead-free ballast
- Conforms to ASTM accuracy requirements
- Glass hydrometer cylinder of size 390 mm x 50 mm

Sedimentation Cylinder

- Glass sedimentation cylinder from Thomas scientific ltd.
- Used in measuring particle size distribution in soil suspensions by means of a hydrometer as per ASTM D 422.
- 457 mm x 63.5 mm and marked for 1000 ml volume.

Dispersing agent

- Sodium hexametaphosphate is the dispersing agent – prepared by using 40 g of powdered sodium hexametaphosphate in a litre of distilled water.
- Used for the complete dispersion of soil particles for the hydrometer analysis.
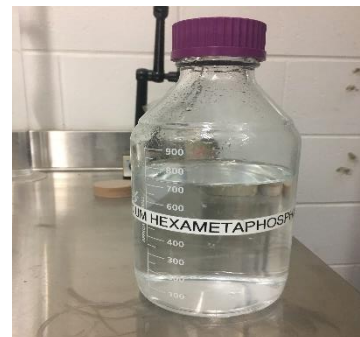
Distilled water station

- Environmental Engineering lab, York University.
- Milli-Q water purification system from Fisher Scientific

Stop-watch

- Extech's 365515 is a digital stopwatch and clock with a backlit display

Acrylic Sheets

- Acrylic platic sheets of 10mm are used to make the brick molds.
- The same Acrylic plastic is used as a levelled surfave for gypsum capping of the masonry units.

Laser cutter

- Simliar Laser cutter used for molds using acrylic sheets.
- Molds are made from 'SandBox'-The 3D Prototype lab in Lassonde School of Engineering , York University equipped with a laser-cutter.

Level

- Digiwave 9" Inch Torpedo Level
- Used during brick making and gypsum capping procesess.

KitchenAid Commercial Countertop Mixer

- Speed control protection
- Commercial bowl-lift design
- Stainless steel bowl guard for added safety
- Motor: 500 Watts ,1.3HP High-Efficiency DC Motor
- Capacity: 8-Qt/7.6L
- Knob Style: Heavy-Duty Metal

Steel Molds

- Steel molds for making brick cubes used for the freeze thaw test
- Size of the cubes were 50mm x50mm x50mm

Centrifuge

- Benchtop Centrifuge from Beckman Coulter
- Faster centrifugation
- Used as one of the dewatering methods of high biopolymer sludge.

Metallic Trays

- Metallic trays of size approximatly 12" x 6" x 1" from Uline used for the drying of the masonry brick units inside the drying oven.

Box Furnace

- Thermo Scientific™ Lindberg/Blue M™ LGO Box Furnace.
- The temperature from 100°C to 1200°C.
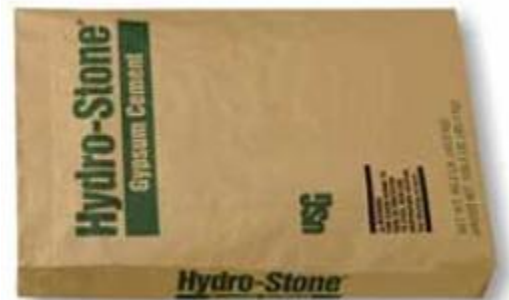- Used for the firing of the maonry units

Rafter Square

- DEWALT Premium Rafter Square, 12"

Gypsum Cement

- Hydro-Stone gypsum cement from home depot used for the capping of masonry brick units.
- Used Consistency of 32 parts of water by weight per 100 parts plaster.
- Set Time (Hand Mix) 17-20 min

Sealer (Lowes)

- Bulls Eye Shellac from Zinsser clear

- It's easy to use, dries quickly, is non-toxic when dry and cleans up easily with ammonia and water.
- Used to prevent water absorption of bricks from gypsum capping

---

Compression strength and splitting tensile strength testing machine

- Controls PILOT 50-C46C02
- Used for testing the Compression strength and splitting tensile strength of the masonry brick units
- Civil Engineering HighBay Lab, York University

MTS

- MTS universal Testing Machine .
- Used for the flexural strength test.
- Civil Engineering HighBay Lab, York University

Silicon Mold

- Silicon mold used to make Geopolymer brick cubes
- 16.5cm (L) x 10.6 (H) x 4.3cm (W)